

CYPRUS

JOURNAL OF MEDICAL SCIENCES

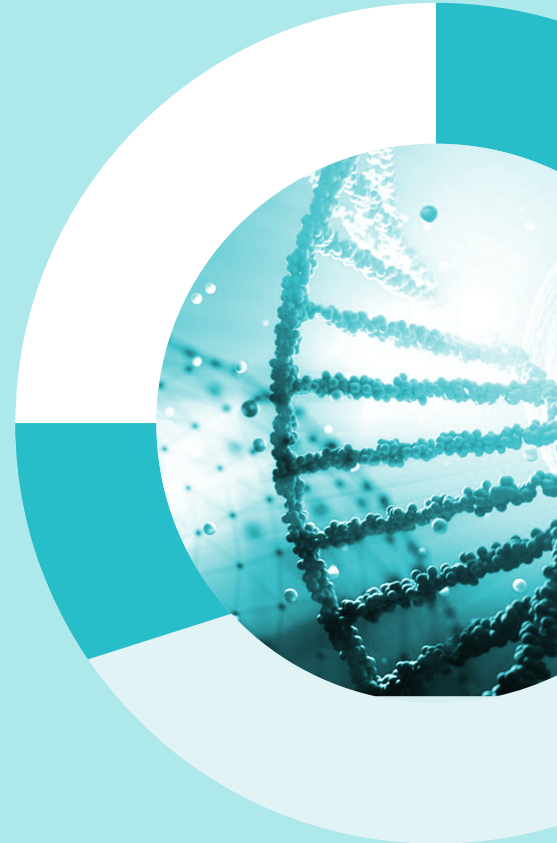
Indexed in the Web of Science

Volume: **10** Issue: **Suppl 1** April 2025



ORIGINAL ARTICLES

- ▶ **Development of an in-House FCoV qRT-PCR Kit**
Tuncel Dereboylu et al.; Nicosia, North Cyprus
- ▶ **Development and Validation of an RP-HPLC Method for the Simultaneous Quantification of Metformin and Curcumin**
Noshadi et al.; Famagusta, Nicosia, North Cyprus
- ▶ **CBCT Assessment of Taurodont and Pyramidal Molars**
Kırmızı et al.; Nicosia, North Cyprus; Ankara, Türkiye
- ▶ **Trueness of Digital Scans**
Önöral et al.; Nicosia, North Cyprus
- ▶ **Biosurfactant-Antifungal Synergy Against *Trichophyton***
Bağkur et al.; Nicosia, North Cyprus
- ▶ **Triazole MCR-1 Inhibitors: Beating Colistin Resistance**
Erdağ et al.; Nicosia, North Cyprus
- ▶ **Requiring New Treatment Strategies for Resistant Pathogens**
Opawoye et al.; Nicosia, North Cyprus
- ▶ **Capsaicin Microemulsion for Neuropathic Pain**
Shayyah et al.; Adana, Van, Türkiye; Nicosia, North Cyprus
- ▶ **Aluminium Chloride Induced Alzheimer's Model in Mice**
Kanan et al.; Niğde, Van, Türkiye; Nicosia, North Cyprus
- ▶ **Renal Artery Variations in Turkish Republic of North Cyprus Population**
Küçükçiloğlu and Tiryakioğlu; Nicosia, North Cyprus
- ▶ **Trueness of Implant Impressions**
Kurtulmus-Yılmaz et al.; Nicosia, North Cyprus
- ▶ **Early Prediction of Mortality in ICU**
Baddal et al.; Nicosia, North Cyprus
- ▶ **Detection of Keratoconus through YOLOv8 and Convolutional Neural Networks**
Anwar and Özbilge; Nicosia, North Cyprus; Erbil, Iraq
- ▶ **Evaluating the Latent Tuberculosis Diagnostic Tests**
Emegano et al.; Nicosia, North Cyprus; Sharjah, United Arab Emirates
- ▶ **MCDM in Rapid Diagnostic Test Selection During Outbreaks**
Arıkan et al.; Nicosia, North Cyprus, Kocaeli, Turkey; Sharjah, UAE
- ▶ **Rosemary Essential Oil and Pancreatic Cancer**
Hoca et al.; Famagusta, Nicosia, North Cyprus; Manisa, Türkiye
- ▶ **Developing RT-qPCR Kit for HDVs**
Günhan et al.; Manisa, Kocaeli, Türkiye; Nicosia, North Cyprus
- ▶ **Biological Network of PCOS and Non-coding RNAs**
Hasanzadeh et al.; Nicosia, North Cyprus; Tehran, Iran
- ▶ **Hypoxia Induces Exosome Secretion in Primary and Metastatic Colon and Breast Cancer Cell Lines**
Gürçınar et al.; Munich, Germany; Manisa, Antalya; Türkiye; Nicosia, North Cyprus
- ▶ **Newcastle Disease Virus**
Siddique and Ali; Nicosia, North Cyprus; Islamabad, Pakistan
- ▶ **RAB31 Play a Role During Exosome Biogenesis from Adipose Derived Mesenchymal Stem Cells**
Vatansever et al.; Manisa, Türkiye; Nicosia, North Cyprus
- ▶ **Menstrual Blood-derived Stem Cell Extraction**
Aktaş et al.; Manisa, Türkiye; Nicosia, North Cyprus
- ▶ **Moringa-Functionalized Chitosan-Zinc Oxide Nanocomposite: Antibacterial and Cytotoxic Evaluation**
Umar et al.; Nicosia, North Cyprus; Sharjah, United Arab Emirates
- ▶ **FSHR SNPs and Biological Network Analysis of PCOS**
Madhher et al.; Nicosia, North Cyprus
- ▶ **Phenolic and Antioxidant Properties of Sarulak Olive Fermented with Red Beetroot**
Güler et al.; Nicosia, North Cyprus; Adana, Türkiye
- ▶ **Diabetes Classification via Voting-Based Ensemble**
Arman et al.; Nicosia, Cyprus; London, United Kingdom
- ▶ **Role of Thiosemicarbazide Compounds on Primary and Metastatic Cancer Cells**
Kabadayı Ensarioğlu et al.; Manisa, İstanbul, Türkiye; Famagusta, Lefke, Nicosia, North Cyprus
- ▶ **Apoptosis and Necroptosis in Testicular Torsion: Impact of Exosomes from Adipose Stem Cells**
Kabadayı Ensarioğlu et al.; Manisa, Ankara, Türkiye; Nicosia, North Cyprus



CYPRUS

JOURNAL OF MEDICAL SCIENCES

Indexed in Web of Science

Volume: **10** | Issue: **Suppl 1** | April 2025

EDITORIAL BOARD

Editor-in-Chief

Sonuç Büyük

Department of Pathology, Dr. Burhan Nalbantoğlu State Hospital, Nicosia, Cyprus

sonucbuyuk@outlook.com

https://ease.org.uk/member_profile/sonuc-buyuk-5661/

Associate Editors

Amber Eker Bakkaloğlu

Department of Neurology, Eastern Mediterranean University, Dr.

Fazıl Küçük Faculty of Medicine, Famagusta, Cyprus

amber.eker@emu.edu.tr

Aysa Ayalı

Department of Oral and Maxillofacial Surgery, European University of Lefke, Faculty of Dentistry, Lefke, North Cyprus

aysaayali@hotmail.com

Ayşe Baha

Department of Chest Diseases, Dr. Akçiçek State Hospital; Girne American University Faculty of Medicine, Kyrenia, Cyprus

dr_aysedemir@hotmail.com

Ayşe Ülgen

Department of Biostatistics, Girne American University Faculty of Medicine, Kyrenia, Cyprus

ayseulgen1@gmail.com

Cemal Gürkan

Turkish Cypriot DNA Laboratory, Nicosia, Cyprus
Eastern Mediterranean University, Dr. Fazıl Küçük Faculty of Medicine, Famagusta, Cyprus

cemal.gurkan@gmail.com

Cenk Conkbayır

Department of Cardiology, Dr. Burhan Nalbantoğlu State Hospital, Nicosia, Cyprus

cenkconk@hotmail.com

Emil Mammadov

Department of Pediatric Surgery, Dr. Burhan Nalbantoğlu State Hospital, Nicosia, Cyprus

dremilmammadov@gmail.com

Erol Dülger

Vip Health Clinic, Nicosia, Cyprus

drerold@yahoo.com

İzgen Karakaya

Department of Restorative Dentistry, European University of Lefke, Faculty of Dentistry, Lefke, North Cyprus

izgen96h@gmail.com

Mümtaz Güran

Department of Medical Microbiology, Eastern Mediterranean University, Dr. Fazıl Küçük Faculty of Medicine, Famagusta, Cyprus

mumtazguran@gmail.com



Publisher Contact

Address: Molla Gürani Mah. Kaçamak Sk. No: 21/1 34093
İstanbul, Türkiye

E-mail: info@galenos.com.tr/yayin@galenos.com.tr

Web: www.galenos.com.tr Publisher Certificate Number: 14521

Publication Date: June 2025

E-ISSN: 2536-507X

ISSN: 2149-7893

International scientific journal published bi-annually.

CYPRUS

JOURNAL OF MEDICAL SCIENCES

Indexed in Web of Science

Volume: 10 | Issue: Suppl 1 | April 2025

EDITORIAL BOARD

Nilüfer Güzoğlu

Department of Neonatology, Eastern Mediterranean University,
Dr. Fazıl Küçük Faculty of Medicine, Famagusta, Cyprus
nilufer.guzoglu@emu.edu.tr

Özüm Tunçyürek

Department of Radiology, Cyprus International University
Faculty of Medicine; Kolan British Hospital, Nicosia, Cyprus
ozum.tuncyurek@neu.edu.tr

Pınar Tunçbilek Özmanevra

Department of Otorhinolaryngology - Head and Neck Surgery,
PrimeMed Clinic, Kyrenia, Cyprus
pinartuncbilek@gmail.com

Ramadan Özmanevra

Department of Orthopaedics and Traumatology, Cyprus
International University Faculty of Medicine, Nicosia, Cyprus
rozmanevra@gmail.com

Cenk Serhan Özverel

Department of Basic Medical Sciences, Near East University
Faculty of Dentistry; DESAM Research Institute, Near East
University, Nicosia, North Cyprus
cenkserhan.ozverel@neu.edu.tr

Section Editors

Ahmet Özent

Private Clinic of Orthodontics, Nicosia, Cyprus
ozantahmet@gmail.com

Ahmet Özyiğit

Universitede-Integrated Clinical Practice/Clinical Skills,
University of Nicosia Faculty of Medicine, Nicosia, Cyprus
dr.ahmet@elitenicosia.com

Ali Cenk Özay

Department of Obstetrics and Gynaecology, Near East University
Faculty of Medicine, Nicosia, Cyprus
drcenkozay@yahoo.com

Ceyhun Dalkan

Department of Pediatrics, Division of Neonatology, Near East
University Faculty of Medicine, Nicosia, Cyprus
dalkanc@yahoo.com

Ersan Berksel

Cyprus Science University Faculty of Health Sciences, Kyrenia,
Cyprus
ersanberksel@su.edu.tr

Eşref Çelik

Department of Medical and Clinical Microbiology, Near East
University Faculty of Medicine, Nicosia, Cyprus
esref.celik@neu.edu.tr

Gökçe Savtekin

Department of Oral and Maxillofacial Surgery, University of City
Island Faculty of Dentistry, Famagusta, Cyprus
gokcesavtekin@gmail.com

Gülten Sucu Dağ

Department of Nursing, Eastern Mediterranean University
Faculty of Health Sciences, Famagusta, Cyprus
sucugulten@gmail.com

Hülya Efetürk

Department of Nuclear Medicine, Near East University Faculty
of Medicine, Nicosia, Cyprus
drhulyaefeturk@gmail.com

Hüseyin Kaya Süer

Department of Infectious Diseases and Clinical Microbiology,
Near East University Faculty of Medicine, Nicosia, Cyprus
kaya.suer@neu.edu.tr

Nail Bulakbaşı

Department of Radiology, Dr. Suat Günsel University of Kyrenia
Hospital, Kyrenia, Cyprus
nbulakbasi@yahoo.com

Necdet Özçay

Department of General Surgery, University of Health Sciences
Türkiye, Gülhane Faculty of Medicine, Ankara, Türkiye
necdetozcay@gmail.com

CYPRUS

JOURNAL OF MEDICAL SCIENCES

Indexed in Web of Science

Volume: **10** | Issue: **Suppl 1** | April 2025

EDITORIAL BOARD

Nedim Sezgin Ilgi

Department of Anatomy, Near East University Faculty of Medicine, Nicosia, Cyprus
sezgin.ilgi@neu.edu.tr

Nerin Bahçeciler

Department of Child Health and Diseases, Division of Allergy and Immunology, Near East University Faculty of Medicine, Nicosia, Cyprus
nerin74@gmail.com

Ömer Taşargöl

Department of Anesthesiology and Reanimation, Dr. Burhan Nalbantoğlu State Hospital, Nicosia, Cyprus
omertasargol@yahoo.com

Özen Aşut

Department of Public Health, Near East University Faculty of Medicine, Nicosia, Cyprus
ozen.asut@neu.edu.tr

Özlem Balcıoğlu

Department of Cardiovascular Surgery, Near East University Faculty of Medicine, Nicosia, Cyprus

Sinem Şiğit İkiz

Department of Radiology, Dr. Burhan Nalbantoğlu State Hospital, Nicosia, Cyprus
sinemsigit@gmail.com

Uğurcan Balyemez

Department of Radiology, Near East University Faculty of Medicine, Nicosia, Cyprus
ubalyemez@gmail.com

Umut Maraşuna

Department of Endocrinology, Dr. Burhan Nalbantoğlu State Hospital, Nicosia, Cyprus
umutmousa@yahoo.co.uk

Zeynep Taşargöl

Department of Obstetrics and Gynaecology, Dr. Burhan Nalbantoğlu State Hospital, Nicosia, Cyprus
zeynepyt84@hotmail.com

Biostatistical Editors

İlker Etikan

Department of Biostatistics, Near East University Faculty of Medicine, Nicosia, Cyprus
ietikan@gmail.com

Ayşe Ülgen

Department of Biostatistics, Girne American University Faculty of Medicine, Kyrenia, Cyprus

National Advisory Board

Ali Ulvi Önder

Department of Urology, Near East University School of Medicine, Nicosia, Cyprus

Ayşe Gökyiğit

Department of Pharmaceutical Services of the Ministry of Health, Nicosia, Cyprus

Beste Kamiloğlu

Department of Orthodontics, Near East University School of Dentistry, Nicosia, Cyprus

Bülent Haydar

Private Clinic of Maxillofacial Surgery, Nicosia, Cyprus

Doğan Ceyhan

Department of Ophthalmology, Near East University School of Medicine, Nicosia, Cyprus

Düriye Deren Oygur

Department of Nephrology, Dr. Burhan Nalbantoğlu State Hospital, Nicosia, Cyprus

Ender Volkan

Cyprus International University School of Pharmacy, Nicosia, Cyprus

Erdem Beyoğlu

Bariş Mental and Neurological Disorders State Hospital, Nicosia, Cyprus

CYPRUS

JOURNAL OF MEDICAL SCIENCES

Indexed in Web of Science

Volume: **10** | Issue: **Suppl 1** | April 2025

EDITORIAL BOARD

Fatma Deniz

Department of Dermatology, Girne Akçiçek State Hospital, Girne, Cyprus

Filiz Besim

Private Clinic of Maxillofacial Surgery, Nicosia, Cyprus

Gamze Mocan Kuzey

Department of Pathology and Cytology, Near East University School of Medicine, Nicosia, Cyprus

Gönül Küçük

Department of Pediatric Surgery, Dr. Burhan Nalbantoğlu State Hospital, Nicosia, Cyprus

Gülşen Bozkurt

Private Clinic of Hematology, Nicosia, Cyprus

Hanife Erçal Ezgi

Department of Dermatology, Dr. Burhan Nalbantoğlu State Hospital, Nicosia, Cyprus

Hasan Besim

Department of General Surgery, Near East University School of Medicine, Nicosia, Cyprus

Hasan Mete İnançlı

Private Clinic of Otorhinolaryngology, Nicosia, Cyprus

İdris Deniz

Department of Forensic Medicine, Dr. Burhan Nalbantoğlu State Hospital, Nicosia, Cyprus

İsmet Başar

Department of Urology, Dr. Burhan Nalbantoğlu State Hospital, Nicosia, Cyprus

Kaan Erler

Department of Orthopaedics, Near East University School of Medicine, Nicosia, Cyprus

Kenan Arifoğlu

Department of Plastic and Reconstructive Surgery, Dr. Burhan Nalbantoğlu State Hospital, Nicosia, Cyprus

Kerem Teralı

Department of Medical Biochemistry, Near East University School of Medicine, Nicosia, Cyprus

Mehmet İnan

Department of General Surgery, Private Magusa Medicine Center, Famagusta, Cyprus

Meltem Nalça

Department of Radiation Oncology, Near East University School of Medicine, Nicosia, Cyprus

Murat Uncu

Department of Biochemistry, Near East University School of Medicine, Nicosia, Cyprus

Mustafa Kalfaoğlu

Department of General Surgery, Magusa State Hospital, Famagusta, North Cyprus

Mustafa Taşeli

Department of Ophthalmology, Near East University School of Medicine, Nicosia, Cyprus

Nahide Gökçora

Department of Nuclear Medicine, East Mediterranean University School of Medicine, Famagusta, Cyprus

Ozan Emiroğlu

Department of Cardiovascular Surgery, Dr. Burhan Nalbantoğlu State Hospital, Nicosia, Cyprus

Özay Önöral

Department of Protetic Medical Therapy, Near East University Faculty of Dentistry, Nicosia, Cyprus

Serap Soytaç İnançlı

Private Clinic of Endocrinology and Metabolic Diseases and Internal Medicine, Nicosia, Cyprus

Sevda Lafcı

Department of Anatomy, Near East University School of Medicine, Nicosia, Cyprus

CYPRUS

JOURNAL OF MEDICAL SCIENCES

Indexed in Web of Science

Volume: **10** | Issue: **Suppl 1** | April 2025

EDITORIAL BOARD

Sezgin Handan

Department of Nursing, Eastern Mediterranean University
School of Health Sciences, Famagusta, Cyprus

Sibel Tozaki

Department of Dermatology, Dr. Burhan Nalbantoğlu State
Hospital, Nicosia, Cyprus

Songül Acar Vaizoğlu

Department of Public Health, Near East University School of
Medicine, Nicosia, Cyprus

Süha Akpınar

Department of Radiology, Near East University School of
Medicine, Nicosia, Cyprus

Şanda Çalı

Department of Public Health, Near East University School of
Medicine, Nicosia, Cyprus

Tarık İzbul

Department of General Surgery, Dr. Burhan Nalbantoğlu State
Hospital, Nicosia, Cyprus

Tevfik Eker

Department of General Surgery, Private Magusa Medicine
Center, Famagusta, Cyprus

Tijen Ataçağ

Department of Obstetrics and Gynecology, Near East University
School of Medicine, Nicosia, Cyprus

Turgay Akalın

Private Clinic of Neurology, Nicosia, Cyprus

Ülvan Özad

Department of Plastic and Reconstructive Surgery, Near East
University School of Medicine, Nicosia, Cyprus

International Advisory Board

A.C. Joao Lima

Department of Radiology, Johns Hopkins Medicine, Baltimore,
USA

Aliye Özenoğlu

Department Nutrition and Dietetics, Üsküdar University School
of Health Science, İstanbul, Türkiye

Alp Usubütün

Department of Pathology, Hacettepe University School of
Medicine, Ankara, Türkiye

Alper Sertçelik

Department of Cardiology, Sanko University School of Medicine,
Gaziantep, Türkiye

Ayla Ünsal

Department Of Nursing, Ahi Evran University School of Health,
Kırşehir, Türkiye

Ayşe Nihal Demircan

Department of Ophthalmology, Çukurova University School of
Medicine, Adana, Türkiye

Aytekin Besim

Private Clinic of Radiology, Ankara, Türkiye

Bengi Semerci

Department of Psychiatrist, Institute of Bengi Semerci, İstanbul,
Türkiye

Barış Doğu Yıldız

Department of General Surgery, Ankara Numune Research and
Training Hospital, Ankara, Türkiye

Çağrı Büke

Department of Infectious Diseases and Clinical Microbiology,
Yeditepe University School of Medicine, İstanbul, Türkiye

Cem Ertan

Department of Emergency Medicine, Akdeniz University School
of Medicine, Antalya, Türkiye

Cem Terzi

Department of General Surgery, Dokuz Eylül University School of
Medicine, İzmir, Türkiye

CYPRUS

JOURNAL OF MEDICAL SCIENCES

Indexed in Web of Science

Volume: **10** | Issue: **Suppl 1** | April 2025

EDITORIAL BOARD

Coşkun Yorulmaz

Department of Forensic Medicine, İstanbul University
Cerrahpaşa School of Medicine, İstanbul, Türkiye

Dilek Yavuz

Department of Internal Medicine and Endocrinology Section,
İstanbul University School of Medicine, İstanbul, Türkiye

Ebru Yılmaz Yalçınkaya

Department of Physical Therapy and Rehabilitation,
Gaziosmanpaşa Taksim Research and Training Hospital,
İstanbul, Türkiye

Elif Arı Bakır

Department of Nephrology, Kartal Dr. Lütfi Kırdar Training
Hospital, İstanbul, Türkiye

Egemen İdiman

Department of Neurology, Dokuz Eylül University School of
Medicine, İzmir, Türkiye

Emre Canda

Department of General Surgery, Dokuz Eylül University School of
Medicine, İzmir, Türkiye

Erkan Göksu

Department of Emergency Medicine, Akdeniz University School
of Medicine, Antalya, Türkiye

Erol Baysal

Dubai Genetic and Thalassemia Center, Dubai Health Authority,
Dubai, UAE

Fatih Köse

Department of Oncology, Başkent University School of Medicine,
Adana Search and Practise Hospital, Adana, Türkiye

Fazıl Tuncay Aki

Department of Urology, Head of Transplantation Unite,
Hacettepe University School of Medicine, Ankara, Türkiye

Funda Tuğcu

Department of Orthodontics, Ankara University School of
Dentistry, Ankara, Türkiye

Gökhan Berktuğ Bahadır

Department of Pediatric Surgery, Mersin University School of
Medicine, Mersin, Türkiye

Gülnur Göllü Bahadır

Department of Pediatric Surgery, Ankara University School of
Medicine, Ankara, Türkiye

Gökhan Nergizoğlu

Department of Internal Medicine-Nephrology, Ankara University
School of Medicine, Ankara, Türkiye

Gölge Acaroğlu

Private Clinic of Ophthalmology, Ankara, Türkiye

Hür Hassoy

Department of Public Health, Ege University School of Medicine,
İzmir, Türkiye

Hakan Altay

Department of Cardiology, Başkent University İstanbul Hospital,
İstanbul, Türkiye

Hüseyin Bakkaloğlu

Department of General Surgery, İstanbul University School of
Medicine, İstanbul, Türkiye

Hüseyin Mertsoylu

Department of Oncology, Başkent University School of Medicine,
Adana Search and Practise Hospital, Adana, Türkiye

İlhami Kuru

Department of Orthopedics and Traumatology, Başkent
University School of Medicine, Ankara, Türkiye

Kemal Bakır

Department of Pathology, Gaziantep University School of
Medicine, Gaziantep, Türkiye

Kemal Dolay

Department of General Surgery, Bezmialem Vakif University,
Bezmialem Hospital, İstanbul, Türkiye

CYPRUS

JOURNAL OF MEDICAL SCIENCES

Indexed in Web of Science

Volume: **10** | Issue: **Suppl 1** | April 2025

EDITORIAL BOARD

Kürşad Türksen

Samuel Lunenfeld Research Institute, Mount Sinai Hospital
University of Toronto, Toronto, Canada

Lale Tokgözoğlu

Department of Cardiology, Hacettepe University School of
Medicine, Ankara, Türkiye

Levent Sennaroğlu

Department of Otorhinolaryngology, Hacettepe University
School of Medicine, Ankara, Türkiye

Mazhar Tokgözoğlu

Department of Orthopaedics and Traumatology, Hacettepe
University School of Medicine, Ankara, Türkiye

Melih Atahan Güven

Department of Gynecology and Obstetrics, Acıbadem University
School of Medicine, İstanbul, Türkiye

Mustafa Camgöz

Department of Life Sciences, Imperial Collage School of Natural
Sciences, London, United Kingdom

Müfit Akyüz

Department of Physical Therapy and Rehabilitation, Karabük
University School of Medicine, Karabük, Türkiye

Müslime Akbaba

Department of Ophthalmology, Acıbadem University School of
Medicine, İstanbul, Türkiye

Mustafa Sertaç Yazıcı

Department of Urology, Hacettepe University School of
Medicine, Ankara, Türkiye

Neval Duman

Department of Internal Medicine-Nephrology, Ankara University
School of Medicine, Ankara, Türkiye

Nihat Yavuz

Department of General Surgery, İstanbul University School of
Medicine, İstanbul, Türkiye

Nilgün Kapucuoğlu

Department of Pathology, Acıbadem University School of
Medicine, İstanbul, Türkiye

Nilüfer Rahmioğlu

Department of Genetics, University of Oxford School of
Medicine, Oxford, United Kingdom

Nuray Başsüllü Kara

Department of Pathology, Acıbadem University School of
Medicine, İstanbul, Türkiye

Nuri Özgirgin

Department of Otorhinolaryngology, Bayındır Hospital, Ankara,
Türkiye

Orçun Şahin

Department of Orthopedics and Traumatology, Başkent
University School of Medicine, Ankara, Türkiye

Oytun Erbaş

Department of Experimental Medicine, The Scientific and
Technological Research Council (TUBITAK-Martek) of Türkiye, IL,
USA

Özgür Deren

Department of Obstetrics and Gynecology, Division of Maternal
Fetal Medicine, Hacettepe University, Ankara, Türkiye

Özgür Özyılkan

Department of Oncology, School of Medicine, Başkent University
Adana Search and Practise Hospital, Adana, Türkiye

Peyman Yalçın

Department of Physical Therapy and Rehabilitation, Ankara
University School of Medicine, Ankara, Türkiye

Pınar Zeyneloğlu

Department of Anesthesiology and Reanimation, Başkent
University, Ankara Hospital, Ankara, Türkiye

Ralph Tufano

Department of Otolaryngology-Head and Neck Surgery, Johns
Hopkins Medicine, Baltimore, USA

CYPRUS

JOURNAL OF MEDICAL SCIENCES

Indexed in Web of Science

Volume: **10** | Issue: **Suppl 1** | April 2025

EDITORIAL BOARD

Rahmi Kılıç

Department of Otorhinolaryngology, Kırıkkale University School of Medicine, Kırıkkale, Türkiye

Salih Marangoz

Department of Orthopaedics and Traumatology, Acıbadem Mehmet Ali Aydınlar University School of Medicine, İstanbul, Türkiye

Selçuk İnanlı

Department of Otorhinolaryngology, Head and Neck Surgery, Marmara University School of Medicine, İstanbul, Türkiye

Serap Öztürkcan

Department of Dermatology, Celal Bayar University School of Medicine, Manisa, Türkiye

Serkan Durdu

Department of Cardiovascular Surgery, Cebeci Kardiac Center, Ankara University School of Medicine, Ankara, Türkiye

Serkan Sertel

Department of Otorhinolaryngology, University of Heidelberg Neuenheimer Feld, Heidelberg, Germany

Serpil Altındoğan

Department of Oral Maxillofacial Surgery, Ankara University School of Dentistry, Ankara, Türkiye

Server Serdaroğlu

Department of Dermatology, İstanbul University Cerrahpaşa School of Medicine, İstanbul, Türkiye

Şaziye Şahin

Department of Anesthesiology and Reanimation, Gazi University Dental School of Dentistry, Ankara, Türkiye

Teslime Atlı

Department of Geriatrics, Ankara University School of Medicine, Ankara, Türkiye

Tolga Karıcı

Department of Orthopaedics and Traumatology, İzmir Şifa University İzmir, Türkiye

Ufuk Ateş

Department of Pediatric Surgery, Ankara University School of Medicine, Ankara, Türkiye

Ufuk Erginoğlu

Department of Neurological Surgery, University of Wisconsin, School of Medicine and Public Health, Madison, USA

Vedat Göröl

Department of Gastroenterology, İstanbul Medipol University School of Medicine, İstanbul, Türkiye

Vural Fidan

Department of Otorhinolaryngology, Yunus Emre State Hospital, Eskişehir, Türkiye

Yeşim Sağlıcan

Department of Pathology, Acıbadem University School of Medicine, İstanbul, Türkiye

Please refer to the journal's webpage (<https://cyprusjmedsci.com/>) for "Aims and Scope", "Instructions to Authors" and "Ethical Policy".

The editorial and publication process of the Cyprus Journal of Medical Sciences are shaped in accordance with the guidelines of ICMJE, WAME, CSE, COPE, EASE, and NISO. The journal is in conformity with the Principles of Transparency and Best Practice in Scholarly Publishing.

Cyprus Journal of Medical Sciences is indexed in **Web of Science-Emerging Sources Citation Index, TUBITAK ULAKBIM TR Index, Embase, EBSCO, J-GATE, CABI, CNKI and Gale.**

The journal is published electronically.

Owner: Ahmet Özant on behalf of Cyprus Turkish Medical Association

Responsible Manager: Sonuç Büyük

CONTENTS

ORIGINAL ARTICLES

- 1** **Development of a qRT - PCR Diagnostic Kit for the Detection of FCoV**
Gülten Tuncel Dereboylu, Gökçe Akan, Melis Kalaycı, Cenk Serhan Özverel, Tamer Şanlıdağ; Nicosia, North Cyprus
- 4** **Development and Validation of an RP-HPLC Method for the Simultaneous Quantification of Metformin and Curcumin**
Bahareh Noshadi, Emine Vildan Burgaz, Leyla Beba Pozharani; Nicosia, North Cyprus
- 8** **Evaluation of Taurodont and Pyramidal Mandibular Molars Prevalence in a Group of Turkish Cypriot Population by Cone Beam Computed Tomography**
Dilan Kırmızı, Umut Aksoy, Seçil Aksoy, Nildem İnönü, Kaan Orhan; Nicosia, North Cyprus; Ankara, Türkiye
- 12** **Influence of Prefabricated Auxiliary Device Design and Intraoral Scanner Type on the 3D Trueness of Intraoral Scans**
Özay Önöral, Selin Çakır, Sevcan Kurtulmuş Yılmaz; Nicosia, North Cyprus
- 16** ***In Silico* Analysis of the Synergistic Interaction Between Biosurfactants and Antifungal Agents Against *Trichophyton* spp.**
Cemile Bağkur, Cenk Serhan Özverel, Emine Erdağ; Nicosia, North Cyprus
- 20** **Triazole Derivatives as Potential MCR-1 Inhibitors: A Promising Approach to Overcome Colistin Resistance**
Emine Erdağ, Cenk Serhan Özverel, Cemile Bağkur; Nicosia, North Cyprus
- 24** **Necessity of Alternative Strategies to Combat Antibiotic Resistant Strains Detected in Northern Cyprus**
Elizabeth Mkpouto Opaoye, Emrah Güler, Kaya Süer, Ayşe Arıkan; Nicosia, Lefke, Kyrenia, North Cyprus
- 29** ***In Vivo* Assessment of a Capsaicin-Containing Microemulsion for Neuropathic Pain Management**
Rumooz Shayyah, Umay Merve Güven Bölgen, Ares Alizade, Serpil Demirci Kayıran, Sonia Ebrahimi, Fazilet Aksu; Adana, Van, Türkiye; Nicosia, North Cyprus
- 34** **Investigation of Behavioral Changes and Histopathological Changes in the Brain in Alzheimer's Modeled Mice with Aluminium Chloride (AlCl₃)**
Derya Deniz Kanan, Işıl Aydemir, Ares Alizade, Sonia Ebrahimi, Fazilet Aksu; Niğde, Van, Türkiye; Nicosia, North Cyprus
- 38** **Renal Artery Variations and Clinical Implications: CT Angiography Study in Turkish Republic of North Cyprus Population**
Yasemin Küçükçiloğlu, Mehtap Tiryakioğlu; Nicosia, North Cyprus
- 42** **Does Scan Aid Use Improve the 3D Trueness of Digital Implant Impressions with Different Inter-Implant Distances?**
Sevcan Kurtulmuş-Yılmaz, Tezcan Muslu, Özay Önöral; Nicosia, North Cyprus
- 46** **Early Prediction of Mortality due to Carbapenem-Resistant Gram-Negative Bacterial Infection in Intensive Care Units Using Machine Learning**
Buket Baddal, Cemile Bağkur, Bardia Arman; Nicosia, North Cyprus
- 50** **Detection of Keratoconus through YOLOv8 Region of Interest Preprocessing and Pre-trained Convolutional Neural Networks Using 2D Images**
Muhammed Sideeq Anwar, Emre Özbilge; Nicosia, North Cyprus; Erbil, Iraq
- 55** **Evaluating the Latent Tuberculosis Diagnostic Tests Using Fuzzy PROMETHEE: A Multi-Criteria Decision Approach**
Declan Emegano, Nazife Sultanoğlu, Efe Precious Onakpojeruo, Berna Uzun, Dilber Uzun Ozsahin, Tamer Şanlıdağ; Nicosia, North Cyprus; Sharjah, United Arab Emirates
- 60** **Contribution of Multi-Criteria Decision-Making Approach in Choosing the Most Appropriate Rapid Diagnostic Tests in an Outbreak**
Ayşe Arıkan, Berna Uzun, Murat Sayan, Dilber Uzun Ozsahin Tamer Şanlıdağ; Nicosia, North Cyprus, Kocaeli, Turkey; Sharjah, UAE

CONTENTS

- 65 The Cytotoxic Activity of Rosemary Essential Oil on PANC-1 Cells**
Mustafa Hoca, Eda Becer, Abdussalam Yakubu, Hafize Seda Vatansever; Famagusta, Nicosia, North Cyprus; Manisa, Türkiye
- 69 Developing RT-qPCR Kit for Detection and Quantification of Hepatitis D Virus Unique Genome**
Kıvanç Günhan, Hafize Seda Vatansever, Tamer Şanlıdağ, Murat Sayan, Sinem Akçalı, Hilal Kabadayı Ensarioğlu, Ferdi Çetin, Gökçe Akan, Gülten Tuncel Dereboylu, Melis Kalaycı; Manisa, Kocaeli, Türkiye; Nicosia, North Cyprus
- 74 Biological Network Analysis of Genes and Non-coding RNAs in Polycystic Ovary Syndrome**
Bitra Ostad Hasanzadeh, Zahra Lotfi Sousefi, Parham Ostad Hasanzadeh, Pınar Tulay; Nicosia, North Cyprus; Tehran, Iran
- 78 Stimulation by Exosomes Under Hypoxia Enhances Tumorigenic Properties of Primary and Metastatic Colon and Breast Cancer Cells**
İbrahim Halil Gürçınar, Hilal Kabadayı Ensarioğlu, Remziye Kendirci-Katirci, Hafize Seda Vatansever; Munich, Germany; Manisa, Antalya; Türkiye; Nicosia, North Cyprus
- 83 Molecular Characterization of Newcastle Disease Virus Circulating in Pakistan**
Uswa Siddique, Ijaz Ali; Nicosia, North Cyprus; Islamabad, Pakistan
- 87 Does RAB31 Continue to Play a Role in Exosome Biogenesis of Adipose-Derived Mesenchymal Stem Cells in 2D and 3D Culture Conditions in a Hypoxic Environment?**
Hafize Seda Vatansever, Hilal Kabadayı Ensarioğlu, Aslınur Aktaş, Burak Kutlu Aydın, Nadire Kıyak, Mehmet Vatansever; Manisa, Türkiye; Nicosia, North Cyprus
- 92 Protocol for Obtaining Stem Cells from Menstrual Blood**
Aslınur Aktaş, Hilal Kabadayı Ensarioğlu, Yıldız Uyar, Hafize Seda Vatansever; Manisa, Türkiye; Nicosia, North Cyprus
- 96 Synthesis of Chitosan Functionalized Zinc Oxide Nanocomposite using *Moringa Stenopetala* Extract and Assessment of its Antibacterial and Cytotoxic Potentials**
Huzaifa Umar, Maryam Rabiü Aliyu, Natacha Usanase, Basil Bartholomew Duwa, Dilber Uzun Ozsahin; Nicosia, North Cyprus; Sharjah, United Arab Emirates
- 101 Investigation of Single Nucleotide Polymorphisms within the *FSHR* Gene and Biological Network Analysis of Non-Coding RNAs in Polycystic Ovary Syndrome Patients**
Sana Madhher, Bitra Ostad-Hasanzadeh, Burcu Özbakır, Ali Cenk Özay, Pınar Tulay; Nicosia, North Cyprus
- 106 Phenolic Profile and Antioxidant Properties of Sarıolak Olive Fermented with Red Beetroot**
Şebnem Güler, Hüseyin Erten, Mehmet Karagözlü; Nicosia, North Cyprus; Adana, Türkiye
- 111 Ensemble Learning for Diabetes Classification Using Voting Classifier on CDC Health Indicators Dataset**
Bardia Arman, Kian Jazayeri, Erbug Celebi, Kezban Alban, Kamil Dimililer; Nicosia, North Cyprus; London, United Kingdom
- 116 Synthesis and Cytotoxic Effects of Various Thiosemicarbazide Compounds on Primary and Metastatic Breast Cancer Cell Lines**
Hilal Kabadayı Ensarioğlu, Eda Becer, Faika Başoğlu, Nuray Ulusoy Güzeldemirci, Hafize Seda Vatansever; Manisa, İstanbul, Türkiye; Famagusta, Lefke, Nicosia, North Cyprus
- 121 Adipose Mesenchymal Stem Cell-Derived Exosomes Prevent Testicular Torsion Injury by Controlling Apoptosis and Necroptosis**
Hilal Kabadayı Ensarioğlu, Fatma Bilgecan Şimşek, Hafize Seda Vatansever, Hasan Çayırılı, Aydın Şencan; Manisa, Ankara, Türkiye; Nicosia, North Cyprus

Development of a qRT - PCR Diagnostic Kit for the Detection of FCoV

✉ Gülten Tuncel Dereboylu¹, ✉ Gökçe Akan¹, ✉ Melis Kalaycı¹, ✉ Cenk Serhan Özverel^{1,2}, ✉ Tamer Şanlıdağ¹

¹DESAM Research Institute, Near East University, Nicosia, North Cyprus

²Department of Basic Medical Sciences, Near East University Faculty of Dentistry, Nicosia, North Cyprus

Abstract

BACKGROUND/AIMS: In recent years, feline infectious peritonitis (FIP), which led to the death of more than 3,000 cats on the island of Cyprus, has become a significant concern. FIP is a fatal disease in cats caused by feline coronavirus (FCoV). Due to its rapid spread among cats, its potential to pose a pandemic threat, and its presentation of symptoms similar to other diseases, accurate and rapid diagnostic methods are essential.

MATERIALS AND METHODS: This study reports the development of a novel quantitative reverse-transcription polymerase chain reaction (qRT-PCR) diagnostic kit specifically designed to detect the presence of FCoV-specific nucleic acid in anal/fecal swab samples. Sequence-specific primer and probe sequences were designed and optimized to specifically target FCoV membrane and *open reading frame 7* genes. The kit was evaluated using clinical samples from suspected FCoV cases.

RESULTS: Designed kit demonstrated high sensitivity and specificity on tested samples. Target genes in all FCoV-positive samples were successfully amplified with no false-positive or false-negative results.

CONCLUSION: Our findings indicate that the designed qRT-PCR kit provides a reliable tool for the rapid and early diagnosis of FCoV infection in cats, thereby aiding in clinical decision-making as well as disease management.

Keywords: Feline coronavirus, FCoV, FIP, qRT-PCR

INTRODUCTION

Feline infectious peritonitis (FIP) is a severe, often fatal systemic disease caused by a virulent strain of feline coronavirus (FCoV).¹ FCoV is an enveloped, positive-sense single-stranded RNA virus belonging to the Coronaviridae family. The FCoV genome is approximately 29.4 kb in length and consists of several open reading frames (ORFs) that encode structural proteins, including the spike (S), envelope, membrane (M), and nucleocapsid proteins, as well as non-structural proteins, which are involved in viral replication and pathogenesis.² The *S protein* gene has been reported as the main factor responsible for the adhesion of the virus to the cells that it will attack. The other important region in

the genome of FCoV is the ORF, which encodes non-structural proteins.³ It is reported that non-structural proteins are responsible for viral replication and transcription. FCoV is reported as highly contagious. It can spread rapidly among cats, particularly in multi-cat environments such as shelters and catteries.^{4,5} In view of its fast transmission rate in cat populations, the importance of early and accurate detection is crucial for proper disease management and prevention of possible outbreaks.⁵ FCoV is mainly transmitted by fecal-oral transmission, where infected cats excrete the virus in their feces or semen.⁶ Close contact with an infected cat, shared litter boxes, or contaminated environments can also be listed as a transmission route for FCoV.

To cite this article: Tuncel Dereboylu G, Akan G, Kalaycı M, Özverel CS, Şanlıdağ T. Development of a qRT - PCR diagnostic kit for the detection of FCoV. Cyprus J Med Sci. 2025;10(Suppl 1):1-3

ORCID IDs of the authors: G.T.D. 0000-0002-3332-471X; G.A. 0000-0002-3878-1135; M.K. 0000-0002-5779-5532; C.S.Ö. 0000-0001-9932-4774; T.Ş. 0000-0001-9932-4774.



Corresponding author: Tamer Şanlıdağ
E-mail: tamer.sanlidag@neu.edu.tr
ORCID ID: orcid.org/0000-0002-6015-8032

Received: 10.12.2024
Accepted: 19.01.2025
Publication Date: 04.06.2025



Copyright© 2025 The Author. Published by Galenos Publishing House on behalf of Cyprus Turkish Medical Association.
This is an open access article under the Creative Commons AttributionNonCommercial 4.0 International (CC BY-NC 4.0) License.

Current testing methods for FCoV rely on antigen testing. However, this method carries a high risk of cross-reactivity, especially with other viruses from the same family, causing false-positive results. Also, antigen tests have lower sensitivity compared to amplification-based polymerase chain reaction (PCR) technology. In this study, we present a novel quantitative reverse-transcription (qRT)-PCR diagnostic kit specifically designed to detect FCoV nucleic acids from anal/fecal swab samples. The kit targets the M and ORF genes, which are known to be crucial for viral replication and indicate the presence of the virus.⁷ By utilizing highly specific primer and probe sets, this PCR kit aims to provide a sensitive and accurate tool for early diagnosis of FCoV.

MATERIALS AND METHODS

Sample Collection and RNA Isolation

By veterinary specialists, a total of 36 blind clinical samples, including anal/fecal swabs, were collected from cats with and without clinical signs of FIP. Near East University Animal Experiments Local Ethics Committee granted the ethical approval for the study (approval number: 2024/192-192, date: 19/12/2024). Control samples were also obtained from healthy cats. RNA isolation from anal swab samples was performed using the commercially available kit, A1 LifeSciences-Diagnovital RTA Viral RNA Isolation Kit (İstanbul, Türkiye), according to the manufacturer's instructions.

Primer and Probe Design

Primers and probes were designed to specifically target the M and *ORF7 protein* genes of the FIP-associated strain of FCoV. The sequences were obtained from the *National Center for Biotechnology Information (NCBI)* gene database. Primer sets were designed using SnapGene and NCBI basic local alignment search tool (BLAST) software. After performing BLAST analysis to ensure that the primers would not result in off-target amplification, had appropriate melting temperatures and no self-annealing risk, the appropriate primer sets were selected.

Polymerase Chain Reaction Assay Development

The PCR assay was developed using a standard protocol with minor modifications to increase sensitivity. The reaction mix included primer and probe sets, PCR mastermix with reverse transcriptase, and extracted RNA. Thermal cycling conditions consisted of an initial reverse transcription step at 55 °C for 15 minimum, followed by an initial denaturation step at 95 °C for 30 30 seconds (sec), then 40 cycles at 95 °C for 10 sec and 58 °C for 30 sec. Fluorescence signals were obtained at Cy5 and FAM channels. The assay was validated using a panel of known FCoV-positive and negative samples. Sensitivity was checked by serial dilution of the target RNA, and specificity was confirmed through in-silico testing against over 30 viral genomes, 20 bacterial genomes, and 10 parasite genomes, along with the feline and *Homo sapiens* genomes.

RESULTS

The PCR assay successfully amplified the target gene in all FCoV-positive samples, with no amplification observed in negative controls or samples from cats with antigen-negative results (Figure 1). Specificity testing showed no cross-reactivity with non-pathogenic FCoV or other feline pathogens, highlighting the assay's robustness and accuracy.

Among the tested samples, 18 were found to be PCR positive, of which 13 indicated active infection and 5 suggested past infection.

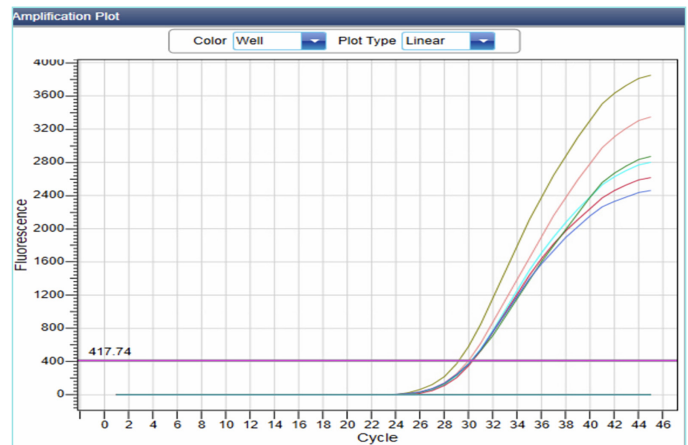


Figure 1. Amplification plot results of FCoV-positive samples.

FCoV: Feline coronavirus.

These findings were consistent with the clinical symptoms observed and antigen results. The kit's performance was further evaluated by comparing its results with serological tests, showing a concordance rate of 100% with serology tests.

DISCUSSION

The ability to diagnose FCoV infections with high specificity and accuracy carries great importance for both clinical and epidemiological purposes since the virus can transmit easily among feline populations worldwide.^{4,8} Conventional diagnostic methods, such as serological testing, have notable limitations, including delayed results and a risk of false positives or negatives.⁹ A major limitation of this study is the relatively small sample size. Further validation studies of the performance of the kit on a larger feline sample size are necessary. One of the key strengths of this qRT-PCR kit is its use of primers and probes designed specifically to target the genes for FCoV.^{8,9} The specificity of this diagnostic method was confirmed not only through laboratory testing but also through in silico analysis against a wide range of viral, bacterial, and parasitic genomes, as well as the feline genome, thus ensuring no cross-reactivity with non-pathogenic strains of FCoV or other common feline pathogens.

The results obtained from clinical samples in this study also emphasize the kit's diagnostic effectiveness. Among the 36 tested samples, the qRT-PCR assay identified 13 active infections and 5 past infections in cats. These findings were consistent with the clinical signs and antigen test results, confirming the kit's effectiveness in identifying not only active infections but also previous exposures to FCoV on account of the designed primers and probes. This capability is especially valuable for disease surveillance in multi-cat environments, such as streets or shelters, where rapid identification and isolation of infected cats are essential for controlling possible outbreaks.^{4,8} From a research perspective, this diagnostic kit study can be a pioneering study for future research and will help in understanding the molecular mechanism of FCoV.⁴

Study Limitations

The main limitation of this study was the small sample size, which may affect the generalizability of the findings; future research could address this by including a larger and more diverse sample.

CONCLUSION

Development of an in-house qRT-PCR kit for the detection of FCoV is an important step for the field of veterinary diagnostics. The kit is designed to specifically target the viral genes which are M and ORF7. Primer and probe sets are designed to ensure high specificity and sensitivity. During optimization studies, the detection performance of the in-house designed kit has been studied with clinical samples suspected for FCoV. Importantly, the results were in concordance with the serological test results. The results prove that the designed kit can be used as a reliable diagnostic tool. Future studies will focus on optimizing the kit for routine use and exploring its applicability across diverse clinical settings.

MAIN POINTS

- The designed diagnostic kit provides a valuable tool for the early and accurate detection of feline coronavirus (FCoV).
- The kit offers rapid and reliable results.
- It is aimed to be prepared for a possible pandemic by targeting the FCoV which can transmit rapidly.
- Sensitivity tests were carried out in comparison with serological tests and completely compatible results were obtained.

ETHICS

Ethics Committee Approval: Near East University Animal Experiments Local Ethics Committee granted the ethical approval for the study (approval number: 2024/192-192, date: 19/12/2024).

Informed Consent: Not available.

Footnotes

Acknowledgements

The authors would like to extend their sincere gratitude to Near East University Animal Hospital and Hospital Veterinary Clinic for providing clinical samples crucial for the completion of this project.

Authorship Contributions

Concept C.S.Ö., T.Ş., Design: G.T.D., G.A., M.K, Data Collection and/or Processing: G.T.D., G.A., M.K, Analysis and/or Interpretation: G.T.D., G.A., M.K, Literature Search: G.T.D., G.A., M.K, Writing: G.T.D., G.A., M.K.

DISCLOSURES

Conflict of Interest: No conflict of interest was declared by the authors.

Financial Disclosure: Near East University.

REFERENCES

1. Sherding RG. Feline Infectious Peritonitis (Feline Coronavirus). Saunders Manual of Small Animal Practice. 2009; 132-43.
2. Lutz M, Steiner AR, Cattori V, Hofmann-Lehmann R, Lutz H, Kipar A, et al. FCoV viral sequences of systemically infected healthy cats lack gene mutations previously linked to the development of FIP. *Pathogens*. 2020; 9(8): 603.
3. Jaimes JA, Whittaker GR. Feline coronavirus: insights into viral pathogenesis based on the spike protein structure and function. *Virology*. 2018; 517: 108-21.
4. Gao YY, Wang Q, Liang XY, Zhang S, Bao D, Zhao H, et al. An updated review of feline coronavirus: mind the two biotypes. *Virus Res*. 2023; 326: 199059.
5. Sykes JE. Feline Coronavirus infection. *Canine and Feline Infectious Diseases*. 2013; 195-208.
6. Stranieri A, Probo M, Pisu MC, Fioletti A, Meazzi S, Gelain ME, et al. Preliminary investigation on feline coronavirus presence in the reproductive tract of the tom cat as a potential route of viral transmission. *J Feline Med Surg*. 2020; 22(2): 178-85.
7. Pedersen NC. An update on feline infectious peritonitis: diagnostics and therapeutics. *Vet J*. 2014; 201(2): 133-41.
8. Roman, N. (2024, January 8). Feline infectious peritonitis. MSD Veterinary Manual. <https://www.msdsvetmanual.com/generalized-conditions/feline-infectious-peritonitis/feline-infectious-peritonitis>
9. Sharif S, Arshad SS, Hair-Bejo M, Omar AR, Zeenathul NA, Alazawy A. Diagnostic methods for feline coronavirus: a review. *Vet Med Int*. 2010; 2010: 809480.

Development and Validation of an RP-HPLC Method for the Simultaneous Quantification of Metformin and Curcumin

✉ Bahareh Noshadi¹, ✉ Emine Vildan Burgaz², ✉ Leyla Beba Pozharani²

¹Department of Pharmaceutical Chemistry, Near East University Faculty of Pharmacy, Nicosia, North Cyprus

²Department of Pharmaceutical Chemistry, Eastern Mediterranean University Faculty of Pharmacy, Famagusta, North Cyprus

Abstract

BACKGROUND/AIMS: Metformin, a common drug for managing type 2 diabetes, and curcumin, a bioactive compound from turmeric, exhibit complementary therapeutic properties, particularly for metabolic disorders. Despite their potential synergy, simultaneous analysis is challenging due to differences in chemical structure and solubility.

MATERIALS AND METHODS: A reverse-phase high-performance liquid chromatography (RP-HPLC) method was developed for the concurrent quantification of metformin and curcumin. The method utilized an Agilent 1260 Infinity HPLC system with a UV-Vis detector and a C18 column, achieving separation with retention times of 1.2 minutes for metformin and 6.0 minutes for curcumin. Validation followed International Conference on Harmonization Guidelines, assessing linearity, precision, accuracy, and sensitivity.

RESULTS: The method demonstrated high linearity ($R^2 > 0.999$), precision (%RSD $< 2\%$), and accuracy with recovery rates close to 100%. Sensitivity tests showed low limits of detection and limits of quantification, indicating robustness and reliability for routine analysis.

CONCLUSION: The validated RP-HPLC method is efficient and cost-effective, enabling robust analysis of metformin and curcumin in combined pharmaceutical formulations. This method is ideal for quality control laboratories and holds potential for biological sample analysis in clinical research on combined treatments.

Keywords: Metformin, curcumin, RP-HPLC, method validation, simultaneous quantification

INTRODUCTION

Metformin is a used antidiabetic medication recognized for its effectiveness in decreasing blood glucose levels by enhancing insulin sensitivity and diminishing hepatic glucose production.^{1,2} Curcumin, a polyphenolic compound obtained from turmeric (*Curcuma longa*), has been the subject of extensive research regarding its anti-inflammatory, antioxidant, and antidiabetic properties.^{3,4} Recent studies suggest that the combination of metformin and curcumin may yield synergistic effects in treating metabolic disorders.^{5,6} Simultaneous analysis of these compounds presents challenges owing to variations in their chemical structures and solubility profiles.⁷ High-performance

liquid chromatography is a technology that is effective in separating and quantifying chemicals that are present in complex mixtures.^{8,9} This study develops and verifies a reverse-phase high-performance liquid chromatography (RP-HPLC) technique for the simultaneous measurement of metformin and curcumin, with the goal of improving the method for use in research as well as quality control.

MATERIALS AND METHODS

In order to carry out this investigation, we utilized laboratory samples and did not involve human participants; consequently, informed consent was not necessary.

To cite this article: Noshadi B, Burgaz EV, Pozharani LB. Development and validation of an RP-HPLC method for the simultaneous quantification of metformin and curcumin. *Cyprus J Med Sci.* 2025;10(Suppl 1):4-7

ORCID IDs of the authors: B.N. 0000-0002-2650-0148; E.V.B. 0000-0003-3245-5934; L.B.P. 0000-0001-5051-4489.



Corresponding author: Bahareh Noshadi
E-mail: Bahareh.noshadi@neu.edu.tr
ORCID ID: orcid.org/0000-0002-2650-0148

Received: 03.11.2024
Accepted: 25.12.2024
Publication Date: 04.06.2025



Copyright © 2025 The Author. Published by Galenos Publishing House on behalf of Cyprus Turkish Medical Association.
This is an open access article under the Creative Commons Attribution-NonCommercial 4.0 International (CC BY-NC 4.0) License.

Chemicals and Reagents

Metformin hydrochloride (analytical grade, catalog no. M9768, Sigma-Aldrich, USA) and curcumin (analytical grade, catalog no: C7727, Sigma-Aldrich, USA) were utilized in this study. HPLC-grade methanol (catalog no: M/4054/17, Fisher Scientific, UK) was obtained from local suppliers. Deionized water was consistently used throughout the study and filtered using a 0.45 µm membrane filter (catalog no: SF14795, Merck Millipore, Germany). All reagents and solvents were of the highest analytical or HPLC grade to ensure accuracy and reproducibility in the analysis.

HPLC Instrumentation and Conditions

Using an Agilent 1260 Infinity HPLC system equipped with a UV-Vis detector, the chromatographic analysis was carried out. The separation process was carried out utilizing a C18 column with dimensions of 150×4.6 mm and a particle size of 5 µm at a temperature of 30 °C. In this step, the gradient elution protocol described in Table 1 was carefully optimized to achieve effective separation of metformin and curcumin, considering their distinct chemical properties. The chosen solvent ratios facilitate clear peak resolution with retention times of 1.2 and 6.0 minutes, minimizing co-elution and baseline drift. Methanol-water mixtures were selected for their compatibility with the analytes and consistency in performance. This protocol balances high separation efficiency with practical runtime, making it suitable for routine quality control applications. The mobile phase comprised two solvents: Solvent A (80:20 water: methanol) and Solvent B (90:10 methanol: water).

A maximum pressure of 400 bar was maintained, with the flow rate at 1.0 milliliters per minute. A wavelength of 254 nm was chosen as the detection wavelength. The retention durations for metformin and curcumin were around 1.2 minutes and 6.0 minutes, respectively, which guaranteed that there was sufficient peak separation in Figure 1.

Preparation of Standard Solutions

Methanol was used as the solvent in the preparation of stock solutions of metformin (100 µg/mL) and curcumin (100 µg/mL). By diluting stock solutions with the mobile phase, standard working solutions were generated. The resultant concentration range for metformin was between 10 and 100 µg/mL, while the concentration range for curcumin was between 1 and 50 µg/mL.

Table 1. The gradient elution protocol

Time (min)	Mobile phase
0:00-2:00	100% A
2:00-3:00	Transition from 100% A to 100% B
3:00-8:00	100% B
8:00-9:00	Transition from 100% B back to 100% A
9:00-20:00	100% A

Table 2. Regression equations and correlation coefficients (R_2) for metformin and curcumin

Compound	Concentration (µg/mL)	Regression equation	R_2
Metformin	10-100	$y = 2.54x + 4.74$	0.9994
Curcumin	10-50	$y = 3.57x + 0.918$	0.9993

Statistical Analysis

Data were analyzed using appropriate statistical methods and presented as means ± standard deviation (SD) to ensure clarity and reliability. The validation of the method was conducted in compliance with the International Conference on Harmonization Q2 (R1) guidelines.¹⁰ The evaluated parameters included linearity, precision, accuracy, limit of detection (LOD), and limit of quantification (LOQ).

Linearity

Linearity was evaluated using distinct concentrations for each analyte. As seen in Figure 2, calibration curves were constructed to illustrate the relationship between peak area and concentration, with regression analysis providing the correlation coefficient R_2 (Table 2). The method exhibited linearity across the evaluated concentration ranges, showing high correlation coefficients.

Precision

Precision was evaluated by analyzing three concentrations of metformin and curcumin on one day (intra-day) and over three consecutive days

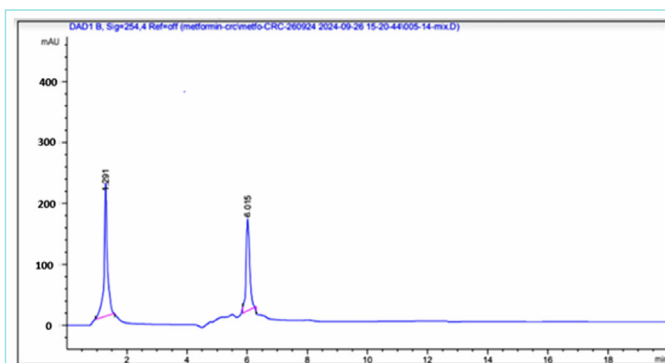


Figure 1. Chromatogram obtained from the RP-HPLC method showing the separation of metformin and curcumin.

RP-HPLC: Reverse-phase high-performance liquid chromatography.

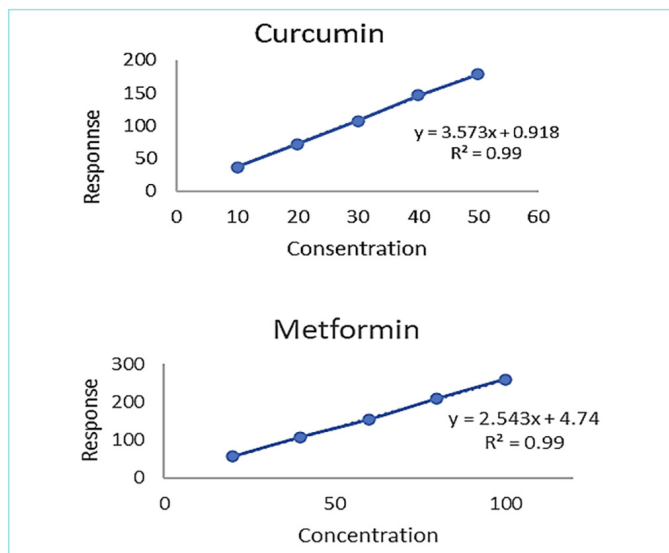


Figure 2. Calibration curves for metformin and curcumin demonstrate the linear relationship between concentration and peak area.

(inter-day). The relative standard deviation (%RSD) values were below 2%, indicating high reproducibility, as detailed in Table 3.

Accuracy

The accuracy of the method was evaluated through recovery studies, where known amounts of metformin and curcumin were added to pre-analyzed samples. The recoveries at three levels (50%, 100%, and 150%) were determined, demonstrating the method's accuracy, and the results are shown in Table 4.

LOD and LOQ

Both the LOD and the LOQ were determined by using the slope of the calibration curve in conjunction with the SD of the response. The findings, which are presented in Table 5, indicate that the method is sensitive enough to detect even minute quantities of both drugs.

Robustness

The robustness of a chromatographic technique reflects its ability to withstand minor intentional variations in operating conditions while maintaining reliable performance. Adjustments to the column temperature (± 5 °C) were made, and percent %RSD values along with system suitability parameters were evaluated. The method demonstrated robustness, with %RSD values (<1) and system suitability parameters remaining stable and within acceptable limits.

RESULTS

The enhanced RP-HPLC method achieved clear separation of metformin and curcumin with excellent linearity, precision, accuracy, and sensitivity. LOD and LOQ values were low, indicating the method's capacity to detect trace levels of both compounds-ideal for pharmacokinetic

Table 3. Precision results for intraday and interday analyses of metformin and curcumin

Compound	Intraday precision (peak area \pm SD) (%RSD)	Inter-day precision (peak area \pm SD) (%RSD)
Metformin	1000 \pm 10.0 (1.00)	1005 \pm 15.0 (1.49)
Curcumin	500 \pm 5.0 (1.00)	505 \pm 7.5 (1.49)

SD: Standard deviation, RSD: Relative standard deviation.

Table 4. Recovery study results for metformin and curcumin

Compound	%	Added amount (μ g/mL)	Recovered amount (μ g/mL)	(%) recovery	(%) average
Metformin	50	50	50 \pm 1.25	100 \pm 0.003	100.02
Metformin	100	100	100 \pm 2.00	100 \pm 0.004	100.10
Metformin	150	150	150 \pm 3.00	100 \pm 0.005	99.98
Curcumin	5	5	5 \pm 0.10	100 \pm 0.002	100.15
Curcumin	10	10	10 \pm 0.20	100 \pm 0.003	99.90
Curcumin	15	15	15 \pm 0.30	100 \pm 0.004	99.87

Table 5. Limits of detection and limits of quantification for metformin and curcumin

Compound	LOD (μ g/mL)	LOQ (μ g/mL)
Metformin	6.85	20.76
Curcumin	3.49	10.56

LOD: Limits of detection, LOQ: Limits of quantification.

applications.¹¹ Recovery ranged from 98.5%-101.2% for metformin and 97.8%-100.9% for curcumin, confirming the method's accuracy. %RSD values were consistently near 2%, supporting its precision.

DISCUSSION

The developed method is suitable for routine pharmaceutical analysis. Its high sensitivity, reliable recovery, and low %RSD make it a strong alternative to more advanced techniques like LC-MS. Furthermore, its compatibility with standard HPLC systems makes it a cost-effective and accessible option for most quality control laboratories.¹²

Study Limitations

One limitation of this study is the inherent instability of curcumin, which is sensitive to light and can degrade over time.¹³ To mitigate this, we used amber-colored volumetric flasks to protect the compound during preparation and analysis. Despite these precautions, curcumin's lack of stability could still impact its quantification under certain conditions. Future studies should consider additional stability assessments to ensure consistent results.

CONCLUSION

This study presents an HPLC method for simultaneous measurement of curcumin and metformin, demonstrating exceptional linearity, accuracy, precision, and sensitivity. Future research may explore its use with biological specimens and clinical trials. The established RP-HPLC method for the simultaneous measurement of metformin and curcumin demonstrates notable improvements over previous techniques. The sensitivity has been enhanced, showing LODs of 6.85 μ g/mL for metformin and 3.49 μ g/mL for curcumin, along with LOQs of 20.76 μ g/mL for metformin and 10.56 μ g/mL for curcumin, aligning with previously documented values. Moreover, the method demonstrates outstanding precision (RSD% <2) and accuracy (recovery rates close to 100%), thereby fostering confidence for regular use. The use of a standard C18 column along with short retention times enhances efficiency, making it an economical option for quality control and investigative purposes.

MAIN POINTS

- A validated reverse-phase high-performance liquid chromatography method quantifies metformin and curcumin with high precision.
- Low limit of detection and limit of quantification ensure suitability for trace-level analysis.
- Cost-effective and ideal for quality control of combined drugs.

ETHICS

Ethics Committee Approval: Not applicable.

Informed Consent: Not applicable.

Footnotes

Authorship Contributions

Concept: B.N., Design: B.N., Data Collection and/or Processing: B.N., E.V.B., Analysis and/or Interpretation: B.N., E.V.B., Literature Search: B.N., E.V.B., L.B.P., Writing: B.N.

DISCLOSURES

Conflict of Interest: No conflict of interest was declared by the authors.

Financial Disclosure: The authors declared that this study had received no financial support.

REFERENCES

1. Bailey CJ, Turner RC. Metformin. *N Engl J Med*. 1996; 334(9): 574-9.
2. Rena G, Hardie DG, Pearson ER. The mechanisms of action of metformin. *Diabetologia*. 2017; 60(9): 1577-85.
3. Aggarwal BB, Harikumar KB. Potential therapeutic effects of curcumin. *Biochem Pharmacol*. 2009; 76(11): 1590-611.
4. Meng B, Li J, Cao H. Antioxidant activities of curcumin. *Curr Pharm Des*. 2013; 19(11): 2101-13.
5. Jin L, Xie T, Ye Y. Combination of curcumin and metformin. *J Pharm Pharmacol*. 2018; 70(2): 236-44.
6. Panahi Y, et al. Curcumin improves insulin resistance. *Phytother Res*. 2014; 28(3): 376-9.
7. Sharma RA, Steward WP, Gescher AJ. Pharmacokinetics and pharmacodynamics of curcumin. *Mol Cancer Ther*. 2007; 6(3): 729-40.
8. Snyder LR, Kirkland JJ. *Modern liquid chromatography*. Wiley; 2010.
9. McCalley DV. RP-HPLC analysis of drugs. *J Chromatogr A*. 2013; 1284: 57-61.
10. ICH Q2 (R1): Validation of Analytical Procedures. 2005.
11. Bisht S, et al. Nanoparticle-encapsulated curcumin. *J Nanobiotechnology*. 2007; 5: 3.
12. Goel A, et al. Curcumin as "Curecumin": From kitchen to clinic. *Cancer Lett*. 2008; 267(1): 133-64.
13. Priyadarsini KI. The chemistry of curcumin: from extraction to therapeutic agent. *Molecules*. 2014; 19(12): 20091-112.

Evaluation of Taurodont and Pyramidal Mandibular Molars Prevalence in a Group of Turkish Cypriot Population by Cone Beam Computed Tomography

✉ Dilan Kırmızı¹, ✉ Umut Aksoy¹, ✉ Seçil Aksoy², ✉ Nildem İnönü¹, ✉ Kaan Orhan³

¹Department of Endodontics, Near East University Faculty of Dentistry, Nicosia, North Cyprus

²Department of Dentomaxillofacial Radiology, Near East University Faculty of Dentistry, Nicosia, North Cyprus

³Department of Dentomaxillofacial Radiology, Ankara University Faculty of Dentistry, Ankara, Türkiye

Abstract

BACKGROUND/AIMS: The purpose of this retrospective study was to determine the prevalence of taurodont and pyramidal mandibular molars among a Turkish Cypriot population.

MATERIALS AND METHODS: This study involved a retrospective evaluation of cone beam computed tomography (CBCT) scans from 285 adult patients (148 males and 137 females, aged, 18-80). A total of 902 molar teeth (including third molars) were evaluated using CBCT images. The recorded data were statistically analyzed to compare the incidence of taurodont and pyramidal teeth between genders and tooth types.

RESULTS: Fifty-seven patients were found to have at least one taurodont tooth (32 males and 25 females), with an incidence of 20%. Among the 902 teeth, 100 (11.1%) mandibular molar teeth exhibited taurodontism, with 51 (11.4%) on the left side and 49 (10.7%) on the right side. Taurodontism occurred in 51 of the 429 teeth from female patients (11.8%) and 49 of the 473 teeth from male patients (10.3%), without statistically significant differences ($p>0.05$). Third molars were the most commonly affected teeth (23.1%), followed by second molars (12.3%) and first molars (3.36%). A statistically significant difference was found in tooth type ($p<0.05$). Pyramidal teeth were detected in 7 patients, representing a prevalence of 2.5%. Of these, 4 patients (2.9%) were females and 3 patients (2%) were males.

CONCLUSION: Taurodont molars exhibited a high prevalence among Turkish Cypriots, particularly in the second and third molars of mandibular teeth. Dental practitioners should be aware of this dental anomaly.

Keywords: Taurodontism, CBCT, pyramidal molar tooth

INTRODUCTION

Dental anomalies may affect both crown and root structures. Crowns often exhibit deviations in shape, size, color, or number, and teeth may appear in abnormal positions or display irregular eruption patterns.¹ Common root abnormalities include taurodontism, pyramidal shapes, dilaceration, short roots, and root fusion.^{2,3} Extensive research has demonstrated that various dental anomalies often manifest concurrently

in different combinations.⁴ Taurodontism was first described by Keith⁵ in 1913 and refers to the molar teeth with an extended pulp chamber below the cemento-enamel junction (CEJ) and apical displacement of the root bifurcation or trifurcation. Taurodont teeth, which exhibit a rectangular shape, are subclassified by Shaw⁶ into mild, moderate, or severe [hypotaurodontism (HT), mesotaurodontism (MT), and hypertaurodontism (HYT), respectively] based on relative degree of pulp

To cite this article: Kırmızı D, Aksoy U, Aksoy S, İnönü N, Orhan K. Evaluation of taurodont and pyramidal mandibular molars prevalence in a group of Turkish Cypriot population by cone beam computed tomography. Cyprus J Med Sci. 2025;10(Suppl 1):8-11

ORCID IDs of the authors: D.K. 0000-0003-0483-1736; U.A. 0000-0001-6768-508X; S.A. 0000-0002-6400-4911; N.İ. 0009-0006-4253-2939; K.O. 0000-0001-6768-0176.



Corresponding author: Nildem İnönü
E-mail: nildem.inonu@neu.edu.tr
ORCID ID: orcid.org/0009-0006-4253-2939

Received: 05.11.2024
Accepted: 17.12.2024
Publication Date: 04.06.2025



Copyright© 2025 The Author. Published by Galenos Publishing House on behalf of Cyprus Turkish Medical Association.
This is an open access article under the Creative Commons Attribution-NonCommercial 4.0 International (CC BY-NC 4.0) License.

chamber displacement. Teeth with normally sized pulp chambers are referred to as cynodonts (CD).⁶ The root configurations of these molar teeth may exhibit separate roots, or partially or completely fused roots. Completely fused roots with a single, wide root canal are attributed to deep taurodontism and pyramidal molars (PM).³ Theories regarding the origins of taurodontism vary widely, but it is often attributed to early invagination of the epithelial root sheath, which is critical for the development of dental structures.⁷ Taurodontism occurs more frequently in permanent teeth, and may be observed in individual teeth or bilaterally. Studies in the literature indicate a higher prevalence of taurodontism among some specific ethnic groups, including the Inuit of Alaska, Aborigines in Australia, and the indigenous populations of Central America.^{8,9}

The endodontic management of taurodont teeth presents some challenges in terms of canal identification, cleaning, shaping, and obturation, and requires an approach that differs from that used for typical teeth. Radiographic imaging is required to diagnose these anomalies, as the clinical appearance of taurodont or pyramidal teeth cannot be distinguished from that of other teeth.¹⁰ In 1978, Shifman and Chanannel¹¹ described an index to determine the severity of taurodontism on radiographic images. Previous studies on the prevalence of taurodontism and PM have mostly relied on two-dimensional (2D) imaging such as panoramic or bitewing radiographs.^{4,10,12} However, cone beam computed tomography (CBCT) is a reliable three-dimensional (3D) imaging modality for determining the prevalence of taurodontism and PM, their diagnosis and classification, making accurate measurements, and managing the treatment processes. A comprehensive literature review has revealed only a few studies using CBCT to examine the prevalence of taurodontism,^{13,14} and no study was found for the Turkish Cypriot population. Hence, the present study was conducted to identify taurodont and pyramidal mandibular molars in a group of the Turkish Cypriot population using CBCT.

MATERIALS AND METHODS

The study protocol was approved by the Near East University, Scientific Research Ethics Committee (approval number: YDU/2019/70-851, date: 27.06.2019). This study involves the retrospective evaluation of CBCT scans obtained from 285 adult (137 female and 148 male) patients aged 18-80 years from 2020 to 2024. CBCT images were obtained for various purposes such as implant planning, impacted tooth assessment, maxillary sinus evaluation, and cysts. The CBCT images were obtained using the Sirona Orthophos XG 3D system with the following parameters: a field of view of 80x80 mm or 110x100 mm, 85 kV, 6 mA, 14.4 seconds of scanning time, and 0.027 mm³ voxel size.

CBCT images, of healthy mandibular molar teeth without endodontic treatment, filling restoration, fixed prosthodontic treatment, open apex, periapical lesion, and root resorption were included in the study. After recording the demographic information of the patients, cross-sectional images were assessed independently by two observers (N.I. and D.K.). The assessment of taurodont mandibular molars was conducted using the Taurodont index (TI), as modified by Shifman and Chanannel.¹¹ In this method, the vertical height of the pulp chamber, defined as the distance from the roof's lowest point to the floor's highest point, is divided by the total distance from the roof's lowest point to the apex of the longest root. This ratio was then multiplied by 100. A tooth was classified as taurodont if the calculated value reached 20 or more, and the distance between the CEJ and the highest point of the pulp chamber

floor measured greater than 2.5 mm. Each taurodont tooth was categorized by severity: hypotaurodont (TI between 20% and 29.9%), mesotaurodont (TI between 30% and 39.9%), and hypertaurodont (TI between 40% and 75%). Mandibular molars with a single, wide canal and completely fused roots were classified as pyramidal mandibular molars.

Statistical Analysis

The gender distribution, anatomical location, and severity levels of taurodont molars, along with their association with pyramidal teeth, were statistically analyzed. All data were analyzed using IBM SPSS Statistics (version 22). Descriptive analyses were performed for all variables. The differences in the frequency of taurodontism anomaly between groups were assessed using the chi-square (χ^2) test for categorical data. A p-value below 0.05 was regarded as indicative of statistical significance.

RESULTS

A total of 902 teeth from 285 patients were evaluated, comprising 148 females and 137 males. The average age of the participants was 36 years. Taurodontism was identified in 57 out of the 285 patients (20%). At least one taurodont tooth was observed in 32 males (21.62%) and 25 females (18.25%). Gender differences in the number and percentages of CD and taurodont teeth subgroups are summarized in Table 1. HT was the predominant type of taurodontism observed, followed by MT; no cases of HYT were detected in either gender. No statistically significant differences were noted between genders ($p>0.05$); however, taurodontism was present in 51 teeth from female participants (11.8%) and 49 teeth from male participants (10.3%) as shown in Figure 1. Taurodontism occurred most frequently in third molars (23.12%), followed by second molars (12.30%) and first molars (3.86%), revealing statistically significant differences ($p<0.05$). Of the 902 mandibular molars assessed, 100 exhibited taurodontism, with 51 (11.4%) on the left side and 49 (10.7%) on the right side, as detailed in Table 2. Furthermore, 86% of the taurodont teeth were classified as HT, and 14% as MT, according to the data presented in Figure 2. Only 7 patients showed evidence of PM, yielding a prevalence rate of 2.5%. Of these, four were female (2.9%) and three were male (2%). Concerning tooth type, five of the identified pyramidal teeth were second molars, and only two were third molars. Notably, none of the teeth evaluated exhibited pyramidal characteristics in the first molars (Table 2).

DISCUSSION

"Taurodontism" combines the Greek terms "tauros," meaning "bull," and "dontia," meaning "teeth," which implies "bull-like teeth". This condition describes teeth characterized by a vertically enlarged pulp chamber and altered root canal structures.¹⁵ Although taurodontism typically presents with a clinically normal appearance and does not

Table 1. Gender differences in the number and percentages of cynodont and taurodont teeth subgroups

	CD (n)	HT (n)	MT (n)	%	PM (n)	%
Male	421	42	7	10.3	3	2.00%
Female	374	44	7	11.8	4	2.90%
Total	795	86	14	11.1	7	2.50%
p=0.533						
CD: Cynodont, HT: Hypotaurodont, MT: Mesotaurodont, PM: Pyramidal molars.						

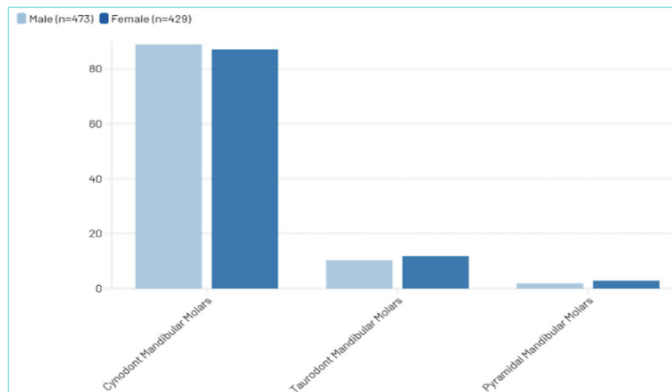


Figure 1. Distribution percentages of cynodont, taurodont and pyramidal mandibular molars according to gender.

Table 2. Distribution of taurodontism and pyramidal mandibular molar teeth according to their localization

	Total (n)	Taurodontism				Pyramidal	
		CD (n)	HT (n)	MT (n)	%	n	%
Right	457	406	39	10	10.70	2	0.40
Left	445	389	47	4	11.40	5	1.10
		CD (n)	HT (n)	MT (n)			
1. Molar	336	323	13	0	3.86	0	0.00
2. Molar	406	351	41	9	12.30	5	1.20
3. Molar	160	121	32	5	23.12	2	1.30

p=0.805, p>0.05

CD: Cynodont, HT: Hypotaurodont, MT: Mesotaurodont.

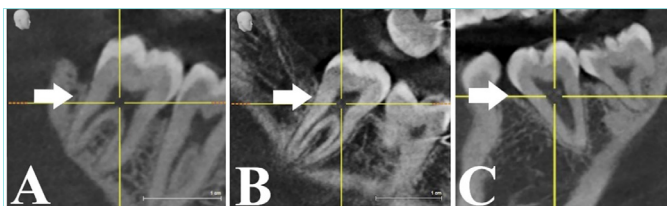


Figure 2. Representative sagittal CBCT sections demonstrating the mandibular molar (white arrow) exhibiting hypotaurodontism (A), mesotaurodontism (B), and pyramidal morphology (C), as observed in the present study.

CBCT: Cone beam computed tomography.

generally affect aesthetics, its presence may complicate endodontic treatment procedures.¹³

Moreover, the occurrence of taurodontism differs across ethnic populations, with these variations potentially linked to disparities in diagnostic methods and criteria.¹⁶ Research on taurodontism prevalence has reported rates ranging from 0.26% to 48%. Sarr et al.¹⁷ observed the highest prevalence in an adult Senegalese population, with taurodontism identified in 48% of individuals. Furthermore, 48.6% of the patients exhibited both taurodontism and pyramidal teeth.¹⁷ MacDonald-Jankowski and Li⁹ reported the second highest prevalence at 46.4% among the young adult Chinese population. Earlier studies in the Turkish population documented prevalence rates varying from 0.26% to 22.8%.¹⁸⁻²⁰ In the present study, taurodontism prevalence was

20%, which is quite similar to the incidence reported by Topçuoğlu et al.²⁰ Previous studies within the Turkish population predominantly employed panoramic radiography.¹⁸⁻²⁰ In contrast, the present study utilized CBCT for assessment. Due to its 2D imaging and inherent magnification issues, a 3D evaluation method was preferred over panoramic radiography in the present study. Typically, earlier studies have included maxillary molars, premolars, and mandibular premolars, with some indicating that taurodontism is significantly more commonly observed in the maxillary molars. Consequently, a plan is in place to include premolar and maxillary molar teeth in future research, which is anticipated to reveal a higher prevalence of taurodontism in our population.

Study Limitations

The limitations of this study are as follows: Unlike previous studies that included maxillary molars, premolars, and mandibular premolars, the current evaluation is restricted solely to permanent mandibular molars. Additionally, this study was conducted at a single center in North Cyprus and did not represent the whole population.

CONCLUSION

In conclusion, the North Cyprus population has a 20% incidence of taurodontic mandibular molars and 2.5% incidence of pyramidal mandibular molars, indicating the need for a meticulous clinical approach in their endodontic treatment. CBCT is more effective for precise diagnosis, classification, and treatment planning. This study establishes a foundation for improving endodontic processes and patient care in North Cyprus.

MAIN POINTS

- This study identifies a 20% prevalence of taurodontism and a 2.5% prevalence of pyramidal molars (PM) in the Turkish Cypriot population.
- Hypotaurodontism is the predominant subtype observed, with no cases of hypertaurodontism reported.
- Cone beam computed tomography has been demonstrated to be superior to conventional 2D imaging techniques for the accurate diagnosis and classification of taurodont and PM.
- The findings emphasize the necessity for individualized endodontic treatment protocols and the importance of precise diagnostic imaging in clinical practice.

ETHICS

Ethics Committee Approval: The study protocol was approved by the Near East University, Scientific Research Ethics Committee (approval number: YDU/2019/70-851, date: 27.06.2019).

Informed Consent: Retrospective study.

FOOTNOTES

Authorship Contributions

Concept: U.A., S.A., K.O., Design: U.A., S.A., Data Collection and/or Processing: D.K., N.İ., Analysis and/or Interpretation: U.A., S.A., Literature Search: D.K., N.İ., Writing: D.K., S.A.

DISCLOSURES

Conflict of Interest: No conflict of interest was declared by the authors.

Financial Disclosure: The authors declared that this study had received no financial support.

REFERENCES

- Klein OD, Oberoi S, Huysseune A, Hovorakova M, Peterka M, Peterkova R. Developmental disorders of the dentition: an update. *Am J Med Genet C Semin Med Genet.* 2013; 163(4): 318-32.
- Lind V. Short root anomaly. *Scand J Dent Res.* 1972; 80(2): 85-93.
- Ackerman JL, Ackerman AL, Ackerman AB. Taurodont, pyramidal, and fused molar roots associated with other anomalies in a kindred. *Am J Phys Anthropol.* 1973; 38(3): 681-94.
- Klein U, Paimagham B, Blumhagen R, Kroehl M, Sain J. Pyramidal and taurodont molars and their association with other tooth anomalies. *Pediatr Dent.* 2017; 39(1): 46-52.
- Keith A. Problems relating to the teeth of the earlier form of prehistoric man. *Proc R Soc Med.* 1913; 6: 103-24.
- Shaw JCM. Taurodont teeth in South African Races. *J Anat.* 1928 ;62: 476-98.
- Goldstein E, Medina JL. Mohr syndrome or oral facial-digital II: report of two cases. *J Am Dent Assoc.* 1974; 89: 377-82.
- Nunn JH, Carter NE, Gillgrass TJ, Hobson RS, Jepson NJ, Meechan JG, et al. The interdisciplinary management of hypodontia: background and role of paediatric dentistry. *Br Dent J.* 2003; 194(5): 245-51.
- MacDonald-Jankowski DS, Li TT. Taurodontism in a young adult Chinese population. *Dentomaxillofac Radiol.* 1993; 22: 140-4.
- Parolia A, Khosla M, Kundabala M. Endodontic management of hypo-, meso-and hypertaurodontism. *Aust Endod J.* 2012; 38(1): 36-41.
- Shifman A, Chanannel I. Prevalence of taurodontism found in radiographic dental examination of 1200 young adult Israeli patients. *Community Dent Oral Epidemiol.* 1978; 6(4): 200-3.
- Bürklein S, Breuer D, Schäfer E. Prevalence of taurodont and pyramidal molars in a German population. *J Endod.* 2011; 37(2): 158-62.
- Jabali AH, Chourasia HR, Wasli AS, Alkhayrat AM, Mahnashi HM, Kamly Mj, et al. Taurodontism in maxillary and mandibular molars using cone beam computed tomography in a dental center in Saudi Arabia. *Ann Saudi Med.* 2021; 41(4): 232-7.
- Li Y, Qian F, Wang D, Wang Y, Wang W, Tian Y. Prevalence of taurodontism in individuals in Northwest China determined by cone-beam computed tomography images. *Heliyon.* 2023; 9(4): 15531.
- Haskova JE, Gill DS, Figueiredo JA, Tredwin, CJ, Naini FB. Taurodontism--a review. *Dent Update.* 2009; 36(4): 235-6, 239-40, 243.
- Manjunatha BS, Kovvuru SK. Taurodontism - a review on its etiology, prevalence and clinical considerations. *J Clin Exp Dent.* 2010; 2(4): 187-90.
- Sarr M, Toure B, Kane AW, Fall F, Wone MM. Taurodontism and the pyramidal tooth at the level of the molar. Prevalence in the Senegalese population 15 to 19 years of age. *Odontostomatol Trop.* 2000; 23(89): 31-4.
- Çolak H, Tan E, Bayraktar Y, Hamidi MM, Çolak T. Taurodontism in a central anatolian population. *Dental Res J.* 2013; 10(29): 260-3.
- Bilge NH, Yeşiltepe S, Törenek Ağırman K, Çağlayan F, Bilge OM. Investigation of prevalence of dental anomalies by using digital panoramic radiographs. *Folia Morphol (Warsz).* 2018; 77(2): 323-8.
- Topçuoğlu HS, Karatas E, Arslan H, Köseoglu M, Evcil MS. The frequency of taurodontism in the Turkish population. *J Clin Exp Dent.* 2011; 3(4): 284-8.

Influence of Prefabricated Auxiliary Device Design and Intraoral Scanner Type on the 3D Trueness of Intraoral Scans

Özay Önöral, Selin Çakır, Sevcan Kurtulmus-Yılmaz

Department of Prosthetic Dentistry, Near East University Faculty of Dentistry, Nicosia, North Cyprus

Abstract

BACKGROUND/AIMS: It was aimed to compare the trueness of digital impressions acquired using prefabricated auxiliary devices (PADs) in 2 different forms, in combination with 2 intraoral scanners (IOSs).

MATERIALS AND METHODS: A master cast of a partially edentulous maxilla with two multi-unit analogues was initially scanned in a laboratory setting, with the resulting data saved as a reference standard tessellation language (STL) file. Subsequently, experimental STL files were generated, by using two different IOSs, the Omnicam and iTero, following three distinct scanning routes: without a PAD, with an indented PAD, and with a plain PAD. Each experimental STL file was superimposed onto the reference STL file; the scan bodies were transformed into virtual hollow cylinders, and the Cartesian coordinates of the centre lines passing through these cylinders were recorded, enabling the calculation of angular deviation (AD) and linear deviations (LD). Statistical analysis was performed using two-way analysis of variance with Tukey's post-hoc test ($\alpha=0.05$).

RESULTS: PAD design, IOS type, and their interaction terms significantly influenced the deviation values ($p<0.05$), except for the PAD design effect on AD values in location #13 and the IOS type effect on LD values in location #13 ($p>0.05$). In both AD and LD data, the Omnicam + no-PAD and iTero + indented PAD, groups exhibited the highest and the lowest values across all locations, respectively. The LD values in all locations and the AD values in location #13 were below the acceptability thresholds ($<100 \mu\text{m}$ and $<0.5^\circ$). However, the AD values of Omnicam + no-PAD, iTero + no-PAD, and Omnicam + plain-PAD groups were clinically unacceptable ($>0.5^\circ$) in location #17.

CONCLUSION: The iTero + indented PAD group outperformed the other groups in terms of trueness.

Keywords: Intraoral-scan, prefabricated-auxiliary-device, scan-aid, superimposition, trueness

INTRODUCTION

Intraoral scanners (IOSs) have gained prominence in dental practice as an effective and practical alternative to traditional impression-making.¹ IOSs offer patient comfort and streamline workflow by eliminating stages such as tray selection, dispensing, and setting of impression materials, and the production of stone casts. Additionally, IOSs offer

accessible storage on electronic databases and significantly improve communication among dental professionals, patients, and technicians, as captured digital images can be used for visual explanations.^{2,3} However, IOSs capture consecutive 2D images via a limited-range sensor, which are subsequently combined into a single 3D image by running the iterative closest point algorithm.² This process, known as image stitching, is supported by solid anatomical landmarks available

To cite this article: Önöral Ö, Çakır S, Kurtulmus-Yılmaz S. Influence of prefabricated auxiliary device design and intraoral scanner type on the 3D trueness of intraoral scans. Cyprus J Med Sci. 2025;10(Suppl 1):12-15

ORCID IDs of the authors: Ö.Ö. 0000-0002-5264-9376; S.Ç. 0009-0004-1893-7093; S.K.Y. 0000-0001-8792-1977.



Corresponding author: Selin Çakır
E-mail: selincakir2016@gmail.com
ORCID ID: orcid.org/0009-0004-1893-7093

Received: 31.10.2024
Accepted: 25.12.2024
Publication Date: 04.06.2025



Copyright© 2025 The Author. Published by Galenos Publishing House on behalf of Cyprus Turkish Medical Association.
This is an open access article under the Creative Commons AttributionNonCommercial 4.0 International (CC BY-NC 4.0) License.

along the scan path.^{1,2} In instances of the loss of several contiguous teeth, image stitching presents challenges due to the extended distance of the edentulous region between scan bodies.^{3,4} The lack of anatomical landmarks can lead to cumulative errors during the stitching process, resulting in distortion. Therefore, previous studies recommend using IOSs as an alternative to conventional techniques for single-unit and short-span fixed partial restorations, where anatomical references are more readily available.⁵⁻⁸ Without anatomical landmarks, IOSs may inaccurately stitch images or misunderstand scan segments as superfluous data.^{1,9-12} To address this drawback, artificial landmarks must be created to maintain continuity between scan bodies, allowing for accurate tracking of the scanning route.¹³⁻¹⁵ Using fiducial markers, applying pressure-indicating paste, splinting scan bodies with different materials, utilising scan bodies with flags, and positioning prefabricated auxiliary devices (PADs) on the scan bodies are the proposed approaches to installing artificial landmarks.¹⁶⁻²¹ However, data supporting the effectiveness of these approaches are scarce. Therefore, this study aimed to compare the trueness, (refers to the closeness of the experimental object to the reference object) of digital implant impressions acquired by using 2 different PADs in combination with 2 different IOSs. The null hypothesis posited that the utilization of a PAD would not affect trueness, that there would be no disparity in trueness among different PADs, and that there would be no disparity in trueness among IOSs.

MATERIALS AND METHODS

A partially edentulous maxillary cast was created by pouring a self-curing acrylic resin (Meliodent Rapid Repair Denture Acrylic; Kulzer GmbH) into a dentulous silicone mould (AG-3 G Silicone Index; Frasco). Two multiunit analogues (T0 32202; NucleOSS) were then positioned within the cast, designating it the master cast. To enable scanning, scan bodies (T0 32033; NucleOSS) were fastened to the multiunit analogues, and the cast was scanned using a benchtop laboratory scanner (inEOS X5; Dentsply Sirona). The resulting data were saved in standard tessellation language format, establishing a reference dataset for further comparison. Experimental scan datasets were obtained with 2 different IOS devices (CEREC Omnicam and iTero Element 5D Plus) across 3 separate routes: 1) with no PAD, 2) with indented PAD, and 3) with plain PAD (Figure 1). Using a software tool (G*power, v.3.1.9.7, Heinrich-Heine-University), the minimum required sample size was calculated to be 18 with 85% power, an effect size of 0.40, and a significance level of 0.05. Indented and plain PADs were first virtually designed, by using a software program (SolidWorks; Dassault Systèmes Corp.) and then 3D printed with the aid of a fused deposition modelling device (Prusa i3 MK3S; Prusa Research AS, Czech Republic) with polylactic acid plus filament. The print nozzle temperature was set at 210 °C, and the print bed temperature was set at 60 °C. Eighteen consecutive scans were performed for each group by an experienced calibrated operator. All datasets were transferred into a metrology software application (Geomagic Control; 3D Systems). Each experimental scan dataset was superimposed over the reference scan dataset, and best-fit alignment was subsequently applied. For the evaluation of angular deviation (AD) and linear distortion (LD), the feature creation tab was utilised to generate the best-fit plane (plane 1) on the occlusal surface of the scan body. An offset plane (plane 2) was then created 10 mm away from plane 1, corresponding to the height of the scan body. Hollow virtual cylinders were designed along the line passing through the centres of both planes, matching the scan body's diameter. The Cartesian coordinates of these centre lines were recorded. AD and LD were calculated as described in a previous study.²

Statistical Analysis

Data were processed in a software program (SPSS Statistics 25.0; SPSS Inc.). The assumption of normal distribution was verified by using the Shapiro-Wilk test. Statistical analysis was performed by using two-way analysis of variance (ANOVA) with Tukey's post-hoc test ($\alpha=0.05$).

RESULTS

The mean AD and LD values \pm standard deviations with pairwise comparisons are presented in Table 1. The results of 2-way ANOVA proved that the PAD design, IOS type, and their interaction terms significantly influenced the deviation values ($p<0.05$), except for the PAD design effect on AD values in location #13 and the IOS type effect on LD values in location #13 ($p>0.05$). In both AD and LD data, the Omnicam + no-PAD and iTero + indented PAD groups exhibited the highest and the lowest values across all locations, respectively. The LD values in all locations and the AD values in location #13 were below the acceptability thresholds ($<100 \mu\text{m}$ for LD and $<0.5^\circ$ for AD). However, the AD values of Omnicam + no-PAD, iTero + no-PAD, and Omnicam + plain-PAD groups were clinically unacceptable ($>0.5^\circ$) in location #17.

DISCUSSION

In a scenario of a partially edentulous case, this study compared the trueness of digital impressions acquired by using PADs in 2 different forms, in combination with 2 IOSs, all null hypotheses were rejected because the PAD design, IOS type, and their interaction terms significantly influenced the AD and LD values. According to the results, Omnicam had higher AD and LD values in all locations. This is consistent with a previous study²² and can be attributed to several reasons. First, Omnicam gathers data via unpolarised white light through active triangulation technology.^{9,22} Omnicam may have encountered confusion while scanning the white PAD. Second, white substrates reflect light diffusely, diminishing the contrast between the substrate and the light emitted by the scanner. White surfaces tend to scatter light in multiple directions, as reflective materials do.⁸ This scattering phenomenon diminishes the quantity of structured light reflected to the scanner's sensors, complicating accurate surface mapping. Third, white might overwhelm

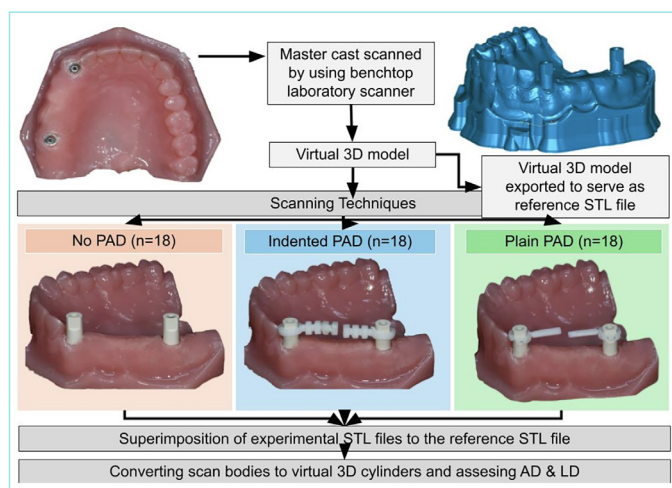


Figure 1. Workflow of study.

PAD: Prefabricated auxiliary device, STL: Standard tessellation language, AD: Angular distortion, LD: Linear distortion.

Table 1. Mean angular and linear deviation values \pm standard deviations with Tukey post-hoc comparisons

Routes	Angular deviation (degrees)			Linear deviation (μm)		
	Omnica	iTero	Total	Omnica	iTero	Total
Data for location #13						
Without PAD	0.21 \pm 0.04 ^{Aa}	0.15 \pm 0.03 ^{Bb}	0.18 \pm 0.04 ^a	4.40 \pm 0.52 ^{A,ab}	3.10 \pm 0.88 ^{Aa}	3.75 \pm 0.97 ^a
With indented PAD	0.19 \pm 0.03 ^{Aa}	0.12 \pm 0.05 ^{Ba}	0.16 \pm 0.05 ^a	4.10 \pm 1.20 ^{Aa}	3.20 \pm 1.32 ^{Aa}	3.65 \pm 1.31 ^a
With plain PAD	0.19 \pm 0.05 ^{Aa}	0.13 \pm 0.03 ^{B,ab}	0.16 \pm 0.05 ^a	5.60 \pm 2.12 ^{A,b}	5.90 \pm 3.18 ^{A,b}	5.75 \pm 2.63 ^b
Total	0.19 \pm 0.04 ^A	0.14 \pm 0.04 ^B	0.16 \pm 0.05	4.70 \pm 1.53 ^A	4.06 \pm 2.38 ^A	4.38 \pm 2.10
Data for location #17						
Without PAD	1.26 \pm 0.15 ^{A,c}	1.10 \pm 0.06 ^{B,c}	1.18 \pm 0.14 ^c	22.00 \pm 2.58 ^{A,c}	19.30 \pm 1.16 ^{B,c}	20.65 \pm 2.39 ^c
With indented PAD	0.43 \pm 0.04 ^{Aa}	0.34 \pm 0.03 ^{Ba}	0.39 \pm 0.06 ^a	7.60 \pm 0.52 ^{Aa}	6.10 \pm 0.74 ^{Ba}	6.85 \pm 0.99 ^a
With plain PAD	0.53 \pm 0.03 ^{A,b}	0.47 \pm 0.02 ^{B,b}	0.50 \pm 0.04 ^b	9.60 \pm 0.84 ^{A,b}	8.50 \pm 0.53 ^{A,b}	9.05 \pm 0.89 ^b
Total	0.74 \pm 0.39 ^A	0.64 \pm 0.34 ^B	0.69 \pm 0.36	13.06 \pm 6.66 ^A	11.30 \pm 5.90 ^B	12.18 \pm 6.30

PAD: Prefabricated auxiliary device. Different superscript lowercase letters indicate significant differences in the same column; different superscript uppercase letters indicate significant differences in the same row.

the sensor due to its high light reflectivity, resulting in overexposure and erroneous scanning data. Fourth, the compact scanner head of Omnica (in comparison to iTero) necessitates stitching together more 2D images or videos, which may compromise trueness. On the other hand, iTero functions with parallel confocal imaging technology. This technology lies in focusing light at a certain depth and detecting only the light that reflects at the same angle.^{9,22} This method reduces the influence of scattered light, which often occurs when surfaces are reflective or white.^{9,22,23} Following the results of this study, iTero better handles diffuse-reflecting materials, such as white substrates, since it filters out the light, which is not in focus, hence reducing noise and improving the clarity of the scan. Comprehensive and stable anatomical landmarks available on the scan path help to achieve accurate image stitching.^{1,2,8,13} Consistently, in the groups where scan bodies were supported with PADs, including artificial landmarks, lower AD and LD values were detected. Both PADs were prepared to extend deliberately toward the edentulous area, serving as an optical bridge with enhanced surface morphology to facilitate stitching. Strikingly, the indented PAD exhibited significantly better performance than the plain PAD. This is due to the irregular surface topography of the indented PAD, which presents more abundant artificial landmarks and will allow for better stitching.^{2,17,18} Moreover, when evaluating the locations, it was found that both AD and LD values increased from location #13 to location #17. This can be attributed to the accumulation of stitching errors.

Study Limitations

This study has several limitations. The PADs with a lateral extension were used. Different PAD designs may present different results. The responsiveness to the scanned substrate with defined optical features can vary widely for different IOSs due to their different data acquisition systems, although only two IOSs were preferred. Neither inter-implant distance nor angulation was included as a variable. Moreover, the presence of saliva and variations in ambient lighting conditions were not evaluated, which can all alter the results.

CONCLUSION

Based on the limitations of this study, the subsequent conclusions can be drawn: 1) the utilisation of PAD improved the trueness values; 2) IOS type affected the trueness, and iTero outperformed Omnica; 3) the group in which iTero was coupled with indentation PAD exhibited

superior trueness compared to the others.

MAIN POINTS

- Intraoral scanners (IOSs) have transformed dental practice by providing a more comfortable and efficient workflow, eliminating traditional impression-making stages, and improving communication among dental professionals, patients, and technicians.
- The study highlights the importance of creating artificial landmarks, such as using prefabricated auxiliary devices (PADs), to enhance the accuracy of digital impressions in the absence of natural anatomical landmarks.
- The study found that PAD design, IOS type, and their interaction significantly influenced the trueness of digital impressions, with the iTero scanner performing better overall. Indented PADs provided more accurate image stitching due to their irregular surface topography, which offered more abundant artificial landmarks, thereby reducing distortion.
- The findings seek to address the challenges of image stitching in extended edentulous regions and to improve the reliability of IOSs in dental practice.

ETHICS

Ethics Committee Approval: Not available.

Informed Consent: Not available.

Footnotes

Authorship Contributions

Concept: S.K.Y., Design: S.K.Y., Data Collection and/or Processing: S.Ç., Analysis and/or Interpretation: Ö.Ö., Literature Search: S.Ç., Writing: Ö.Ö., S.Ç.

DISCLOSURES

Conflict of Interest: No conflict of interest was declared by the authors.

Financial Disclosure: The authors declared that this study had received no financial support.

REFERENCES

- Waldecker M, Bömicke W, Awounvo SA, Rammelsberg P, Rues S. Influence of artificial landmarks on the accuracy of complete arch scans in the partially edentulous maxilla: an in vitro study. *J Prosthet Dent.* 2024; 132(4): 829-37.
- Eddin MB, Önoral Ö. Influence of splinting scan bodies or incorporating three-dimensionally printed scan aids on the trueness of complete arch digital scans. *J Prosthet Dent.* 2024; 132(4): 828.
- Park GH, Son K, Lee KB. Feasibility of using an intraoral scanner for a complete-arch digital scan. *J Prosthet Dent.* 2019; 121(5): 803-10.
- Waldecker M, Rues S, Behnisch R, Rammelsberg P, Bömicke W. Effect of scan-path length on the scanning accuracy of completely dentate and partially edentulous maxillae. *J Prosthet Dent.* 2024; 131(1): 146-54.
- Sanda M, Miyoshi K, Baba K. Trueness and precision of digital implant impressions by intraoral scanners: a literature review. *Int J Implant Dent.* 2021; 7(1): 97.
- Knechtle N, Wiedemeier D, Mehl A, Ender A. Accuracy of digital complete-arch, multi-implant scans made in the edentulous jaw with gingival movement simulation: an in vitro study. *J Prosthet Dent.* 2022; 128(3): 468-78.
- Rutkunas V, Gedrimiene A, Adaskevicius R, Al-Haj Husain N, Özcan M. Comparison of the clinical accuracy of digital and conventional dental implant impressions. *Eur J Prosthodont Restor Dent.* 2020; 28(4): 173-81.
- Wu HK, Wang J, Chen G, Huang X, Deng F, Li Y. Effect of novel prefabricated auxiliary devices attaching to scan bodies on the accuracy of intraoral scanning of complete-arch with multiple implants: an in-vitro study. *J Dent.* 2023; 138: 104702.
- Mangano FG, Admakin O, Bonacina M, Lerner H, Rutkunas V, Mangano C. Trueness of 12 intraoral scanners in the full-arch implant impression: a comparative in vitro study. *BMC Oral Health.* 2020; 20: 1-21.
- Rutkunas V, Gedrimiene A, Akulauskas M, Fehmer V, Sailer I, Jegelevicius D. In vitro and in vivo accuracy of full-arch digital implant impressions. *Clin Oral Implants Res.* 2021; 32(12): 1444-54.
- Mangano FG, Hauschild U, Veronesi G, Imburgia M, Mangano C, Admakin O. Trueness and precision of 5 intraoral scanners in the impressions of single and multiple implants: a comparative in vitro study. *BMC Oral Health.* 2019; 19(1): 101.
- Wulfman C, Naveau A, Rignon-Bret C. Digital scanning for complete-arch implant-supported restorations: a systematic review. *J Prosthet Dent.* 2020; 124(2): 161-7.
- Kim JE, Amelya A, Shin Y, Shim JS. Accuracy of intraoral digital impressions using an artificial landmark. *J Prosthet Dent.* 2017; 117(6): 755-61.
- Rutkunas V, Gedrimienė A, Husain NA, Pletkus J, Barauskis D, Jegelevičius D, Özcan M. Effect of additional reference objects on accuracy of five intraoral scanners in partially and completely edentulous jaws: an in vitro study. *J Prosthet Dent.* 2023; 130(1): 111-8.
- Iturrate M, Eguiraun H, Solaberrieta E. Accuracy of digital impressions for implant-supported complete-arch prosthesis, using an auxiliary geometry part-An in vitro study. *Clin Oral Implants Res.* 2019; 30(12): 1250-8.
- Kernen F, Brändle D, Wagendorf O, Recca M, Mehrhof J, Vach K, et al. Enhancing intraoral scanner accuracy using scan aid for multiple implants in the edentulous arch: an in vivo study. *Clin Oral Implants Res.* 2023; 34(8): 793-801.
- Kernen FR, Recca M, Vach K, Nahles S, Nelson K, Flügge TV. In vitro scanning accuracy using different aids for multiple implants in the edentulous arch. *Clin Oral Implants Res.* 2022; 33(10): 1010-20.
- Pan Y, Tsoi JK, Lam WY, Zhao K, Pow EH. Improving intraoral implant scanning with a novel auxiliary device: an in-vitro study. *Clin Oral Implants Res.* 2021; 32(12): 1466-73.
- Liu M, Fu XJ, Lai HC, Shi JY, Liu BL. Accuracy of traditional open-tray impression, stereophotogrammetry, and intraoral scanning with prefabricated aids for implant-supported complete arch prostheses with different implant distributions: An in vitro study. *J Prosthet Dent.* 2024; 132(3): 602.
- Huang R, Liu Y, Huang B, Zhang C, Chen Z, Li Z. Improved scanning accuracy with newly designed scan bodies: An in vitro study comparing digital versus conventional impression techniques for complete-arch implant rehabilitation. *Clin Oral Implants Res.* 2020; 31(7): 625-33.
- Masu R, Tanaka S, Sanda M, Miyoshi K, Baba K. Effect of assistive devices on the precision of digital impressions for implants placed in edentulous maxilla: an in vitro study. *Int J Implant Dent.* 2021; 7(1): 116.
- Farah RF, Alresheedi B, Alazmi S, Al-Haj Ali SN. Evaluating the impact of scan body angulation and geometric attachments on the accuracy of complete-arch digital implant impressions: a comparison of two intraoral scanners. *J Prosthodont.* 2025; 34(2): 174-81.
- Kachhara S, Nallaswamy D, Ganapathy DM, Sivaswamy V, Rajaraman V. Assessment of intraoral scanning technology for multiple implant impressions-a systematic review and meta-analysis. *J Indian Prosthodont Soc.* 2020; 20(2): 141-52.

In silico Analysis of the Synergistic Interaction Between Biosurfactants and Antifungal Agents Against *Trichophyton* spp.

© Cemile Bağkur¹, © Cenk Serhan Özverel^{1,2}, © Emine Erdağ³

¹DESAM Research Institute, Near East University, Nicosia, North Cyprus

²Department of Basic Medical Sciences, Near East University Faculty of Dentistry, Nicosia, North Cyprus

³Department of Pharmaceutical Chemistry, Near East University Faculty of Pharmacy, Nicosia, North Cyprus

Abstract

BACKGROUND/AIMS: Dermatophytosis, caused by *Trichophyton* species such as *T. rubrum*, *T. mentagrophytes*, and *T. indotinea*, is a common fungal infection with rising terbinafine resistance, particularly in *T. indotinea* strains in South Asia. This study investigates the potential of biosurfactant (rhamnolipid and sophorolipid) and antifungal (terbinafine, itraconazole, fluconazole) combinations in the battle against antifungal resistance.

METHODS: Homology modeling was used to generate 3D structures of 14-alpha-demethylase and squalene epoxidase. Molecular docking and molecular mechanics/poisson-boltzmann surface area calculations were performed via GROMACS 2020.6.

RESULTS: Itraconazole/sophorolipid combination demonstrated the highest combined energy in *T. mentagrophytes* (-82.24 kJ/mol) and *T. indotinea* (-85.35 kJ/mol). The terbinafine/rhamnolipid combination exhibited strong synergistic effects in *T. mentagrophytes* (-84.23 kJ/mol), but it was found not to be an ideal combination for *T. rubrum*.

CONCLUSION: Combining biosurfactants with conventional antifungals is reported to be a promising strategy for treating resistant *Trichophyton* infections, particularly via co-administration of itraconazole/sophorolipid and terbinafine/rhamnolipid combinations.

Keywords: Dermatophytosis, *Trichophyton* species, antifungal resistance, biosurfactants, molecular docking

INTRODUCTION

Dermatophytosis is the most prevalent fungal infection worldwide, caused by various dermatophyte species. These include *Trichophyton*, *Microsporum*, and *Epidermophyton*, which infect keratinized tissues such as skin, hair, and nails. Among *Trichophyton* species, *T. rubrum*, *T. mentagrophytes*, and *T. interdigitale* are the most common in humans.¹ *T. indotinea*, a hypervirulent strain previously known as *T. mentagrophytes* genotype 8, has been responsible for persistent dermatophytosis outbreaks in South Asia.² *T. indotinea* manifests primarily as tinea faciei, corporis, or cruris, and is highly transmissible.³

Increasing cases of terbinafine-resistant *T. indotinea* and other *Trichophyton* species globally have raised concerns about treatment effectiveness.^{4,5}

Tinea in the genital region is rare, mostly caused by *T. rubrum*, but a new genotype of *T. mentagrophytes* (type 7) has been linked to severe infections in this part of the body.⁶ These infections, reported among men who have sex with men, are suspected to be sexually transmitted, although no terbinafine resistance has been observed in this strain.⁷

Common treatments for dermatophytosis include topical and oral antifungals, with oral therapies (primarily terbinafine) reserved for

To cite this article: Bağkur C, Özverel CS, Erdağ E. *In silico* analysis of the synergistic interaction between biosurfactants and antifungal agents against *Trichophyton* spp. Cyprus J Med Sci. 2025;10(Suppl 1):16-19

ORCID IDs of the authors: C.B. 0000-0003-0998-4176; C.S.Ö. 0000-0001-9932-4774; E.E. 0000-0002-1431-935X.



Corresponding author: Cemile Bağkur
E-mail: cemile.bagkur@neu.edu.tr
ORCID ID: orcid.org/0000-0003-0998-4176

Received: 31.10.2024
Accepted: 26.01.2025
Publication Date: 04.06.2025



Copyright© 2025 The Author. Published by Galenos Publishing House on behalf of Cyprus Turkish Medical Association.
This is an open access article under the Creative Commons AttributionNonCommercial 4.0 International (CC BY-NC 4.0) License.

severe cases. However, rising resistance to azoles and allylamines in *T. rubrum* and *T. indotineae* presents a significant challenge.⁸ Resistance mechanisms include mutations in the *ERG11* gene (targeting azoles) and *SQLE* gene (affecting terbinafine), which alter enzyme structures, reducing drug binding.^{8,9}

Biosurfactants, like rhamnolipids and sophorolipids, are regarded as promising alternatives in antifungal therapy due to their ability to disrupt biofilms and cell membranes.^{10,11} Rhamnolipids reduce the minimum inhibitory concentrations of azoles and allylamines in resistant strains like *T. rubrum*, while sophorolipids enhance drug permeability, particularly in *Candida albicans* and *T. mentagrophytes*.¹² Given the rise in drug-resistant *Trichophyton* species,¹³ the growing resistance underscores the urgent need for novel treatment strategies, such as combining biosurfactants with conventional antifungals to enhance therapeutic effectiveness.

This study aims to address the critical challenge of antifungal resistance by exploring the synergistic potential of combining biosurfactants, known for their biofilm-disrupting and permeability-enhancing properties, with conventional antifungal agents. Through *in silico* analysis of binding interactions with key enzymes in three *Trichophyton* species, this research seeks to identify more effective therapeutic options, providing a basis for targeted, species-specific treatment approaches for drug-resistant dermatophytosis.

MATERIALS AND METHODS

Homology Modeling and Molecular Docking

AutoDock Vina was used to assess the binding affinities of antifungal agents (fluconazole, itraconazole, terbinafine) and biosurfactants (rhamnolipid, sophorolipid) against *Trichophyton* species. The target proteins 14- α -demethylase and squalene epoxidase, involved in fungal sterol biosynthesis, were modeled via homology using I-TASSER (<https://zhanggroup.org/>). Ligands and proteins were prepared with AutoDockTools, and docking focused on the active sites using a grid box of $28 \times 28 \times 28$ Å. The Lamarckian genetic algorithm generated 10 docking poses per ligand, with the lowest energy pose chosen for molecular dynamics (MD) simulations.¹⁴

MD Simulations and MM/PBSA Calculations

MD simulations were performed using GROMACS 2020.6 to evaluate the stability of ligand-protein complexes as described in previous research.¹⁴ Post-MD simulations, molecular mechanics/poisson-boltzmann surface area binding free energy calculations were performed using g_mmpbsa

to estimate the free energy of ligand-protein complexes.¹⁴ The stability of combination-enzyme complexes was illustrated using a root mean square deviation (RMSD) plot.

Ethical approval was not applicable for this study as no human participants or animals were involved.

RESULTS

The binding energies of antifungal agents and biosurfactants against 14- α -demethylase and squalene epoxidase in *T. mentagrophytes*, *T. indotineae*, and *T. rubrum* were calculated by AutoDock Vina. As a result of this analysis, the most effective combinations for *T. mentagrophytes* were found to be terbinafine/rhamnolipid (-84.23 ± 1.63 kJ/mol), itraconazole/sophorolipid (-82.24 ± 1.32 kJ/mol), and itraconazole/rhamnolipid (-73.46 ± 1.75 kJ/mol). For *T. indotineae*, the highest interactions in terms of combined binding energies were observed in the following order: itraconazole/sophorolipid (-85.35 ± 1.64 kJ/mol), itraconazole/rhamnolipid (-81.57 ± 2.18 kJ/mol), and terbinafine/rhamnolipid (-72.27 ± 2.04 kJ/mol). When compared to the other two *Trichophyton* species, the binding energies in *T. rubrum* exhibited less negative binding energies, with the highest affinity observed in the combinations of itraconazole/rhamnolipid (-74.73 ± 1.87 kJ/mol), fluconazole/rhamnolipid (-56.23 ± 2.05 kJ/mol), and fluconazole/sophorolipid (-48.54 ± 1.54 kJ/mol). The binding energies of the combinations of antifungal drugs (terbinafine, itraconazole, fluconazole) with biosurfactants (rhamnolipid, sophorolipid) at the binding sites (squalene epoxidase and 14- α -demethylase) in different *Trichophyton* species are shown in Table 1.

Higher additive energy values for terbinafine/rhamnolipid and terbinafine/sophorolipid (-54.60 ± 2.04 and -64.70 ± 2.26 kJ/mol, respectively) were obtained in *T. rubrum* compared to the combined energy values for terbinafine/rhamnolipid and terbinafine/sophorolipid (-51.73 ± 1.38 and -45.29 ± 2.14 kJ/mol, respectively). This indicates that terbinafine alone is more effective than its combinations with biosurfactants, particularly for this species (Figure 1a).

RMSD analysis was performed to assess the stability of the MD simulations in the drug-biosurfactant combinations that exhibited the highest binding energy in each *Trichophyton* species. As a result, the terbinafine/rhamnolipid combination in *T. mentagrophytes* was found to be the most stable combination (Figure 1b). The itraconazole/rhamnolipid combination in *T. rubrum* was reported to be more stable than the itraconazole/sophorolipid combination in *T. indotineae*, and all MD were within the expected range (RMSD value <2).

Table 1. Additive and combined binding energies (kJ/mol) of drug-biosurfactant combinations with squalene epoxidase and 14- α -demethylase in *Trichophyton* species

Combinations	<i>Trichophyton mentagrophytes</i>		<i>Trichophyton indotineae</i>		<i>Trichophyton rubrum</i>	
	Additive energy	Combined energy	Additive energy	Combined energy	Additive energy	Combined energy
Fluconazole + rhamnolipid	-27.00 \pm 2.04	-34.73 \pm 2.23	-28.00 \pm 2.74	-48.39 \pm 1.83	-45.00 \pm 2.94	-56.23 \pm 2.05
Fluconazole + sophorolipid	-35.00 \pm 2.26	-38.23 \pm 1.26	-25.00 \pm 2.59	-32.33 \pm 1.64	-25.00 \pm 2.46	-48.54 \pm 1.54
Itraconazole + rhamnolipid	-47.00 \pm 1.95	-73.46 \pm 1.75	-48.00 \pm 2.59	-81.57 \pm 2.18	-55.00 \pm 2.57	-74.73 \pm 1.87
Itraconazole + sophorolipid	-55.00 \pm 2.17	-82.24 \pm 1.32	-45.00 \pm 2.43	-85.35 \pm 1.64	-35.00 \pm 2.00	-41.84 \pm 1.45
Terbinafine + rhamnolipid	-70.00 \pm 1.91	-84.23 \pm 1.63	-50.00 \pm 2.33	-72.27 \pm 2.04	-54.60 \pm 2.04	-51.73 \pm 1.38
Terbinafine + sophorolipid	-55.00 \pm 2.35	-78.37 \pm 2.16	-40.00 \pm 2.07	-52.38 \pm 1.83	-64.70 \pm 2.26	-45.29 \pm 2.14

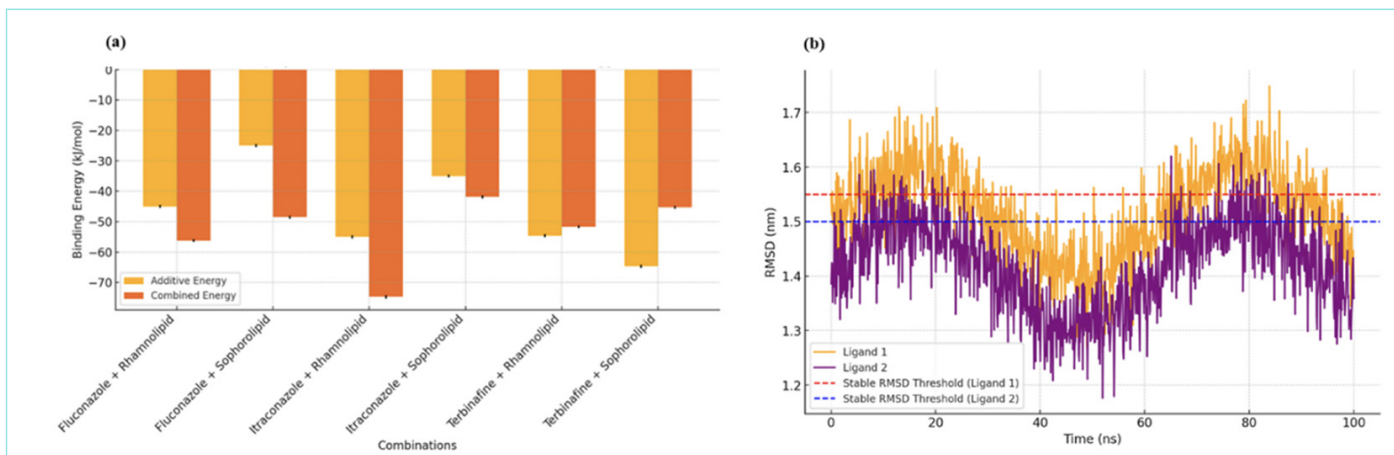


Figure 1. (a) Comparison of additive and combined binding energies for drug-biosurfactant combinations in *Trichophyton rubrum*. (b) The RMSD analysis of terbinafine (purple) and rhamnolipid (orange) in complex with *Trichophyton mentagrophytes* was conducted over a 100 ns simulation period.

RMSD: Root mean square deviation.

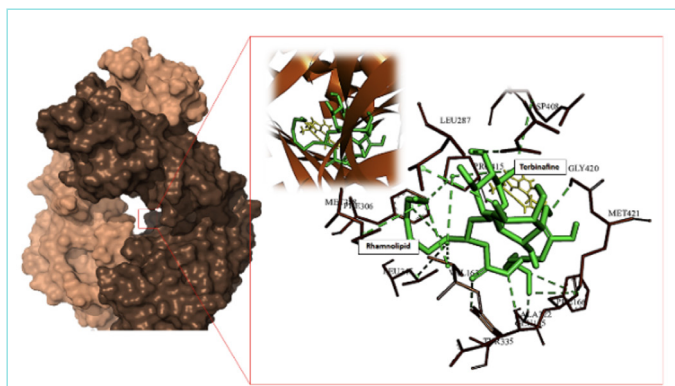


Figure 2. The interaction of terbinafine (yellow) and rhamnolipid (green) at the squalene epoxidase binding site of *Trichophyton mentagrophytes*.

DISCUSSION

In this study, we aimed to investigate the combined use of biosurfactants with the efficacy of conventionally used antifungal agents over three different *Trichophyton* species in combating antifungal resistance. For this purpose, both the additive and combined energies of each combination were calculated for specific *Trichophyton* species included in the study.

Additive energy represents the sum of the binding energies of each agent individually, whereas combined energy refers to the binding energy when both agents interact simultaneously. Data revealed that, relatively higher combined binding energies were obtained in all combinations except for the combinations of *T. rubrum* with terbinafine, meaning that the combinations with biosurfactants were shown to be more effective than conventional agents used alone. The ability of rhamnolipid to disrupt fungal biofilm and the capacity of sophorolipids to alter membrane permeability may contribute to the enhanced drug interactions, as previously reported in studies exploring biosurfactants as drug-delivery enhancers.¹⁵⁻¹⁷ This could be attributed

to the possibility of having higher combined binding energies in combinations over antifungals alone.

When examining the combinations that exhibited the highest combined binding energy for all three *Trichophyton* species, it is observed that the top three combinations with the highest affinity vary for each species. While the azole group combination, itraconazole/sophorolipid, and the allylamine group combination terbinafine/rhamnolipid are common options for *T. mentagrophytes* and *T. indotinea*, the itraconazole/rhamnolipid combination is shared between *T. indotinea* and *T. rubrum*. However, there is no common factor combination that shows the highest interaction for both *T. mentagrophytes* and *T. rubrum*. Interestingly, fluconazole, which is less potent than itraconazole, demonstrated better binding when combined with biosurfactants, particularly for *T. rubrum* compared to the other two species. This discrepancy might be attributed to species-specific differences in the structure of the targeted enzymes, influencing how biosurfactants interact with antifungals. These findings are consistent with previous research showing that genetic variability among *Trichophyton* species impacts drug efficacy, which might explain the varying effectiveness of certain drug combinations across different *Trichophyton* species.^{18,19}

The findings of the present study indicated that the combination application of biosurfactants and antifungals demonstrated enhanced antifungal activity particularly in *T. mentagrophytes* and *T. indotinea* as they possess higher combined energy than additive energies. The combination of terbinafine and rhamnolipid demonstrated the highest synergism at the squalene epoxidase binding site, especially on *T. mentagrophytes* (Figure 2).

CONCLUSION

In conclusion, this study emphasizes the necessity of personalized antifungal treatment strategies due to species-specific responses and genetic variability among *Trichophyton* species, which influence drug efficacy. It emphasizes accurate species identification to optimize treatment and reduce antifungal resistance. This paves the way for future research on developing more precise diagnostic tools and targeted therapies to enhance efficacy.

MAIN POINTS

- Biosurfactants combined with antifungals significantly improved efficacy against *Trichophyton* species.
- Sophorolipid/itraconazole and rhamnolipid/terbinafine combinations showed strong antifungal effects.
- The combinations effectively targeted drug-resistant strains, offering a promising approach for overcoming antifungal resistance.

ETHICS

Ethics Committee Approval: Ethical approval was not applicable for this study as no human participants or animals were involved.

Informed Consent: Not available.

Footnotes**Authorship Contributions**

Concept: C.S.Ö., Design: C.S.Ö., Data Collection and/or Processing: E.E., Analysis and/or Interpretation: C.B., E.E., Literature Search: C.B., Writing: C.B.

DISCLOSURES

Conflict of Interest: No conflict of interest was declared by the authors.

Financial Disclosure: The authors declared that this study had received no financial support.

REFERENCES

1. De Hoog GS, Dukik K, Monod M, Packeu A, Stubbe D, Hendrickx M, et al. Toward a novel multilocus phylogenetic taxonomy for the dermatophytes. *Mycopathologia*. 2017; 182(1-2): 5-31.
2. Shen JJ, Arendrup MC, Verma S, Saunte DML. The emerging terbinafine-resistant *Trichophyton* epidemic: what is the role of antifungal susceptibility testing? *Dermatology*. 2022; 238(1): 60-79.
3. Uhrhlaß S, Verma SB, Gräser Y, Rezaei-Matehkolaei A, Hatami M, Schaller M, et al. *Trichophyton indotineae*-an emerging pathogen causing recalcitrant dermatophytoses in India and worldwide-a multidimensional perspective. *J Fungi (Basel)*. 2022; 8(7): 757.
4. Cañete-Gibas CF, Mele J, Patterson HP, Sanders CJ, Ferrer D, Garcia V, et al. Terbinafine-resistant dermatophytes and the presence of *Trichophyton indotineae* in North America. *J Clin Microbiol*. 2023; 61(8): 56223.
5. Abdolrasouli A, Borman AM, Johnson EM, Hay RJ, Arias M. Terbinafine-resistant *Trichophyton indotineae* causing extensive dermatophytosis in a returning traveller, London, UK. *Clin Exp Dermatol*. 2024; 49(6): 635-7.
6. Luchsinger I, Bosshard PP, Kasper RS, Reinhardt D, Lautenschlager S. *Tinea genitalis*: a new entity of sexually transmitted infection? Case series and review of the literature. *Sex Transm Infect*. 2015; 91(7): 493-6.
7. Jabet A, Dellièrre S, Seang S, Chermak A, Schneider L, Chiarabini T, et al. Sexually transmitted *Trichophyton mentagrophytes* genotype VII infection among men who have sex with men. *Emerg Infect Dis*. 2023; 29(7): 1411-4.
8. Sonogo B, Corio A, Mazzeletti V, Zerbato V, Benini A, di Meo N, et al. *Trichophyton indotineae*, an emerging drug-resistant dermatophyte: a review of the treatment options. *J Clin Med*. 2024; 13(12): 3558.
9. Osborne CS, Leitner I, Favre B, Ryder NS. Amino acid substitution in *Trichophyton rubrum* squalene epoxidase associated with resistance to terbinafine. *Antimicrob Agents Chemother*. 2005; 49(7): 2840-4.
10. Sen S, Borah SN, Bora A, Deka S. Production, characterization, and antifungal activity of a biosurfactant produced by *Rhodotorula babjevae* YS3. *Microb Cell Fact*. 2017; 16(1): 95.
11. dos Santos JRA, Rocha AA, de Macedo AT, Santana AA, da Silva JBS, de Souza MEP, et al. Antifungal activity of biosurfactant against profound mycosis. *Green Sustainable Process for Chemical and Environmental Engineering and Science*. 2022; 257-87.
12. Sen S, Borah SN, Bora A, Deka S. Rhamnolipid exhibits anti-biofilm activity against the dermatophytic fungi *Trichophyton rubrum* and *Trichophyton mentagrophytes*. *Biotechnol Rep*. 2020; 27: 516.
13. Bristow IR, Joshi LT. Dermatophyte resistance-on the rise. *J Foot Ankle Res*. 2023; 16(1): 69.
14. Sultanoglu N, Erdag E, Ozverel CS. A single antiviral for a triple epidemic: is it possible? *Future Virol*. 2023; 18(10): 633-42.
15. Thakur P, Saini NK, Thakur VK, Gupta VK, Saini RV, Saini AK. Rhamnolipid the glycolipid biosurfactant: emerging trends and promising strategies in the field of biotechnology and biomedicine. *Microb Cell Fact*. 2021; 20(1): 1.
16. Hmingthansanga V, Singh N, Banerjee S, Manickam S, Velayutham R, Natesan S. Improved topical drug delivery: role of permeation enhancers and advanced approaches. *Pharmaceutics*. 2022; 14(12): 2818.
17. Som I, Bhatia K, Yasir M. Status of surfactants as penetration enhancers in transdermal drug delivery. *J Pharm Bioallied Sci*. 2012; 4(1): 2-9.
- 18.
19. Sacheli R, Hayette MP. Antifungal resistance in dermatophytes: genetic considerations, clinical presentations and alternative therapies. *J Fungi (Basel)*. 2021; 7(11): 983.
20. Yamada T, Maeda M, Alshahni MM, Tanaka R, Yaguchi T, Bontems O, et al. Terbinafine resistance of *Trichophyton* clinical isolates caused by specific point mutations in the squalene epoxidase gene. *Antimicrob Agents Chemother*. 2017; 61(7): 115-7.

Triazole Derivatives as Potential MCR-1 Inhibitors: A Promising Approach to Overcome Colistin Resistance

Emine Erdağ¹, Cenk Serhan Özverel^{2,3}, Cemile Bağkur³

¹Department of Pharmaceutical Chemistry, Near East University Faculty of Pharmacy, Nicosia, North Cyprus

²Department of Basic Medical Sciences, Near East University Faculty of Dentistry, Nicosia, North Cyprus

³DESAM Research Institute, Near East University, Nicosia, North Cyprus

Abstract

BACKGROUND/AIMS: Colistin, a last-resort antibiotic, is crucial in treating multidrug-resistant Gram-negative infections. However, the rise of colistin resistance, particularly due to plasmid-mediated *MCR-1* genes, poses a significant challenge. This study explored the possibility of using triazole derivatives as potential MCR-1 inhibitors. The study aimed to explore various triazole derivatives as bioisosteric replacements for these heterocycles, given their similar electronic properties and interactions with biological targets to design new molecules with improved efficacy and pharmacokinetic profiles.

MATERIALS AND METHODS: Triazole derivatives were created by applying modifications to their R1 groups on the triazole ring. After modifications, their efficacy was evaluated through molecular docking and molecular dynamics simulations using AutoDock4 and GROMACS software.

RESULTS: The results demonstrated that triazole derivatives with the N-phenylsulfonamide modification exerted superior activity and pharmacokinetic profile over other derivatives formed. Notably, this compound interacted strongly with MCR-1 residues in the catalytic domain, making it a promising candidate to combat colistin resistance.

CONCLUSION: This study highlights that triazole derivatives might be promising candidates for MCR-1 inhibition to combat colistin-resistant infections.

Keywords: MCR-1, colistin-resistance, multidrug-resistant Gram-negative infections, triazoles, computer-aided drug design

INTRODUCTION

Polymyxins, such as colistin, are effective against Gram-negative bacteria like *Acinetobacter* spp., *Pseudomonas aeruginosa*, and *Klebsiella* spp.¹⁻³ Colistin targets bacterial membranes by interacting with lipid A in lipopolysaccharides, disrupting membrane integrity and causing cell death.⁴ Resistance to polymyxins has evolved through chromosomal mutations and plasmid-mediated mechanisms, particularly via the *MCR-1* gene.⁵ This gene, discovered in 2015, encodes a phosphoethanolamine (pEtN) transferase (MCR-1) that modifies lipid A, reducing the binding

and antimicrobial efficacy of colistin.⁶ The *MCR-1* gene, which encodes pEtN transferase, modifies lipid A by adding pEtN, thereby reducing the negative charge on the membrane and enhancing lipid packing.⁷ This alteration decreases the binding and penetration of polymyxins, leading to increased resistance by reinforcing the membrane and reducing antimicrobial peptide efficacy.⁷ The dissemination of plasmid-borne *MCR-1* confers colistin resistance, with mobile *MCR-1* gene cassettes facilitating genetic transfer across various hosts, including animals, food products, and humans.⁸ Recent studies have identified inhibitors featuring pyrazolone, imidazole, and oxazole structures

To cite this article: Erdağ E, Özverel CS, Bağkur C. Triazole derivatives as potential MCR-1 inhibitors: a promising approach to overcome colistin resistance. Cyprus J Med Sci. 2025;10(Suppl 1):20-23

ORCID IDs of the authors: E.E. 0000-0002-1431-935X; C.S.Ö 0000-0001-9932-4774; C.B. 0000-0003-0998-4176.



Corresponding author: Emine Erdağ
E-mail: emine.erdag@neu.edu.tr
ORCID ID: orcid.org/0000-0002-1431-935X

Received: 25.10.2024
Accepted: 26.01.2025
Publication Date: 04.06.2025



Copyright© 2025 The Author. Published by Galenos Publishing House on behalf of Cyprus Turkish Medical Association.
This is an open access article under the Creative Commons AttributionNonCommercial 4.0 International (CC BY-NC 4.0) License.

as agents targeting *MCR* genes (MCR-1 to MCR-10).⁹⁻¹¹ These inhibitors aimed to restore the effectiveness of colistin against resistant bacterial strains by inhibiting the enzymatic activity of MCR proteins. Beyond pyrazolone and other derivatives, various other bioisosteric heterocyclic compounds, including triazoles, could be explored as promising candidates for the development of MCR inhibitors. The ultimate goal of this approach is to address the growing challenge of colistin resistance and to enhance treatment options for multidrug-resistant Gram-negative infections.

MATERIALS AND METHODS

Preparation of Data Set and Molecular Docking

This study does not involve the use of human or animal samples; therefore, ethical approval is not applicable. In this study, seven triazole derivatives (Ligand 1-7), each varying by the R groups attached to the N-4 position of the triazole ring, were chosen from the ZINC and ChemDiv ligand libraries. The main differences between triazole-containing ligands are illustrated in Figure 1. Ligand preparation was performed using LigandScout 4.0, followed by molecular optimization with the Avogadro tool (<https://avogadro.cc/>). AutoDock4 was utilized to conduct molecular docking studies to determine the binding affinities of the triazole derivatives to the MCR-1 catalytic domain (PDB ID: 5LRM).¹² The docking results were assessed by analyzing binding energies and protein-ligand interactions.

Statistical Analysis

GROMACS software was used to assess the statistical analysis of the complex stability, and Molecular Mechanics/Poisson-Boltzmann Surface Area (MM/PBSA) calculations were performed with *g_mmpbsa* to estimate binding free energies with mean standard deviations.¹³ The stability of the most effective ligand was confirmed further by the root mean square (RMSD) plot.

Pharmacokinetic Predictions

Pharmacokinetic properties absorption, distribution, metabolism, excretion, toxicity of the triazole derivatives were assessed using ProTox II and SwissADME, analyzing key factors like LogP, gastrointestinal (GI) absorption, plasma protein binding, and enzyme inhibition potential to evaluate their pharmacokinetic profile and drug interaction risks.¹⁴

RESULTS

The *in silico* analysis of the seven triazole derivatives demonstrated varying levels of interaction with MCR-1, with Ligand 6 emerging as the most promising candidate. The MM/PBSA binding energy of Ligand 6 was calculated to be -29.72 ± 1.82 kJ/mol, representing the strongest binding affinity among the compounds. Its docking score of -12.4 kcal/mol further confirmed this high affinity, indicating robust interactions with the MCR-1 protein. This was likely due to the presence of a 4-sulfonamide moiety in Ligand 6, which facilitated stronger interactions with critical amino acid residues in the protein's active site (Figure 2). Specifically, aspartate and arginine amino acids were key residues involved in stabilizing the ligand-protein complex. The RMSD values for both the MCR-1 and Ligand 6 indicated a stable interaction throughout the molecular dynamics simulation (Figure 3). Similarly, Ligand 5 exhibited favorable results, with a binding energy of -26.33 ± 1.63 kJ/mol and a docking score of -11.7 kcal/mol, making it the second most effective compound in the series. While slightly less

potent than Ligand 6, Ligand 5 still showed a strong potential for MCR-1 inhibition due to its high binding energy and favorable interactions with the protein. However, other ligands such as Ligand 1 and Ligand 3 showed weaker binding energies and docking scores. For instance, Ligand 1 presented a binding energy of -16.23 ± 1.32 kJ/mol and a docking score of -7.3 kcal/mol, while Ligand 3 had the weakest values among the derivatives, with a binding energy of -14.84 ± 1.72 kJ/mol, and a docking score of -6.7 kcal/mol. Moreover, pharmacokinetic predictions revealed optimal properties for all ligands, with Ligand 6

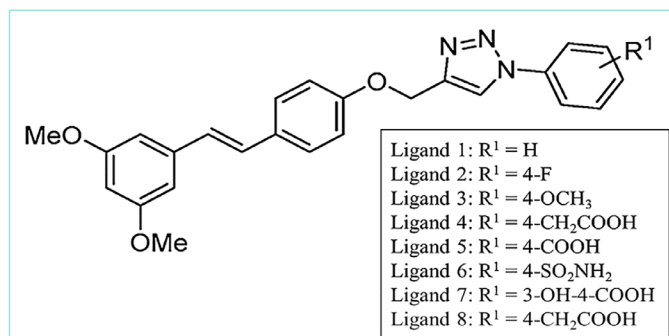


Figure 1. General structure of triazole derivatives with different R1 groups on triazole ring.

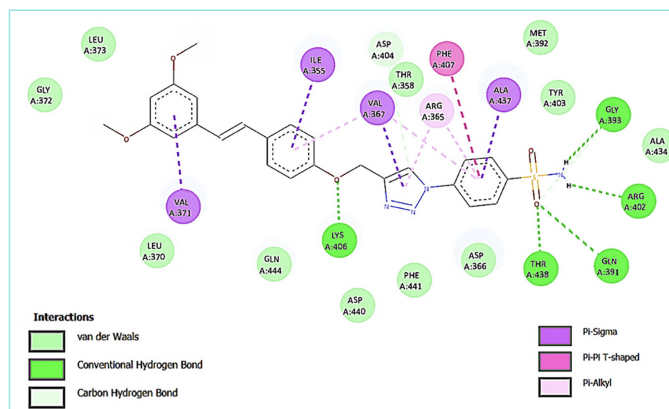


Figure 2. 2D interaction map of Ligand 6 within the MCR-1 active site, highlighting various interactions contributing to its binding affinity.

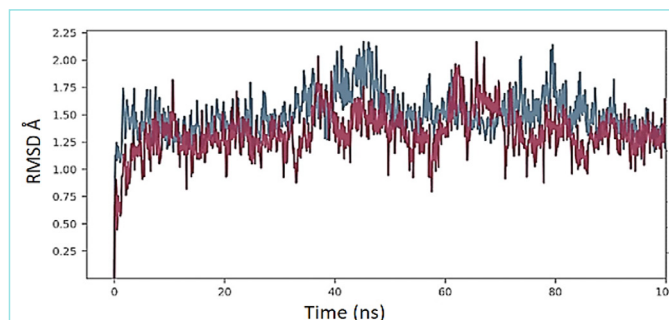


Figure 3. RMSD graph of Ligand 6 and MCR-1 in a 100 ns simulation period. The blue color indicates the RMSD of MCR-1, while the red color indicates the RMSD of Ligand-6.

RMSD: Root mean square deviation.

emerging as the most promising. It exhibited a favorable LogP value of 0.472, which supports good membrane permeability and absorption, as confirmed by a GI absorption score of 0.511. Ligand 6 also had 73% plasma protein binding, ensuring sufficient free drug in circulation, and showed no inhibition of major CYP450 enzymes, indicating low drug-drug interaction potential. In addition, the half-life of Ligand 6 was predicted as 5.242 hours, making it suitable for regular dosing intervals.

DISCUSSION

Resistance to colistin, especially driven by the *MCR-1* gene, poses a major global health concern, as it compromises the effectiveness of one of the last-resort antibiotics used to treat multidrug-resistant Gram-negative bacterial infections.¹⁵ In the current study, several triazole derivatives were evaluated as potential inhibitors of MCR-1. Ligand 6 showed the most promising results, with strong binding energy and favorable docking scores. The presence of a 4-sulfonamide group facilitated significant interactions in the MCR-1 binding pocket. As mentioned earlier, these interactions are crucial for the inhibition of MCR-1 activity, indicating the potential of Ligand 6 for restoring the efficacy of colistin. The strong binding interactions at aspartate and arginine residues suggested that Ligand 6 could inhibit the activity of MCR-1, potentially restoring the efficacy of colistin against resistant bacterial strains. The results from the present study aligned with earlier research on MCR-1 inhibitors. For instance, Hanpaibool et al.¹⁶ investigated pyrazolone-based compounds as potential MCR-1 inhibitors. The study reported that some of these compounds enhanced colistin efficacy by lowering the minimal inhibitory concentration of colistin in *MCR-1*-expressing *E. coli* strains. Compared to research by Hanpaibool et al.¹⁶, reporting the most effective compound (Py4i) exhibiting a binding free energy of -6.64 kcal/mol, the current study on the triazole derivative Ligand 6 demonstrated a significantly stronger binding affinity with a docking score of -12.4 kcal/mol, suggesting that triazoles may provide a more effective approach for overcoming colistin resistance.

In the present study, MM/PBSA calculations were used to estimate the binding free energies, providing a detailed insight into the strength of the ligand-protein interactions, similar to previous reports.¹³ The superior inhibitory effects of Ligands 5 and 6 might be due to the nature of their functional groups and interactions with the MCR-1 catalytic domain. The carboxyl group (COOH) of Ligand 5 at the 4-position is negatively charged and highly polar. This might be attributed to its enhanced binding affinity and inhibitory potency. Likewise, the sulfonamide group (SO₂NH₂) of Ligand 6 exhibited strong polarity and electrostatic interaction potential, forming extensive hydrogen and ionic bonds with the active site. The large size of the sulfonamide group further increased surface interactions, leading to stronger binding affinity and inhibitory efficacy. On the other hand, Ligand 3, which contains a methoxy group (OCH₃), demonstrated weaker interactions with the MCR-1 catalytic site. The methoxy group is electron-donating and lacks significant polarity, reducing its ability to engage in strong electrostatic interactions. As a result, the binding energy and docking scores for Ligand 3 were less favorable. Ligand 2, which contains a fluorine atom (F) at the 4-position, exhibited slightly stronger binding than Ligand 3 due to the electron-withdrawing nature of fluorine. However, its small size might limit the extent of its interactions with the binding pocket, resulting in weaker inhibition compared to Ligands 5 and 6. In addition, Ligand

6 exhibited a highly favorable pharmacokinetic profile, particularly with its optimal LogP and GI absorption values, indicating desirable membrane permeability and potential for effective oral bioavailability. Furthermore, its lack of CYP450 enzyme inhibition suggests a low risk of drug-drug interactions, making it a promising candidate for further development.

Study Limitations

The key limitation of this study is its reliance on *in silico* methods, meaning that the results need to be validated through experimental *in vitro* and *in vivo* studies.

CONCLUSION

This study highlighted the potential of triazole derivatives, particularly Ligand 6, as promising MCR-1 inhibitors to combat colistin resistance. Despite the limitations of this *in silico* study, the results provided a solid foundation for further *in vitro* and *in vivo* studies, with the long-term goal of developing alternative strategies to combat antibiotic resistance in critical bacterial infections.

MAIN POINTS

- All triazole derivatives exhibited optimal pharmacokinetic properties.
- A triazole derivative with a 4-sulfonamide group demonstrated the highest binding affinity.
- Strong interactions with MCR-1 residues, particularly aspartate and arginine, confirmed the inhibitory potential of all triazole derivatives.

ETHICS

Ethics Committee Approval: Not applicable.

Informed Consent: Not applicable.

Footnotes

Authorship Contributions

Concept: E.E., C.S.Ö., C.B., Design: E.E., C.S.Ö., C.B., Data Collection and/or Processing: E.E., Analysis and/or Interpretation: E.E., C.S.Ö., C.B., Literature Search: C.B., Writing: E.E., C.S.Ö., C.B.

DISCLOSURES

Conflict of Interest: No conflict of interest was declared by the authors.

Financial Disclosure: The authors declared that this study had received no financial support.

REFERENCES

1. Lim LM, Ly N, Anderson D, Yang JC, Macander L, Jarkowski A III, et al. Resurgence of colistin: a review of resistance, toxicity, pharmacodynamics, and dosing. *Pharmacotherapy*. 2010; 30(12): 1279-91.
2. Poirel L, Jayol A, Nordmann P. Polymyxins: antibacterial activity, susceptibility testing, and resistance mechanisms encoded by plasmids or chromosomes. *Clinical microbiology reviews*. 2017; 30(2): 557-96.
3. Yang S, Wang H, Zhao D, Zhang S, Hu C. Polymyxins: recent advances and challenges. *Frontiers in Pharmacology*. 2024; 15: 1424765.

4. Ayoub Moubareck C. Polymyxins and bacterial membranes: a review of antibacterial activity and mechanisms of resistance. *Membranes (Basel)*. 2020; 10(8): 181.
5. Anyanwu MU, Jaja IF, Nwobi OC. Occurrence and characteristics of mobile colistin resistance (*mcr*) gene-containing isolates from the environment: a review. *Int J Environ Res Public Health*. 2020; 17(3): 1028.
6. Schwarz S, Johnson AP. Transferable resistance to colistin: a new but old threat. *J Antimicrob Chemother*. 2016; 71(8): 2066-70.
7. Khondker A, Dhaliwal AK, Saem S, Mahmood A, Fradin C, Moran-Mirabal J, et al. Membrane charge and lipid packing determine polymyxin-induced membrane damage. *Commun Biol*. 2019; 2(1): 1-11.
8. Schwarz S, Johnson AP. Transferable resistance to colistin: a new but old threat. *J Antimicrob Chemother*. 2016; 71(8): 2066-70.
9. Pietschmann S, Hoffmann K, Voget M, Pison U. Synergistic effects of miconazole and polymyxin B on microbial pathogens. *Vet Res Commun*. 2009; 33: 489-505.
10. Semenyuta I, Hodyna D, Kovalishyn V, Demydchuk B, Kachaeva M, Pilyo S, et al. Development and application of *in silico* models to design new antibacterial 5-amino-4-cyano-1,3-oxazoles against colistin-resistant *E. coli* strains. *Artif Intell Chem*. 2023; 1(2): 100024.
11. Frantz R, Gwozdziński K, Gisch N, Doijad SP, Hudel M, Wille M, et al. A single residue within the MCR-1 protein confers anticipatory resilience. *Microbiol Spectr*. 2023; 11(3): e0359222.
12. Hinchliffe P, Yang QE, Portal E, Young T, Li H, Tooke CL, et al. Insights into the mechanistic basis of plasmid-mediated colistin resistance from crystal structures of the catalytic domain of MCR-1. *Sci Rep*. 2017; 7: 39392.
13. Ozverel CS, Erdağ E. Enhancing quality of life in multiple sclerosis patients through coadministration of FDA-approved immunomodulators and melatonin. *Chronobiol Med*. 2024; 6(3): 135-142.
14. Li Y, Meng Q, Yang M, Liu D, Hou X, Tang L, et al. Current trends in drug metabolism and pharmacokinetics. *Acta Pharm Sin B*. 2019; 9(6): 1113-44.
15. Mondal AH, Khare K, Saxena P, Debnath P, Mukhopadhyay K, Yadav D. A review on colistin resistance: an antibiotic of last resort. *Microorganisms*. 2024; 12(4): 772.
16. Hanpaibool C, Ounjai P, Yotphan S, Mulholland AJ, Spencer J, Ngamwongsatit N, et al. Enhancement by pyrazolones of colistin efficacy against *mcr-1*-expressing *E. coli*: an *in silico* and *in vitro* investigation. *J Comput Aided Mol Des*. 2023; 37(10): 479-89.

Necessity of Alternative Strategies to Combat Antibiotic Resistant Strains Detected in Northern Cyprus

Elizabeth Mkpouto Opawoye¹, Emrah Güler², Kaya Sürer³, Ayşe Arıkan^{1,4,5}

¹Department of Medical Microbiology and Clinical Microbiology, Near East University Faculty of Medicine, Nicosia, North Cyprus

²Department of Molecular Biology and Genetics, European University of Lefke Faculty of Arts and Sciences, Lefke, North Cyprus

³Department of Infectious Diseases and Clinical Microbiology, Near East University Faculty of Medicine, Nicosia, North Cyprus

⁴DESAM Research Institute, Near East University, Nicosia, North Cyprus

⁵Department of Medical Microbiology and Clinical Microbiology, Kyrenia University Faculty of Medicine, Kyrenia, North Cyprus

Abstract

BACKGROUND/AIMS: Antibiotic resistance is becoming an important global health crisis. This study aims to investigate the alteration in the distribution and antibiotic resistance patterns of pathogens isolated from aspirate and sputum samples of patients admitted to a microbiology laboratory in Northern Cyprus over a period of 5 years.

MATERIALS AND METHODS: A total of 3669 samples between 2018 and 2022 were involved in the study retrospectively. The VITEK 2 (bioMérieux) compact automated system was used for microorganism identification and antibiotic susceptibility tests. Antibiotic susceptibility tests were evaluated according to the European Committee on Antimicrobial Susceptibility Testing criteria, and antibiotics detected as intermediate were considered resistant.

RESULTS: While the five-year growth rate was 52.7%, these rates were 52.0%, 51.6%, 45.5%, 52.2% and 61.1% in 2018, 2019, 2020, 2021 and 2022, respectively. Of the bacterial growth, 82.7% (n=1597) were gram-negative, 8.9% (n=171) were gram-positive, and 8.5% (n=164) were *Candida* species. Accordingly, the most frequently isolated gram-negative bacteria were *Pseudomonas aeruginosa* (20.3%) and *Acinetobacter baumannii*-calcoaceticus complex (18.3%), which were most resistant to aztreonam (78%), levofloxacin (70.5%), and imipenem (69.1%). *Klebsiella pneumoniae* (18.0%) showed resistance to ampicillin (91.1%) and cefuroxime (63.1%). The most frequently isolated gram-positive bacteria were *Staphylococcus aureus* (62%) and *Enterococcus* spp. (29.2%) The rate of methicillin-resistant *S. aureus*, extended-spectrum beta-lactamase, and vancomycin-resistant enterococci was 55.7%, 43.3%, and 6%, respectively, with high resistance to erythromycin (45.5%) and tetracycline (40.7%).

CONCLUSION: Identifying highly resistant pathogens indicates the need for close monitoring of patients and the development of alternative treatment approaches to reduce antibiotic resistance against commonly used antibiotics.

Keywords: Drug resistance, anti-bacterial agents, infectious diseases

INTRODUCTION

Antibiotics have been among the most important medical achievements in treating infectious diseases over the last few decades.¹ The use of antimicrobials, while critical to improving

our health and quality of life, has led to the development of antimicrobial resistance (AMR) in recent years, which poses a major threat. The most important consequences of AMR are treatment failure, the risk of global spread of resistant infections, the triggering of serious diseases, prolonged hospital

To cite this article: Opawoye EM, Güler E, Sürer K, Arıkan A. Necessity of alternative strategies to combat antibiotic resistant strains detected in Northern Cyprus. Cyprus J Med Sci. 2025;10(Suppl 1):24-28

ORCID IDs of the authors: E.M.O. 0000-0002-8029-9887; E.G. 0000-0002-1635-0051; K.S. 0000-0002-2565-3425; A.A. 0000-0003-1942-1203.



Corresponding author: Ayşe Arıkan
E-mail: ayse.arikansarioglu@neu.edu.tr
ORCID ID: orcid.org/000-0003-1942-1203

Received: 01.11.2024
Accepted: 16.01.2025
Publication Date: 04.06.2025



Copyright © 2025 The Author. Published by Galenos Publishing House on behalf of Cyprus Turkish Medical Association.
This is an open access article under the Creative Commons Attribution-NonCommercial 4.0 International (CC BY-NC 4.0) License.

stay and treatment, and consequently increased healthcare costs and significant mortality rates. More and more organisms are becoming multidrug-resistant (MDR), and the infections they cause are more difficult to treat. However, extensively drug-resistant and pandrug-resistant organisms, which are the serious and dangerous forms, are of critical concern.² The World Health Organization (WHO) estimated that AMR directly caused 1.27 million deaths and contributed to 4.95 million deaths worldwide in 2019.³ In addition to its negative impact on mortality and morbidity, AMR has a significant economic impact. The Centers for Disease Control and Prevention estimates that healthcare costs of AMR infections are 4 to 5 billion United States Dollars (USD), annually. Additionally, the World Bank projects estimate an increase of 1 trillion USD in healthcare expenditures by 2050 and alongside annual gross domestic product losses ranging from 1 trillion to 3.4 trillion USD by 2030.³⁻⁵

The increase in AMR infections, especially following the coronavirus disease-2019 (COVID-19) pandemic, is considered a global public health crisis at the human, veterinary and environmental levels.⁶ There will be an impact on the ecosystem, agricultural output, impoverished conditions, health security, and the United Nations Sustainable Development Goals, highlighting the necessity of a multisectoral One Health plan to reduce AMR.⁴ The continuous prevalence of this silent pandemic particularly affects clinically significant *Enterococcus faecium*, *Staphylococcus aureus*, *Klebsiella pneumoniae*, *Acinetobacter baumannii*, *Pseudomonas aeruginosa*, *Enterobacter species*, and *Escherichia coli* (ESKAPEE) pathogens. This is putting increased pressure on the healthcare, veterinary, and agricultural sectors.⁷ Although official statistics on antibiotic use and AMR in the Turkish Republic of Northern Cyprus (TRNC) are not available on the official websites of the Ministry of Health, studies on AMR in the TRNC have revealed that AMR poses an increasing threat to both the health sector and society in Northern Cyprus.^{8,9} Therefore, the study aimed to demonstrate the distribution and antibiotic resistance patterns of pathogens isolated from aspirate and sputum samples, and to raise awareness about the necessity of alternative treatments in the fight against AMR.

MATERIALS AND METHODS

The study involved 3669 sputum and aspirate samples taken from both inpatients and outpatients admitted to the University Hospital between 2018 and 2022. The results of the patients were evaluated as a single study group and not as community and hospital environment groups. The patient's demographic data, such as age and gender, were included. Microbial detection and antibiotic susceptibility testing were performed using the VITEK 2 (bioMérieux) automated system and were evaluated according to the European Committee on Antimicrobial Susceptibility Testing criteria.¹⁰ The ethical approval of the study was obtained from the Near East University Ethical Committee (approval number: 2023/112, date: 30.03.2023). Informed consent forms were not obtained from the patients as the study was conducted retrospectively.

Statistical Analysis

The SPSS Demo Ver 22 (SPSS Inc., Chicago, IL, USA) software package was used for statistical analysis. Pearson chi-square,

Fisher's exact test, and one-way ANOVA tests were used to analyze variables, and p-values <0.05 were considered significant.

RESULTS

Of the samples, n=1121 (57.6%) were aspirates and n=424 (42.4%) were sputum. Microbial growth was reported in 52.7% (n=1932/3669) of the samples. Of those with growth, 58% were aspirates and 42% were sputa. No growth was detected in 47.3% (n=1737) of the specimens in the study. Sixty-five percent (n=1254) of the patients with bacterial growth were male, while 35.1% (n=678) were female. The mean age of these female patients was 69.63±17.17 years (range 0-100 years). In the study, the growth rate in males was higher than that of females (p=0.012). By years, the growth rates were 52.0% (270/519), 51.6% (313/607), 45.5% (363/798), 52.2% (n=467/895) and 61.1% (519/850), in 2018-2022 respectively. The highest growth rate was detected in 2022, with an increase of 61.1% compared to the previous years, indicating statistical significance (p=0.0001). Of the bacterial growth, the rates of gram-negative bacteria, gram-positive bacteria, and *Candida* species were found to be 82.7% (n=1597), 8.9% (n=171), and 8.5% (n=164), respectively. The most commonly identified gram-positive bacteria were *S. aureus* (62%, 106/171) and *Enterococcus* spp. (29.2%, 50/171). Methicillin-resistant *S. aureus* (MRSA) was detected at a rate of 55.7% (59/106). The rate of vancomycin-resistant enterococci (VRE) was 6% (3/50). Amongst gram-negative bacteria, enteric and non-enteric bacteria were reported at 46.6% (n=744) and 53.4% (n=853), respectively. *K. pneumoniae* (46.6%, 347/744) and *E. coli* (19.5%, 145/744) were the most commonly isolated enteric bacteria, while *P. aeruginosa* (46.0%, 392/853) and *A. baumannii* (42.1%, 359/853) were the most common non-enteric bacteria (Figure 1). The extended-spectrum beta-lactamase (ESBL) positivity rate in gram-negative enteric bacteria was 43.3%. This rate was 41.3% (202/489) in males and 47.1% (120/255) in females; no statistically significant relationship was found between sex and ESBL positivity (p=0.133). When we compared gender and MRSA rates, it was found that females (62.7%, 32/51) had more MRSA strains in cultures compared to males (41.7%, 20/48), which was statistically significant (p=0.036)

Antibiotic resistance patterns in enteric bacteria (Table 1) between 2018 and 2022 show that the highest resistance was detected in ampicillin (91.1%), cefuroxime (63.1%), and ceftriaxone (49.5%) while the highest sensitivity was reported for amikacin (87.5%), gentamicin (85.1%), and meropenem (83.7%). Amongst non-enteric bacteria (Table 1), the highest resistance was reported to aztreonam (78%), levofloxacin (70.5%), and imipenem (69.1%), while the highest sensitivity was observed for colistin with a rate of 93.4%. For gram-positive bacteria, the highest resistance was reported against erythromycin (45.5%), clindamycin (35.4%), and tetracycline (40.7%), while the highest sensitivity was reported for tigecycline, linezolid, and daptomycin with rates of 99.2%, 98.1%, and 92.1%, respectively (Table 2). Table 2 shows antibiotic profiles in gram-positive bacteria between 2018 and 2022. The highest resistance was reported against tetracycline (40.7%), erythromycin (45.5%), and clindamycin (35.4%).

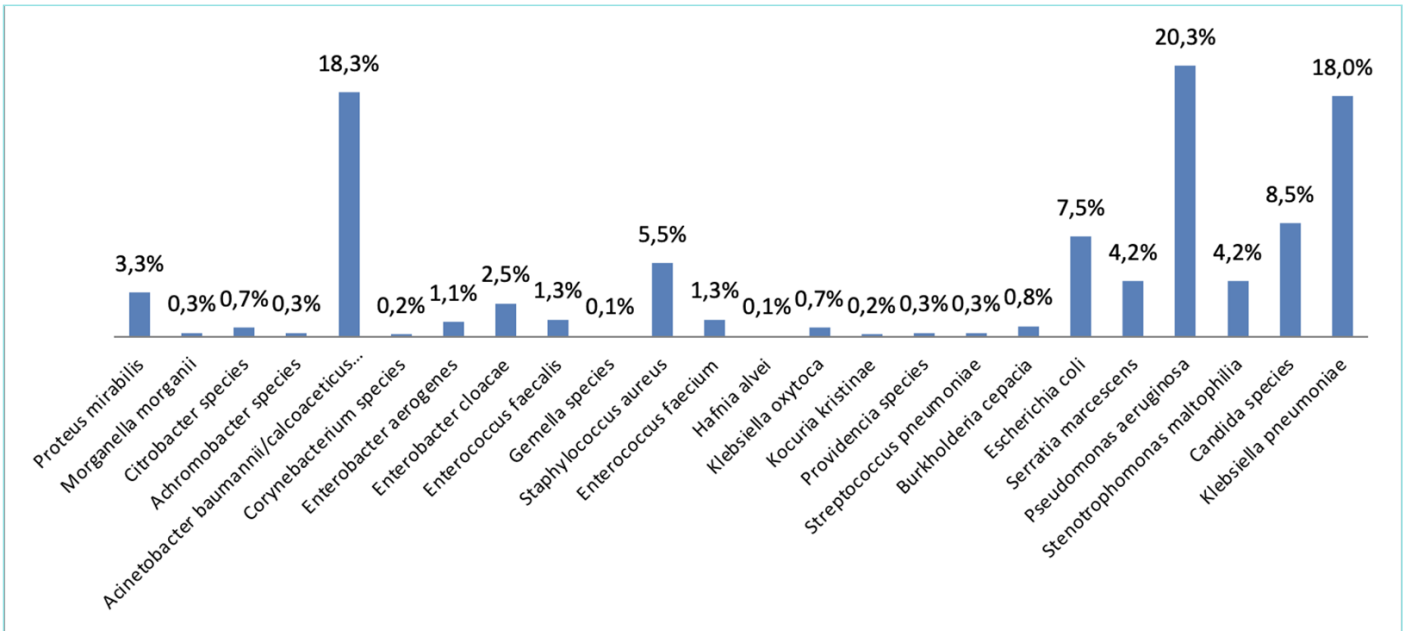


Figure 1. Distribution of bacteria isolated from sputum and aspirate samples between 2018-2022 (%).

Table 1. The antibiotic resistance patterns in gram-negative bacteria

Antibiotic	Enteric bacteria (%)		Antibiotic	Non-enteric bacteria (%)	
	sensitive	resistant		sensitive	resistant
Amikacin	87.5	12.5	Amikacin	58.1	41.9
Ampicillin	8.9	91.1	Aztreonam	22.0	78.0
Aztreonam	60.6	39.4	Cefepime	45.2	54.8
Cefepime	55.8	44.2	Ceftazidime	49.6	50.4
Ceftazidime	56.3	43.7	Ciprofloxacin	32.3	67.7
Ceftriaxone	50.5	49.5	Colistin	93.4	6.6
Cefuroxime	36.9	63.1	Gentamicin	46.3	53.7
Ciprofloxacin	56.2	43.8	Imipenem	30.9	69.1
Ertapenem	72.1	27.9	Levofloxacin	29.5	70.5
Gentamicin	85.1	14.9	Meropenem	31.4	68.6
Imipenem	82.5	17.5	Netilmicin	38.7	61.3
Meropenem	83.7	16.3	TZP	42.8	57.2
TZP	66.4	33.6	Tigecycline	83.4	16.6
Tigecycline	72.2	27.8	Tobramycin	57.3	42.7
SXT	64.4	35.6	SXT	34.9	65.1

TZP: Tazobaktam, SXT:Sulfamethoxazole + Trimethoprim (Bactrim, Septra).

Table 2. The antibiotic resistance patterns in Gram-positive bacteria

Antibiotic	Sensitive (%)	Resistant (%)
Ciprofloxacin	73.6	26.4
Clindamycin	64.6	35.4
Daptomycin	92.1	7.9
Erythromycin	54.5	45.5
Gentamicin	84.2	15.8
Levofloxacin	76.0	24.0
Linezolid	98.1	1.9
Teicoplanin	91.5	8.5
Tetracycline	59.3	40.7
Tigecycline	99.2	0.8
SXT	65.4	34.6
Vancomycin	95.8	4.2

SXT: Sulfamethoxazole.

DISCUSSION

AMR continues to pose an increasing threat globally. This study investigated the distribution of pathogens and drug resistance profiles against various antibiotics over 5 years. Bacterial growth was detected in aspirate/sputum samples over 50%, the peak growth rate was detected in 2022 (61.1%), and the lowest growth rate was detected in 2020 (45.5%). The restrictions implemented during the last pandemic may have caused a decrease in access to healthcare systems in 2020, which may have led to a false report of a reduction in bacterial growth rates. However, by

2022, many countries had lifted COVID-19 restrictions (such as masks and distancing), which increased person-to-person contact and bacterial transmission. Additionally, people who avoided hospitals in previous years may have contracted more severe bacterial infections in 2022. These factors may have also contributed to the increased growth rate. Additionally, the significant difference in microbial growth between males and females may be due to various factors such as underlying diseases, smoking, and exposure to infection.

Our findings revealed that high levels of resistance to some important pathogens including *P. aeruginosa*, *A. baumannii*/calcoaceticus complex, *K. pneumoniae*, MRSA, VRE, and ESBL were in circulation in Northern Cyprus between 2018 and 2022. Additionally, due to ESBL detection at notable rates and the presence of significant MRSA resistance especially in women, it is

important to investigate the underlying causes such as access to health care, predisposing factors, or healthcare-related exposure. The isolated pathogens in the study were highly resistant to major antibiotics such as ampicillin (91.1%), aztreonam (78%), levofloxacin (70.5%), imipenem (69.1%), cefuroxime (63.1%), erythromycin (45.5%) and tetracycline (40.7%). The high rate of resistance to these antibiotics appears to pose a serious risk to public health and hospital infection management. The WHO reported that overuse of antibiotics in COVID-19-infected hospitalized patients during the pandemic triggered AMR. Globally, although only 8% of these patients had bacterial co-infections requiring antibiotics, approximately 75% of them received prophylactic antibiotic treatment, which may have triggered the trend of antibiotic overuse.¹¹ During the COVID-19 outbreak in Northern Cyprus, the application of prophylaxis regimens to hospitalized patients and unnecessary antibiotic use by the community may have led to an increase in resistant pathogens. This situation demonstrated the importance of antimicrobial stewardship policies. A similar study conducted in Nepal revealed that *P. aeruginosa* (30.7%), *A. baumannii* (29.8%), *Burkholderia* spp. (1%) and *Stenotrophomonas* spp. (2.8%) had high growth rates, and these pathogens were highly resistant to cefepime (95%), imipenem (92%), and levofloxacin (86%), highlighting the need to monitor resistant pathogens to reduce mortality.¹² In China, *P. aeruginosa*, *A. baumannii*, and *K. pneumoniae* were the most commonly isolated pathogens in sputum samples with the highest resistance to all antibiotics tested except colistin, indicating AMR that AMR is widespread worldwide.¹³ On the other hand, colistin, used as one of the last resort antibiotics against MDR infections, has excellent efficacy against *A. baumannii* and *K. pneumoniae*, indicating the appropriate use of colistin in our hospital.

Study Limitations

Firstly, since the study only included sputum/aspire samples, it may not reflect the resistance patterns of all microorganisms circulating in the population. Secondly, we did not separately evaluate the community and hospitalized patients or their antibiotic resistance profiles. Therefore, the study does not provide the main origin of the resistant strains. Also, molecular analysis was not performed to identify resistant strains and virulence genes in the study.

CONCLUSION

The detection of antibiotic-resistant pathogens suggests that infection control measures should be implemented alongside antibiotic resistance surveillance. Due to increasing resistance rates, more research is needed on developing alternative treatment options such as phage therapy, CRISPR-Cas 9, and new antibiotics, to combat resistant bacterial strains effectively. In addition, unnecessary and excessive use of antimicrobials should be monitored, and the community should be educated on limiting such use in the country.

MAIN POINTS

- Highly resistant pathogens were in circulation between 2018 and 2022 in Northern Cyprus.

- Close monitoring of patients and the development of alternative treatment approaches are needed to reduce antibiotic resistance to commonly used antibiotics.
- Unnecessary and excessive use of antimicrobials should be monitored in the country.

ETHICS

Ethics Committee Approval: The ethical approval of the study was obtained from the Near East University Ethical Committee (approval number: 2023/112, date: 30.03.2023).

Informed Consent: Informed consent forms were not obtained from the patients as the study was conducted retrospectively.

Footnotes

Authorship Contributions

Concept: E.G., K.S., A.A., Design: E.G., K.S., A.A., Data Collection and/or Processing: E.M.O., E.G., Analysis and/or Interpretation: E.M.O., E.G., K.S., A.A., Literature Search: E.M.O., Writing: E.M.O., E.G., K.S.

DISCLOSURES

Conflict of Interest: No conflict of interest was declared by the authors.

Financial Disclosure: The authors declared that this study had received no financial support.

REFERENCES

1. Bo L, Sun H, Li YD, Zhu J, Wurpel JND, Lin H, et al. Combating antimicrobial resistance: the silent war. *Front Pharmacol*. 2024; 15: 1347750.
2. Murugaiyan J, Kumar PA, Rao GS, Iskandar K, Hawser S, Hays JP, et al. Progress in alternative strategies to combat antimicrobial resistance: Focus on antibiotics. *Antibiotics*. 2022; 11(2): 200.
3. The World Health Organization (WHO). Antimicrobial resistance. Available from URL: <https://www.who.int/news-room/fact-sheets/detail/antimicrobial-resistance>. accessed 21 November 2023.
4. The Centers for Disease Control and Prevention (CDC). CDC Partners estimate healthcare cost of antimicrobial resistant infections Available from URL: <https://www.cdc.gov/antimicrobial-resistance/stories/partner-estimates.html> accessed at 22 April 2024.
5. World Bank. Drug-resistant infections: a threat to our economic future. Available from URL: <https://documents.worldbank.org/en/publication/documents-reports/documentdetail/323311493396993758/final-report> accessed at 18 October 2024.
6. Antimicrobial resistance: a silent pandemic. *Nat Commun* 2024; 15, 6198. doi: 10.1038/s41467-024-50457-z
7. Mancuso G, Midiri A, Gerace E, Biondo C. Bacterial Antibiotic Resistance: The most critical pathogens. *Pathogens*. 2021; 10(10): 1310.
8. Ilman MJM, Lajunen TJ, Baddal B, Apostolou M. Antibiotics knowledge, attitudes and behaviours among the population living in Cyprus. *Antibiotics (Basel)*. 2023; 12(5): 897.
9. Baddal B, Potindji TMF, Güler E. Evaluation of frequency, antimicrobial resistance and multidrug resistance patterns of methicillin-resistant *Staphylococcus aureus* isolates at a university hospital in northern Cyprus, 2016 to 2020. *Turk Hij Den Biyol Derg*. 2024; 81(1): 11-22.
10. European Society of Clinical Microbiology and Infectious Diseases (EUCAST) guidelines for the detection of resistance mechanisms and specific resistances

- of clinical and/or epidemiological importance. Available from URL: https://www.eucast.org/fileadmin/src/media/PDFs/EUCAST_files/Resistance_mechanisms/EUCAST_detection_of_resistance_mechanisms_170711.pdf. accessed 18 October 2024.
11. The World Health Organization (WHO). WHO reports widespread overuse of antibiotics in patients hospitalized with COVID-19. *Saudi Med J*. 2024; 45(5): 547-8.
 12. Ghimire R, Gupte HA, Shrestha S, Thekkur P, Kharel S, Kattel HP, et al. High drug resistance among Gram-negative bacteria in sputum samples from an intensive care unit in Nepal. *Public Health Action*. 2021; 11(1): 64-9.
 13. Hao L, Yang X, Chen H, Wei S, Xu B, Zhao Z. Distribution and drug resistance of bacterial infection in hospitalized patients at the respiratory department before and after the COVID-19 pandemic in Guangzhou, China. *Microorganisms*. 2023; 11(10): 2542.

In Vivo Assessment of a Capsaicin-Containing Microemulsion for Neuropathic Pain Management

© Rumooz Shayyah¹, © Umay Merve Güven Bölgen², © Ares Alizade³, © Serpil Demirci Kayıran⁴, © Sonia Ebrahimi⁵, © Fazilet Aksu⁶

¹Department of Biotechnology, Çukurova University Institute of Natural and Applied Sciences, Adana, Türkiye

²Department of Pharmaceutical Technology, Çukurova University Faculty of Pharmacy, Adana, Türkiye

³Department of Medical Pharmacology, Van Yüzüncü Yıl University Faculty of Medicine, Van, Türkiye

⁴Department of Pharmaceutical Botany, Çukurova University Faculty of Pharmacy, Adana, Türkiye

⁵Department of Medical Pharmacology, Near East University Faculty of Medicine, Nicosia, North Cyprus

⁶Department of Medical Pharmacology, DESAM Research Institute, Near East University Faculty of Medicine, Nicosia, North Cyprus

Abstract

BACKGROUND/AIMS: Capsaicin (CAP) has been used in clinical applications for the treatment of neuropathic pain (NP). The main disadvantages of CAP are its short half-life, low water solubility and low bioavailability. This study intended to produce a therapeutically effective microemulsion (ME) formulation comprising CAP to decrease NP.

MATERIALS AND METHODS: ME was prepared using oleic acid, Tween 80, propylene glycol, ethanol, and water. Neuropathy was induced by partial sciatic nerve ligation (PSL) in mice. Two weeks after, PSL NP was tested using the cold plate (CP) and von Frey (VF) tests. The mice in the treatment group were administered 10 mg/kg CAP by oral gavage. The effects on NP of conventional CAP and ME CAP were compared.

RESULTS: The prepared ME formulation of (CAP) was a homogeneous, transparent, thermodynamically stable dispersion of water and oil. The classic CAP was not effective on NP, while ME CAP was effective in the CP. The ME CAP was more effective on mice, than classic CAP using the VF test.

CONCLUSION: The developed novel ME formulation at lower doses could reduce side effects and improve the bioavailability of the oral administration of CAP in the treatment of NP, and thus, would achieve good patient compliance.

Keywords: Capsaicin, mice, microemulsion formulation, neuropathic pain

INTRODUCTION

Neuropathic pain (NP) is an inappropriate response caused by a primary lesion or dysfunction in the nervous system. It is a chronic type of pain that is difficult to treat and does not respond to known analgesics. Since

NP may not respond in part or at all to common analgesic therapies, adjuvant analgesics such as antiepileptics, antiarrhythmics, and antidepressants are widely used in the medical treatment of NP.¹ As a second line therapy, capsaicin (CAP) is recommended for NP.² CAP is an

To cite this article: Shayyah R, Güven Bölgen UM, Alizade A, Demirci Kayıran S, Ebrahimi S, Aksu F. *In vivo* assessment of a capsaicin-containing microemulsion for neuropathic pain management. Cyprus J Med Sci. 2025;10(Suppl 1):29-33

ORCID IDs of the authors: R.S. 0000-0003-4638-6327; U.M.G.B. 0000-0003-1547-0817; A.A. 0000-0003-0334-8152; S.D.K. 0000-0001-8340-3347; S.E. 0000-0001-5371-4646; F.A. 0000-0003-3585-2599.



Corresponding author: Fazilet Aksu

E-mail: faziletaksu@gmail.com

ORCID ID: orcid.org/0000-0003-3585-2599

Received: 04.11.2024

Accepted: 18.12.2024

Publication Date: 04.06.2025



Copyright © 2025 The Author. Published by Galenos Publishing House on behalf of Cyprus Turkish Medical Association.

This is an open access article under the Creative Commons Attribution-NonCommercial 4.0 International (CC BY-NC 4.0) License.

active ingredient found in chili peppers and similar plants of the capsicum plant family, and has long been used as an analgesic agent.³ There are preparations of CAP obtained from hot red pepper that can be applied to the skin as creams and patches. On the other hand, CAP has some disadvantages. The main disadvantage of CAP is its short half-life and low bioavailability. Another significant drawback of using it as a medication is the burning sensation, which negatively affects patient compliance.⁴ For this reason, various strategies such as hydrogel formation, encapsulation in liposomes, iontophoresis, and sustained-release formulations were developed to eliminate these disadvantages and ultimately increase its bioavailability. In addition, the development of drug delivery systems has intensified in recent years to enhance the bioavailability of CAP and increase its therapeutic index.⁵ Drug delivery systems have generally been developed for transdermal and oral administration of CAP.⁶ In the past years, microemulsion (ME) systems have been widely studied for their superior advantages such as ease of preparation, homogeneity, improved solubility, and permeability. MEs are transparent, thermodynamically stable dispersions of oil, water, and surfactant (S), often significantly combined with a cosurfactants (CoS). The oil-in-water (o/w) MEs seem to be promising because they can dissolve components with poor water solubility in the oil phase, enhancing their solubility.⁷ Therefore, in this study, we aimed to develop an orally effective delivery system, o/w MEs, in order to increase the solubility and *in vivo* bioavailability, and to decrease adverse effects of CAP.

MATERIALS AND METHODS

Chemicals

CAP (Sigma Aldrich, Cas no:404-86-4) as an active agent, oleic acid (Sigma Aldrich, Cas no:112-80-1) as an oil phase, Tween® 80 (Sigma Aldrich, Cas no:9005-65-6) as a S, propylene glycol (Sigma Aldrich, Cas no:57-55-6) and ethanol (Sigma Aldrich, Cas no:64-17-5) as co-S and water as an aqueous phase.

Ternary Phase Diagram Construction

The preparation of a self-emulsifying system used pseudo-ternary phase diagrams of MEs. The regions such as the ME and nanoemulsion, which vary according to the amount and ratio of oil, water, and S, were determined on the pseudo ternary phase diagrams.⁸ Different concentrations of S and CoS were studied with oleic acid, Tween® 80, propylene glycol, and ethanol. Tween® 80 was used as a S while propylene glycol and ethanol were selected as the CoS in an S/CoS weight ratio of 2:1, 3:2, and 3:1.⁹

Characterization of Formulation

Globule size, zeta potential, polydispersity index (PDI), and pH were measured to determine the physicochemical properties of ME. Zeta potential and globule sizes of MEs were measured using Zetasizer nano ZS (Malvern, United Kingdom) at 25 °C, and the PDI was reported. results Samples were placed in clear, one-use zeta cells, and results were obtained.⁹ After preparing the MEs, the pH value of those emulsions was measured.

Pharmacological Evaluation

25-30 g Swiss albino male mice, obtained from Çukurova University Health Sciences Experimental Application and Research Center, were used. Approval was obtained from the Çukurova University Experimental Animals Ethics Committee (approval number: 4, date: 08.07.2019). Partial sciatic nerve ligation was performed to produce neuropathy, as described previously in rats by Seltzer et al.¹⁰ In sham-operated mice, the nerve was exposed, but not ligated. NP has tested two weeks after sciatic nerve ligation using the cold plate [(CP), cold allodynia] and von Frey [(VF), mechanical allodynia] tests. CP analgesiometer (Ugo Basile, Hot/CP Analgesia, Italy, Cat. No. 35150) and VF filaments (Ugo Basile, VF Hairs, Semmes-Weinstein set of monofilaments, Code: 37450-275) were used for CP and VF tests, respectively. In the CP test, mice were placed on a metal plate at 5 degrees and their reaction times [CP latency (CPL)] were measured.¹¹ In the VF test, the filaments are applied on the plantar surfaces of mice's feet with a series of increasing forces until the animal gives a reaction [VF Threshold (VFTH)].¹² A dose of 10 mg/kg (ME CAP), and a dose of 10 mg/kg classic CAP, were administered via oral gavage, 2 h before the tests. The placebo (control) group was given a placebo without active pharmaceutical ingredients.

Statistical Analysis

Variables were summarized as mean and standard deviation. For comparison of groups, One-Way ANOVA was used. Tukey's Games-Howell tests were used for multiple comparisons of groups regarding the homogeneity of variances. IBM SPSS Statistics Version 20.0 statistical software package was used to perform all analyses. The statistical level of significance for all tests was considered to be 0.05 (IBM Corp. Released 2011).

RESULTS

The ternary phase diagram describes the ideal experimental conditions, for putting the components together to form a clear preparation. The S and CoS were weighed at different ratios (2:1, 3:2 and 3:1) in each tube. The pseudo-ternary phase diagram has been created by means of a computer program. The percentage of ME area in most of phase diagrams was largest at an S/CoS weight ratio of 2:1, compared to others (Table 1). The prepared blank and CAP -loaded MEs were clear, transparent, liquid, single-phase, free of drug precipitation, and homogeneous in appearance. Table 1 shows the physicochemical parameters of MEs in the presence and absence of CAP.

CPL and VFTH of the groups were measured two weeks after the neuropathy and sham operation. ME CAP and classic CAP were administered by oral gavage 2 hours before the tests. According to results, CPL and VFTH of the sham group were not different from the control, whereas a significant decrease was observed in the CPL and VFTH in the NP group (Figures 1, 2 respectively). In experiments examining the effects of ME CAP and classical CAP on NP, it was observed that CPL of the ME CAP group was significantly increased; however, CPL of the classical CAP group was not increased compared to

Table 1. Optimum formulation ingredients and characterization of microemulsion formulations

Code/formulation	Oil (%)	Water (%)	S (%)	CoS (%)	CAP (%)	pH	Zeta potential (mV)	Globule size (nm)	PDI
Splacebo	7.6	34.5	38.6	19.3	-	5.42±0.01	0.56±0.18	124.6±2.8	0.2±0.02
Scapsaicin	7.6	34.2	38.6	19.3	3	5.31±0.02	0.60±0.36	156.6±3.4	0.3±0.04

CoS: Cosurfactant, CAP: Capsaicin, S: Surfactant, PDI: Polydispersity index.

the NP group (Figure 3). According to these results, the ME CAP reduced NP in CP test, but classic CAP did not show any effect on NP. On the other hand, both classic CAP and ME CAP decreased NP in the VF test. Furthermore, a significant increase in VFTH was observed in the ME CAP group compared with the classic CAP group in the VF test (Figure 4). It can be suggested that ME CAP is more effective on NP than classic CAP

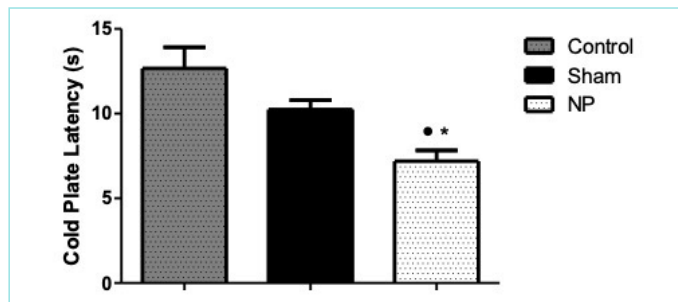


Figure 1. CPL latencies in Control, Sham and NP groups. One-way ANOVA, according to Tukey’s multiple comparison test: *: Significantly different from the control group. (p<0.05). •: Significantly different from Sham group (p<0.05).

CPL: Cold plate latency, NP: Neuropathic pain.

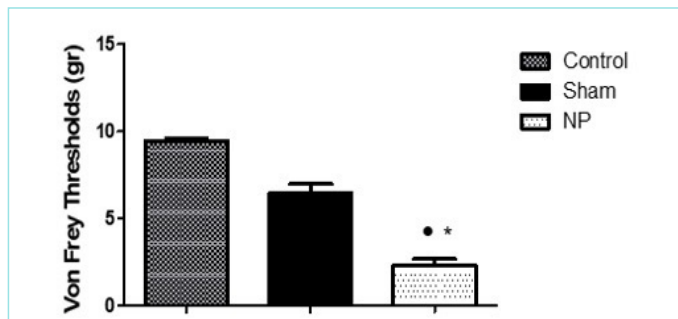


Figure 2. VFTH in control, sham and NP groups. One-Way ANOVA, according to Tukey’s multiple comparison test; *: Significantly different from the control group. (p<0.05). •: Significantly different from Sham group (p<0.05).

VFTH: von Frey Thresholds, NP: Neuropathic pain.

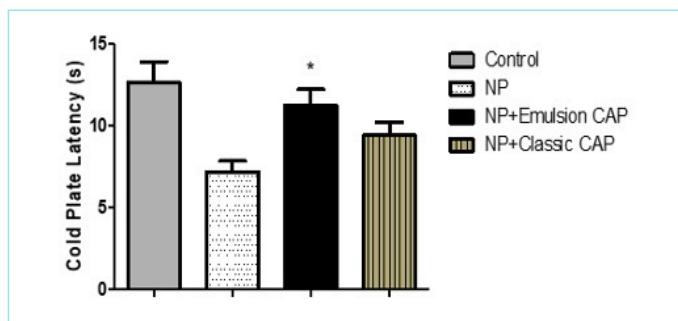


Figure 3. The effects of ME and classic CAP Formulation in the CP test. One-Way ANOVA, according to Tukey’s multiple comparison test; *: Significantly different from the NP group (p<0.05).

ME: Microemulsion, CAP: Capsaicin, CP: Cold plate, NP: Neuropathic pain.

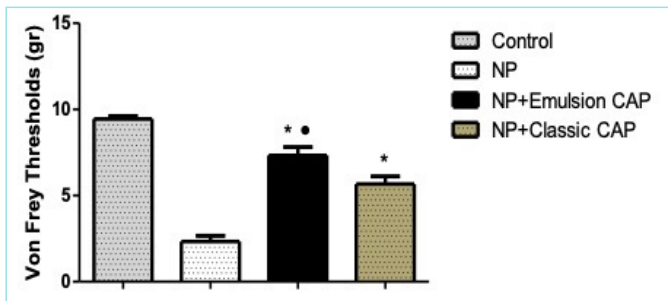


Figure 4. The effects of ME and Classic CAP Formulation in the VF test. One-Way ANOVA, according to Tukey’s multiple comparison test: *: Significantly different from the NP group (p<0.05), •: Significantly different from NP + classic CAP group (p<0.05).

ME: Microemulsion, CAP: Capsaicin, VF: von Frey, NP: Neuropathic pain.

in the VF test.

DISCUSSION

Nanotechnological drug delivery systems like MEs have been widely investigated for a variety of pharmaceutical applications. MEs, with their excellent solubilization, permeability, and bioavailability-enhancing properties, have already been applied in clinics to improve oral drug delivery.¹³ Globule sizes of CAP loaded formulations were slightly larger than the blank formulations, but this difference was not statistically significant (p>0.05). Based on previous studies, the pH value of these formulations is suitable for oral administration, and there are no significant differences between them (Table 1). The Zeta potential value is crucial for studying emulsion stability.¹⁴ Due to compounds like non-ionic S, the zeta potential of MEs is nearly neutral.

In a study conducted by Sethuram and Thomas¹⁵, ME-loaded nanofibrous membranes with a homogeneous distribution were fabricated. The developed formulations demonstrated controlled and sustained release in the wound environment and were suggested to be suitable for use in wound infection treatment. In another study, baicalin-loaded MEs were found to improve transdermal delivery by enhancing solubility, skin permeation, and retention. Additionally, the formulation demonstrated good efficacy and a high safety profile in anti-inflammatory and analgesic experiments.¹⁶

In our study, the pSLN model, defined by Seltzer et al.¹⁰ was used to create experimental NP. Pain behaviors observed in animals in the pSLN model are similar to many symptoms (allodynia; hyperalgesia) in humans with NP syndrome.¹⁷ It was shown that cold allodynia and mechanical allodynia, which are the most important symptoms of NP, occur as a result of partial ligation of the sciatic nerve.¹⁸ The use of the sciatic nerve to create experimental peripheral NP is common because it is easy to access and suitable for performing paw tests.

As a result of the CP test, there was no significant difference between the CPL of control and sham groups; however, the CPLs of the animals ligated to the sciatic nerve (NP group) were significantly lower than those of the control and sham groups (Figure 1). This result shows that cold allodynia occurs with our method and is consistent with the literature and the results of our previous studies.¹⁹⁻²⁰ In addition, ME CAP significantly prolonged CPL compared to the NP group, but no difference was observed between classical CAP and the NP group in the CP test. According to this result, ME CAP is effective for NP pain, but

classic CAP is not, and we may say that ME CAP is superior to classic CAP in the CP test (Figure 3).

In the VF test, the VFTH of the animals in the control and sham groups was similar, and there was no significant difference between them. However, the VFTH of sciatic nerve ligated mice (NP group) was significantly reduced when compared to the control and sham groups (Figure 2). This result shows that mechanical allodynia occurs with our method, and the results are consistent with the literature.^{22,23} Differently from CP test both ME CAP and classic CAP groups were effective on NP in VF test. Furthermore, a significant increase in VFTH was observed in the ME CAP group compared with the classic CAP group (Figure 4). Thus, we can say that the novel ME CAP formulation is more effective than classic CAP formulation in VF test.

We found that the o/w ME CAP formulation seems to be promising because it was more effective against cold and mechanical allodynia. Probably this formulation improves the solubility, absorption, and thus bioavailability of CAP. It is reported that oral CAP ingestion may cause several side effects because it needs to be used in high doses to be effective.²⁴ On the other hand, topical CAP causes a burning sensation.⁴ So, our study provided the opportunity to develop a preparation suitable for oral use. These results show that the new oral formulation prepared in the study can be used at lower doses, thus having fewer side effects and providing better patient compliance.

Study Limitations

In this study, although we planned to investigate the effectiveness of CAP in NP by preparing new oral and topical formulations, only the oral formulation was prepared and its effectiveness was examined. The main purpose of the study was to prepare a more effective oral formulation. If there was no response to the oral formulation, we considered the topical formulation, as plan B. Since the expected results were obtained from the oral formulation we prepared, the topical formulation was not studied, in order not to use more animals in terms of animal ethics.

CONCLUSION

While classical CAP was not effective against cold allodynia due to NP, the new oral CAP formulation was found to be effective, which was the purpose of this study. Furthermore, the new formulation was found to be more effective against mechanical allodynia due to NP than the oral form currently used. Based on these results, the effects of the new formulation we have prepared warrant further detailed examination with additional studies. In conclusion, the developed ME formulation improves the solubility of CAP, enhances its oral bioavailability, and is a promising basis for further development as a formulation for oral administration.

MAIN POINTS

- By using a titration method with a small particle size and polydispersity index range, a capsaicin (CAP)-loaded microemulsion (ME) can be successfully prepared.
- Classical CAP is ineffective against cold allodynia, but is effective against mechanical allodynia.
- CAP prepared in ME form is effective against both cold allodynia and mechanical allodynia.

- The ME formulation of CAP is more effective than classical CAP in the treatment of neuropathic pain.
- The oral efficacy of drugs can be increased by administering them in ME form.

ETHICS

Ethics Committee Approval: Approval was obtained from the Çukurova University Experimental Animals Ethics Committee (approval number: 4, date: 08.07.2019).

Informed Consent: Not available.

Footnotes

Authorship Contributions

Surgical and Medical Practices: R.S., A.A., S.E., Concept: R.S., U.M.G.B., S.D.K., F.A., Design: R.S., U.M.G.B., S.D.K., F.A., Data Collection and/or Processing: R.S., U.M.G.B., A.A., Analysis and/or Interpretation: U.M.G.B., S.D.K., F.A., Literature Search: R.S., U.M.G.B., S.D.K., S.E., Writing: R.S., U.M.G.B., S.D.K., F.A.

DISCLOSURES

Conflict of Interest: No conflict of interest was declared by the authors.

Financial Disclosure: This study is supported by Çukurova University Research Foundation Grant No: TYL-2019-2599.

REREFENCES

1. Orza F, Boswell MV, Rosenberg SK. Neuropathic pain: review of mechanisms and pharmacologic management, *NeuroRehabilitation*. 2000; 14(1): 15-23.
2. Finnerup NB, Kuner R, Jensen TS. Neuropathic pain: from mechanisms to treatment. *Physiol Rev*. 2021; 101: 259-301.
3. Arora V, Campbell JN, Chung MK. Fight fire with fire: neurobiology of capsaicin-induced analgesia for chronic pain. *Pharmacol Ther*. 2021; 220: 107743.
4. Üçeyler N, Sommer C. High-dose capsaicin for the treatment of neuropathic pain: what we know and what we need to know. *Pain Ther*. 2014; 3(2): 73-84.
5. Rollyson WD, Stover CA, Brow KC, Perry HE, Stevenson CD, McNees CA, et al. Bioavailability of capsaicin and its implications for drug delivery. *J Control Release*. 2014;196: 96-105.
6. Peppin JF, Pappagallo M. Capsaicinoids in the treatment of neuropathic pain: a review. *Ther Adv Neurol Disord*. 2014; 7(1): 22-32.
7. Bajaj A, Rao MR, Khole I, Munjapara G. Self-nanoemulsifying drug delivery system of cefpodoxime proxetil containing tocopherol polyethylene glycol succinate. *Drug Dev Ind Pharm*. 2013; 39(5): 635-45.
8. Gursoy RN, Benita S. Self-emulsifying drug delivery systems (SEDDS) for improved oral delivery of lipophilic drugs, *Biomed Pharmacother*. 2004; 58(3): 173-82.
9. Güven UM, Kayıran SD, Aygül A, Nenni M, Kirici S. Design of microemulsion formulations loaded *Scutellaria salviifolia* Benth, *Sideritis libanotica* Labill. subsp. *linearis* (Benth) Bornm, and *Ziziphora clinopodioides* Lam. extracts from Turkey and in vitro evaluation of their biological activities. *Turk J Bot*. 2021; 45(8): 789-99.
10. Seltzer ZE, Dubner R, Shir Y. A novel behavioral model of neuropathic pain disorders produced in rats by partial sciatic nerve injury. *Pain*. 1990; 43(2): 205-18.

11. Ji G, Zhou S, Kochukov MY, Westlund KN, Carlton SM. Plasticity in intact A δ -and C-fibers contributes to cold hypersensitivity in neuropathic rats. *Neuroscience*. 2007; 150(1): 182-93.
12. Deuis JR, Dvorakova LS, Vetter I. Methods used to evaluate pain behaviors in rodents. *Front Mol Neuroscience*. 2017; 10: 284.
13. Kalepu S, Nekkanti V. Insoluble drug delivery strategies: review of recent advances and business prospects. *Acta Pharm Sin B*. 2015;5: 442-53.
14. Bhatt N, Prasad RK, Singh K, Panpalia G.M. Stability study of O/W emulsions using zeta potential. *J Chem Pharm Res*. 2010; 2(1): 512-27.
15. Sethuram L, Thomas J. Synthesis, fabrication and biosafety profiles of biobased microemulsions reinforced electrospun nanofibers for wound dressing applications. *Nano-Struct. Nano-Objects*. 2023; 33: 100940.
16. Wang Y, Liu M, Li J, Jiang P, Han D, Zhang H, et al. Preparing a novel baicalin-loaded microemulsion-based gel for transdermal delivery and testing its anti-gout effect. *Saudi Phar J*. 2024; 32(6): 102100.
17. Bennett GJ, Xie YK. A peripheral mononeuropathy in rat that produces disorders of pain sensation like those seen in man. *Pain*. 1988; 33(1): 87-107.
18. Korah HE, Cheng K, Washington SM, Flowers ME, Stratton HJ, Patwardhan A, et al. Partial sciatic nerve ligation: a mouse model of chronic neuropathic pain to study the antinociceptive effect of novel therapies. *J Vis Exp*. 2022; 6: 188.
19. Mete S, Aksu F. The role of nitrergic system on the effects of tramadol and agmatine in an experimental neuropathic pain model. *Cukurova Med J*. 2015; 40(1): 42-54.
20. Senay Dagilgan, Seref Erdogan, Fazilet Aksu. Tramadol reverses the effects of neuropathic pain on oocyte maturation and copulation ratio in mice. *Eurasian J Med*. 2018; 50(3): 182-6.
21. Yalcin I, Megat S, Barthas F, Waltisperger E, Kremer M, Salvat E, et al. The sciatic nerve cuffing model of neuropathic pain in mice. *J Vis Exp*. 2014; 89: 51608.
22. Richner M, Bjerrum OJ, Nykjaer A, Vaegter CB. The spared nerve injury (SNI) model of induced mechanical allodynia in mice. *J Vis Exp*. 2011; 54: 3092.
23. Arnold JT, Stewart SB, Sammut L. Oral capsaicin ingestion: a brief update-dose, tolerance and side effects. *Res Rev: J Herb Sci*. 2016; 5(2): 2278-57.

Investigation of Behavioral Changes and Histopathological Changes in the Brain in Alzheimer's Modeled Mice with Aluminium Chloride (AlCl₃)

© Derya Deniz Kanan¹, © Işıl Aydemir², © Ares Alizade³, © Sonia Ebrahimi⁴, © Fazilet Aksu⁵

¹Department of Physiology, Niğde Ömer Halisdemir University Faculty of Medicine, Niğde, Türkiye

²Department of Histology, Niğde Ömer Halisdemir University Faculty of Medicine, Niğde, Türkiye

³Department of Medical Pharmacology, Van Yüzüncü Yıl University Faculty of Medicine, Van, Türkiye

⁴Department of Medical Pharmacology, Near East University Faculty of Medicine, Nicosia, North Cyprus

⁵Department of Medical Pharmacology, DESAM Research Institute, Near East University Faculty of Medicine, Nicosia, North Cyprus

Abstract

BACKGROUND/AIMS: Aluminium (Al) is related with many brain diseases including Alzheimer's disease, however the relation between Al and neurodegenerative diseases is still controversial. In this study behavioral and histopathological changes were investigated in the AlCl₃ induced Alzheimer's model in mice.

MATERIALS AND METHODS: Male and female mice divided into control (tap water) and test (50 mg/kg/day AlCl₃) groups. After ninety days of AlCl₃/water intake, rota rod, elevated plus maze, Passive Avoidance tests were performed to assess motor coordination, spatial and emotional learning and memory, respectively. After the behavioural experiments, histopathological examination was made in the brain.

RESULTS: No difference was found between the groups and the genders in the rota-rod test. Learning and memory were impaired in both gender. Long term memory impaired female mice in the test group. Neuron loss was observed in both the cerebral cortex and hippocampus CA1 regions in the test group, while an increase in pycnotic nucleated cells was observed. Neurofibrillary tangles were also observed in the hippocampus, with neurons with basophilic nuclei prominently.

CONCLUSION: As a result, long-term exposure to low doses of aluminum may cause behavioral changes and histopathological changes in the brain.

Keywords: Aluminium chloride, Alzheimer's disease, behaviour, learning, memory, mice

INTRODUCTION

Alzheimer's disease (AD) is a neurodegenerative illness. The most important symptoms of progressive and irreversible AD are memory loss, decreased cognitive functions, and disorders in spatial perception, daily life activities, and speech.¹ The most important pathological

findings of the disease are neurofibrillary tangles (NFT) and amyloid beta plaque formation.² In addition, factors such as oxidative stress, inflammation, and glutamate excitotoxicity are also thought to promote this neurodegeneration.³⁻⁵ The pathophysiology of the disease is still not completely elucidated, and the search for new treatments continues.

To cite this article: Kanan DD, Aydemir I, Alizade A, Ebrahimi S, Aksu F. Investigation of behavioral changes and histopathological changes in the brain in Alzheimer's modeled mice with aluminium chloride (AlCl₃). Cyprus J Med Sci. 2025;10(Suppl 1):34-37

ORCID IDs of the authors: D.D.K. 0000-0002-4357-4966; I.A. 0000-0002-4143-7319; A.A. 0000-0003-0334-8152; S.E. 0000-0001-5371-4646; F.A. 0000-0003-3585-2599.



Corresponding author: Fazilet Aksu

E-mail: faziletaksu@gmail.com

ORCID ID: orcid.org/0000-0003-3585-2599

Received: 05.11.2024

Accepted: 17.12.2024

Publication Date: 04.06.2025



Copyright © 2025 The Author. Published by Galenos Publishing House on behalf of Cyprus Turkish Medical Association.

This is an open access article under the Creative Commons Attribution-NonCommercial 4.0 International (CC BY-NC 4.0) License.

We aimed to investigate behavioral and histopathological changes by using an experimental AD model in mice in the present study.

MATERIALS AND METHODS

Animals, Chemical and Experimental Design

Study approval was obtained from the Animal Ethics Committee of Çukurova University (approval number: 2020/09, date: 10.12.2020). Swiss albino mice were obtained from Health Sciences Experimental Application and Research Center of Çukurova University. Mice were kept in standard conditions. Male and female control groups (n=20) and experimental groups (n=30) were created. Control groups were given tap water while the test (AlCl₃) group was given AlCl₃ solution (50 mg/kg/day) via a feeding bottle for ninety days.

The Rota Rod test was used to evaluate the motor coordination of the mouse on a rotating rod (10 rpm).⁶ Learning and spatial memory were evaluated by using the elevated plus maze (EPM) test.⁷ Long-term memory was examined using the Passive Avoidance (PA) test.⁸

Histological Analysis

The brains were fixed with 10% neutral formalin solution, and a routine paraffin embedding protocol was performed. Hematoxylin and eosin staining was performed. The differences between the groups were evaluated under a light microscope with a camera attachment.⁹

Statistical Analysis

Categorical measurements were expressed as numbers and percentages, and numerical measurements as mean and standard deviation (median and interquartile range where appropriate). Whether the numerical measurements met the assumption of normal distribution was assessed using the Shapiro-Wilk test. In the comparison of numerical

measurements between the groups, Student's t-test for independent groups was used if the assumptions were met and Mann-Whitney U test was used if the assumptions were not met. The IBM SPSS Statistics version 20.0 software package was used. Statistical significance was decided when p<0.05

RESULTS

No significant difference was found between the AlCl₃ and the control groups of each sex in the Rota Rod test.

According to EPM test, there was no difference between the sexes in the control mice, while a statistically significant difference was found between male and female mice in the AlCl₃ group (p<0.05, Table 1). The latency time (LT) of male and female mice in the light arm decreased, while LT in the dark arm increased, on the second day. These time changes were statistically significant in female mice (p<0.05).

In the PA test setup, the time spent by mice in the light and in the dark box (LT), for 300 seconds was recorded. There was a significant difference between male and female mice with regard to LT in the light box in the AlCl₃ group (p<0.05, Table 2). No significant difference was found between male and female mice in the control group.

Histopathologic Findings

Cerebral cortex regions of all groups were examined using hematoxylin and eosin staining. The histologic structure of the cerebral cortex regions of male and female mice belonging to the control group was found to be normal. Six layers, including stratum granularis externa and interna, stratum pyramidalis externa and interna, and stratum multiformis, were preserved from the pia mater to the medulla. Especially in pyramidal neurons, the cell borders were smooth and the cell nuclei were round and centrally located (Figure 1).

Table 1. Two-day comparison of the time (sec.) spent by male and female mice in the elevated plus maze

Groups	Day 1 LT (light arm) (X ± SD, sec), p-value	Day 2 LT (light arm) (X ± SD, sec.), p-value	Day 1 LT (dark arm) (median ± IQR, sec.), p-value	Day 2 LT (dark arm) (median ± IQR, sec.), p-value
Control male (n=9); Control female (n=6)	105.1±15.5 112.3±9.1 0.325	82.1±28.7 88.7±25.2 0.657	20.0±24.0 5.0±15.0 0.388	53.0±48.0 32.0±27.0 0.689
AlCl ₃ -t male (n=12); AlCl ₃ -t female (n=11)	115.2±8.7 94.4±16.8 0.001*	102.9±22.2 88.8±21.8 0.140	0.0±9.5 28.0±14.0 0.001*	5.0±39.0 32.0±34.0 0.134

Data are presented as mean ± standard deviation for normally distributed groups and median ± interquartile range for non-normally distributed groups. *Shows significance in AlCl₃ group female mice. LT: Latency time, SD: Standard deviation, IQR: Interquartile range.

Table 2. Comparison of the time (sec.) spent by male and female mice in the Passive Avoidance test

Groups	Day 1 LT (light box) (median ± IQR, sec.)	Day 2 LT (light box) (X ± SD, sec.)	Day 2 LT (dark box) (median ± IQR, sec.)
Control male (n=9) Control female (n=6)	27.0±10.0 30.0±34.0	256.1±48.6 287.8±24.6	21.0±86.0 2.0±7.0
p-value	0.102		0.224
AlCl ₃ -male (n=12) AlCl ₃ -female (n=11)	27.5±16.5 26.0±47.0	298.1±5.7 274.8±48.0	0.0±0.0 0.0±43.0
p-value	0.04*		0.566

Data are presented as mean ± standard deviation for normally distributed groups and median ± interquartile range for non-normally distributed groups. *Shows significance in AlCl₃ group female mice. LT: Latency time, SD: Standard deviation, IQR: Interquartile range.

It was found that the cerebral cortex of the $AlCl_3$ groups, consisted of six layers, but there was cellular damage. An increased number of cells with pyknotic nuclei and the formation of cerebral vacuoles was observed. The damage in the cerebral cortex of male mice was greater compared to that of female mice (Figure 2). Large euchromatic nuclei and smooth cell borders were seen in the CA1 region neurons in both sexes of control mice (Figure 3). In the CA1 region of the $AlCl_3$ groups, the number of normal-looking neurons decreased and was replaced by neurons with pyknotic nuclei and basophilic stained nuclei. Neurons with basophilic nuclei showed prominent NFT. Histopathologic findings in the hippocampus CA1 region of male mice were higher compared to the control group (Figure 4).

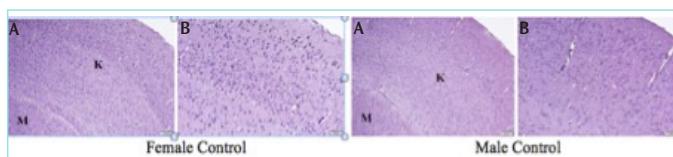


Figure 1. The histologic images of brain tissue from control female and male mice show hematoxylin and eosin staining. K: Cortex, M: Medulla. Magnifications: 100 µm (A), 50 µm (B).

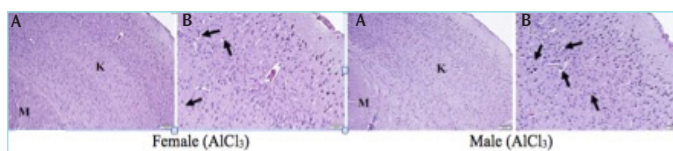


Figure 2. Histologic images of brain tissue of $AlCl_3$ group female and male mice, hematoxylin and eosin staining. K: Cortex, M: Medulla, Arrows: Cerebral vacuoles. Magnifications: 100 µm (A), 50 µm (B).

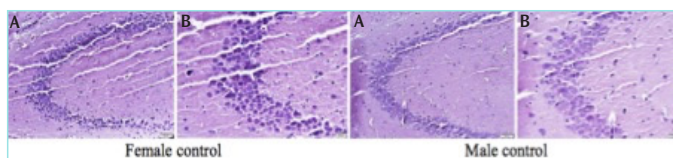


Figure 3. Histologic images of the hippocampus region of the brain of control group female and male mice, stained with hematoxylin and eosin, show characteristic features. Magnifications: 50 µm (A), 20 µm (B).

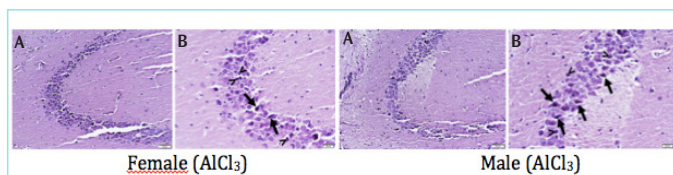


Figure 4. Histologic images of the hippocampus region of the brain of $AlCl_3$ groups female and male mice, Hematoxylin and Eosin staining. Arrows: Neurofibrillary tangles, Arrow heads: Pyknotic nucleated cells. Magnifications: 50 µm (A), 20 µm (B).

DISCUSSION

We used long-term oral administration of $AlCl_3$ to induce experimental AD, since people are exposed to aluminum in their daily lives, either in kitchen utensils or through food and medicines. Our results showed that this model is suitable for the study and in accordance with some other studies.¹⁰ The motor coordination of both control and $AlCl_3$ groups was not impaired. This result shows that the EPM and PA tests' findings are not related to a motor coordination disorder. Exploratory, anxiety, and motor behaviors, as well as memory and spatial learning, were evaluated using the EPM test in control and $AlCl_3$ groups. In their natural habitat, mice tend to explore unfamiliar environments by sniffing and crawling, and if they feel anxious and fearful, they prefer to enter a closed, dark environment. In this study, LT in the light arm decreased and LT in the dark arm increased on the second day in the control and $AlCl_3$ groups. The decrease of LT in the light arm and the increase of LT in the dark arm, were statistically significant in the control group mice. This was an expected result, as control mice learned the safe area on the first day and remembered it on the second day, whereas memory was impaired in mice receiving $AlCl_3$. In terms of gender, no difference was found between the control group and the treatment group mice. On the other hand, a significant difference was found in female mice in the $AlCl_3$ group. In fact, AD is more common in women.¹¹ Emotional, and long-term memory and learning were assessed in the PA test. Female mice entered the closed box earlier, while male mice stayed in the light box longer. The findings here corroborate those of the EPM. Female mice were more stressed than male mice and had an increased desire to enter the dark zone. However, despite the electric shock on the second day, the female mice entered the closed box before the male mice. Based on these findings, it may be suggested that long-term memory is more impaired in female mice with an Alzheimer's model than in male mice.

It was observed that the histologic structure of the control group was normal, while in the $AlCl_3$ group, the cells were damaged, and the number of cells with pyknotic nuclei increased. In the $AlCl_3$ group, the normal-appearing number of neurons in the hippocampus CA1 region was decreased. NFTs were prominently seen in neurons with basophilic nuclei in the hippocampus. These findings were in accordance with some other studies.^{12,13} In histopathologic examinations, no change was observed in the control group, but damage was observed in the CA1 region of the cortex and hippocampus, in male and female mice in the $AlCl_3$ group.

Study Limitations

Although we had made plans to measure, we could not measure serum Brain-Derived Neurotrophic Factor concentrations because the ELISA kits could not be obtained on time. We evaluated aluminum effects on AD, using behavioral and histopathological examinations.

CONCLUSION

In our study, aluminum exposure was found to cause changes in behavior and negatively affect learning and memory. Histopathological examinations have also shown changes in the brain.

MAIN POINTS

- Long-term oral use of low-dose $AlCl_3$ can be used in Alzheimer's disease research as an experimental model.

- Long-term exposure to aluminum can impair learning and memory.
- Female mice were more affected by aluminum than male mice.

ETHICS

Ethics Committee Approval: Study approval was obtained from the Animal Ethics Committee of Çukurova University (approval number: 2020/09, date: 10.12.2020).

Informed Consent: Patient approval has not been obtained as it is performed on animals.

Acknowledgements: The authors thank to Assoc. Prof. İlker Ünal (Çukurova Faculty of Medicine, Department of Biostatistics) for his kindly contribution to statistical analysis of this study.

Footnotes

Authorship Contributions

Surgical and Medical Practices: D.D.K., I.A., A.A., S.E., Concept: D.D.K., I.A., F.A., Design: D.D.K., F.A., Data Collection and/or Processing: D.D.K., I.A., A.A., Analysis and/or Interpretation: D.D.K., I.A., F.A., Literature Search: D.D.K., I.A., S.E., F.A., Writing: D.D.K., I.A., F.A.

DISCLOSURES

Conflict of Interest: No conflict of interest was declared by the authors.

Financial Disclosure: This study was supported by Çukurova University Research Foundation Grant No: TYL-2021-13480.

REFERENCES

1. Sonkusare SK, Kaul CL, Ramarao P. Dementia of Alzheimer's disease and other neurodegenerative disorders-memantine, a new hope. *Pharmacol Res.* 2005; 51(1): 1-17.
2. Haass C, Selkoe DJ. Soluble protein oligomers in neurodegeneration: lessons from the Alzheimer's amyloid beta-peptide. *Nat Rev Mol Cell Biol.* 2007; 8(2): 101-12.
3. Chong ZZ, Li F, Maiese K. Stress in the brain: novel cellular mechanisms of injury linked to Alzheimer's disease. *Brain Res Rev.* 2005; 49(1): 1-21.
4. Salminen A, Ojala J, Kauppinen A, Kaarniranta K, Suuronen T. Inflammation in Alzheimer's disease: amyloid- β oligomers trigger innate immunity defence via pattern recognition receptors. *Prog Neurobiol.* 2009; 87(3): 181-4.
5. Hynd MR, Scott HL, Dodd PR. Glutamate-mediated excitotoxicity and neurodegeneration in Alzheimer's disease. *Neurochem Int.* 2004; 45(5): 583-95.
6. Nehru B, Verma R, Khanna P, Sharma SK. Behavioral alterations in rotenone model of Parkinson's disease: attenuation by co-treatment of centropheoxine. *Brain Res.* 2008; 1201: 122-7.
7. Carola V, D'Olimpio F, Brunamonti FE, Mangia F, Renzi P. Evaluation of the elevated plus maze and open-field tests for the assessment of anxiety-related behaviour in inbred mice. *Behav Brain Res.* 2002; 134(1-2): 49-57.
8. Moosavi M, SoukhakLari R, Moezi L, Pirsalami F. Scopolamine-induced passive avoidance memory retrieval deficit is accompanied with hippocampal MMP2, MMP-9 and MAPKs alteration. *Eur J Pharmacol.* 2018; 819: 248-53.
9. Baban D. The effect of selenium on the morphological changes in the hippocampus and cerebral cortex of scopolamine induced Alzheimer's type dementia rat model by histological analysis. Yeditepe University, Institute of Health Sciences, Department of Histology and Embryology, Master Thesis, 2021, İstanbul.
10. Oshima E, Ishihara T, Yokota O, Nakashima-Yasuda H, Nagao S, Ikeda C, et al. Accelerated tau aggregation, apoptosis and neurological dysfunction caused by chronic oral administration of aluminum in a mouse model of tauopathies. *Brain Pathol.* 2013; 23: 633-44.
11. Beam CR, Kaneshiro C, Jang JY, Reynolds CA, Pedersen NL, Gatz M. Differences between women and men in incidence rates of dementia and alzheimer's disease. *J Alzheimers Dis.* 2018; 64(4): 1077-83.
12. Nakanishi K, Sakakima H, Norimatsu K, Otsuka S, Takada S, Tani A, et al. Effect of low-intensity motor balance and coordination exercise on cognitive functions, hippocampal AB deposition, neuronal loss, neuroinflammation, and oxidative stress in a Mouse model of Alzheimer's disease. *Exp Neurol.* 2021; 337: 113590.
13. Padurariu M, Ciobica A, Mavroudis I, Fotiou D, Baloyannis S. Hippocampal neuronal loss in the CA1 and CA3 areas of Alzheimer's disease patients. *Psychiatr Danub.* 2012; 24: 152-8.

Renal Artery Variations and Clinical Implications: CT Angiography Study in Turkish Republic of North Cyprus Population

✉ Yasemin Küçükçiloğlu¹, ✉ Mehtap Tiryakioğlu²

¹Department of Radiology, Near East University Faculty of Medicine, Nicosia, North Cyprus

²Department of Anatomy, Near East University Faculty of Medicine, Nicosia, North Cyprus

Abstract

BACKGROUND/AIMS: Arteries of the kidneys [renal arteries (RA)] typically emerge from the sides of the abdominal aorta usually at the intervertebral disc level between the lumbar 1st and 2nd vertebrae. Due to the large quantity of renal surgeries and urological and radiological procedures, awareness of renal artery anomalies has gained importance. In this study, we aimed to examine the variations in RA within the Turkish Republic of North Cyprus (TRNC) population.

MATERIALS AND METHODS: Multidetector computed tomography angiography examinations of 108 patients were retrospectively analyzed to document the origins of the RA alongside the presence and quantity of the accessory RA.

RESULTS: RA variations were detected in 32 patients and classified into five categories. In type 1, a unilateral accessory renal artery on the right side (RaccRA) was observed in 13 patients (40.6%). In type 2, a unilateral accessory renal artery on the left side (LaccRA) was observed in 14 patients (43.8%). Type 3 was characterized by the bilateral accessory RA and was found in 3 patients (9.4%). Type 4 consisted of one case with 2 accRRA (3.1%). Type 5 was characterized by 2 RaccRA and 1 LaccRA, which reached the left renal hilum by ascending towards the left renal artery, and was encountered in only one case (3.1%).

CONCLUSION: Supernumerary RA should be considered during procedures such as vascular surgery, nephrectomy, kidney transplants, biopsies, and interventional radiology to prevent complications that could lead to kidney failure or ischemia. Further studies with larger sample sizes are needed to better understand the prevalence and clinical implications of supernumerary RA in the TRNC population.

Keywords: Renal artery, accessory renal artery, CT angiography, renal transplant

INTRODUCTION

Each kidney receives a substantial volume of blood from the heart: about 20% of cardiac output.¹ This large blood supply enables the kidneys to filter blood efficiently. The renal arteries (RA) supply blood to the kidneys and typically branch off from the abdominal aorta

(AA).² They emerge just below the superior mesenteric artery, at the level of the intervertebral disc between the first and second lumbar vertebrae (L1-L2).^{1,3,4} In approximately 70% of the population, each kidney is supplied by a single RA.^{1,4,5} Each segmental branch supplies a distinct region of the kidney. Understanding RA variations is crucial

To cite this article: Küçükçiloğlu Y, Tiryakioğlu M. Renal artery variations and clinical implications: CT angiography study in Turkish Republic of North Cyprus population. Cyprus J Med Sci. 2025;10(Suppl 1):38-41

ORCID IDs of the authors: Y.K. 0000-0002-1572-1375; M.T. 0000-0001-7176-2764.



Corresponding author: Yasemin Küçükçiloğlu

E-mail: yasemin.kucukciloglu@neu.edu.tr

ORCID ID: orcid.org/0000-0002-1572-1375

Received: 04.11.2024

Accepted: 25.12.2024

Publication Date: 04.06.2025



Copyright © 2025 The Author. Published by Galenos Publishing House on behalf of Cyprus Turkish Medical Association.

This is an open access article under the Creative Commons Attribution-NonCommercial 4.0 International (CC BY-NC 4.0) License.

for clinicians performing surgeries or other interventional procedures on the kidneys.³

Accessory RA, also known as supernumerary or multiple RA, emerge from the aorta (25% of cases) or from another source, such as one of the mesenteric, lumbar, or thoracic arteries.² The origin and number of accessory RA vary and are influenced by renal embryogenesis, as the failure to eliminate mesonephric arteries leads to supernumerary RA.^{1,4,6,7} With the increase in kidney transplants, renal laparoscopy, vascular reconstruction, and various surgical, urological, and radiological procedures, awareness of RA variations has become crucial.^{1,3,4}

Accessory RA occur unilaterally in 25% of cases (equally on each side) and bilaterally in 10% of cases, entering the kidney at the renal hilum, superior pole, or inferior pole.¹ The widespread use of multidetector computed tomography (CT) angiography (CTA) has enhanced knowledge about the deviations in the arterial blood supply to the kidneys.³

This study aims to investigate RA variations in the Turkish Republic of North Cyprus (TRNC) population using CTA and to compare the findings with existing literature. To our knowledge, this is the first study to investigate RA variations in the TRNC population.

MATERIALS AND METHODS

This study was piloted in collaboration with the Anatomy and Radiology departments of Near East University, Faculty of Medicine, Lefkosa, TRNC.

One hundred and eight CTA images of 25 female and 83 male patients in the population of the TRNC were retrospectively evaluated. In this study, the vertebral level where the RA originate from the AA as well as the numbers and branching patterns of the existing accessory arteries were taken into consideration.

The study received approval from the Near East University Ethics Committee (approval number: 2019/73-906, date: 24.10.2019).

Statistical Analysis

RA variations were detected in 32 of 108 patients and grouped in five categories (Table 1).

Table 1. Renal artery variations were detected in 32 cases out of 108 CTA images (29.6%). Five types of cases were grouped according to the numbers, sides, and branching patterns of the accessory renal arteries. Blue lines represent the abdominal aorta and the main renal arteries, while yellow lines represent the right and/or left accessory renal arteries

types of the RA variations	number of the cases (n)	branching patterns of the renal arteries coming out of the abdominal aorta				%
		x3	x7	x3		
type 1	13					40,6
type 2	14					43,8
type 3	3					9,4
type 4	1					3,1
type 5	1					3,1
TOTAL	32					100

RA: Renal artery, CTA: Computed tomography angiography.

RESULTS

RA variations were observed in 32 patients and categorized into five types (Table 1):

Type 1: Unilateral right accessory renal artery (RaccRA) in 13 patients (40.6%) (Figure 1).

Type 2 was found: Unilateral left accessory renal artery (LaccRA) in 14 patients (43.8%) (Figure 2).

Type 3: Bilateral accessory RA on each side in 3 patients (9.4%) (Figure 3).

Type 4: Two RaccRAs in 1 patient (3.1%).

Type 5: Two RaccRAs and one LaccRA ascending toward the left RA, reaching the left renal hilum, in 1 patient (3.1%) (Figure 4).

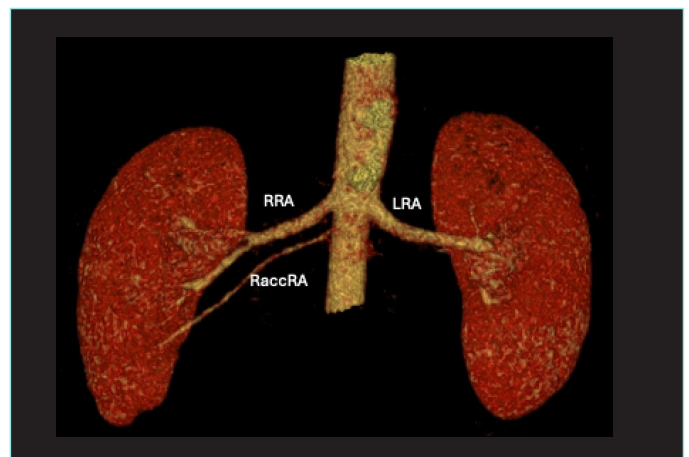


Figure 1. Type 1: the RaccRA runs inferior to the main renal artery. RRA: Right renal artery, LRA: Left renal artery, RaccRA: Right accessory renal artery.

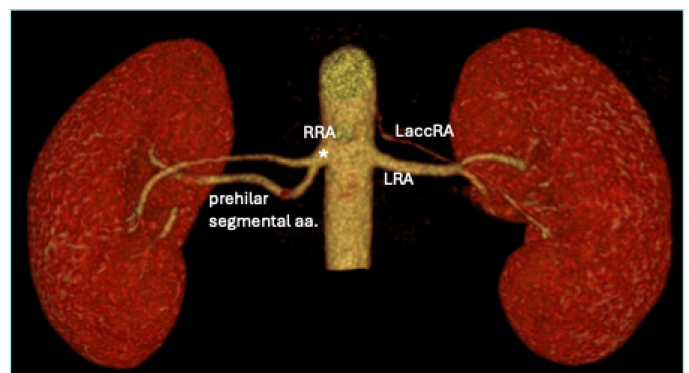


Figure 2. Type 2: the early segmental branches originated from the short main RRA, while LaccRA originated from the lateral aspect of the AA superior to the LRA and crossed the main artery to enter the renal hilum. RRA: Right renal artery, LaccRA: Left accessory renal artery, AA: Abdominal aorta, LRA: Left renal artery.

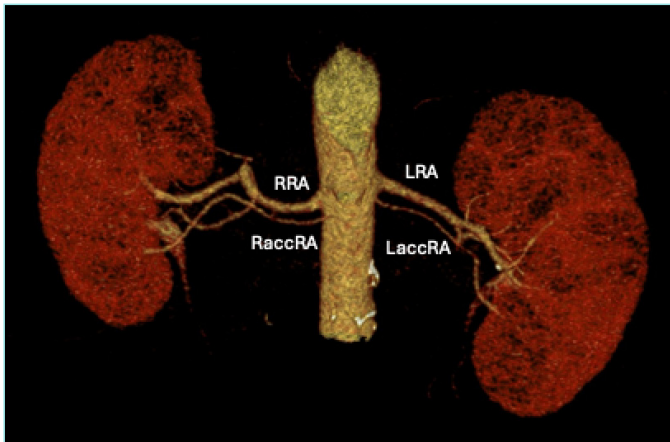


Figure 3. Type 3: the bilateral accRAs arose inferior to the main renal arteries.

RRA: Right renal artery, LRA: Left renal artery, RaccRA: Right accessory renal artery, LaccRA: Left accessory renal artery.

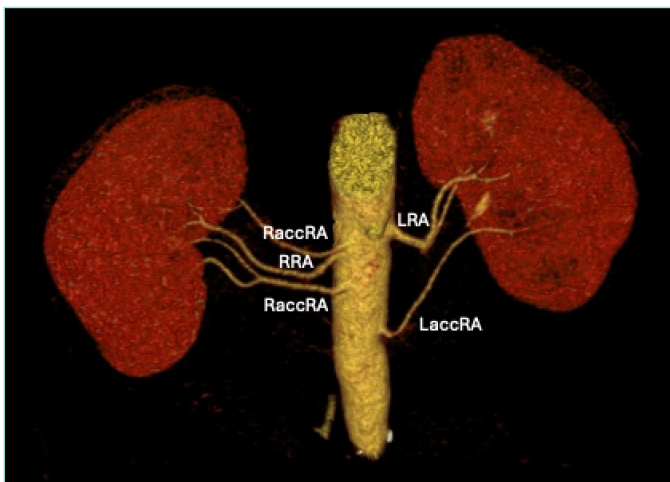


Figure 4. Type 5: 2 RaccRAs one on the inferior and another on the superior to the main renal artery (RRA). LaccRA is reaching the left renal hilum by ascending towards the LRA.

RRA: Right renal artery, LRA: Left renal artery, RaccRA: Right accessory renal artery, LaccRA: Left accessory renal artery.

DISCUSSION

While a single RA supplies each kidney in 70% of cases, this study found RA variations in 32 of the 108 cases (29.6%), consistent with literature findings.^{1,4,5,8}

In our study, type 1 consisted of a unilateral RaccRA, while type 2 involved a unilateral LaccRA. All accessory RA in this sample originated from the AA, in line with other studies, although the literature notes rare cases where accessory RAs arise from other sources, like the inferior or superior mesenteric artery, lumbar, iliac arteries, or other visceral sources.^{1,4} Abba et al.⁴ in their case report, found an accessory right RA originating from the AA at the level of L3 vertebra in a male cadaver.

Prehilar branching was noted in 3.1% of cases in our study. In the study by Kornafel et al.⁵, prehilar branching was found in 24 (11.9%) patients.

Additionally, we observed bilateral accessory RAs in 3 cases (9.4%), which aligns with the literature. Kornafel et al.⁵ found bilateral accessory RAs in 20 (10%) patients.

Previous literature has documented cases with 2-6 RAs on one side (commonly the right). In this study, the maximum number of RA observed was 5, found in a case with 2 RaccRA, and 1 LaccRA (Figure 4). Interestingly, accessory RA were seen in 12% of female CTAs compared to 35% of male CTAs, a variation that has shown significant differences across populations.

Given the risk of anastomotic complications due to the presence and complicated branching patterns of accessory RA, patients with these deviations are generally not preferred as surgical donors.^{7,8}

Study Limitations

Our study has some limitations. The most important limitation is the small size of the study group. We believe that further studies with larger study groups may reveal new, previously unreported variations of CT. The second limitation is the low quality of some figures due to patient-related factors or technical issues.

CONCLUSION

Supernumerary RA should be considered during procedures such as vascular surgery, nephrectomy, kidney transplants, biopsies, and interventional radiology to prevent complications that could lead to kidney failure or ischemia. Further studies with larger sample sizes are needed to understand better the prevalence and clinical implications of supernumerary RA in the TRNC population.

MAIN POINTS

- About 30% of populations have accessory renal arteries (RA).
- The origin and number of accessory RA vary and are influenced by renal embryogenesis.
- The variations in renal vascularity should be considered during procedures to prevent complications that could lead to kidney failure or ischemia.

ETHICS

Ethics Committee Approval: The study received approval from the Near East University Ethics Committee (approval number: 2019/73-906, date: 24.10.2019).

Informed Consent: Retrospective study.

Footnotes

Authorship Contributions

Surgical and Medical Practices: Y.K., Concept: Y.K., M.T., Design: Y.K., M.T., Data Collection and/or Processing: Y.K., M.T., Analysis and/or Interpretation: Y.K., M.T., Literature Search: Y.K., M.T., Writing: Y.K., M.T.

DISCLOSURES

Conflict of Interest: No conflict of interest was declared by the authors.

Financial Disclosure: The authors declared that this study had received no financial support.

REFERENCES

1. Leckie A, Tao MJ, Narayanasamy S, Khalili K, Schieda N, Krishna S. The renal vasculature: what the radiologist needs to know. *Radiographics*. 2021; 41: 1531-48.
2. Standring S, Borley NR, Gray H. *Gray's Anatomy: The Anatomical Basis of Clinical Practice*. Churchill Livingstone/Elsevier. 2008: pp. 1074.
3. White RD, Moore KS, Salahia MG, Thomas WR, Gordon AC, Williams IM, et al. Renal arteries revisited: anatomy, pathologic entities, and implications for endovascular management. *Radiographics*. 2021; 41(3): 909-28.
4. Abba S, Tesfay A, Ekanem P. Accessory renal artery and its clinical significance. *Int J Anat Res*. 2013; 3: 155-7.
5. Kornafel O, Baran B, Pawlikowska I, Laszczyński P, Guziński M, Sęsiadek M. Analysis of anatomical variations of the main arteries branching from the abdominal aorta, with 64-detector computed tomography. *Pol J Radiol*. 2010; 75(2): 38-45.
6. Cases C, García-Zoghby L, Manzorro P, Valderrama-Canales FJ, Muñoz M, Vidal M, et al. Anatomical variations of the renal arteries: cadaveric and radiologic study, review of the literature, and proposal of a new classification of clinical interest. *Ann Anat*. 2017; 211: 61-8.
7. Chow AK, Deane LA. Five supernumerary renal arteries originating from the aorta associated with ureteropelvic junction extrinsic compression. *Urology*. 2018; 112: 5-6.
8. Mir NS, Ul Hassan A, Rangrez R, Hamid S, Sabia, Tabish SA, et al. Bilateral duplication of renal vessels: anatomical, medical and surgical perspective. *Int J Health Sci*. 2008; 2(2): 179-85.

Does Scan Aid Use Improve the 3D Trueness of Digital Implant Impressions with Different Inter-Implant Distances?

Sevcan Kurtulmus-Yilmaz, Tezcan Muslu, Özay Önöral

Department of Prosthetic Dentistry, Near East University Faculty of Dentistry, Nicosia, North Cyprus

Abstract

BACKGROUND/AIMS: The aim was to compare the trueness of digital scans with and without the use of scan aids in the case of different inter-implant distances.

MATERIALS AND METHODS: Three mandibular edentulous models with 4 implants were prepared by altering the inter-implant distance between the implants (12, 15, and 18 mm) on the left side. The models were lab-scanned and reference data were acquired. An intraoral scanner (iTero Element 5D Plus) was used to obtain experimental scan data of the models. Twenty digital scans were recorded from each model with or without using scan aids (n=10). The best-fitting alignment strategy (Geomagic Control 3D Systems) was used for the superimposition of the reference scan data onto the experimental scan data. Angular deviation (AD) and linear deviation (LD) were determined, and the data were statistically analyzed.

RESULTS: The inter-implant distance significantly affected both the AD and LD values only in the left posterior implants ($p<0.001$). The use of scan aid significantly improved ADs and LDs in the left anterior, left posterior, and right anterior implants ($p<0.001$). However, no significant effect was noted in the deviation values of right posterior implants ($p=0.26$ and $p=0.18$, respectively). The interaction between scan-aid use and inter-implant distance, was significant for both ADs and LDs, concerning the left posterior implant ($p<0.001$).

CONCLUSION: The use of scan aids significantly enhances the trueness of digital implant impressions, particularly in cases with varying inter-implant distances.

Keywords: All-on-4, auxiliary-device, implant-impression, scan-aid, trueness

INTRODUCTION

The advancements in digital dentistry provide a fully digital workflow in implantology (Albanchez-González, 2022). Digital implant impressions have the advantages of shorter chairside time, higher patient comfort, elimination of impression and cast materials, thereby reducing the distortion risk associated with these materials, and enhanced communication with both dental technicians and patients through the use of virtual visualization.^{1,2} The accuracy of the intraoral

scanners (IOSs) is crucial to obtaining a passive fit between the prosthetic framework and implant components. A lack of passive fit results in manifold biological and mechanical complications, which jeopardize the clinical success of implant-supported restorations.³ The span length is one of the parameters that influence the accuracy of IOSs.⁴ In short-span restorations, the accuracy of intraoral scans was comparable with conventional impressions.⁵ However, in the case of a larger span or complete edentulism, a significant decrease in the accuracy

To cite this article: Kurtulmus-Yilmaz S, Muslu T, Önöral Ö. Does scan aid use improve the 3D trueness of digital implant impressions with different inter-implant distances? Cyprus J Med Sci. 2025;10(Suppl 1):42-45

ORCID IDs of the authors: S.K.Y. 0000-0001-8792-1977; T.M. 0009-0001-0806-4610; Ö.Ö. 0000-0002-5264-9376.



Corresponding author: Tezcan Muslu
E-mail: tezcan.muslu@neu.edu.tr
ORCID ID: orcid.org/0009-0001-0806-4610

Received: 31.10.2024
Accepted: 25.12.2024
Publication Date: 04.06.2025



Copyright© 2025 The Author. Published by Galenos Publishing House on behalf of Cyprus Turkish Medical Association.
This is an open access article under the Creative Commons AttributionNonCommercial 4.0 International (CC BY-NC 4.0) License.

of digital scans has been reported.⁶⁻⁹ The absence of stable anatomic reference points on the mucosa between the implants makes the image stitching process of IOS challenging. Therefore, a larger scanning area and longer inter-implant distance lead to accumulated errors during stitching, which culminates in higher inaccuracies in impression.^{10,11} Several methods have been proposed to overcome this drawback and provide a continuous scanning path for IOSs, including creating artificial landmarks on the mucosa¹², splinting the scan bodies¹³, using scan bodies with extensions¹⁴, and employing prefabricated auxiliary geometric devices (scan aids).¹⁵⁻¹⁷ Although the employment of scan aids has been shown to improve the trueness of IOSs^{13,15,17,18}, to the best of the authors' knowledge, no consensus exists on a device that does not require complex or additional procedures for fabrication and clinical application, and that offers flexible use regardless of implant position or angulation. The available literature provides limited data on both the relationship between the inter-implant distance and intraoral scan accuracy and the threshold inter-implant distance at which a scan aid becomes necessary. This study aimed to compare the trueness of digital scans with and without the use of scan aids in the case of different inter-implant distances in all-on-4 configuration. The null hypothesis was that neither the inter-implant distance nor the scan aid use would affect the trueness of scans.

MATERIALS AND METHODS

Three mandibular edentulous models were created by pouring a self-polymerizing acrylic resin (Meliodent Rapid Repair; Kulzer GmbH, Hanau, Germany) into a mould (AG-3 Edentulous Rubber Mould; Frasaco GmbH). Four sockets were prepared on the models by a rotary instrument to place multi-unit implant analogues (Nobel Active Multiunit Analog, Ø4.8 mm, Nobel Biocare) according to the all-on-4 configuration. In all models, anterior implants were inserted in the canine region and the right posterior implant was inserted in the second premolar region. The position of the left posterior implant was altered, and distances of 12 mm, 15 mm, and 18 mm were set between the anterior and posterior implants on the left side of the arch in models 1 to 3, respectively (Figure 1). Four PEEK scan bodies (Elos Accurate Scan Body IO 2C-A; Elos Medtech) were attached to the multi-unit implant analogues to facilitate scanning. The models were first lab-scanned (inEOS X5; Dentsply Sirona) to obtain reference scan data. An IOS (iTerm Element 5D Plus; Align Technology) was then utilized to capture experimental scan data of the models. A single experienced operator (T.M), conducted the digital scanning procedure of models following the manufacturer's instructions. Scan aids were fabricated by using a fused deposition modelling device (Prusa i3 MK3S, Prusa Research AS) with a filament type of. Scan aids were mechanically attached to the scan bodies. Twenty digital scans were recorded for each model with or

without using scan aids (n=10) (Figure 2). A metrology software program (Geomagic Control X, 3D Systems) was used for the 3D analysis of data. The reference and experimental data were superimposed by a single operator to calculate the deviation values. Identical virtual cylinders were created from scan bodies on both reference, and experimental data. The centre lines of these virtual cylinders were measured by recording their x, y, and z coordinates. The angular deviation (AD) and linear deviation (LD) between the centre lines of the reference and experimental cylinders were calculated according to the method outlined in a previous study.¹⁷

Statistical Analysis

All statistical computations were performed using specialized analytical software (IBM SPSS Statistics, version 23, IBM Corp). The Shapiro-Wilk test was employed to evaluate data normality, confirming a normal distribution ($p>0.05$). Subsequently, a parametric two-way analysis of variance (ANOVA) was performed, complemented by Tukey's honest significant difference test for examining the effects of two variables- inter-implant distance and scan aid usage-on AD and LD values.

RESULTS

Table 1 presents the mean AD and LD values \pm standard deviations with pairwise comparisons. According to the 2-way ANOVA results, the inter-implant distance (factor 1) significantly influenced both the AD and LD values in the left posterior site ($p<0.001$); however, no significant differences were detected in other sites ($p>0.05$). The use of a scan aid (factor 2) significantly affected both the AD and LD values in all sites ($p<0.001$), except for the right posterior site ($p=0.26$ for AD and $p=0.18$ for LD). The interaction term between the tested factors was significant for AD and LD values in all sites ($p<0.001$), except for AD values in the right posterior site ($p>0.05$). Not only AD, but also LD values increased progressively from the right posterior site to the left posterior site. The LD values of all groups in all sites were below the acceptability threshold ($<100 \mu\text{m}$). The AD values of scans with SA were lower than the acceptability threshold (<0.5 degrees). For the scans without SA, only the AD values of the right posterior site were clinically acceptable.

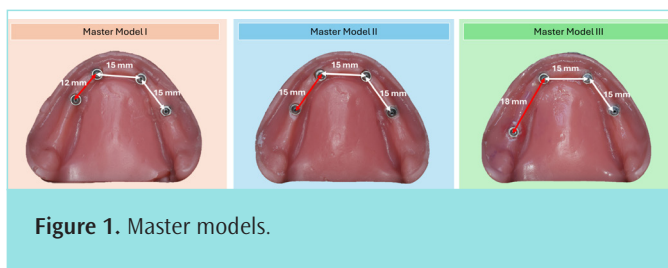


Figure 1. Master models.



Figure 2. Experimental groups.

Table 1. Mean AD (degrees) and LD (μm) values \pm standard deviations with Tukey Post Hoc comparison

Site	Model	Angular deviations			Linear deviations		
		Without SA	With SA	Total	Without SA	With SA	Total
Left posterior	Model 1	0.83 \pm 0.07 ^{A,a}	0.31 \pm 0.04 ^{B,a}	0.57 \pm 0.29 ^a	15.33 \pm 2.31 ^{A,a}	5.67 \pm 0.58 ^{B,a}	10.50 \pm 5.50 ^a
	Model 2	1.14 \pm 0.11 ^{A,b}	0.37 \pm 0.04 ^{B,ab}	0.76 \pm 0.42 ^b	20.00 \pm 1.73 ^{A,b}	6.67 \pm 0.58 ^{B,ab}	13.33 \pm 7.39 ^b
	Model 3	1.42 \pm 0.07 ^{A,c}	0.44 \pm 0.09 ^{B,b}	0.85 \pm 0.52 ^c	25.67 \pm 1.15 ^{A,c}	8.67 \pm 0.58 ^{B,b}	17.17 \pm 9.35 ^c
	Total	1.13 \pm 0.27 ^A	0.39 \pm 0.77 ^B	0.76 \pm 0.42	20.33 \pm 4.74 ^A	7.00 \pm 1.41 ^B	13.67 \pm 7.65
Left anterior	Model 1	0.72 \pm 0.06 ^{A,a}	0.24 \pm 0.03 ^{B,a}	0.48 \pm 0.27 ^a	13.67 \pm 1.15 ^{A,a}	4.67 \pm 0.58 ^{B,a}	9.17 \pm 5.00 ^a
	Model 2	0.75 \pm 0.01 ^{A,a}	0.28 \pm 0.07 ^{B,a}	0.52 \pm 0.24 ^a	13.00 \pm 0.00 ^{A,a}	6.00 \pm 1.00 ^{B,a}	9.50 \pm 3.89 ^a
	Model 3	0.76 \pm 0.03 ^{A,a}	0.31 \pm 0.03 ^{B,a}	0.53 \pm 0.26 ^a	14.67 \pm 1.53 ^{A,a}	6.33 \pm 1.53 ^{B,a}	10.50 \pm 4.76 ^a
	Total	0.74 \pm 0.04 ^A	0.28 \pm 0.05 ^B	0.51 \pm 0.24	13.78 \pm 1.20 ^A	5.67 \pm 1.22 ^B	9.72 \pm 4.34
Right anterior	Model 1	0.61 \pm 0.05 ^{A,a}	0.18 \pm 0.03 ^{B,a}	0.39 \pm 0.24 ^a	11.67 \pm 1.15 ^{A,a}	3.33 \pm 0.58 ^{B,a}	7.50 \pm 4.64 ^a
	Model 2	0.63 \pm 0.02 ^{A,a}	0.19 \pm 0.03 ^{B,a}	0.41 \pm 0.24 ^a	11.00 \pm 0.02 ^{A,a}	4.33 \pm 1.15 ^{B,a}	7.67 \pm 3.72 ^a
	Model 3	0.62 \pm 0.03 ^{A,a}	0.21 \pm 0.02 ^{B,a}	0.42 \pm 0.23 ^a	10.67 \pm 0.58 ^{A,a}	4.67 \pm 1.53 ^{B,a}	7.67 \pm 3.44 ^a
	Total	0.62 \pm 0.03 ^A	0.19 \pm 0.03 ^B	0.41 \pm 0.22	11.11 \pm 0.78 ^A	4.11 \pm 1.17 ^B	7.61 \pm 3.73
Right posterior	Model 1	0.15 \pm 0.01 ^{A,a}	0.13 \pm 0.05 ^{A,a}	0.14 \pm 0.03 ^a	4.00 \pm 1.00 ^{A,a}	2.67 \pm 0.58 ^{B,a}	3.33 \pm 1.03 ^a
	Model 2	0.17 \pm 0.06 ^{A,a}	0.14 \pm 0.04 ^{A,a}	0.15 \pm 0.05 ^a	4.07 \pm 0.58 ^{A,a}	3.33 \pm 0.58 ^{B,a}	4.00 \pm 0.89 ^a
	Model 3	0.16 \pm 0.01 ^{A,a}	0.15 \pm 0.20 ^{A,a}	0.16 \pm 0.02 ^a	4.60 \pm 0.02 ^{A,a}	4.00 \pm 1.00 ^{B,a}	3.50 \pm 0.84 ^a
	Total	0.16 \pm 0.03 ^A	0.14 \pm 0.03 ^A	0.15 \pm 0.03	3.89 \pm 0.93 ^A	3.33 \pm 0.87 ^B	3.61 \pm 0.92

Distinct superscript uppercase letters denote statistically significant differences within the same row, while distinct superscript lowercase letters indicate significant differences within the same column. SA: Scan aid, AD: Angular deviation, LD: Linear deviation.

DISCUSSION

This study aimed to investigate the effect of inter-implant distance and scan-aid use on the 3D trueness of digital implant impressions. The null hypothesis of the study was rejected, since both the scan-aid use and inter-implant distances significantly affected the AD and LD values. The use of IOSs for complete-arch implant impressions is still considered controversial¹⁹ due to limited reference points between scan bodies, which may lead to the misinterpretation of data during the stitching process.¹⁰ In the present study, 3 inter-implant distances were simulated in the left posterior arch, and the scanning process using IOS was initiated from the right posterior implant site. The deviation values increased from the right posterior arch to the left posterior arch; this increase can be attributed to the accumulation of stitching errors, increasing in parallel with the amount of scanned area.²⁰ A limited number of studies^{11,21,22} have evaluated the effect of inter-implant distance on the trueness of digital scans. The findings of the current study were consistent with previous studies, as higher deviation values were observed with the longer inter-implant distances.^{11,21,22} Scan aids act as artificial landmarks providing a continuous scan between the implants, and thereby enhancing the trueness of the stitching process.¹⁸ The scan aid used in this study was designed to be practically attached to the scan body and adjustable in length according to varying inter-implant distances. The scan aid had a lateral extension, which was directed towards the edentulous region to increase the reference points between implants. Statistical analysis revealed that when a scan aid was used, significantly lower LD and AD values were found in all models and all implant sites, except for right posterior implants. The starting points of the intraoral scanning have been shown to exhibit lower deviation values in comparison to the most distal implants of the scanned arch.²³ The lower deviation values in the right posterior implant may be attributed to the scan path followed in this study. Although the

LD values were below the clinical acceptability threshold ($<100 \mu\text{m}$), the AD values were detected in the right anterior, left anterior, and left posterior implants of all models were above this threshold (<0.5 degrees)²⁴ when scan-aids were not used. AD has been reported to impose more stress on implant components than LD.²⁵ Therefore, the use of scan aids is an effective method to reduce AD in complete arch implant impressions. In addition to being an *in vitro* study, this research has several other limitations, including the utilization of a single IOS, the use of only one scan aid design, and the evaluation of only the trueness. The findings of the current study suggest that incorporating scan aids into the digital workflow for implant impressions can significantly enhance accuracy, especially in cases with extended inter-implant distances. This improvement may lead to better prosthetic fit, reduced risk of complications, and increased efficiency in clinical practice, making scan aids a valuable addition to digital implantology. Further studies investigating both trueness and precision, comparing different IOSs and scan aid designs in cases of varying inter-implant distances are needed.

CONCLUSION

Within the limitations of this *in vitro* investigation, it can be inferred that incorporating a scan aid may serve as an efficacious approach to enhancing the three-dimensional accuracy of digital implant impressions in fully edentulous arches, particularly when addressing extended inter-implant distances.

Within the limitations of this *in vitro* study, it can be concluded that the use of a scan aid may be an effective method for improving the 3D trueness of digital implant impressions in complete edentulous arches, especially in longer inter-implant distances.

MAIN POINTS

- Intraoral scanners (IOSs) have significantly improved dental workflows by eliminating traditional impression methods, offering increased patient comfort, and fostering better communication between dental teams and patients.
- The study emphasizes the critical role of artificial landmarks, specifically prefabricated auxiliary devices, in enhancing the precision of digital impressions, especially when natural anatomical landmarks are not available.
- The study seeks to overcome challenges associated with image stitching in extended edentulous areas, aiming to enhance the overall performance and reliability of IOS technology in clinical dental practice.

ETHICS

Ethics Committee Approval: Not available.

Informed Consent: Not available.

Footnotes

Authorship Contributions

Concept: S.K.Y., Design: S.K.Y., Data Collection and/or Processing: T.M., Analysis and/or Interpretation: Ö.Ö., Literature Search: T.M., Writing: T.M., Ö.Ö.

DISCLOSURES

Conflict of Interest: No conflict of interest was declared by the authors.

Financial Disclosure: The authors declared that this study had received no financial support.

REFERENCES

- Mangano F, Gandolfi A, Luongo G, Logozzo S. Intraoral scanners in dentistry: a review of the current literature. *BMC Oral Health*. 2017; 17(1): 149.
- Flügge T, van der Meer WJ, Gonzalez BG, Vach K, Wismeijer D, Wang P. The accuracy of different dental impression techniques for implant-supported dental prostheses: a systematic review and meta-analysis. *Clin Oral Implants Res*. 2018; 29(Suppl 16): 374-92.
- Abduo J, Judge RB. Implications of implant framework misfit: a systematic review of biomechanical sequelae. *Int J Oral Maxillofac Implants*. 2014; 29(3): 608-21.
- Abduo J, Elseyoufi M. Accuracy of Intraoral Scanners: a Systematic Review of Influencing Factors. *Eur J Prosthodont Restor Dent*. 2018; 26(3): 101-21.
- Ahlholm P, Sipilä K, Vallittu P, Jakonen M, Kotiranta U. Digital versus conventional impressions in fixed prosthodontics: a review. *J Prosthodont*. 2018; 27(1): 35-41.
- Fukazawa S, Odaira C, Kondo H. Investigation of accuracy and reproducibility of abutment position by intraoral scanners. *J Prosthodont Res*. 2017; 61(4): 450-9.
- Imburgia M, Logozzo S, Hauschild U, Veronesi G, Mangano C, Mangano FG. Accuracy of four intraoral scanners in oral implantology: a comparative in vitro study. *BMC Oral Health*. 2017; 17(1): 92.
- Vandeweghe S, Vervack V, Dierens M, De Bruyn H. Accuracy of digital impressions of multiple dental implants: an in vitro study. *Clin Oral Implants Res*. 2017; 28(6): 648-53.
- Mangano FG, Hauschild U, Veronesi G, Imburgia M, Mangano C, Admakin O. Trueness and precision of 5 intraoral scanners in the impressions of single and multiple implants: a comparative in vitro study. *BMC Oral Health*. 2019; 19(1): 101.
- Wulfman C, Naveau A, Rignon-Bret C. Digital scanning for complete-arch implant-supported restorations: a systematic review. *J Prosthet Dent*. 2020; 124(2): 161-7.
- Thanasrisuebwong P, Kulchotirat T, Anunmana C. Effects of inter-implant distance on the accuracy of intraoral scanner: an in vitro study. *J Adv Prosthodont*. 2021; 13(2): 107-16.
- Kim JE, Amelya A, Shin Y, Shim JS. Accuracy of intraoral digital impressions using an artificial landmark. *J Prosthet Dent*. 2017; 117(6): 755-61.
- Pozzi A, Arcuri L, Lio F, Papa A, Nardi A, Londono J. Accuracy of complete-arch digital implant impression with or without scanbody splinting: an in vitro study. *J Dent*. 2022; 119: 104072.
- Huang R, Liu Y, Huang B, Zhang C, Chen Z, Li Z. Improved scanning accuracy with newly designed scan bodies: an in vitro study comparing digital versus conventional impression techniques for complete-arch implant rehabilitation. *Clin Oral Implants Res*. 2020; 31(7): 625-33.
- Pan Y, Tsoi JK, Lam WY, Zhao K, Pow EH. Improving intraoral implant scanning with a novel auxiliary device: an in-vitro study. *Clin Oral Implants Res*. 2021; 32(12): 1466-73.
- Kernen FR, Recca M, Vach K, Nahles S, Nelson K, Flügge TV. In vitro scanning accuracy using different aids for multiple implants in the edentulous arch. *Clin Oral Implants Res*. 2022; 33(10): 1010-20.
- Eddin MB, Önöral Ö. Influence of splinting scan bodies or incorporating three-dimensionally printed scan aids on the trueness of complete arch digital scans. *J Prosthet Dent*. 2024; 132(4): 828.
- Wu HK, Wang J, Chen G, Huang X, Deng F, Li Y. Effect of novel prefabricated auxiliary devices attaching to scan bodies on the accuracy of intraoral scanning of complete-arch with multiple implants: an in-vitro study. *J Dent*. 2023; 138: 104702.
- Revilla-León M, Att W, Özcan M, Rubenstein J. Comparison of conventional, photogrammetry, and intraoral scanning accuracy of complete-arch implant impression procedures evaluated with a coordinate measuring machine. *J Prosthet Dent*. 2021; 125(3): 470-8.
- van der Meer WJ. Application of intra-oral dental scanners in the digital workflow of implantology. *PLoS One*. 2012; 7(8): 43312.
- Andriessen FS, Rijkens DR, Van Der Meer WJ, Wismeijer DW. Applicability and accuracy of an intraoral scanner for scanning multiple implants in edentulous mandibles: a pilot study. *J Prosthet Dent*. 2014; 111(3): 186-94.
- Tan MY, Hui Xin Yee S, Wong KM, Tan YH, Tan KB. Comparison of three-dimensional accuracy of digital and conventional implant impressions: effect of interimplant distance in an edentulous arch. *Int J Oral Maxillofac Implants*. 2019; 34(2): 366-80.
- Meneghetti PC, Li J, Borella PS, Mendonça G, Burnett Jr LH. Influence of scanbody design and intraoral scanner on the trueness of complete arch implant digital impressions: an in vitro study. *Plos One*. 2023; 18(12): 0295790.
- Gintaute A, Papatiantafyllou N, Aljehani M, Att W. Accuracy of computerized and conventional impression-making procedures for multiple straight and tilted dental implants. *Int J Esthet Dent*. 2018; 13(4): 550-65.
- Winter W, Möhrle S, Holst S, Karl M. Bone loading caused by different types of misfits of implant-supported fixed dental prostheses: a three-dimensional finite element analysis based on experimental results. *Int J Oral Maxillofac Implants*. 2010; 25(5): 947-52.

Early Prediction of Mortality due to Carbapenem-Resistant Gram-Negative Bacterial Infection in Intensive Care Units Using Machine Learning

✉ Buket Baddal¹, ✉ Cemile Bağkur², ✉ Bardia Arman³

¹Department of Medical Microbiology and Clinical Microbiology, Near East University Faculty of Medicine, Nicosia, North Cyprus

²DESAM Research Institute, Near East University, Nicosia, North Cyprus

³Artificial Intelligence Application and Research Center, Cyprus International University Faculty of Engineering, Nicosia, North Cyprus

Abstract

BACKGROUND/AIMS: The occurrence of hospital-acquired infections due to carbapenem-resistant Gram-negative bacteria (CR-GNB) is on the rise globally. Studies show that infections with multidrug-resistant Gram-negative bacteria are associated with high mortality mainly in intensive care units (ICUs). This study aims to develop machine learning (ML) algorithms to identify variables correlated with mortality and construct a prediction model for ICU mortality due to CR-GNB infections.

MATERIALS AND METHODS: Data from patients admitted to a private hospital between 2016 and 2023 were included. The dataset included patients from the ICU who had a positive culture of CR-GNB after 3 days of admission (n=788). Demographic data, vital signs, important blood test indicators, intubation, and catheterization history were collected. The proposed models included a classifier and a mortality prediction system, utilizing seven ML algorithms: Extreme Gradient Boosting (XGBoost), logistic regression, random forest (RF), k-nearest neighbors, support vector machine, naive bayes, and decision tree (DT).

RESULTS: Analysis showed that blood C-reactive protein, urea, creatinine, platelet-large cell ratio, along with patient age and presence of endotracheal intubation, were strong predictors of mortality in ICU patients. In terms of accuracy, XGBoost (96.2%) outperformed RF (93.7%) and DT (91.8%). The area under the receiver operating characteristic curve for these models was 0.98, 0.99, and 0.93, while F1 scores were 0.97, 0.95, and 0.94, respectively.

CONCLUSION: ML prediction models can predict patient mortality in ICUs due to CR-GNB and guide medical staff to identify high-risk groups in advance.

Keywords: Carbapenem-resistant Gram-negative bacteria, machine learning, intensive care unit, mortality prediction

INTRODUCTION

Carbapenem resistance is a global public health issue. The excessive application and escalating misuse of the carbapenem class of antibiotics have caused a significant rise in the occurrence of carbapenem-resistant Gram-negative bacterial (CR-GNB) infections.¹ This is particularly due to

the existence of β -lactamase genes, which are found on mobile genetic elements that can be disseminated among bacteria within a hospital environment.² Indeed, the World Health Organization 2017 priority list of pathogens ranked carbapenem-resistant *Pseudomonas aeruginosa*, carbapenem-resistant *Acinetobacter baumannii*, and carbapenem-resistant *Enterobacteriaceae* within the top priority category, which

To cite this article: Baddal B, Bağkur C, Arman B. Early prediction of mortality due to carbapenem-resistant Gram-negative bacterial infection in intensive care units using machine learning. Cyprus J Med Sci. 2025;10(Suppl 1):46-49

ORCID IDs of the authors: B.B. 0000-0003-3319-2179; C.B. 0000-0003-0998-4176; B.A. 0009-0001-9449-2688.



Corresponding author: Buket Baddal
E-mail: buket.baddal@neu.edu.tr
ORCID ID: orcid.org/0000-0003-3319-2179

Received: 05.11.2024
Accepted: 13.12.2024
Publication Date: 04.06.2025



Copyright© 2025 The Author. Published by Galenos Publishing House on behalf of Cyprus Turkish Medical Association.
This is an open access article under the Creative Commons AttributionNonCommercial 4.0 International (CC BY-NC 4.0) License.

was termed the critical category.³ Infections by these pathogens are associated with longer stays, added healthcare costs, and higher mortality, particularly in those within the intensive care unit (ICU).⁴

Infections in ICUs are central causes of morbidity and mortality due to the increased vulnerability of these patients to nosocomial infections. ICUs are termed the epicenter of multidrug-resistant (MDR)-GNB, which primarily arise from the frequent and irrational use of broad-spectrum antibiotics, that lead to the evolution of drug-resistant strains.⁵ ICU-admitted patients are also more prone to MDR-GNB infections due to numerous invasive medical procedures such as mechanical ventilation, catheterization, and intubation.⁶

The present study aims to develop machine learning (ML) algorithms to identify variables correlated with CR-GNB-associated mortality in patients admitted to the ICU; provide a prediction model for ICU mortality; and evaluate the performance of ML models in the prediction of mortality in individuals that require ICU admission.

MATERIALS AND METHODS

This study was approved by the Ethics Committee of Near East University (NEU/2023/110-1685, date: 26.01.2023). Due to the retrospective nature of the study, informed consent was waived.

Data Collection, Study Design, and Population

This retrospective study evaluated patients from the ICU at Near East University Hospital between January 2016 and December 2023. The inclusion criteria were: (1) age ≥ 18 years; (2) ICU admission; (3) a positive culture of CR-GNB after 3 days of ICU admission; (4) the presence of important blood test indicators. The exclusion criteria were: (1) outpatients; (2) patients transferred to the general ward within 3 days.

Demographic data including age, gender, as well as clinical features such as prognostic scores, vital signs, laboratory blood examination results, history of invasive catheterization, and endotracheal intubation were collected. In terms of blood test variables, serum albumin; alanine aminotransferase (serum pyruvic transaminase); aspartate aminotransferase (serum glutamate oxaloacetate transaminase); C-reactive protein (CRP); glucose; white blood cell count; neutrophil number (NEU#); neutrophil percentage (NEU%); lymphocyte number (LYM#); lymphocyte percentage (LYM%); monocyte number (MONO#); monocyte percentage (MONO%); eosinophil number (EOS#); eosinophil percentage (EOS%); basophil number (BASO#); basophil percentage (BASO%); red blood cell count; hemoglobin; mean corpuscular hemoglobin; mean corpuscular hemoglobin concentration; platelet count; red blood cell distribution width; mean platelet volume; plateletcrit; platelet-large cell ratio (P-LCR); nucleated red blood cell count; chlorine; creatinine; potassium; procalcitonin; sodium; urea and calcium were used.

Data Splitting and Preprocessing

The preprocessing of the dataset involved mapping categorical values for “gender”, “invasive catheterization”, “endotracheal intubation”, and “CR-GNB infection” into their binary numerical representations: 0 and 1. Numerical feature missing values were handled by converting data into numeric format and missing values of numerical features were handled by filling them with zero. For the purpose of prediction the target variable “death” was separated from the rest of the predictor

variables. Following this, the dataset was divided into a training set and a test set in the ratio of 80:20, using the function `train_test_split`. Standardization of the variables was performed prior to the evaluation of different ML models.

Statistical Analysis

The performance of several models including logistic regression (LR), decision trees (DT), k-nearest neighbors (KNN), support vector machine (SVM), random forest (RF), extreme gradient boosting (XGBoost), and naive bayes (NB) was compared using area under the receiver operating characteristic curve (AU-ROC) curves and classification metrics such as accuracy, precision, recall, and F1 score. This enabled the comparison of each model's performance by plotting the ROC curves, highlighting key features that contribute to mortality prediction. These model developments and statistical tests were performed in Python version 3.6.

RESULTS

Variable Importance and Feature Selection

The selected predictors of in-ICU mortality due to CR-GNB infection are shown in Figure 1A. From a total of 37 variables, the top six variables to correlate with mortality in descending order were CRP, urea, creatinine, age, endotracheal intubation, and P-LCR. Variables such as CRP, urea, and creatinine were moderately positively correlated with mortality, indicating that the higher these biomarkers are, the worse the outcome. Age and endotracheal intubation, although with weaker correlations, represented well-established risk factors of mortality in the ICU. The low correlation observed in the correlation matrix suggested minimal multicollinearity in the dataset, indicating that each variable provided unique information supporting model accuracy (Figure 1B).

Overall Performance of the ML Models

The comparison of different models is necessary to identify the most accurate and reliable approach for predicting biomarkers associated with mortality. The prognostic performance and accuracy of the prediction models for ICU mortality due to CR-GNB infection are summarized in Table 1. Overall, the XGBoost classifier had the highest accuracy with 95.6%, followed by the RF classifier (93.7%). Indeed, both models demonstrated positive performance, with precision, recall, and F1-scores above 0.93. The DT model also performed well with an accuracy of 91.8%, although it was lower than that of the ensemble models.

On the contrary, The KNN model exhibited had a reasonable performance with a reasonable accuracy of 78.5%, performing well in terms of precision while giving a slightly lower recall. The LR and the SVM were also less effective, with accuracy values at 69% and 71%, respectively. The worst performing model was NB, with an accuracy of 62% and lower F1-scores, giving a poor performance for the correct classification of survived patients. Overall, the tree-based models resulted in the best predictive performance for predicting mortality.

The prediction algorithm using RF had the highest predictive value, for mortality due to CR-GNB infection in ICU with an area under the curve (AUC) of 0.99, for mortality due to CR-GNB infection in ICU (Figure 2).

DISCUSSION

In this study, the predictive capabilities of several ML models were evaluated for ICU mortality due to CR-GNB infections. Among the models examined, XGBoost, RF, and DT were identified as the top performers. XGBoost demonstrated superior predictive accuracy at 96.2%, followed by RF at 93.7%, and DT at 91.8%. These models proved highly effective in identifying high-risk ICU patients, with XGBoost achieving an AU-ROC of 0.99, indicating excellent performance in distinguishing between mortality outcomes. Tree-based models, such as XGBoost and LightGBM, are widely recognized for their strong predictive capabilities and

frequently outperform other ML models. Consistent with our findings, Jeon et al.⁷ reported that LightGBM (AU-ROC; 0.827) outperformed LR and conventional clinical scoring systems in predicting ICU mortality, reinforcing the value of ML models in critical care settings. Both studies identified similar key parameters influencing predictions, including CRP, urea, and creatinine levels, which emerged as crucial indicators of mortality risk.⁷ CRP, a well-established biomarker of inflammation, plays a central role in assessing mortality risk, particularly in septic conditions. Elevated CRP levels, particularly those measured on the third day of ICU admission, have been linked to increased mortality. Similarly, elevated urea and creatinine levels are critical predictors of mortality, particularly when a high urea-to-creatinine ratio is observed.⁸⁻¹⁰ In addition to CRP and other biochemical markers, P-LCR emerged as a significant predictor of mortality in our study. Elevated P-LCR, indicative of systemic inflammation, was also strongly correlated with mortality in Coronavirus disease-2019 patients in the study by Çelik et al.¹¹, reflecting the role of inflammation-driven markers in ICU settings. This highlights the diverse applicability of both complex ML models and simpler clinical biomarkers in predicting ICU outcomes across different conditions.

A unique feature of the current study was the use of a local hospital database rather than publicly available datasets. Other studies, such as Iwase et al.'s¹² work on a broader ICU population, achieved similarly high predictive accuracy (AU-ROC; 0.945, using a RF model) but relied on more generalized datasets.

Study Limitations

The study's single-center data allow for specific healthcare applications but limits broader generalizability. The inclusion of multiple datasets with the same variables from different hospitals within the same region would improve the accuracy of the prediction models. The prediction models lack external validation, restricting their use in other clinical environments.

CONCLUSION

This study shows that ML prediction models can predict patient mortality in ICUs due to CR-GNB and guide medical staff to identify high-risk groups in advance. The localized approach in this study offers a more relevant predictive model for clinical decision-making in the hospital setting, potentially improving patient care by offering customized risk assessment for CR-GNB infections in ICUs. This focus on local data strengthens the real-world applicability of our findings, making them more directly actionable for improving patient outcomes in specific healthcare environments.

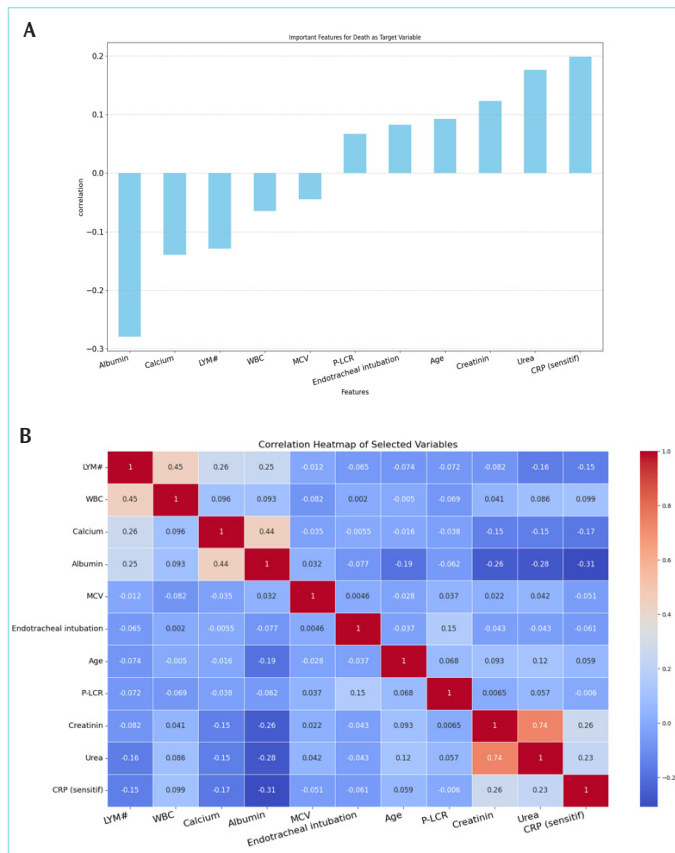


Figure 1. (A,B) Importance of the selected variables and their correlation matrix.

LTM: Lymphocyte, WBC: White blood cell count, MCV: Mean corpuscular volume, P-LCR: Platelet-large cell ratio, CRP: C-reactive protein, ROC: Receiver operating characteristic curve, AUC: Area under the curve.

Table 1. Overall performance of the prediction models

Model	Accuracy	Precision (class 0)	Precision (class 1)	Recall (class 0)	Recall (class 1)	F1-score (class 0)	F1-score (class 1)
XGBoost	95.6	0.92	0.97	0.94	0.96	0.93	0.97
Random forest	93.7	0.87	0.97	0.94	0.94	0.90	0.95
Decision tree	91.8	0.82	0.97	0.94	0.91	0.88	0.94
K-nearest neighbors	78.5	0.66	0.84	0.63	0.85	0.65	0.85
Support vector machine	71	0.67	0.71	0.12	0.97	0.21	0.82
Logistic regression	69	0.5	0.76	0.43	0.81	0.46	0.78
Naive bayes	62	0.42	0.77	0.57	0.64	0.48	0.7

XGBoost: Extreme gradient boosting.

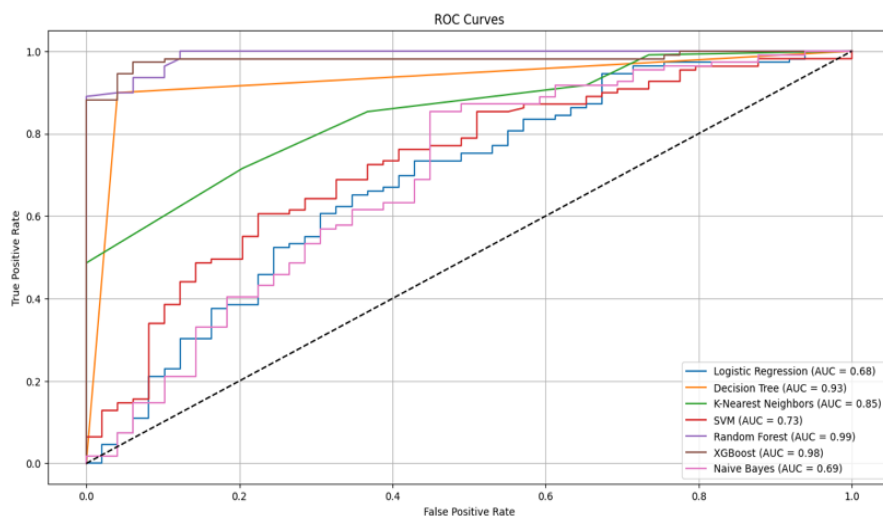


Figure 2. ROC curves and AUCs for ICU mortality were obtained using machine learning methods.

AUC: Area under the curve, SVM: Support vector machine, XGBoost: Extreme gradient boosting, LYM: Lymphocytes, MVC: Mean corpuscular volume, P-LCR: Platelet large cell ratio, CRP: C-reactive protein, WBC: White blood cell, ICU: Intensive care unit.

MAIN POINTS

- This study focuses on machine learning (ML) models to identify variables correlated with mortality due to carbapenem-resistant Gram-negative bacterial (CR-GNB) infection in intensive care units (ICUs).
- Analysis results indicated that blood C-reactive protein, urea, creatinine, platelet-large cell ratio, along with patient age and presence of endotracheal intubation, were strong predictors of mortality in ICU patients.
- In terms of accuracy, XGBoost had the highest accuracy among random forest and decision tree.
- ML prediction models can predict patient mortality in ICUs due to CR-GNB and can guide medical staff to identify high-risk groups in advance.

ETHICS

Ethics Committee Approval: This study was approved by the Ethics Committee of Near East University (NEU/2023/110-1685, date: 26.01.2023).

Informed Consent: Retrospective study.

Footnotes

Authorship Contributions

Concept: B.B., C.B., Design: B.B., C.B., Data Collection and/or Processing: C.B., B.A., Analysis and/or Interpretation: B.B., C.B., B.A., Literature Search: B.B., C.B., B.A., Writing: B.B., C.B., B.A.

DISCLOSURES

Conflict of Interest: No conflict of interest was declared by the authors.

Financial Disclosure: The authors declared that this study had received no financial support.

REFERENCES

1. Nordmann P, Poire L. Epidemiology and diagnostics of carbapenem resistance in gram-negative bacteria. *Clin. Infect Dis.* 2019; 69(7): 521-8.
2. Logan LK, Weinstein RA. The epidemiology of carbapenem-resistant enterobacteriaceae: The impact and evolution of a global menace. *J Infect Dis.* 2017; 215(1): 28-36.
3. World Health Organization. WHO publishes list of bacteria for which new antibiotics are urgently needed. 2017. Available from: <https://www.who.int/news/item/27-02-2017-who-publishes-list-of-bacteria-for-which-new-antibiotics-are-urgently-needed>
4. van Loon K, Voor In 't Holt AF, Vos MC. A systematic review and meta-analyses of the clinical epidemiology of carbapenem-resistant enterobacteriaceae. *Antimicrob Agents Chemother.* 2018; 62(1): 1730-17.
5. Breijyeh Z, Jubeh B, Karaman R. Resistance of gram-negative bacteria to current antibacterial agents and approaches to resolve it. *Molecules.* 2020; 25(6): 1340.
6. Sengupta S, Barman P, Lo J. Opportunities to overcome implementation challenges of infection prevention and control in low-middle income countries. *Curr Treat Options Infect Dis.* 2019; 11(3): 267-80.
7. Jeon ET, Lee HJ, Park TY, Jin KN, Ryu B, Lee HW, et al. Machine learning-based prediction of in-ICU mortality in pneumonia patients. *Sci Rep.* 2023; 13(1): 11527.
8. Devran O, Karakurt Z, Adıgüzel N, Güngör G, Moçin OY, Balcı MK, et al. C-reactive protein as a predictor of mortality in patients affected with severe sepsis in intensive care unit. *Multidiscip Respir Med.* 2012; 7(1): 47.
9. Qu R, Hu L, Ling Y, Hou Y, Fang H, Zhang H, et al. C-reactive protein concentration as a risk predictor of mortality in intensive care unit: a multicenter, prospective, observational study. *BMC Anesthesiol.* 2020; 20(1): 292.
10. van der Slikke EC, Star BS, de Jager VD, Leferink MBM, Klein LM, Quinten VM, et al. A high urea-to-creatinine ratio predicts long-term mortality independent of acute kidney injury among patients hospitalized with an infection. *Sci Rep.* 2020; 10(1): 15649.
11. Çelik O, Laloğlu E, Çelik N. The role of platelet large cell ratio in determining mortality in COVID-19 patients. *Medicine (Baltimore).* 2024; 103(18): 38033.
12. Iwase S, Nakada TA, Shimada T, Oami T, Shimazui T, Takahashi N, et al. Prediction algorithm for ICU mortality and length of stay using machine learning. *Sci Rep.* 2022; 12(1): 12912.

Detection of Keratoconus through YOLOv8 Region of Interest Preprocessing and Pre-trained Convolutional Neural Networks Using 2D Images

© Muhammed Sideeq Anwar^{1,2}, © Emre Özbilge¹

¹Department of Computer Engineering, Cyprus International University Faculty of Engineering, Nicosia, North Cyprus

²Department of Computer Education, Tishk International University Faculty of Education, Erbil, Iraq

Abstract

BACKGROUND/AIMS: This study presents a methodology for detecting keratoconus using pre-trained convolutional neural network (CNN) models. Five models were evaluated, namely, Xception, InceptionV3, ResNet152, InceptionResNetV2, and EfficientNetV2S.

MATERIALS AND METHODS: Model performance was assessed in two stages: in the initial stage, raw image data were used with a YOLOv8 object detector to extract the region of interest (ROI) around the eyes, and the subsequent stage involved training the pre-trained CNN model through transfer learning to classify the extracted eye region image as normal, mild, or advanced keratoconus.

RESULTS: The results showed that the Xception and InceptionResNetV2 models achieved accuracies of 93.80% and 94.23%, respectively, with ROI cropping, outperforming the other CNN architectures. Without ROI preprocessing, their accuracy decreased to 91.43% and 91.45%, respectively, highlighting the importance of targeted image cropping.

CONCLUSION: Additional metrics corroborated these findings and demonstrated improved diagnostic capabilities when trained using extracted ROI data. This methodology demonstrates the potential of targeted image preprocessing and transfer learning to enhance early detection and management of keratoconus.

Keywords: Keratoconus, CNN, transfer learning, YOLOv8

INTRODUCTION

Keratoconus is a visual impairment characterised by the thinning and protrusion of the cornea into a conical shape. It typically affects both eyes, with one eye often being impacted more severely. The condition usually manifests between late adolescence and early adulthood, progressing over ten years or more. Initially, the visual impairments were corrected using spectacles or soft contact lenses. As the disease progresses, rigid gas-permeable or scleral lenses may become necessary. Severe cases may require corneal transplantations. Corneal collagen

cross-linking aims to halt or decelerate keratoconus progression, potentially averting transplant surgery.¹ Symptoms include blurred or distorted vision, sensitivity to bright light and glare, frequent changes in eyeglass prescriptions, and sudden deterioration of vision or cloudiness. Rapid vision deterioration, particularly irregular astigmatism, warrants prompt ophthalmological evaluation. The precise aetiology remains unknown; however, it is hypothesised to involve genetic and environmental factors. Risk factors include family history, vigorous eye rubbing, and conditions such as retinitis pigmentosa, Down syndrome, and connective tissue disorders.^{1,2}

To cite this article: Anwar MS, Özbilge E. Detection of keratoconus through YOLOv8 ROI preprocessing and pre-trained convolutional neural networks using 2d images. Cyprus J Med Sci. 2025;10(Suppl 1):50-54

ORCID IDs of the authors: M.S.A. 0009-0008-9444-6404; E.Ö. 0000-0002-2295-752X.



Corresponding author: Emre Özbilge
E-mail: eozbilge@ciu.edu.tr
ORCID ID: orcid.org/0000-0002-2295-752X

Received: 03.12.2024
Accepted: 27.01.2025
Publication Date: 04.06.2025



Copyright © 2025 The Author. Published by Galenos Publishing House on behalf of Cyprus Turkish Medical Association.
This is an open access article under the Creative Commons Attribution-NonCommercial 4.0 International (CC BY-NC 4.0) License.

Complications of keratoconus include rapid corneal swelling (hydrops) leading to sudden vision loss and scarring, as well as progressive corneal scarring requiring transplant surgery, particularly in advanced cases. However, convolutional neural network (CNN) algorithms typically analyse entire ocular images, including nonessential structures, resulting in redundant data processing that may diminish their ability to accurately detect keratoconus-related abnormalities. By isolating the region of interest (ROI), our objective was to facilitate the processing for subsequent algorithms, enhancing their capacity to identify relevant features associated with keratoconus pathology. Traditional methods, such as support vector machines (SVM) and random forests (RF), rely on manually engineered features, which may fail to capture the nuanced patterns of keratoconus progression. To define the ROI, we employed YOLOv8, which is recognised for its high object detection accuracy. This ensures that classification algorithms focus on diagnostic challenges without extraneous elements.^{3,4} This preprocessing step enables algorithms to discern differences in crucial features, potentially achieving a higher accuracy in keratoconus detection. By eliminating redundant information, we reduce the computational burden, resulting in a shorter execution time. We aimed to improve both the accuracy and efficiency of the classification algorithms, benefiting ophthalmology diagnostic practices and patient outcomes.

In summary, this study proposes a two-stage keratoconus detection approach using YOLOv8 for ROI extraction and CNN-based classification to improve the diagnostic performance. This study aimed to develop an advanced methodology for detecting keratoconus, a progressive corneal disorder, using pre-trained CNNs and targeted image preprocessing techniques. By employing a two-stage process, using YOLOv8 for eye region extraction and leveraging transfer learning on extracted regions, this approach highlights the role of ROI cropping in improving diagnostic accuracy. This study demonstrates how integrating ROI-based preprocessing with robust CNN models, such as Xception and InceptionResNetV2, can significantly enhance the detection accuracy and other diagnostic metrics. This innovation has the potential to facilitate earlier detection and better management of keratoconus, improving patient outcomes. The main contributions of this study are as follows:

Significant accuracy improvement through region of interest extraction: Utilizing YOLOv8 for precise eye-region extraction enhances the CNN classifier accuracy.

Enhanced diagnostic metrics: Integrating ROI preprocessing with transfer learning improved recall, precision, and F1-score, emphasising the benefits of focusing on diagnostically relevant regions.

Efficient two-stage detection pipeline: The proposed methodology reduces redundant data processing and computational load while maintaining high performance, enabling more efficient early detection of keratoconus in clinical settings.

The remainder of this paper is organised as follows. We begin with an introduction (section 1) that establishes the context and purpose of the investigation. The literature review (section 2) examines current research in the field, identifying gaps and significant findings that informed our work. The methodology (section 3) explains the study design, data collection, and analytical methods employed. We then present the experimental results (section 4), discuss our findings, and elucidate

their significance. Finally, we reflect on the challenges encountered and propose areas for future research (section 5).

Literature Review

Keratoconus is an eye condition that involves thinning and conical bulging of the cornea, creating challenges for analysis and treatment. With technological advances, machine learning (ML) and CNN have become valuable in clinical photograph evaluation, offering more accurate detection of keratoconus. In this literature review, we studied ML and CNN strategies to identify keratoconus and discussed their benefits, drawbacks, and functionality in scientific settings.

Traditional Machine Learning-Based Approaches

In early keratoconus detection, researchers used conventional devices to develop algorithms, such as SVM, multilayer perceptrons, and RF, focusing on features from corneal topography or tomography images.⁵ Applied an SVM to corneal topography data to differentiate normal eyes from keratoconus-affected eyes, achieving promising accuracy. However, traditional methods such as SVM and RF rely on manually engineered features, which may fail to capture nuanced, non-linear patterns of keratoconus progression.⁶

Deep Learning-Based Approaches

CNN models have revolutionised medical image analysis by automatically extracting features from raw images, thereby eliminating the need for manual feature extraction. They have shown excellent performance in detecting keratoconus, particularly in anterior segment optical coherence tomography (AS-OCT) and corneal tomography images.⁷ Developed a CNN architecture for screening keratoconus using AS-OCT images, achieving high sensitivity and specificity.⁸

Transfer learning has become prevalent in keratoconus detection. This technique involves fine-tuning pre-trained CNN models for specific tasks and leveraging knowledge from large datasets. It enhances model performance and reduces the need for extensive labeled data. Researchers are exploring innovative deep learning architectures for keratoconus detection, such as attention mechanisms and generative adversarial networks (GANs), to improve diagnostic accuracy.^{8,9} Recent advances have demonstrated the effectiveness of combining attention mechanisms with neural networks, including GANs, to enhance corneal image analysis. In¹⁰, a U-Net model with edge and spatial attention mechanisms improved OCT image segmentation accuracy, achieving a Dice score of 94.99%.¹¹ used attention-enhanced CNNs to focus on retinal fundus images for glaucoma classification, highlighting important regions, such as the optic disc.¹² proposed a constrained GAN for medical image enhancement, incorporating structural and illumination constraints with attention mechanisms to enhance corneal images, outperforming traditional methods in NIQE and PIQE metrics. A semi-supervised multi-scale self-transformer-GAN was proposed in¹³, to segment corneal ulcers from slit-lamp images, capture long-range dependencies, and enhance performance in labeled and unlabelled datasets.¹⁴ Combined local extrema information and quantised Haralick features from fundus images, with a long short-term memory network to classify diabetic retinopathy symptoms and capture texture and multiresolution details, while analysing retinal vasculature and hard-exudate patterns with high precision.

MATERIALS AND METHODS

Dataset

Sample input images for keratoconus in the normal, mild, and advanced cases are shown in Figure 1. A total of 1,000 images were obtained and separated into severe, mild, and normal eye condition categories. These images were collected, under a non-disclosure agreement, at the North Eye Center in Iraq with a non-disclosure agreement. Mild and advanced cases accounted for 70% of the total samples, with approximately 35% for each of these classes, while 30% were normal cases. Half of the images were used to train the object detection model in stage 1, and the other half to train the classification model in stage 2. The datasets for each stage were split into training, validation, and test sets at ratios of 70%, 20%, and 10%, respectively. The performance of these stages was evaluated using a test set to evaluate the validity of both models.

To improve the performance of both models, data augmentation, including contrast adjustment, rotation, linear translation, zooming, and flipping, was applied to enhance the model generalization and mitigate overfitting. This augmentation process was applied only to the training datasets before training, and each method was randomly applied to the original images with a certain probability. This process was repeated six times to generate different variations in the original image. The original images were retained without modifying the training dataset.

Keratoconus Diagnosis System

The proposed keratoconus detection method was implemented in two stages (Figure 2). The raw facial image was presented to the trained

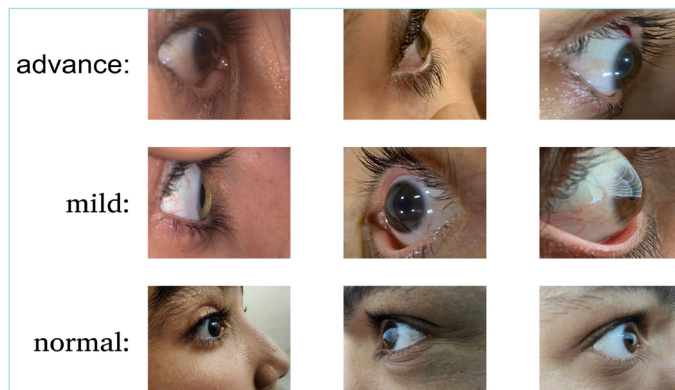


Figure 1. Sample keratoconus image for advance, mild and normal eye conditions.

YOLOv8 model, and the extracted eye region images were fed to the pre-trained ImageNet model for keratoconus stage classification (normal, mild, or advanced). Both models were trained using separate datasets. However, during inferencing, they were combined sequentially, with the YOLOv8 object detector's output becoming the classifier model's input, constituting the complete pipeline for keratoconus identification.

YOLOv8 Object Detection Model

YOLOv8, introduced by Ultralytics,¹⁵ significantly enhances end-to-end object detection. It employs an efficient backbone architecture for feature extraction and integrates a Feature Pyramid Network to improve detection across multiple scales. YOLOv8 adopts an anchor-free approach that directly predicts the center, width, and height of bounding boxes, simplifying detection by eliminating the predefined anchor boxes. This method enhances speed and accuracy. The algorithm processes the entire image in a single pass, consistent with its "you only look once" principle, and applies non-maximum suppression to remove overlapping boxes, retaining only the most confident detections. The YOLOv8 model was trained to detect eye regions in facial images, and the extracted regions were then presented to the CNN classifier for keratoconus stage identification.

Transfer Learning for Classification

Transfer learning has been widely applied in deep learning. The weights of a pre-trained CNN model's weights, learned on the ImageNet challenge dataset, were used for the custom task by replacing the classifier head, which allowed the transferred model to learn a new task. This method is more robust and accurate than a deep learning model trained from scratch. Five pre-trained CNN models (Xception, InceptionV3, ResNet152, InceptionResNetV2, and EfficientNetV2S) were evaluated. Classifier heads were replaced to adapt the models to keratoconus diagnostic tasks. A global average pooling layer flattened the extracted features, followed by two fully connected dense layers (512 and 256 nodes) and one output dense layer with three a softmax activation to learn the keratoconus stages. The models were trained using the Adam optimiser, with a 0.01 learning rate up to 100 epochs.

Experimental Results and Discussions

The performance of the pre-trained models was evaluated with and without ROI extraction using the YOLOv8 object detector. Table 1 presents the results of the pre-trained CNN models when raw facial images were directly inputted into them. Table 2 illustrates the results when the eye region was initially extracted using YOLOv8 and subsequently presented to the classification models. This is evidenced by the consistent improvement in the model performance when

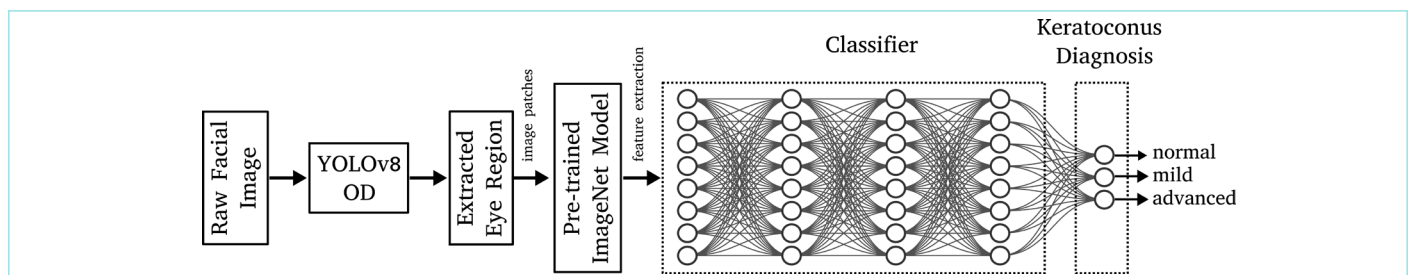


Figure 2. Proposed keratoconus diagnostic system through detecting image patches from the facial image and then classifying input image patches (eye regions) with the stage of keratoconus disease.

Table 1. Comparison results of CNN models without performing YOLOv8 detection.

Model	Accuracy	Recall	Precision	F1-score
Xception	91.43%	89.02%	89.05%	89.04%
InceptionV3	87.98%	80.13%	80.11%	80.11%
Resnet152	85.18%	79.43%	76.22%	77.79%
InceptionResNetV2	91.45%	88.23%	88.08%	88.16%
EfficientNetV2S	90.55%	86.78%	83.79%	86.42%

CNN: Convolutional neural network.

Table 2. Comparison results of CNN models after performing YOLOv8 detection.

Model	Accuracy	Recall	Precision	F1-score
Xception	93.80%	90.98%	89.05%	90.00%
InceptionV3	90.15%	82.99%	81.61%	82.29%
Resnet152	87.51%	81.46%	77.98%	79.68%
InceptionResNetV2	94.23%	89.82%	89.64%	89.73%
EfficientNetV2S	93.11%	87.93%	84.97%	86.42%

CNN: Convolutional neural network.

employing YOLOv8 object detection. With ROI extraction, the Xception model demonstrated a 2.37% improvement in accuracy, rising from 91.43% to 93.80%, whereas InceptionResNetV2 showed the highest accuracy at 94.23%. The recall metric of Xception improved from 89.02% to 90.98%. InceptionV3, which initially demonstrated an accuracy of 87.98% without an object detector, improved to 90.15% after eye-region extraction. These improvements suggest that ROI extraction facilitates focusing on sample characteristics, thereby enhancing its ability to generalize and identify key data patterns.

However, not all the models exhibited the same trend. InceptionResNetV2 demonstrated a modest increase in accuracy from 91.45% to 94.23% and a slight improvement in recall and the F1 scores. This indicates that although YOLOv8 object detection, enhances the model performance, the extent of its effect may depend on the model's inherent architecture. ResNet152 exhibited one of the largest improvements in accuracy, increasing from 85.18% to 87.51%. Overall, extracting the eye region appears to be valuable for enhancing model performance, particularly for increasing recall and precision. The results in Table 2 highlight the efficacy of YOLOv8 preprocessing in improving classification performance. Among the evaluated models, InceptionResNetV2 demonstrated the highest accuracy, whereas ResNet152 demonstrated modest gains.

CONCLUSION

Despite significant advancements, challenges persist in developing and applying ML and CNN for keratoconus detection. Limited annotated datasets, variability in imaging protocols, and generalisability to diverse populations pose constraints. The capacity to train deep learning models and their integration into clinical workflows warrants further investigation. ML and CNN approaches demonstrate considerable potential for enhancing the early diagnosis and management of keratoconus. Continued research on data standardisation, model interpretation, and clinical validation is essential to translate this technology into routine clinical practice, benefiting keratoconus patients globally. In refining keratoconus diagnostic techniques, we encountered the following obstacle: the incorporation of extraneous data into ocular images. Traditional CNN algorithms exhibit limitations

owing to redundant information from nontrivial sources, which affects accuracy and efficiency. To address this, an object detection method that emphasises a ROI extraction from ocular images is proposed. Future integration of explainable AI methods could improve clinical adoption by enabling transparent decision making for keratoconus diagnosis.

MAIN POINTS

- Novel dataset was collected in this study.
- Two stages deep learning based approach was developed to detect the keratoconus eye disease.
- Comparing several deep learning architectures to evaluate the performance of deep learning models.
- Compare the performance of the deep learning models with and without using object detection algorithm.

ETHICS

Ethics Committee Approval: Not available.

Informed Consent: Prior to participation, all individuals were fully informed about the objectives and procedures of the study and voluntarily provided verbal consent to the researchers. Furthermore, ethical approval and authorization for data collection were granted by North Eye Center.

Footnotes

Authorship Contributions

Concept: M.S.A., E.Ö., Design: M.S.A., E.Ö., Data Collection and/or Processing: M.S.A., Analysis and/or Interpretation: M.S.A., Literature Search: M.S.A., E.Ö., Writing: M.S.A., E.Ö.

DISCLOSURES

Conflict of Interest: No conflict of interest was declared by the authors.

Financial Disclosure: The authors declared that this study had received no financial support.

REFERENCES

1. Santodomingo-Rubido J, Carracedo G, Suzaki A, Villa-Collar C, Vincent SJ, Wolffsohn JS. Keratoconus: an updated review. *Contact Lens and Anterior Eye*. 2022; 45(3): 101559.
2. Zhang X, Munir SZ, Sami Karim SA, Munir WM. A review of imaging modalities for detecting early keratoconus. *Eye*. 2021; 35(1): 173-87.
3. Reis D, Kupec J, Hong J, Daoudi A. Real-time flying object detection with YOLOv8. *arXiv preprint arXiv:2305.09972*. 2023 May 17.
4. Terven J, Córdova-Esparza DM, Romero-González JA. A comprehensive review of yolo architectures in computer vision: from yolov1 to yolov8 and yolo-nas. *Machine Learning and Knowledge Extraction*. 2023; 5(4): 1680-716.
5. Arbelaez MC, Versaci F, Vestri G, Barboni P, Savini G. Use of a support vector machine for keratoconus and subclinical keratoconus detection by topographic and tomographic data. *Ophthalmology*. 2012; 119(11): 2231-8.
6. Lavric A, Popa V, Takahashi H, Yousefi S. Detecting keratoconus from corneal imaging data using machine learning. *IEEE Access*. 2020;8:149113-21.
7. Michl M, Fabianska M, Seeböck P, Sadeghipour A, Najeeb BH, Bogunovic H, et al. Automated quantification of macular fluid in retinal diseases and their response to anti-VEGF therapy. *British Journal of Ophthalmology*. 2022; 106(1): 113-20.
8. Lavric A, Valentin P. KeratoDetect: keratoconus detection algorithm using convolutional neural networks. *Comput Intell Neurosci*. 2019; 2019(1): 8162567.
9. Al-Timemy AH, Ghaeb NH, Mosa ZM, Escudero J. Deep transfer learning for improved detection of keratoconus using corneal topographic maps. *Cognitive Computation*. 2022; 14(5): 1627-42.
10. Jocher G, Chaurasia A, Qiu J. Ultralytics YOLO (Version 8.0.0)[Computer software]. Available from: <https://github.com/ultralytics/ultralytics>. 2023.
11. Karn PK, Abdulla WH. Advancing ocular imaging: a hybrid attention mechanism-based u-net model for precise segmentation of sub-retinal layers in OCT images. *Bioengineering*. 2024; 11(3): 240.
12. Cho YS, Song HJ, Han JH, Kim YS. Attention mechanism-based glaucoma classification model using retinal fundus images. *Sensors*. 2024; 24(14): 4684.
13. Ma Y, Liu J, Liu Y, Fu H, Hu Yan, Cheng J. Structure and illumination constrained GAN for medical image enhancement. *Transactions on Medical Imaging*. 2021; 40(12): 3955-67.
14. Wang T, Wang M, Zhu W, Wang L, Chen Z, Peng Y, et al. Semi-MsST-GAN: a semi-supervised segmentation method for corneal ulcer segmentation in slit-lamp images. *Front Neurosci*. 2022; 15: 793377.
15. Ashir AM, Ibrahim S, Abdulghani M, Ibrahim AA, Anwar MS. Diabetic retinopathy detection using local extrema quantized haralick features with long short-term memory network. *Int J Biomed Imaging*. 2021; 2021: 6618666.

Evaluating the Latent Tuberculosis Diagnostic Tests Using Fuzzy PROMETHEE: A Multi-Criteria Decision Approach

✉ Declan Emegano¹, ✉ Nazife Sultanoğlu², ✉ Efe Precious Onakpojeruo^{1,3}, ✉ Berna Uzun^{1,4}, ✉ Dilber Uzun Ozsahin^{1,5,6}, ✉ Tamer Şanlıdağ²

¹Operational Research Center in Healthcare, Near East University, Nicosia, North Cyprus

²DESAM Research Institute, Near East University, Nicosia, North Cyprus

³Department of Biomedical Engineering, Near East University Faculty of Medicine, Nicosia, North Cyprus

⁴Department of Mathematics, Near East University Faculty of Medicine, Nicosia, North Cyprus

⁵Department of Medical Diagnostic Imaging, College of Health Sciences, University of Sharjah, Sharjah, United Arab Emirates

⁶Research Institute for Medical and Health Sciences, University of Sharjah, Sharjah, United Arab Emirates

Abstract

BACKGROUND/AIMS: Latent tuberculosis infection (LTBI) remains a critical challenge in global tuberculosis (TB) control efforts, necessitating effective diagnostic techniques. This study provides a comprehensive analysis of 7 diagnostic methods for LTBI, including QuantiFERON-TB and T-SPOT.TB.

MATERIALS AND METHODS: Seven different diagnostic techniques were evaluated against criteria such as specificity to *Mycobacterium tuberculosis*, sensitivity, cost-effectiveness, accessibility, limitations, turnaround time, etc. using multi-criteria decision-making methods (MCDMs). Weightings for each criterion were applied to account for their relative importance in clinical decision-making. To validate the results obtained using the fuzzy preference ranking organization method for enrichment evaluations we applied two additional MCDMs: the weighted sum method and the technique for order of preference by similarity to ideal solution using the same criteria, alternatives, and weightings.

RESULTS: Indicate that QuantiFERON-TB with a NetFlow of 0.0577 ranks highest in overall performance. T-SPOT.TB and Diaskintest followed closely, with minor variations in their rankings between the methods, while traditional methods such as Tuberculin Skin tests ranked lower due to their limitations in specificity and cross-reactivity. Sensitivity analysis further validated these rankings, suggesting that modern blood-based assays offer superior diagnostic accuracy and operational efficiency.

CONCLUSION: This study highlights the potential of fuzzy-based MCDM for selecting diagnostic tools for LTBI, contributing to more informed clinical practices and effective TB control strategies.

Keywords: Latent tuberculosis infection, diagnosis, comparison, multi-criteria decision-making methods

To cite this article: Emegano D, Sultanoğlu N, Onakpojeruo EP, Uzun B, Uzun Ozsahin D, Şanlıdağ T. Evaluating the latent tuberculosis diagnostic tests using fuzzy PROMETHEE: a multi-criteria decision approach. Cyprus J Med Sci. 2025;10(Suppl 1):55-59

ORCID IDs of the authors: D.E. 0000-0003-0258-9624; N.S. 0000-0002-5140-6938; E.P.O. 0000-0001-8582-409X; B.U. 0000-0002-5438-8608; D.U.O. 0000-0002-3873-1410; T.Ş. 0000-0002-6015-8032.



Corresponding author: Efe Precious Onakpojeruo

E-mail: efeprecious.onakpojeruo@neu.edu.tr

ORCID ID: orcid.org/0000-0001-8582-409X

Received: 01.11.2024

Accepted: 21.01.2025

Publication Date: 04.06.2025



Copyright© 2025 The Author. Published by Galenos Publishing House on behalf of Cyprus Turkish Medical Association.

This is an open access article under the Creative Commons AttributionNonCommercial 4.0 International (CC BY-NC 4.0) License.

INTRODUCTION

Tuberculosis (TB) is a transmissible disease caused by *Mycobacterium tuberculosis*, a bacteria which predominantly affects the lungs.¹ TB is transmitted via airborne particles when individuals infected with pulmonary TB cough, sneeze, or expectorate. Inhalation of a few pathogens is sufficient to contract an infection.² Upon acquiring the pathogen, individuals can be classified as having either active tuberculosis (aTB), characterized by clinical symptoms that may spread to multiple organs, or latent tuberculosis infection (LTBI), an asymptomatic state in which 5-10% of individuals may develop aTB in the following months or years.^{3,4} Although latent TB is not contagious, there is a significant risk of developing aTB later unless it is not diagnosed and treated, which presents a major obstacle to preventing TB.⁴ Therefore, diagnosing and treating LTBI play a crucial role in eliminating the disease. Diagnosing LTBI is challenging, despite the availability of a variety tests.⁵ No single test is sufficient, and evaluating the illness requires thorough clinical and radiographic assessment, as well as interpretation of immunological testing. Hence, there is still no gold standard test available for diagnosing LTBI. The available diagnostic procedures can be grouped to include: immune-based responses such as Tuberculin Skin test, Diaskintest, Combination Tuberculosis Skin test, T-SPOT.TB, QuantiFERON-TB Gold and Conventional Tuberculin Skin test, and Enzyme-Linked Immunoassay for Cytokines test. The use of multiple criteria decision-making methods (MCDM) has been widely recognized for its effectiveness in evaluating diverse strategies and alternatives across various domains.⁶ An example of MCDM-

Preference Ranking Organization METHOD for Enrichment Evaluations (PROMETHEE) with fuzzy logic, focuses on enhancing decision quality through rigorous analyses and could be employed in assessing the LTBI treatment strategies. Therefore, this study aims to use one of the successfully applied MCDM approaches, fuzzy preference ranking organization method for enrichment evaluations (F-PROMETHEE), for assessing the effectiveness of the 7 available LTBI diagnostic strategies.

MATERIALS AND METHODS

Fuzzy PROMETHEE Approach

F-PROMETHEE is an MCDM approach that employs fuzzy set theory to address uncertainty and imprecision in alternative evaluations, and was implemented in this study. Multiple criteria are suggested for ranking the alternatives (LTBI diagnostics). The parameters most frequently considered in the literature when determining the most effective diagnostic alternatives for LTBI include specificity, sensitivity, effectiveness, accessibility, limitations, ability to discriminate between latent and aTB, cost-effectiveness, cross-reactivity, turnaround time, and Food and Drug Administration (FDA) approval. Criteria serve as a benchmark for evaluating different alternatives. The relative importance of each criterion was assessed to determine its weight. Consequently, experts were consulted to assign relative importance levels to the selected criteria analyzed. Table 1 presents the decision matrix of the TB diagnostic strategies, which are evaluated using a linguistic scale shown in Table 2. The Yager index is used for defuzzification, and the Gaussian preference function is applied in the PROMETHEE analysis.

Table 1. The decision matrix of the selected TB strategies

Weightings	M	M	VH	M	M	M	L	H	M	H	
Alternatives/criteria	Specificity	Sensitivity	Effectiveness	Accessibility	Limitation	ADLATB	CE	CR	Avg. TT	FDA approved	References
Tuberculin Skin test	L	M	H	H	Requires two visits, FP, FN, skilled personnel, induration [H]	Yes	VL	Yes	4 days	Yes	1,7,8
Diaskintest	VH	H	VH	H	Induration [L]	No	H	Yes	3 days	Yes	2,9
Combination Tuberculosis Skin test	M	M	M	M	FN, impaired immune response [L]	Yes	L	Yes	1 day	Yes	2,10
T-SPOT.TB	H	H	H	M	Specific time for sample collection assay, induration [M]	No	L	Yes	1 day	Yes	2,11,12
QuantiFERON	VH	VH	VH	M	Inability to distinguish LTBI and aTB, FP/ FN, accessibility, requires skilled personnel [M]	No	H	No	1 day	Yes	2,13,14
ELISA	VH	VH	H	M	Cross reactivity, inability to different A and LTBI, needs skilled personnel [H]	No	M	Yes	2 days	No	2
Conventional Tuberculin Skin test	VH	H	VL	H	Positive predictive value, skin reactivity [L]	No	M	No	4 days	No	15,16

LTBI: Latent tuberculosis infection, aTB: Active tuberculosis, FP: False positive, FN: False negative, ADLATB: Ability to discriminate between latent and active TB, Avg.: Average, TT: Turnaround time, CR: Cross-reactivity, CE: Cost effect, VH: Very high, H: High, M: Moderate, L: Low, VL: Very low.

Statistical Analysis

Sensitivity Analysis

In this section, a sensitivity analysis was conducted to evaluate the robustness of the prior results. This study examines the impact of altering the weights of the evaluation criteria on the final ranking of the alternatives. The objective was to assess how changes in the relative significance of the selected criteria could influence the reliability of the conclusive outcome. In the sensitivity analysis, the weight of only two criteria was adjusted while keeping all other criteria constant. In the current study, significance weights were established for each criterion using a linguistic scale (Table 2). The weight of two essential criteria was adjusted: "Effectiveness," formerly rated as "very high", was decreased to "moderate", while "sensitivity," previously rated as "moderate", was elevated to "high". These modifications led to QuantiFERON-TB retaining its premier status, with a slightly decreased NetFlow (0.0475) (Table 3). This implies that altering the relative weights of individual criteria does not substantially impact the final ranking order. The single minor alteration is observed between the Conventional Tuberculin Skin Test and the Tuberculin Skin Test, characterized by a modest variance in NetFlow rankings. The initially integrated comprehensive ranking remained unchanged, despite variations in the outranking net flow values.

RESULTS

In this study, one of the decision-making tools known as F-PROMETHEE was proposed to rank 7 diagnostic methods for identifying LTBI based on selected parameters. This included sensitivity, specificity for *Mycobacterium tuberculosis*, cost, limitations, effectiveness, accessibility, cross-reactivity, FDA approval, and the time it takes to generate the result (Table 1). Among all the investigated methods, QuantiFERON-TB Gold proved to be the most efficient diagnostic tool with a NetFlow of 0.0557, indicating superior performance in specificity, sensitivity, and cost-efficiency. After QuantiFERON-TB, Diaskintest achieved the second-highest NetFlow (0.0296), indicating its high sensitivity and accessibility, especially for immunocompromised individuals. Conventional diagnostic methods, including the Tuberculin Skin tests, had a relatively lower NetFlow of -0.0407 and -0.0732, a consequence of low specificity and cross-reactivity, particularly in subjects vaccinated with Bacillus Calmette-Guérin. Results are summarized in Table 4.

Validation of Results with Weighted Sum and TOPSIS MCDM Methods

To validate the results obtained using the F-PROMETHEE approach, two more MCDM methods were applied: The weighted sum method (WSM) and the Technique for Order of Preference by Similarity to Ideal Solution (TOPSIS). The same criteria, alternatives, and weightings from

Table 4. Ranking of the latent tuberculosis infection tests using F-PROMETHEE

Rank	Alternatives	NetFlow (Phi)	Positive outranking flow (Phi+)	Negative outranking flow (Phi-)
1	QuantiFERON	0.0557	0.0687	0.0130
2	Diaskintest	0.0296	0.0514	0.0218
3	T-SPOT.TB	0.0236	0.0404	0.0168
4	ELISA	0.0070	0.0373	0.0302
5	Combination Tuberculin Skin test	-0.0021	0.0390	0.0411
6	Tuberculin Skin test	-0.0407	0.0311	0.0718
7	Conventional Tuberculin Skin test	-0.0732	0.0285	0.1016

F-PROMETHEE: Fuzzy Preference Ranking Organization METHOD for Enrichment Evaluations

Table 2. Linguistic scale and the weights assigned to criteria

Ranking Linguistic scale	Fuzzification scale	Criteria
VH	(0.75, 1, 1)	Effectiveness
H	(0.50, 0.75, 1)	Cross-reactivity, FDA-approved
M	(0.25, 0.50, 0.75)	Average turnaround time, ability to discriminate between latent and active TB, limitation, accessibility, sensitivity, specificity
L	(0, 0.25, 0.50)	Cost effectiveness
VL	(0, 0, 0.25)	

FDA: Food and Drug Administration, VH: Very high, H: High, M: Moderate, L: Low, VL: Very low.

Table 3. Sensitivity analysis results

Rank	Alternatives	NetFlow (Phi)	Positive outranking flow (Phi+)	Negative outranking flow (Phi-)
1	QuantiFERON	0.0475	0.0615	0.0140
2	Diaskintest	0.0209	0.0377	0.0167
3	T-SPOT.TB	0.0193	0.0428	0.0235
4	ELISA	0.0031	0.0343	0.0312
5	Combination Tuberculin Skin test	0.0026	0.0395	0.0369
6	Conventional Tuberculin Skin test	-0.0449	0.0307	0.0757
7	Tuberculin Skin test	-0.0485	0.0277	0.0762

Table 5. Comparison between fuzzy PROMETHEE, weighted sum method and TOPSIS methods

Alternatives	PROMETHEE net flow	Rank (PROMETHEE)	WSM score	Rank (WSM)	TOPSIS score	Rank (TOPSIS)
QuantiFERON	0.0557	1	0.8785	1	0.9201	1
T-SPOT.TB	0.0236	3	0.8602	2	0.8932	2
Diaskintest	0.0296	2	0.8157	3	0.8450	3
ELISA	0.0070	4	0.7820	4	0.8104	4
Combination Tuberculin Skin test	-0.0021	5	0.7455	5	0.7793	5
Tuberculin Skin test	-0.0407	6	0.6924	6	0.7245	6
Conventional Tuberculin Skin test	-0.0732	7	0.6712	7	0.7004	7

PROMETHEE: Preference Ranking Organization METHOD for Enrichment Evaluations, WSM: Weighted sum method, TOPSIS: Technique for Order of Preference by Similarity to Ideal Solution

the F-PROMETHEE analysis were applied to ensure consistency and comparability. The rankings obtained using F-PROMETHEE, WSM, and TOPSIS methods are presented in Table 5.

The results indicate strong agreement among the three methods, with minor variations in rankings for certain alternatives. QuantiFERON-TB Gold consistently emerged as the top-ranking diagnostic method. The Conventional Tuberculin Skin Test ranked lower across all methods due to its limitations in specificity, sensitivity, and turnaround time.

DISCUSSION

This study highlights the effectiveness of modern blood-based diagnostic tools like QuantiFERON-TB and T-SPOT.TB for detecting LTBI. Consistent with findings in the literature,^{2,12} our results demonstrate that traditional methods such as the Tuberculin Skin test are being surpassed due to their limitations, including cross-reactivity, false positives, and prolonged turnaround times, particularly in Bacillus Calmette-Guérin-vaccinated populations. QuantiFERON-TB emerged as the most reliable diagnostic tool, achieving the highest ranking across all methods (PROMETHEE, WSM, and TOPSIS). Its superior performance is attributed to high sensitivity, high specificity, minimal cross-reactivity, and a quick turnaround time of 24 hours. T-SPOT.TB and Diaskintest followed closely, with minor variations in their rankings between the methods. Notably, T-SPOT.TB exhibited strong performance regarding sensitivity, while Diaskintest demonstrated slightly better specificity and reliability in certain evaluations. The lower rankings of traditional methods, such as Tuberculin Skin test and the Conventional Tuberculin Skin test, further underscore their limitations in diagnostic accuracy and operational efficiency due to their prolonged turnaround time and operational complexity. The close agreement between the F-PROMETHEE, WSM, and TOPSIS results validates the robustness and reliability of findings, similar to the approach.¹⁷ This study represents the first application of F-PROMETHEE for a comprehensive comparison of 7 LTBI diagnostic tests, making it challenging to conduct a comparative analysis with previous studies in the field.

Study of Limitations

The evaluation of the study was simplified to seven LTBI diagnostic tests and ten criteria. Incorporating more diagnostic tests, such as biomarkers, and diagnostic criteria would change the rankings and potentially improve the study.

CONCLUSION

The results emphasize the role of improved diagnostics like QuantiFERON-TB, Diaskintest, and T-SPOT.TB for the diagnosis and

management of LTBI. The sensitivity analysis further validates these findings, showing that even when the weights applied to the evaluation measures are different, the modern blood-based assays are still the most accurate diagnostic tools for LTBI. These findings will provide knowledge to clinicians and policymakers in the enhancement of TB control, especially where the identification of LTBI cases remains paramount.

MAIN POINTS

- QuantiFERON-TB is the most favorable latent tuberculosis infection (LTBI) diagnosis amongst the 7 compared LTBI tests, considering selected criteria.
- Following QuantiFERON-TB, the next best ranks are T-SPOT.TB and Diaskintest for LBTI diagnosis.
- Validation of Fuzzy Preference Ranking Organization METHOD for Enrichment Evaluations results using Technique for Order of Preference by Similarity to Ideal Solution and weighted sum method confirms QuantiFERON-TB as the top-rank

ETHICS

Ethics Committee Approval: Not applicable.

Informed Consent: Not applicable.

Footnotes

Authorship Contributions

Concept: D.E., N.S., E.P.O., B.U., D.U.O., T.Ş., Design: D.E., N.S., E.P.O., B.U., D.U.O., T.Ş., Data Collection and/or Processing: D.E., N.S., E.P.O., B.U., D.U.O., T.Ş., Analysis and/or Interpretation: D.E., N.S., E.P.O., B.U., D.U.O., T.Ş., Literature Search: D.E., N.S., E.P.O., B.U., D.U.O., T.Ş., Writing: D.E., N.S., E.P.O., B.U., D.U.O., T.Ş.

DISCLOSURES

Conflict of Interest: No conflict of interest was declared by the authors.

Financial Disclosure: The authors declared that this study had received no financial support.

REFERENCES

1. Jonas DE, Riley SR, Lee LC, Coffey CP, Wang SH, Asher GN, et al. Screening for latent tuberculosis infection in adults: updated evidencen report and systematic review for the US preventive services task force. *JAMA*. 2023; 329(17): 1495-509.

2. Gong W, Wu X. Differential diagnosis of latent tuberculosis infection and active tuberculosis: a key to a successful tuberculosis control strategy. *Front Microbiol.* 2021; 12: 745592.
3. Kiazky S, Ball T. Latent tuberculosis infection: an overview. *Can Commun Dis Rep.* 2017; 43(3-4): 62-6.
4. Frahm M, Goswami ND, Owzar K, Hecker E, Mosher A, Cadogan E, et al. Discriminating between latent and active tuberculosis with multiple biomarker responses. *Tuberculosis.* 201; 91(3): 250-6.
5. Ho CS, Feng PJI, Narita M, Stout JE, Chen M, Pascopella L, et al. Comparison of three tests for latent tuberculosis infection in high-risk people in the USA: an observational cohort study. *Lancet Infect Dis.* 2022; 22(1): 85-96.
6. Onakpojeruo EP, Uzun B, David LR, Ozsahin I, Efe CC, Ozsahin DU. Integrating ANFIS, ANN, & MLR with MCDM for accurate prediction of lung cancer for improved clinical decision support. In 2024 17th International Conference on Development in eSystem Engineering (DeSE). 2024. pp. 445-450. IEEE.
7. Price C, Nguyen AD. Latent tuberculosis. In: StatPearls [Internet]. Treasure Island (FL): StatPearls Publishing; 2024 [cited 2024 Sep 18]. Available from: <http://www.ncbi.nlm.nih.gov/books/NBK599527/>
8. CDC. Tuberculosis (TB). 2024 [cited 2024 Sep 20]. Clinical Testing Guidance for Tuberculosis: Tuberculin Skin Test. Available from: <https://www.cdc.gov/tb/hcp/testing-diagnosis/tuberculin-skin-test.html>
9. Simeonov L. [Interpretation of the tuberculin reaction in BCG-vaccinated subjects]. *Tuberkuloza.* 1962;14:193-216.
10. Shenoy B, Reddy HT. C-Tb skin test: a step toward tuberculosis eradication. *Pediatric Infectious Disease.* 2024; 15;6(2); 55.
11. Carranza C, Pedraza-Sanchez S, De Oyarzabal-Mendez E, Torres M. Diagnosis for latent tuberculosis infection: new alternatives. *Front Immunol.* 2020; 11: 2006.
12. Xu M, Lu W, Li T, Li J, Du W, Wu Q, et al. Sensitivity, specificity, and safety of a novel ESAT6-CFP10 skin test for tuberculosis infection in China: 2 randomized, self-controlled, parallel-group phase 2b trials. *Clin Infect Dis.* 2022; 74(4): 668-77.
13. Takasaki J, Manabe T, Morino E, Muto Y, Hashimoto M, Iikura M, et al. Sensitivity and specificity of QuantiFERON-TB Gold Plus compared with QuantiFERON-TB Gold In-Tube and T-SPOT.TB on active tuberculosis in Japan. *J Infect Chemother.* 2018; 24(3): 188-92.
14. CDCTB. Centers for Disease Control and Prevention. 2022 [cited 2024 Sep 20]. Tuberculosis (TB) - Deciding When to Treat Latent TB Infection. Available from: <https://www.cdc.gov/tb/topic/treatment/decideltbi.htm>
15. Lalvani A, Berrocal-Almanza LC, Halliday A. Predicting progression to active tuberculosis: a rate-limiting step on the path to elimination. *PLoS Med.* 2019; 16(5): 1002814.
16. Hamada Y, Surkova E, Kontsevaya I, Wang TT, Liu V, Ziganshina IE, et al. Accuracy of Mycobacterium tuberculosis antigen-based skin tests: a systematic review and meta-analysis. In: WHO consolidated guidelines on tuberculosis: Module 3: Diagnosis – Tests for tuberculosis infection [Internet]. World Health Organization; 2022 [cited 2024 Sep 20]. Available from: <https://www.ncbi.nlm.nih.gov/books/NBK586667/>
17. Ozsahin I, Onakpojeruo EP, Uzun B, Uzun Ozsahin D, Butler TA. A Multi-criteria decision aid tool for radiopharmaceutical selection in Tau PET imaging. *Pharmaceutics.* 2023; 15(4): 1304.

Contribution of Multi-Criteria Decision-Making Approach in Choosing the Most Appropriate Rapid Diagnostic Tests in an Outbreak

✉ Ayşe Arıkan^{1,3}, ✉ Berna Uzun^{4,5}, ✉ Murat Sayan^{1,6}, ✉ Dilber Uzun Ozsahin^{4,7,8}, ✉ Tamer Şanlıdağ¹

¹DESAM Research Institute, Near East University, Nicosia, North Cyprus

²Department of Medical Microbiology and Clinical Microbiology, Near East University Faculty of Medicine, Nicosia, North Cyprus

³Department of Medical Microbiology and Clinical Microbiology, Kyrenia University Faculty of Medicine, Kyrenia, North Cyprus

⁴Operational Research Center in Healthcare, Near East University, Nicosia, North Cyprus

⁵Department of Mathematics, Near East University Faculty of Arts and Sciences, Nicosia, North Cyprus

⁶PCR Unit, Research and Education Hospital, Kocaeli University, Kocaeli, Türkiye

⁷Department of Medical Diagnostic Imaging, Sharjah University College of Health Sciences, Sharjah, United Arab Emirates

⁸Research Institute for Medical and Health Sciences, University of Sharjah, Sharjah, United Arab Emirates

Abstract

BACKGROUND/AIMS: Rapid diagnostic tests are designed to enable rapid diagnosis of infectious diseases, especially during outbreaks and pandemics. This study aims to retrospectively list the rapid antigen (Ag) tests used in the recent pandemic with the multi-criteria decision-making (MCDM) technique to evaluate the role of the MCDM technique in determining the most appropriate diagnostic techniques during a future outbreak.

MATERIALS AND METHODS: Twenty-eight Ag diagnostic tests authorized for emergency use by the Food and Drug Administration during the coronavirus disease-2019 pandemic were retrospectively included. Limit of detection, positive and negative percent agreement, point-of-care test, sample type, test technique, Ag target, and result time were evaluated. The overall performance of the 28 Ag diagnostic tests was investigated using the fuzzy preference ranking organization method (F-PROMETHEE) of the MCDM approaches.

RESULTS: According to the F-PROMETHEE analysis; clip coronavirus disease rapid ag test was ranked in first place, Sofia 2 Flu + severe acute respiratory syndrome (SARS) Ag fluorescent immunoassay, BD Veritor System, and VITROS Immunodiagnostic Products severe acute respiratory syndrome-coronavirus-2 (SARS-CoV-2) test kits were ranked second, and third, respectively. The VITROS Immunodiagnostic Products SARS-CoV-2 Ag Reagent Pack was ranked last, due to the selected parameters in the ranking.

CONCLUSION: The F-PROMETHEE method, one of the MCDM methods, can be applied to evaluate the tests used in the rapid diagnosis of pathogens, and can support clinicians and laboratories in choosing the most reliable and accurate diagnostic tests in future outbreaks and pandemics.

Keywords: Disease outbreaks, diagnostic tests, fuzzy logic, MCDM, PROMETHEE

To cite this article: Arıkan A, Uzun B, Sayan M, Uzun Ozsahin D, Şanlıdağ T. Contribution of multi-criteria decision-making approach in choosing the most appropriate rapid diagnostic tests in an outbreak. Cyprus J Med Sci. 2025;10(Suppl 1):60-64

ORCID IDs of the authors: A.A. 0000-0003-1942-1203; B.U. 0000-0002-5438-8608; M.S. 0000-0002-4374-7193; D.U.O. 0000-0002-3873-1410; T.Ş. 0000-0002-6015-8032.



Corresponding author: Ayşe Arıkan

E-mail: aysearıkancy@yahoo.com

ORCID ID: orcid.org/0000-0003-1942-1203

Received: 01.11.2024

Accepted: 21.01.2025

Publication Date: 04.06.2025



Copyright© 2025 The Author. Published by Galenos Publishing House on behalf of Cyprus Turkish Medical Association.

This is an open access article under the Creative Commons AttributionNonCommercial 4.0 International (CC BY-NC 4.0) License.

INTRODUCTION

Nucleic acid amplification with the real-time polymerase chain reaction technique is the gold standard in the identification of emerging microbial pathogens; however, antigen (Ag) testing, which detects virus-specific proteins, is widely used in the rapid diagnosis of pathogens, especially in extraordinary situations and disasters like pandemics.¹ Ag tests can be performed using both the nasopharyngeal swab and anterior nares. These tests are easy to use and are more suitable for point-of-care (POC) testing. As Ag diagnostic tests provide rapid and accurate results at a relatively low cost compared to the reference methods, they have made critical contributions in the control of the last pandemic.² During the pandemic, Ag tests were recommended for people with symptoms, asymptomatic individuals at high risk of infection, and for the purposes of contact tracing and screening of severe acute respiratory syndrome-coronavirus-2 (SARS-CoV-2) infected persons for epidemiologic investigations.³ Various Ag diagnostic tests were classified as “emergency-use authorized” for SARS-CoV-2 patient management during the global crisis.⁴ During the coronavirus disease-2019 (COVID-19) pandemic, many companies contributed to the management of the pandemic by specifically developing Ag tests in a short time frame. However, as the pandemic progressed, different measurements were needed to monitor the efficiency and clinical performance of these options. Multi-criteria decision making (MCDM) techniques are approaches that assist decision-makers (DMs) when faced with a selection problem involving multiple criteria.

Numerous issues, including the weights of the criteria, preference dependence, and conflicts between criteria, seem to exacerbate problems when DM evaluates the alternatives. This process requires the use of more advanced techniques to resolve them.^{5,6} Hwang and K. Yoon⁷ proposed that MCDM problems can be divided into two major categories: multiple attribute DMs and multiple objective DMs, due to the various purposes and various types of data. Fuzzy logic theory, published by Lotfi A. Zadeh^{8,9}, was the first to study the fuzzy logic process⁶ mathematically. Zadeh⁸ has brought many concepts to science, such as fuzzy sets, fuzzy logic, approximate reasoning, linguistic variables, and fuzzy if-then rules.

This study aimed to demonstrate the role and usability of the MCDM method in deciding the most appropriate diagnostic test during extraordinary circumstances by ranking the Ag tests that were used during the COVID-19 pandemic. The key advantage of the current study is that the fuzzy MCDM algorithms will serve as a model for evaluating diagnostic alternatives designed for future outbreaks and pandemics.

MATERIALS AND METHODS

One of the most successful MCDM techniques, the fuzzy preference ranking organization method (F-PROMETHEE) technique, was preferred to analyze Ag tests used for SARS-CoV-2 detection. The study was retrospectively performed, and the most frequently performed Ag testing during the COVID-19 pandemic was utilized to mimic the testing methodology of a similar global health problem. In the current study, linguistic triangular fuzzy sets were applied to determine the criteria and their weights numerically. As a preprocessing step for the data, the defuzzification process was then applied via Yager¹⁰ index to gather numerical information for the selected variables, preparing it for use in the PROMETHEE approach. The PROMETHEE approach enables DMs to rank the alternatives that contain various features.¹¹ The PROMETHEE

approach, with fuzzy logic, is a recent MCDM technique that compares alternatives under an ambiguous environment. In this approach, the triangular fuzzy sets are used to determine the linguistic data numerically as fuzzy numbers.

Twenty-eight different SARS-CoV-2 Ag kits that had been authorized for emergency use by the Food and Drug Administration (FDA) during the pandemic were evaluated in this study. These criteria were included according to the information provided by the FDA.⁴ While predominantly lateral flow assay (72%) and chemiluminescent immunoassay (28%) were used in the study, paramagnetic micro-based immunoassays, bulk acoustic wave biosensors, and chromatographic digital immunoassay were also evaluated using mathematical tools. We preferred to use PROMETHEE for analysis since it provides different types of preference functions to determine the superiority of each decision option for each criterion. This distinguishes it from other MCDM models and shows the advantages and disadvantages of each decision option, allowing experts to control for result validation. The criteria used for analysis were: limit of detection (LoD); sensitivity/specificity; POC testing; specimen options (nasopharyngeal swab/anterior nasal swab); test techniques; Ag target [nucleocapsid (N)/spike (S)]; testing for SARS-CoV-2 and flu; time to result; first sampling after symptom onset; reagent storage conditions; requiring analyzer.

F-Promethee Analysis

These criteria were evaluated as linguistic triangular fuzzy sets: “very high (0.75, 1, 1)”, “high (0.5, 0.75, 1)”, “moderate/(0.25,0.5,0.75)”, “low/(0, 0.25, 0.75)”, and “very low/(0, 0, 0.25)” and the SARS-CoV-2 pandemic was considered during this scoring. After data collection, defuzzification was applied to convert fuzzy numbers to single numbers. Then the PROMETHEE method was applied with the Gaussian preference function. The detailed process of the PROMETHEE approach is given in.^{11,12} In this study, the importance values of the selected criteria were obtained based on experts’ preferences as follows: very high: the LoD, positive predictive value/sensitivity, negative predictive value/specificity: high: the point of care testing, specimen option, target, sampling days after symptom onset, result time: moderate: the requiring analyzer, attributes-visual read, test for SARS-CoV-2/Flu, storage.

Ethical Approval

Ethical approval, including patient-informed consent, was not needed as the study involved publicly available data and did not involve human clinical samples.

RESULTS

Among 28 FDA emergency use authorization Ag diagnostic tests for SARS-CoV-2, clip COVID rapid Ag test [Luminostics, Inc., California, United States of America (USA)] was determined to be the most favorable one, followed by Sofia 2 Flu + SARS Ag fluorescent immunoassay (Quidel Corporation, San Diego, USA) and BD Veritor System for Rapid Detection of SARS-CoV-2 (Becton Dickinson and Company, New York, USA). Our finding showed that the clip COVID rapid Ag test (Luminostics, Inc, California, USA), which was the most feasible Ag testing kit according to the ranking, is a POC test that gives results with a portable clip analyzer. Due to its sensitivity and specificity of 96.9% and 100%, respectively, with a LoD of 0.88×10^2 TCID50 per milliliter, this method is highly reliable for diagnostic purposes. Furthermore, nasal swabs obtained within 5 days after the onset of symptoms were used, which still provided reliable

results.⁴ The complete ranking of Ag tests against SARS-CoV-2 is given in Table 1. This table includes more than 28 Ag tests because some tests can be performed either by nasopharyngeal swab or anterior nasal swab, which affects the sensitivity of the test results. Therefore, they were evaluated independently in this study, and different specimen options of the same test were differentiated with asterisks in Table 1. Test kits with an asterisk indicate that both nasopharyngeal swabs and nasal swabs can be used as specimen collection options. Test kits without an asterisk indicate that a nasopharyngeal swab is the only specimen collection option. These results were obtained using the Decision Lab program.

DISCUSSION

Recently, disease outbreaks with unknown new pathogens have been reported.¹³ In the most recent COVID-19 pandemic, a fluctuating increase in cases was detected during the timeline of the pandemic.¹⁴ Therefore, measures have been taken to control the number of cases. However, implementations such as the closure of borders, schools, and workplaces have also had disparate effects.¹⁵ For this reason, control measurements were extended by continuing the screening tests during the later phases of the pandemic. Throughout the pandemic, Ag tests were useful in rapidly screening large populations. Although definitive detection of the virus is dependent on the detection of RNA gene targets such as S, envelope, N, RNA-dependent RNA polymerase, ORF1 by nucleic acid amplification testing, detection of virus-specific

Table 1. Ranking results of SARS-CoV-2 antigen tests during the pandemic

Rank	Ag test	Technique	Phi	Phi+	Phi-
1	Clip	LFA	0.1063	0.1191	0.0128
2	Sofia 2 flu + SARS	LFA	0.0981	0.1156	0.0195
3	BD veritor	Chromatographic immunoassay	0.0906	0.1196	0.029
4	Sofia SARS Ag FIA	LFA	0.0890	0.1032	0.0141
5	LumiraDx*	Micro-fluid immunoassay	0.0872	0.1293	0.0420
6	Celltrion DiaTrust	LFA	0.0766	0.1169	0.0403
7	LumiraDx	Micro-fluid immunoassay	0.0705	0.1193	0.0488
8	QuickVue Ag	LFA	0.0681	0.0978	0.0297
9	Sampinute	Magnetic force immunoassay	0.0617	0.1163	0.0546
10	Status COVID-19/flu	LFA	0.0467	0.0935	0.0469
11	GenBody	LFA	0.0341	0.0861	0.0519
12	SCoV-2	LFA	0.0336	0.0894	0.0558
13	CareStart	LFA	0.0304	0.0843	0.0539
14	Ellume	LFA	0.0236	0.0846	0.0610
15	The LIAISON**	CLIA	0.0063	0.0878	0.0815
16	Simoa	CLIA	-0.0087	0.1156	0.1244
17	CareStart*	LFA	-0.0148	0.0589	0.0737
18	The BD Veritor™ flu A + B	Chromatographic immunoassay	-0.0172	0.0495	0.0668
19	TheBinaxNOW self test	LFA	-0.0218	0.0460	0.0678
19	BinaxNOW	LFA	-0.0218	0.0460	0.0678
21	The LIAISON®	CLIA	-0.0225	0.0738	0.0964
22	Qorvo omnia	Immunoassay	-0.0245	0.0636	0.0882
23	BinaxNOW Ag2	LFA	-0.0260	0.0426	0.0685
24	BinaxNOW Ag Card 2	LFA	-0.0297	0.0422	0.0719
25	QuickVue at home	LFA	-0.0382	0.0401	0.0783
26	Sienna-clarity	LFA	-0.0441	0.0454	0.0895
27	QuickVue at home OTC	LFA	-0.0446	0.0388	0.0834
28	BinaxNOW	LFA	-0.0539	0.0364	0.0903
29	InteliSwab Rx	LFA	-0.0544	0.0351	0.0895
29	InteliSwab	LFA	-0.0544	0.0351	0.0895
31	InteliSwab pro	LFA	-0.0553	0.0351	0.0879
32	Ellume.lab	LFA	-0.0622	0.0367	0.0989
33	VITROS*	CLIA	-0.1348	0.0229	0.1677
34	VITROS	CLIA	-0.1937	0.0147	0.2

Ag: Antigen, LFA: Lateral flow assay, CLIA: Chemiluminescent immunoassay, Phi: Net ranking, Phi+: Positive outranking flow, Phi-: Negative outranking flow, COVID-19: Coronavirus disease-2019, SARS: Severe acute respiratory syndrome, OTC: Over-the-counter

proteins by Ag testing has been preferred during the global crisis.¹⁶ Many manufacturers developed diagnostic alternatives for SARS-CoV-2 to combat the global crisis. However, it was not easy to choose the most accurate test among many alternatives. This study revealed the effective role of the F-PROMETHEE technique in diagnostic microbiology. The applicability of the technique in making correct choices in similar public health concerns was demonstrated.

Throughout the world, preventing and controlling widespread outbreaks is a priority. Clemente-Suárez et al.¹⁷ provided information on the performance of fuzzy MCDM analysis of emergency systems regarding the applications of the technique in hospital settings during the pandemic, as currently applied. As the pandemic continues, the emergence of new variants may cause difficulties with the virus's diagnosis, treatment, and prevention. Therefore, MCDM methods have been widely implemented to address this complexity. Sayan et al.¹¹ evaluated the capacity of SARS-CoV-2 diagnostic tests using MCDM.¹¹ The study on COVID-19 diagnostic tests was conducted at the beginning of the pandemic and focused on diagnostic testing techniques. Similarly, treatment alternatives for COVID-19 were evaluated by Yildirim et al.⁶ using a fuzzy MCDM approach, and they revealed the most appropriate diagnostic and treatment options to support healthcare professionals.

To our knowledge, this work presents a new study evaluating test kits for microbial diagnosis using the F-PROMETHEE technique. This study revealed that the performance of rapid diagnostic tests, widely used in the rapid diagnosis of infectious diseases, especially during disasters, can be evaluated with mathematical approaches before clinical use. Such approaches can guide diagnostic laboratories to choose the most appropriate rapid diagnostic tests to manage future outbreaks and pandemics effectively.

Study Limitations

To point out the study's limitations, positive and negative control samples could not be used because the study was based on mathematical data analysis and was not conducted with clinical samples. Secondly, the results were obtained based on the nature of the analytical DMs process, selected parameters, and the experts' preferences for determining the importance of the criteria; thus, these parameters can be updated according to the DMs' priorities. Thirdly, the study was based on data from the test kit insert rather than clinical data. This data did not include positive and negative controls, which may have altered the results. Additionally, only the F-PROMETHEE technique was used in the study. Comparison of results with other MCDM techniques such as Technique for Order Preference by Similarity to Ideal Solution, Analytic Hierarchy Process, and Elimination and Choice Expressing REality may have affected the ranking.

CONCLUSION

In outbreaks, low-cost rapid diagnostic tests can be prioritized to reduce the workload of healthcare systems. By applying MCDM methods, DMs can systematically analyze multiple factors and prioritize tests according to their importance and necessity in outbreaks. The F-PROMETHEE method can be applied in this field, supporting DM in deciding on the most reliable and accurate rapid test for pathogen detection throughout outbreaks in the future. Additionally, each country can use appropriate diagnostic solutions according to its resources.

MAIN POINTS

- Severe acute respiratory syndrome coronavirus-2 (SARS-CoV-2) clip coronavirus disease rapid antigen (Ag) test is the most reliable test to be used in SARS-CoV-2 Ag detection based on the selected data.
- The fuzzy preference ranking organization method can support clinicians and laboratories in choosing the most reliable and accurate Ag tests.
- Multi-criteria decision-making methods can be implemented to tests.

ETHICS

Ethics Committee Approval: Not applicable.

Informed Consent: Not applicable.

Footnotes

Authorship Contributions

Concept: A.A., B.U., M.S., D.U.O., T.Ş., Design: A.A., B.U., M.S., D.U.O., T.Ş., Data Collection and/or Processing: A.A., M.S., T.Ş., Analysis and/or Interpretation: B.U., D.U.O., Literature Search: A.A., M.S., Writing: A.A., B.U.

DISCLOSURES

Conflict of Interest: No conflict of interest was declared by the authors.

Financial Disclosure: The authors declared that this study had received no financial support.

REFERENCES

1. Dinnes J, Sharma P, Berhane S, van Wyk SS, Nyaaba N, Domen J, et al. COVID-19 diagnostic test accuracy group. Rapid, point-of-care antigen tests for diagnosis of SARS-CoV-2 infection. *Cochrane Database Syst Rev.* 2022; 7(7): 013705.
2. Truong TT, Dien Bard J, Butler-Wu SM. Rapid antigen assays for SARS-CoV-2: promise and peril. *Clin Lab Med.* 2022; 42(2): 203-22.
3. Polechová J, Johnson KD, Payne P, Crozier A, Beiglböck M, Plevka P, et al. SARS-CoV-2 rapid antigen tests provide benefits for epidemic control - observations from Austrian schools. *J Clin Epidemiol.* 2022; 145: 14-9.
4. The Food and Drug Administration (FDA). *Vitro Diagnostics EUAs - Antigen diagnostic tests for SARS-CoV-2*, Available from URL: <https://www.fda.gov/medical-devices/covid-19-emergency-use-authorizations-medical-devices/in-vitro-diagnostics-euas-antigen-diagnostic-tests-sars-cov-2>. Accessed: Jun. 26, 2023.
5. Tzeng GH, Huang JJ. *Multiple attribute decision making: methods and applications*. New York: Chapman and Hall/CRC. 2011; pp. 352.
6. Yildirim FS, Sayan M, Sanlidag T, Uzun B, Ozsahin DU, Ozsahin I. Comparative evaluation of the treatment of COVID-19 with multi-criteria decision-making techniques. *J Healthc Eng.* 2021; 2021: 8864522.
7. Hwang CL, Yoon K. *Methods for multiple attribute decision making*. In: *Multiple Attribute Decision Making. Lecture Notes in Economics and Mathematical Systems*. Springer, Berlin, Heidelberg; 1981; pp. 58-191.
8. Zadeh LA. "Fuzzy sets", *Information and Control.* 1965; 8(3): pp. 338-53.
9. Ozsahin DU, Uzun B, Ozsahin I, Mustapha M, Musa M. *Fuzzy logic in medicine.* 2020; pp. 153-182.

10. Yager R. A procedure for ordering fuzzy subsets of the unit interval. *Information Sciences*. 1981; 24(2): 143-61.
11. Sayan M, Sarigul Yildirim F, Sanlidag T, Uzun B, Uzun Ozsahin D, Ozsahin I. Capacity evaluation of diagnostic tests for COVID-19 using multi-criteria decision-making techniques. *Comput Math Methods Med*. 2020; 6: 2020.
12. Uzun B, Almasri A, Ozsahin DU. Preference ranking organization method for enrichment evaluation (Promethee), in application of multi-criteria decision analysis in environmental and civil engineering, Ozsahin DU, Gökçekuş H, Uzun B, LaMoreaux J. Eds., in *Professional Practice in Earth Sciences*. Cham: Springer International Publishing, 2021; pp. 37-41.
13. Guo C, Wu JY. Pathogen discovery in the post COVID-Era. *Pathogens*. 2024; 13(1): 51.
14. The CDC Museum COVID-19 Timeline. Available from URL: <https://www.cdc.gov/museum/timeline/covid19.html> accessed 30 June 2023.
15. Deb P, Furceri D, Ostry JD, Tawk N. The economic effects of COVID-19 containment measures. *Open Econ. Rev*. 2022; 33(2022): 1-32.
16. Jalali Nadoushan M, Ahmadi S, Jalali Nadoushan P. Serology testing for SARS-CoV-2: benefits and challenges. *Iran J Pathol*. 2020; 15(3): 154-5.
17. Clemente-Suárez VJ, Navarro-Jiménez E, Ruisoto P, Dalamitos AA, Beltran-Velasco AI, Hormeño-Holgado A, et al. Performance of fuzzy multi-criteria decision analysis of emergency system in COVID-19 pandemic. An extensive narrative review. *Int J Environ Res Public Health*. 2021; 18(10): 5208.

The Cytotoxic Activity of Rosemary Essential Oil on PANC-1 Cells

Mustafa Hoca^{1,2}, Eda Becer³, Abdussalam Yakubu⁴, Hafize Seda Vatansever^{5,6}

¹Department of Nutrition and Dietetics, Near East University Faculty of Health Sciences, Nicosia, North Cyprus

²Research Center for Science, Technology and Engineering (BILTEM), Near East University, Nicosia, North Cyprus

³Eastern Mediterranean University Faculty of Pharmacy, Famagusta, North Cyprus

⁴Near East University Faculty of Pharmacy, Nicosia, North Cyprus

⁵DESAM Research Institute, Near East University, Nicosia, North Cyprus

⁶Department of Histology and Embryology, Manisa Celal Bayar University Faculty of Medicine, Manisa, Türkiye

Abstract

BACKGROUND/AIMS: The goal of this research was to analyze the cytotoxic impacts of rosemary essential oil on pancreatic cancer.

MATERIALS AND METHODS: The human pancreatic cancer cell line (PANC-1) was used. The leaves of rosemary cultivated in North Cyprus were collected during the flowering stage. Rosemary essential oil was obtained after air-dried leaves (100 g) were distilled with water for 3 hours. Rosemary essential oil solutions were prepared and diluted in culture medium using various concentrations (100, 200, 300, 400, 500, and 600 µM) for 24 hours and 48 hours incubation periods. The analysis of cytotoxicity was conducted using the MTT [3-(4,5-dimethylthiazol-2-yl)-2,5-diphenyl tetrazolium bromide].

RESULTS: Rosemary oil at 500 µM was more effective in diminishing the proliferation of PANC-1 cells than other concentrations during 48 hours. Cell viability was significantly greater at 100 µM for 24 hours (100%) than 600 µM for 48 hours (81.48%). It was determined that substantially greater cell viability was observed at 200 µM for 24 hours (97.05%) when compared to 600 µM for 48 hours (81.48%). In addition, when various concentrations were evaluated during 48 hours, significant differentiation was found between 100 µM and 600 µM. It was shown that there was a significant differentiation between 200 µM and 600 µM for 48 hours.

CONCLUSION: Cell viability was substantially less at 600 µM than at 100 µM and 200 µM, 81.48%, 95.18%, and 90.23%, respectively.

Keywords: Cytotoxic, essential oil, pancreatic cancer, rosemary

INTRODUCTION

Pancreatic cancer has a five-year survival rate of less than 5%, having the worst prognosis. The maximum survival rate has been reported to be approximately 2 years, even in individuals in the early stages, who have undergone surgery or chemotherapy treatment. The reasons for this situation can be explained by various factors. First, because of the lack of effective tools for early diagnosis, most patients present with

metastatic disease when diagnosed. In addition to metastasis, early recurrence is a specific feature of pancreatic cancer and worsens the prognosis of the disease. Resistance to chemotherapy or radiation treatments also increases the risk of mortality.¹

A large number of spices and medicinal plants are reported in the literature. Among these, *Rosmarinus officinalis L.*, known as rosemary, is highlighted for its various potential activities, including anti-cancer

To cite this article: Hoca M, Becer E, Yakubu A, Vatansever HS. The cytotoxic activity of rosemary essential oil on PANC-1 cells. Cyprus J Med Sci. 2025;10(Suppl 1):65-68

ORCID IDs of the authors: M.H. 0000-0003-3609-5868; E.B. 0000-0002-2378-128X; A.Y. 0009-0005-1984-0792; H.S.V. 0000-0002-7415-9618.



Corresponding author: Mustafa Hoca
E-mail: mustafa.h.91@hotmail.com
ORCID ID: orcid.org/0000-0003-3609-5868

Received: 02.11.2024
Accepted: 10.01.2025
Publication Date: 04.06.2025



Copyright© 2025 The Author. Published by Galenos Publishing House on behalf of Cyprus Turkish Medical Association.
This is an open access article under the Creative Commons AttributionNonCommercial 4.0 International (CC BY-NC 4.0) License.

activity.² Rosemary is one of the most popular herbs used for culinary purposes. Native to the Mediterranean region, this herb is grown in different regions around the world.³ Rosemary essential oil is obtained from the leaves of the rosemary plant. Rosemary oil is rich in certain compounds. These include carnosol, carnosic acid, and rosmarinic acid.⁴ Rosemary essential oil is obtained by the hydrodistillation extraction method. There may be variation depending on the age of the plant and harvest time. Its volume is generally stated as 10 mL/kg of dry plant material. Various effects (anti-inflammatory, anti-proliferative, anti-obesity, antioxidant, anti-tumor, anti-microbial, and neuroprotective) of rosemary have been shown in the literature.⁵

Rosemary and its derivatives may show potential anti-cancer effects owing to their anti-oxidant, anti-angiogenic, and anti-inflammatory features, as well as increasing the expression of onco-suppressor genes.⁶ Studies have been conducted in the literature on rosemary essential oil and various types of cancer.⁷⁻¹²

There have been a limited number of studies in the literature examining the relationship between rosemary oil and pancreatic cancer. Therefore, the objective of this study was to interpret the cytotoxic impacts of rosemary essential oil on pancreatic cancer cells.

MATERIALS AND METHODS

Cell Culture

Human pancreatic cancer cell line-1 (PANC-1) was used for this study. Medium containing Dulbecco's modified Eagle's medium (DMEM), 10% heat-inactivated fetal bovine serum, 1% penicillin-streptomycin, and 1% L-glutamine was used for maintaining the PANC-1. Since this was a cell study, not a human study, informed consent was not obtained.

Plant and Essential Oil Isolation Process

The storage and identification of samples were carried out according to the study by Becer et al.⁹ The leaves of rosemary cultivated in North Cyprus were collected during the flowering stage. Rosemary essential oil was obtained after air dried leaves (100 g) were distilled with water for 3 hour. A temperature of 4 °C was preferred for storing the essential oil until analysis.

Cell Viability

MTT was used for the cytotoxicity analysis. The protocol for MTT was adopted according to the study by Hoca et al.¹³ Various concentrations of rosemary essential oil (100-200-300-400-500-600- μ M) were used to treat PANC-1 cells for two incubation periods (24 hours and 48 hours). Absorbance values were evaluated at 570 nm finally.

Statistical Analysis

Data were presented as mean and standard deviation values. The outcomes were evaluated using Statistical Package for the Social Sciences 18.0. Kruskal-Wallis test and/or Mann-Whitney U tests were employed for differences among groups. When evaluated statistically, $p < 0.05$ was considered significant.

RESULTS

The cell viability was analyzed with MTT. Rosemary oil, in all concentrations, reduced the growth of PANC-1 cells in a time- and/or dose-dependent manner. It was indicated that rosemary oil at 500 μ M,

was more efficient in decreasing the proliferation of cells than other concentrations for 48 hours (Figure 1).

When diverse concentrations (100-200-300-400-500-600 μ M) and incubation conditions (24 and 48 hours) were examined, the cell viability was substantially greater at 100 μ M for 24 hours (100%) than 600 μ M for 48 hours (81.48%) ($p < 0.05$). It was also determined that cell viability was substantially greater at 200 μ M for 24 hours (97.05%) than at 600 μ M for 48 hours (81.48%), ($p < 0.05$). Moreover, when various concentrations were examined during 48 hours, significant differentiation was found between 100 μ M and 600 μ M ($p < 0.05$). There was a significant difference between 200 μ M and 600 μ M for 48 hours ($p < 0.05$). When the viability of cells was examined, cell viability was substantially less at 600 μ M (81.48%) than 100 μ M (95.18%) and 200 μ M (90.23%) (Table 1).

DISCUSSION

Rosemary and its components can show anti-cancer activity due to their apoptotic characteristics.¹⁴ Santos et al.⁷ showed that rosemary essential oil exhibited no substantial effect on cell viability in cervical cancer cells (HeLa) compared with human liver cells (HepG2). This study emphasized that rosemary oil at a concentration of 500 μ M was more effective in declining PANC-1 cell proliferation than other concentrations during the 48-hour period. Al-otaibi¹⁵ showed that 50% decline of human breast adenocarcinoma cell growth when breast cancer cells were treated with 1% (v/v) nano-emulsified rosemary oil + 1.49 μ M of mitomycin C. Thus, this study stated that rosemary oil can increase the effect of the anti-neoplastic agent mitomycin C.

Rosmarinus officinalis white extract showed a significant effect on human colon cancer HT-29 cells: a 50% reduction was achieved at 49.6231 μ g/mL after 48 hours.¹⁶ Rosemary extracts have been shown to be more powerful in reducing cell viability of colon cancer cells

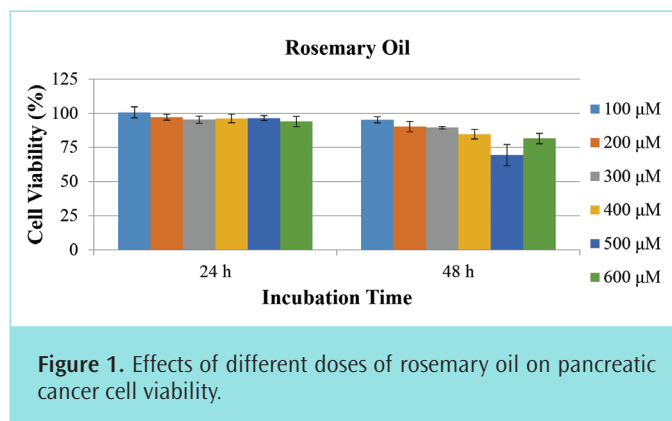


Figure 1. Effects of different doses of rosemary oil on pancreatic cancer cell viability.

	Cell viability-24 hour	Cell viability-48 hour
100 μ M	100%	95.18%
200 μ M	97.05%	90.23%
300 μ M	95.30%	89.41%
400 μ M	96.20%	84.61%
500 μ M	96.47%	69.41%
600 μ M	93.96%	81.48%

than pancreatic cancer cells. Thus, it has been demonstrated that colon cancer cells are more susceptible, and it has been demonstrated that pancreatic cancer cells, especially the PANC-1 cell line, are more resistant.¹⁷ In this research, when the effect of rosemary oil on their viability was evaluated, it was observed that there was no decrease below 50% in cell viability, supporting the idea that the PANC-1 cell line may be resistant.

In a study examining cell viability using the MTT test, it was found that the use of rosemary reduced the viability of glioblastoma cells by approximately 57.2%. However, when 500 µg/mL acyclovir and rosemary were used in combination, they had a 10% greater reductive effect on the viability of glioblastoma cells, unlike their separate effects.¹⁸ In this study, especially after 48 hours, rosemary oil reduced cancer cell viability more at higher concentrations (500 µM) compared to other concentrations, supported its cytotoxic effect. The number of live cells was determined by metabolic activity using the MTT method through a series of steps. It was found that the number of live cells was the least at a concentration of 500 µM after 48 hours.

Due to its antioxidant properties, it can act as a defense against oxidative damage by neutralizing free radicals. It can also have a cytotoxic effect through the release of reactive oxygen species. In addition, it has an effect on the antioxidant defense system by activating nuclear factor erythroid 2-related factor 2 and increasing glutathione levels.⁶ Moreover, it was emphasized that rosemary essential oil affected the mitotic phase and slowed down mitosis significantly.¹⁹ In an experimental study using the human hepatoma HepG2 cell line, when rosemary essential oil was applied at high concentrations, apoptotic substances were observed in the cells. In addition, when the cell cycle was analyzed, after 24 hours of application, it was found that cells in the G1 phase accumulated, accompanied by a decrease in the number of cells in the S phase. In this context, it was observed that cell division slowed down or paused and eventually cell death occurred.²⁰

Different cell lines, have been mainly examined in the above paragraphs due to the limited number of studies in the literature on pancreatic cancer and rosemary oil. At the same time, this situation shows the strength of the study.

Study Limitations

The reliance on cell viability analysis alone is a limitation of the study. In addition, higher doses and incubation periods can be used to show greater or additional effects. The use of specific markers or methods for cell viability is essential to represent the effects more clearly.

CONCLUSION

The cytotoxic activity of rosemary oil was tested in PANC-1 cells using diverse concentrations. Rosemary oil has been shown to reduce cell viability in pancreatic cancer cells. To clarify the specific anti-oncogenic effects of rosemary oil on pancreatic cancer cells, relevant signaling pathways need to be defined. Further studies on various pancreatic cancer cell lines, animals, and humans are needed to elucidate the impacts of rosemary oil on pancreatic cancer, which is one of the rapidly progressive types.

MAIN POINTS

- Rosemary oil at 500 µM was more effectual in diminishing the proliferation of pancreatic cancer cell line-1 cell than another concentrations during 48 hour.
- A significant differentiation was found between 100 µM and 600 µM after 48 hours.
- It was shown that there was a significative differentiation between 200 µM and 600 µM for 48 hour.
- Rosemary oil has been shown to reduce cell viability in pancreatic cancer cells.

ETHICS

Ethics Committee Approval: Not applicable.

Informed Consent: Not applicable.

Footnotes

Authorship Contributions

Concept: M.H., E.B., A.Y., H.S.V., Design: M.H., E.B., A.Y., H.S.V., Data Collection and/or Processing: M.H., E.B., A.Y., H.S.V., Analysis and/or Interpretation: M.H., E.B., A.Y., H.S.V., Literature Search: M.H., E.B., A.Y., H.S.V., Writing: M.H., E.B., A.Y., H.S.V.

DISCLOSURES

Conflict of Interest: No conflict of interest was declared by the authors.

Financial Disclosure: The authors declared that this study had received no financial support.

REFERENCES

1. Zhou P, Li B, Liu F, Zhang M, Wang Q, Liu Y, et al. The epithelial to mesenchymal transition (EMT) and cancer stem cells: implication for treatment resistance in pancreatic cancer. *Mol Cancer*. 2017; 16(1): 52.
2. Mrđanović J, Bogdanović V, Kiprović B, Malenčić Đ, Mikulić-Petkovšek M, Milovanović I, et al. Novel insights to the anti-proliferative activity of rosemary (*Rosmarinus officinalis* L.) co-treatment. *Lekovite Sirovine*. 2019; 39: 45-52.
3. Bourhia M, Laasri FE, Aourik H, Boukhris A, Ullah R, Bari A, et al. Antioxidant and antiproliferative activities of bioactive compounds contained in *Rosmarinus officinalis* used in the Mediterranean diet. *Evid Based Complement Alternat Med*. 2019; 2019: 7623830.
4. Yang J, Goksen G, Zhang W. Rosemary essential oil: chemical and biological properties, with emphasis on its delivery systems for food preservation. *Food Control*. 2023; 154: 110003.
5. Aziz E, Batool R, Akhtar W, Shahzad T, Malik A, Shah MA, et al. Rosemary species: a review of phytochemicals, bioactivities and industrial applications. *S Afr J Bot*. 2022; 151: 3-18.
6. Allegra A, Tonacci A, Pioggia G, Musolino C, Gangemi S. Anticancer activity of *Rosmarinus officinalis* L.: mechanisms of action and therapeutic potentials. *Nutrients*. 2020; 12(6): 1739.
7. Santos PASR, Avanço GB, Nerilo SB, Marcelino RIA, Janeiro V, Valadares MC, et al. Assessment of cytotoxic activity of rosemary (*Rosmarinus officinalis* L.), turmeric (*Curcuma longa* L.), and ginger (*Zingiber officinale* R.) essential oils in cervical cancer cells (HeLa). *Sci World J*. 2016; 2016: 9273078.

8. El Sala AA, Khawaja G, Khalil M, Salam SA. Rosemary essential oil potentiates the antitumor activity of 5-fluorouracil in human colorectal carcinoma cells. *J Pharm Pharmacol*. 2024; 76(6): 691-700.
9. Becer E, Altundağ EM, Güran M, Vatansever HS, Ustürk S, Hanoğlu DY, et al. Composition and antibacterial, anti-inflammatory, antioxidant, and anticancer activities of *Rosmarinus officinalis* L. essential oil. *S Afr J Bot*. 2023; 160: 437-45.
10. Huang Y, Xu H, Ding M, Li J, Wang D, Li H, et al. Screening of rosemary essential oils with different phytochemicals for antioxidant capacity, keratinocyte cytotoxicity, and anti-proliferative activity. *Molecules*. 2023; 28(2): 586.
11. Ahamad J, Uthirapathy S, Mohammed Ameen MS, Anwer ET. Essential oil composition and antidiabetic, anticancer activity of *Rosmarinus officinalis* L. leaves from Erbil (Iraq). *J Essent Oil-Bear Plants*. 2019; 22(6): 1544-53.
12. Dolghi A, Coricovac D, Dinu S, Pinzaru I, Dehelean CA, Grosu C, et al. Chemical and antimicrobial characterization of *Mentha piperita* L. and *Rosmarinus officinalis* L. essential oils and in vitro potential cytotoxic effect in human colorectal carcinoma cells. *Molecules*. 2022; 27(18): 6106.
13. Hoca M, Becer E, Kabadayı H, Yücecan S, Vatansever HS. The effect of resveratrol and quercetin on epithelial-mesenchymal transition in pancreatic cancer stem cell. *Nutr Cancer*. 2020; 72(7): 1231-42.
14. Rahbardar MG, Hosseinzadeh H. Toxicity and safety of rosemary (*Rosmarinus officinalis*): a comprehensive review. *Naunyn-Schmiedeberg's Archives of Pharmacology*. 2024; 398(1): 9-23.
15. Al-otaibi W. Rosemary oil nano-emulsion potentiates the apoptotic effect of mitomycin C on cancer cells in vitro. *Pharmacia*. 2021; 68(1): 201-9.
16. Urquiza-López A, Álvarez-Rivera G, Ballesteros-Vivas D, Cifuentes A, Del Villar-Martínez AA. Metabolite profiling of rosemary cell lines with antiproliferative potential against human HT-29 colon cancer cells. *Plant Foods Hum Nutr*. 2021; 76(3): 319-25.
17. Gonzalez-Vallinas M, Molina S, Vicente G, Zarza V, Martin-Hernandez R, Garcia-Risco MR, et al. Expression of microRNA-15b and the glycosyltransferase GCNT3 correlates with antitumor efficacy of Rosemary diterpenes in colon and pancreatic cancer. *PLoS One*. 2014; 9(6): 98556.
18. Özdemir MD, Göktürk D. The concurrent effect of acyclovir and rosemary on glioblastoma cell culture. *Cell Mol Biol*. 2019; 65(3): 66-71.
19. Stojanović-Radić Z, Nešić M, Čomić L, Radulović N. Antimicrobial activity and cytotoxicity of commercial rosemary essential oil (*Rosmarinus officinalis* L.). *Biologica Nyssana*. 2010; 1(1-2): 83-8.
20. Melušová M, Jantová S, Horváthová E. Carvacrol and rosemary oil at higher concentrations induce apoptosis in human hepatoma HepG2 cells. *Interdiscip Toxicol*. 2014; 7(4): 189-94.

Developing RT-qPCR Kit for Detection and Quantification of Hepatitis D Virus Unique Genome

✉ Kıvanç Günhan¹, ✉ Hafize Seda Vatansever^{2,4}, ✉ Tamer Şanlıdağ⁴, ✉ Murat Sayan^{4,5}, ✉ Sinem Akçalı³,
✉ Hilal Kabadayı Ensarioğlu², ✉ Ferdi Çetin³, ✉ Gökçe Akan⁴, ✉ Gülten Tuncel Dereboylu⁴, ✉ Melis Kalaycı⁴

¹Department of Ear, Nose and Throat, Manisa Celal Bayar University Faculty of Medicine, Manisa, Türkiye

²Department of Histology and Embryology, Manisa Celal Bayar University Faculty of Medicine, Manisa, Türkiye

³Department of Microbiology, Manisa Celal Bayar University Faculty of Medicine, Manisa, Türkiye

⁴DESAM Research Institute, Yakın Doğu University, Nicosia, North Cyprus

⁵Clinic of PCR Laboratory, Kocaeli University Research and Application Hospital, Kocaeli, Türkiye

Abstract

BACKGROUND/AIMS: Hepatitis D virus (HDV) is a significant global health problem identified in the 1970s in Hepatitis B virus (HBV) positive patients. HDV is classified under the Kolmioviridae family and has a unique single-stranded negative-sense circular RNA genome. Its replication relies on HBV surface antigens making HBV co-infection essential. HDV infection can occur either simultaneously with HBV or as a superinfection. This virus frequently leads to progressive liver disease, with approximately 70% of cases developing cirrhosis, highlighting the critical need for early diagnosis. This study aims to develop a high sensitivity and specificity quantitative reverse transcription polymerase chain reaction (RT-qPCR) (diagnostic kit for detecting HDV RNA in plasma samples. The newly developed kit is expected to provide reliable diagnosis and facilitate the early detection of HDV, thereby improving clinical outcomes and epidemiological surveillance.

MATERIALS AND METHODS: Following the RNA isolation step using the RN easy RNA Purification commercial kit (QIAGEN, Cat. No: 74104), the samples underwent a heat-shock protocol, 95 °C for 10 minutes, followed by rapid freezing at -20 °C to disrupt the secondary structure of the HDV RNA and enhance primer binding efficiency. The single-step RT-qPCR assay was carried out using a specific primer-probe set targeting conserved regions of the HDV genome, along with a human *ribosomal protein (RP)* gene as an internal control, to validate RNA extraction and the absence of sample degradation. RT-qPCR was performed using the QIAGEN Rotor-Gene Q-5plex device.

RESULTS: Developed RT-qPCR diagnostic kit successfully detected HDV RNA in all patient samples with high specificity. The fluorescence signals obtained from both the FAM (HDV target) and HEX (*RP* gene) channels confirmed the accurate amplification of the target regions. The kit was further validated using blind samples obtained from the Molecular Diagnosis and Quality Control Laboratory to ensure its clinical applicability and robustness.

CONCLUSION: The development of a novel HDV-specific RT-qPCR diagnostic kit provides a valuable tool for the early, accurate detection and quantification of HDV RNA in clinical samples. The kit's ability to offer rapid and reliable results, coupled with its high sensitivity and specificity, makes it an excellent candidate for widespread clinical use and epidemiological monitoring. Further validation studies are recommended to

To cite this article: Günhan K, Vatansever HS, Şanlıdağ T, Sayan M, Akçalı S, Kabadayı Ensarioğlu H, et al. Developing RT-qPCR kit for detection and quantification of hepatitis d virus unique genome. Cyprus J Med Sci. 2025;10(Suppl 1):69-73

ORCID IDs of the authors: K.G. 0000-0001-6682-3841; H.S.V. 0000-0002-7415-9618; T.Ş. 0000-0002-6015-8032; M.S. 0000-0002-4374-7193; S.A. 0000-0001-7090-2673; H.K.E. 0000-0001-7429-1478; F.Ç. 000-0001-5015-169X; G.A. 0000-0002-3878-1135; G.T.D. 0000-0002-3332-471X; M.K. 0000-0002-5779-5532.



Corresponding author: Melis Kalaycı
E-mail: melis.kalayci@neu.edu.tr
ORCID ID: orcid.org/0000-0002-5779-5532

Received: 24.12.2024
Accepted: 22.04.2025
Publication Date: 04.06.2025



Copyright© 2025 The Author. Published by Galenos Publishing House on behalf of Cyprus Turkish Medical Association.

This is an open access article under the Creative Commons AttributionNonCommercial 4.0 International (CC BY-NC 4.0) License.

Abstract

expand its application across diverse clinical settings and to evaluate its performance in different HDV genotypes. Furthermore, the in-house kit that was produced is thought to be a more affordable alternative to the current commercial kits, which might make it more accessible, particularly in low-income nations.

Keywords: Hepatitis delta, hepatitis delta virus, real time PCR, reverse transcriptase PCR

INTRODUCTION

The global burden of hepatitis D virus (HDV)-related liver disease is significant, affecting an estimated 12 to 72 million people worldwide, with a high risk of severe liver complications such as cirrhosis and hepatocellular carcinoma.^{1,2} Despite its severity, HDV remains underdiagnosed due to inadequate screening practices, particularly in populations co-infected with hepatitis B virus (HBV).^{3,4} Recent studies indicate significant increases in reported HDV cases, particularly in regions including the United States (US) and parts of South America. Areas such as the Amazon basin and parts of Colombia show high HDV prevalence, exacerbated by poor healthcare access.^{5,6}

There are several difficulties in the prevention of hepatitis D infections, including co-infection with HBV. Additionally, there is a lack of adequately effective and widespread processes for monitoring or detecting HDV, such as routine HDV antibody testing. There is also insufficient screening focused on high-risk groups. These groups include injection drug users, individuals with multiple and/or unprotected sexual partners-particularly among men who have sex with men-and migrants from endemic regions. Furthermore, there is limited availability and access to treatment options.^{1-4,7} There are currently no Food and Drug Administration (FDA)-approved drugs for the treatment of HDV in the US. However, bulevirtide is conditionally approved in the European Union and is under review with the US FDA. Current treatment strategies in many countries are based on the use of pegylatedinterferonalfa2a, which has limited efficacy.³

PCR-based diagnostics, particularly reverse transcription polymerase chain reaction (RT-qPCR) and (Droplet Digital Polymerase Chain Reaction), play a crucial role in monitoring HDV transmission and treatment outcomes. These methods enhance the detection and quantification of HDV-RNA, providing valuable insights into disease progression and therapeutic efficacy.^{8,9} HDV has a circular and small RNA genome (1.7 kb) that exhibits high intramolecular base pairing, complicating amplification efforts.¹⁰ However, there are at least eight known genotypes of HDV, each with distinct sequences, leading to variability in assay performance.¹¹ While PCR technologies significantly enhance the monitoring of HDV, challenges remain in the widespread implementation of these technologies, particularly in resource-limited settings where access to advanced diagnostic tools may be restricted. Our aim in this study was to develop an HDV-specific RT-qPCR diagnostic kit and position it as a valuable tool for the early and accurate detection and quantification of HDV RNA in clinical samples. Additionally, it is believed that the developed in-house kit offers a more cost-effective option compared to existing commercial kits, making it potentially more accessible, especially in low-income countries.

MATERIALS AND METHODS

Sample Collection and RNA Isolation

The evaluation panel included plasma samples obtained from 10 HDV positive patients from Kocaeli, Türkiye, that were referred to the laboratory previously and stored at -70 °C. RNA isolation from plasma samples was performed with the QIAGEN EZ1 automated sample purification device using the RNeasy RNA Purification commercial kit (QIAGEN, Cat. No:74104), according to the manufacturer's instructions. After isolation, to reduce the likelihood of natural internal base pairing being restored in the HDV genome, thermal shock was performed by incubating 10 µL of isolate at 95 °C for 10 minutes (min), followed by immediate cooling to -20 °C. The study received approval from Manisa Celal Bayar University Ethics Committee (approval number: 330, date: 19.09.2022) and Informed consent forms were signed by all participants and/or legal guardians

HDV-specific RT-qPCR Diagnostic Kit Design

Sequence alignment of HDV strains (genotype 1-8) full-length genome was performed to locate conserved regions suitable for primer and probes. Primers and probes are designed for the HDV Ag) region.

Our forward primer (19bp) is positioned between 721 to 739 bp of the HDV genome, which corresponds to a palindromic sequence region. The reverse primer (20 bp) binds to the 1085-1104 bp region, located between the overlapping large hepatitis delta antigen (L-HDAg) and small hepatitis delta antigen regions encoded by ORF1. Our primers were designed to be diagnostically compatible with all 8 genotypes of HDV. For this purpose, SnapGene (GSL Biotech, available at snapgene.com) and the NCBI BLAST program were utilized. The sequences of the target gene were obtained from the HDVdb database.¹² The SnapGene tool was used for primer and probe design for HDV and human *ribosomal protein (RP)* genes as the internal control. Gene-specific probes were labelled with different fluorescent dyes. FAM for HDV L-HDAg region and HEX for the human *RP* gene were used. In silico specificity tests of designed primer and probe sequences were performed for 32 different viral and bacterial strains to avoid any possible cross-reaction during PCR. The PCR assay was performed using Takyon™ One-Step Low Rox Probe 5X MasterMix dTTP (Cat No: UF-LP5X-RT0501, Takyon™, Eurogentec Belgium) on the Rotor-Gene Q 5Plex Real-Time PCR (QIAGEN, Hilden, Germany). The optimized PCR reaction started with cDNA synthesis step at 55 °C for 40 min followed by an initial denaturation step at 95 °C for 15 min and 50 cycles of amplification consisting of denaturation at 95 °C for 20 s, at 62 °C for 60 s for annealing and fluorescent signal acquisition at FAM and HEX channels. The optimized reaction mix included 10 µL of one-step master mix, 0.4 µM final primer concentration, 0.2 µM final probe concentration, 6 µL of nucleic acid sample, and RNase/DNase-free ddH₂O to a final volume of 20 µL.

Diagnostic Performance, Amplification Efficiency and Analytical Sensitivity

Validation and performance experiments of the designed HDV detection kit were performed by testing 38 blind samples from Quality Control Program in Molecular Diagnosis (MOTAKK, Ankara, Türkiye). The commercially available Fluorion Real-Time PCR HDV 1.0 (Iontek, İstanbul, Türkiye) kit was used for the validation of the designed HDV detection kit; and the validation study was conducted with 10 plasma pooled samples. The limit of detection was tested by five replicates of serial dilutions, (17x10¹ to 17x10⁵ copies per reaction) of the HDV RNA standard (HDV RNA Viral Load Quantitative & Qualitative Setup Kit, MOTAKK, Ankara, Türkiye). The amplification efficiency (Ex) was determined using the formula $Ex = [10^{(-1/slope)} - 1] \times 100$ for the HDV cDNA standard dilution series. A standard curve was generated using cycle threshold values of serial dilutions of the HDV standard.

RESULTS

Standardization of the RT-qPCR Conditions

The Multiplex RT-qPCR assay was optimized for the diagnosis of HDV infection, simultaneously targeting a conserved region of the HDV genome (L-HDAg gene region) and human *RP* gene, as the internal control. Upon primer and probe optimization, plasma samples were obtained from 10 patients previously diagnosed with HDV infection. RNA isolates obtained from plasma samples were tested with the RT-qPCR assay in optimized conditions. In HDV-positive samples and a positive control sample, RP (human internal control), and HDV target region were amplified simultaneously, forming sigmoidal curves. In the negative control reactions, ddH₂O was used as the template, which led to no amplification line (Figure 1).

Performance and Assay Validation

Thirty-eight blind samples from Quality Control Program in Molecular Diagnosis, (MOTAKK, Ankara, Türkiye) were analyzed using the developed kit. Among these, 22 samples tested positive and 16 tested negative. Results were confirmed by the quality control program. For assay validation, commercially available Fluorion Real-Time PCR HDV 1.0 (Iontek, İstanbul Türkiye) kit was used. Samples from 10 clinically confirmed HDV positive patients, 10 HDV negative patients,

MOTAKK samples, and no template control samples were analyzed simultaneously with both kits following the manufacturer's instructions. The in-house kit exhibited 100% positive percent agreement with the commercially available diagnostic kit.

RT-qPCR Efficiency and Limit-of-Detection

The standard curve analysis was performed to test the efficiency, sensitivity, and LOD of the assay. A dilution series was prepared with HDV RNA standard (HDV RNA Viral Load Quantitative & Qualitative Setup Kit, MOTAKK, Ankara, Türkiye) ranging from 1.7+ E1 to 1.7+ E5 copies per reaction. According to that, the LOD of the designed kit was established as 1.7+ E1 copy per reaction. Triplicate RT-qPCR analysis revealed that the results were consistent across technical replicates (Figure 2).

DISCUSSION

The detection of HDV through PCR presents several significant challenges. These difficulties may stem from the unique characteristics of the virus and the limitations of current methodologies. The technical limitations of HDV PCR significantly impact the accuracy of results, primarily due to the inherent complexities of the HDV and the methodologies employed in testing. These limitations include viral heterogeneity, intra-host diversity, and challenges in assay standardization, which collectively contribute to variability in performance across different laboratories. HDV with a unique genome, exhibits at least eight genotypes, each with distinct genetic characteristics, complicating the design of universal assays.¹¹ On the other hand, the circular genome of HDV has high intramolecular base pairing, which can hinder effective amplification during PCR.¹⁰ These unique genome features of HDV were considered challenges and were approached strategically during our development of the HDV RT-qPCR kit.

In the HDV PCR test kit development process, the methodology is particularly emphasized. Variability in RNA extraction methods and primer/probe design may lead to inconsistent results across different assays.¹¹ The lack of automation in some testing environments may increase the risk of human error, affecting reproducibility.¹³ In our HDV RT-qPCR kit development studies, we focused on automation to minimize human error, to work with variables in a controlled manner, and to establish standard processes. Examples of these include RNA

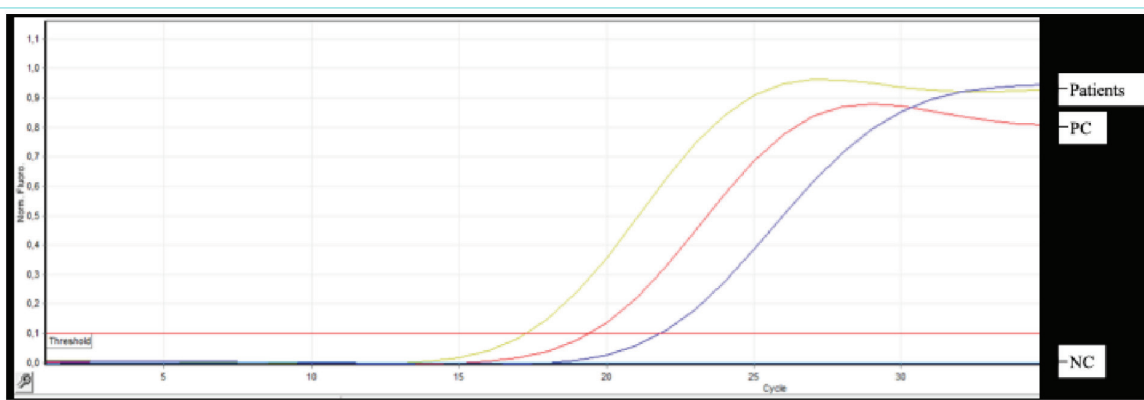


Figure 1. RT-qPCR amplification curve graphs of positive control (PC), no template control (NTC) and patient samples for HDV gene-specific region represented in the graph.

HDV: Hepatitis D virus.

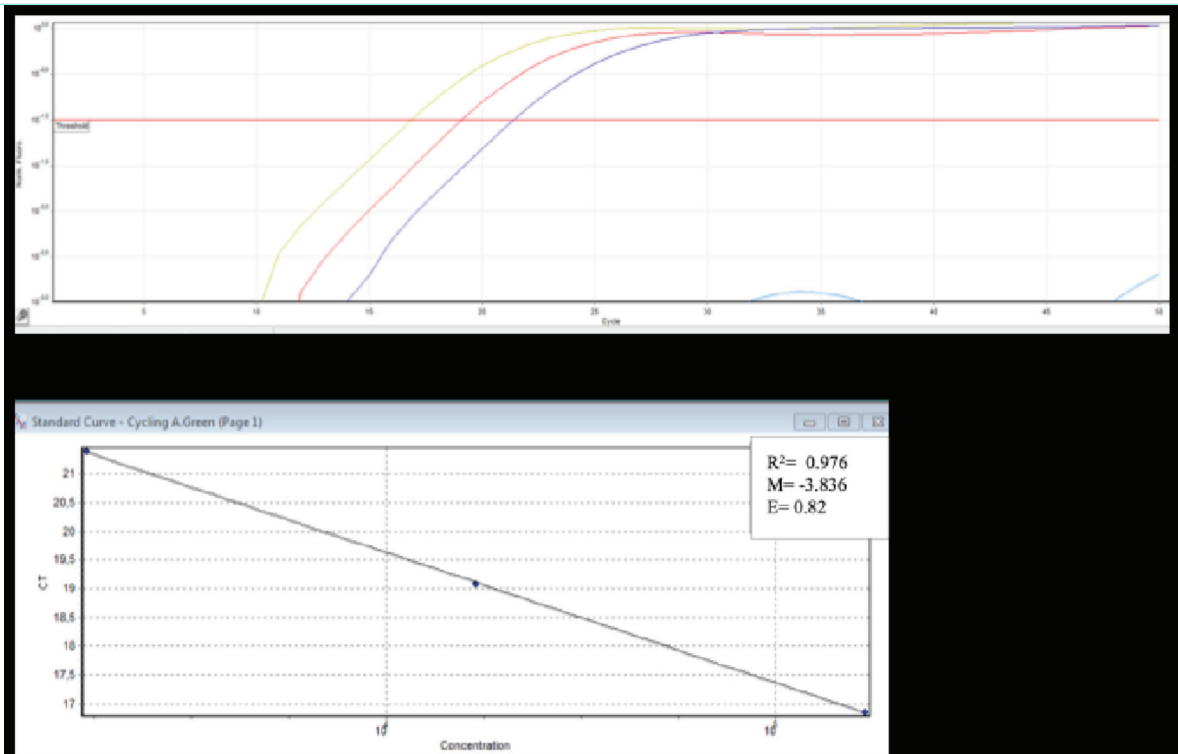


Figure 2. Standard curve analysis for multiplex RT-qPCR of *HDV-specific* gene primers. The reactions were carried out in triplicate. The amplification efficiency (E) is shown on the graph.

HDV: Hepatitis D virus.

extraction with EZ1 magnetic particle isolation, and PCR product extraction with Rotorgene Q 5plex thermal cycling. On the other hand, the lack of a universally accepted standard for HDV RNA quantification is a variable that may cause inconsistencies in test sensitivity and specificity.^{11,14} In the current study, we tried to overcome this difficulty by using MOTAKK HDV RNA standards. In conclusion, HDV surveillance may need to be increased to better understand the international HDV incidence and etiology. The HDV-specific RT-qPCR diagnostic kit developed in this study may be a valuable tool for early, accurate, and quantitative detection of HDV RNA in clinical samples.

Study Limitations

Although the HDV-specific RT-qPCR diagnostic kit developed in this study provides important advantages, the study has some limitations. Firstly, the performance of the kit was tested with a limited number of clinical samples. Verification studies with samples containing different HDV genotypes covering a wider geographical region are necessary to better assess the inter-genotype consistency and generalizability of the kit. This may affect the sensitivity of the test.

In addition, the cost of technologies such as the RNA isolation method used in the study and PCR devices may limit the applicability of the kit in low-resource laboratories. Therefore, it is important to explore more accessible and low-cost alternatives.

Finally, only MOTAKK HDV RNA standards were used in the study, and no comparative analysis was performed with international standards. This may affect the comparability of results between different laboratories.

Future studies may address these limitations through validation with international standards and evaluation of the kit in further clinical settings.

CONCLUSION

The specifically designed HDV qRT-PCR detection kit enables the detection of HDV's RNA for early, accurate, and quantitative results. Standardization and validation studies were made possible by comparing the results with a commercially available qRT-PCR kit, which shows 100% concordance. The PCR protocol was optimized because of the unique structure of the HDV genome and its limitations. Furthermore, the results of the designed kit's sensitivity and accuracy were consolidated using MOTAKK standards.

Despite the limitations of the current methods used in the diagnosis of HDV, this study has made significant progress in the molecular diagnosis of HDV with a standardized approach. The designed and developed kit not only improves clinical diagnostic processes but also provides a valuable tool for studies aimed at better understanding the international prevalence and etiology of HDV. In this context, the expansion and increasing accessibility of PCR-based technologies in HDV diagnosis and monitoring will contribute to global HDV control efforts. The cost-effectiveness of the developed kit, particularly in low-income countries, provides a significant contribution to healthcare services in these regions.

MAIN POINTS

- Due to the circular nature of the hepatitis D virus (HDV) genome, molecular diagnostic methods such as reverse transcription polymerase chain reaction face diagnostic challenges. This study aims to overcome these difficulties.
- In today's world, viral hepatitis has become increasingly significant due to large-scale migration.
- There are limited commercial kits available for HDV diagnosis. Therefore, our study focuses on addressing this gap by developing a reliable diagnostic approach.

ETHICS

Ethics Committee Approval: The study received approval from Manisa Celal Bayar University Ethics Committee (approval number: 330, date: 19.09.2022).

Informed Consent: Informed consent forms were signed by all participants and/or legal guardians.

Footnotes

Authorship Contributions

Concept: K.G., H.S.V., T.Ş., M.S., S.A., H.K.E., F.Ç., G.A., G.T.D., M.K., Design: H.S.V., T.Ş., M.S., G.A., G.T.D., M.K., Data Collection and/or Processing: H.S.V., T.Ş., M.S., G.A., G.T.D., M.K., Analysis and/or Interpretation: K.G., H.S.V., T.Ş., M.S., S.A., H.K.E., F.Ç., G.A., G.T.D., M.K., Literature Search: S.A., H.K.E., F.Ç., Writing: H.S.V., T.Ş., M.S., G.A., G.T.D., M.K.

DISCLOSURES

Conflict of Interest: No conflict of interest was declared by the authors.

Financial Disclosure: The authors declared that this study had received no financial support.

REFERENCES

1. Negro F, Lok AS. Hepatitis D: A Review. *JAMA*. 2023; 330(24): 2376-87.
2. Terrault NA, Ghany MG. Enhanced screening for hepatitis d in the USA: overcoming the delta blues. *Dig Dis Sci*. 2021; 66(8): 2483-5.
3. Khattak A, Vongsavath T, Haque L, Narwan A, Gish RG. The forgotten virus, hepatitis d: a review of epidemiology, diagnosis, and current treatment strategies. *J Clin Exp Hepatol*. 2024; 14(5): 101395.
4. Tharwani A, Hamid S. Elimination of HDV: Epidemiologic implications and public health perspectives. *Liver Int*. 2023; 43(Suppl 1):101-7.
5. Fallon BS, Cooke EM, Hesterman MC, Norseth JS, Akhundjanov SB, Weller ML. A changing landscape: tracking and analysis of the international HDV epidemiology 1999-2020. *PLOS Glob Public Health*. 2023; 3(4): 0000790.
6. Vlachogiannakos J, Papatheodoridis GV. New epidemiology of hepatitis delta. *Liver Int*. 2020; 40(Suppl 1): 48-53.
7. Örmeci N, Erdem H. Changing trends in the epidemiology of delta virus infection. *Viral Hepat J*. 2023; 29(1): 1-9.
8. da Silva Queiroz JA, Roca TP, Souza RB, de Souza LFA, Passos-Silva AM, da Silva ALF, et al. Development of quantitative multiplex RT-qPCR one step assay for detection of hepatitis delta virus. *Sci Rep*. 2023; 13(1): 12073.
9. Olivero A, Rosso C, Ciancio A, Abate ML, Nicolosi A, Troshina G, et al. Clinical application of droplet digital PCR for hepatitis delta virus quantification. *Biomedicines*. 2022; 10(4): 792.
10. Pflüger LS, Volz T, Giersch K, Allweiss L, Dandri M, Lütgehetmann M. Method for Quantitative HDV RNA Detection: I, manual workflow (serum and Liver Tissue) and II, fully automated high throughput workflow for diagnostic Use. *Methods Mol Biol*. 2024; 2837: 171-84.
11. Wedemeyer H, Leus M, Battersby TR, Glenn J, Gordien E, Kamili S, et al. HDV RNA Assays Writing Group at the HBV Forum. HDV RNA assays: performance characteristics, clinical utility, and challenges. *Hepatology*. 2025; 81(2): 637-50.
12. HDVdb - Database Commons. (2020). Cnbc.ac.cn. <https://ngdc.cnbc.ac.cn/databasecommons/database/id/7022> (Access date; 24 November 2024)
13. Pflüger LS, Nörz D, Volz T, Giersch K, Giese A, Goldmann N, Glebe D, Bockmann JH, Pfefferle S, Dandri M, Schulze Zur Wiesch J, Lütgehetmann M. Clinical establishment of a laboratory developed quantitative HDV PCR assay on the cobas6800 high-throughput system. *JHEP Rep*. 2021; 3(6): 100356.
14. Russo D, Malnati MS. Absolute quantification of viral DNA: the quest for perfection. *Methods Mol Biol*. 2014; 1160: 75-86.

Biological Network Analysis of Genes and Non-coding RNAs in Polycystic Ovary Syndrome

✉ Bitá Ostad Hasanzadeh¹, ✉ Zahra Lotfi Sousefi², ✉ Parham Ostad Hasanzadeh³, ✉ Pinar Tulay^{1,4,5}

¹Department of Medical Genetics, Near East University Faculty of Medicine, Nicosia, North Cyprus

²Department of Nanobiotechnology and Biomimetic, University of Tehran Faculty of New Science and Technology, Tehran, Iran

³Department of Pharmacy, Cyprus International University Faculty of Pharmacy, Nicosia, North Cyprus

⁴DESAM Research Institute, Near East University, Nicosia, North Cyprus

⁵Center of Excellence, Genetics and Cancer Diagnosis, Near East University, Nicosia, North Cyprus

Abstract

BACKGROUND/AIMS: Polycystic ovary syndrome (PCOS) is a neuroendocrine and metabolic disorder. This study aimed to explore interactions among differentially expressed genes (DEGs) and Food and Drug Administration (FDA)-approved drugs relevant to PCOS using bioinformatics approaches. The relationships between top-ranked hub genes, DE-microRNAs (miRNAs), and DE-long non-coding RNAs (lncRNAs) within the competing endogenous RNA (ceRNA) network framework were also investigated.

MATERIALS AND METHODS: Expression profiles for miRNA (GSE138572), lncRNA (GSE159466), and mRNA (GSE84958, GSE156067) were obtained from the GEO database. Data analysis was performed using R Project and relevant annotation packages. Drug-gene interactions (DGI) were explored using DGIdb, and Cytoscape software was employed to construct DEG-drug interaction networks.

RESULTS: Analysis of GSE84958 and GSE156067 datasets identified 71 common DEGs. Moreover, 11 DE-miRNAs and 203 DE-lncRNAs were DE in PCOS samples compared to controls. DGIdb analysis showed that FDA-approved drugs could potentially target the identified DEGs. Nine genes- *PDE5A*, *ETFB*, *COL11A1*, *SLC25A20*, *DAPK1*, *ICAM1*, *FABP5*, *GBE1*, and *SLC2A3*-were identified as hub genes within the DGI network and were considered promising therapeutic targets. Dysregulated miRNAs were significantly enriched in the ceRNA network. This suggests their potential role in PCOS therapeutic strategies. Gene ontology and Kyoto Encyclopedia of Genes and Genomes enrichment analyses yielded hub genes primarily associated with secretory granule membranes, extracellular exosomes, and postsynaptic density.

CONCLUSION: Based on a combined analysis of DEGs, DE-miRNAs and DE-lncRNAs, the present study sheds light on the molecular mechanisms underlying PCOS. The findings may help to identify potential therapeutic targets and contribute to the understanding of the pathogenesis of PCOS.

Keywords: PCOS, biological network analysis, DEGs

INTRODUCTION

Polycystic ovary syndrome (PCOS) is a common disease, with estimated prevalence varying from 5% to 20%.¹ Recent literature suggests the involvement of dysregulation of noncoding RNAs, such as microRNAs

(miRNAs), along with long non-coding RNAs (lncRNAs) in the development of PCOS.² For example, a balance between “coding” RNAs (mRNAs) and non-coding RNAs is necessary to control gene transcription and cellular activity.³ Other comparative studies have shown particular non-coding and coding RNAs that are DE in PCOS, enabling the

To cite this article: Hasanzadeh BO, Lotfi Sousefi Z, Hasanzadeh PO, Tulay P. Biological network analysis of genes and non-coding RNAs in polycystic ovary syndrome. *Cyprus J Med Sci*. 2025;10(Suppl 1):74-77

ORCID IDs of the authors: B.O.H. 0009-0000-9496-6276; Z.L.S. 0009-0002-4727-0414; P.O.H. 0009-0002-7724-9384; P.T. 0000-0002-6793-7805.



Corresponding author: Pinar Tulay
E-mail: pinar.tulay@neu.edu.tr
ORCID ID: orcid.org/0000-0002-6793-7805

Received: 23.01.2025
Accepted: 22.04.2025
Publication Date: 04.06.2025



Copyright © 2025 The Author. Published by Galenos Publishing House on behalf of Cyprus Turkish Medical Association.
This is an open access article under the Creative Commons Attribution-NonCommercial 4.0 International (CC BY-NC 4.0) License.

development of strategies for clinical diagnosis and treatment of this syndrome.⁴ Moreover, a better understanding of the complexity of interrelations between coding and non-coding RNAs might help to build targeted methods of treatment, including the use of medications like metformin, ethinyl estradiol, and levonorgestrel, that have Food and Drug Administration (FDA)-approved. These drugs have been demonstrated to address a number of PCOS symptoms, including insulin sensitivity and hormone regulation, with well-established mechanisms of action. These mechanisms of action that call for additional research using bioinformatic techniques. Significant alterations in mRNA, miRNA, and lncRNA expression among PCOS patients relative to healthy individuals have been used to explain the pathophysiology of the disease.⁵ From these studies, genes and regulatory networks that could be potential therapeutic targets have been identified. Nevertheless, there are still unanswered questions about the initial targets and modes of action of FDA-approved medications in relation to PCOS. By addressing the research gaps and emphasizing the novelty of this work, the current study aims to concentrate on the communication between different miRNAs, lncRNAs, and mRNAs in PCOS patients and how these molecular pathways might be implicated in the action of FDA-approved medications.

MATERIALS AND METHODS

We obtained the expression profiles of mRNA (GSE84958 and GSE156067), miRNA (GSE138572), and lncRNA (GSE159466) from the Gene Expression Omnibus database (<https://www.ncbi.nlm.nih.gov/geo/>).¹ We then processed and analyzed these data using R Project (version 4.0.1). Due to the limited sample sizes, potential batch effects were addressed by applying the remove Batch Effect function from the limma package (version 3.46.0). Differentially expressed genes (DEGs) were subsequently identified by employing the edgeR (version 3.32.1) and limma (version 3.46.0) packages. The normalization of read counts was performed using the trimmed mean of M-values method to correct for compositional biases between libraries. Normalized counts were then transformed into log counts per million values via the voom function from the limma package. The selection of DEGs was based on a threshold of $|\log_2 \text{ fold change}| \geq 1$ and an adjusted p-value false discovery rate (FDR) < 0.05 . Overlapping DEGs between the two mRNA datasets (GSE84958 and GSE156067) were identified for further analysis. To analyze regulatory interactions, a ceRNA network was constructed by integrating mRNA, miRNAs, and long non-coding RNA expression data. Experimentally validated interactions between miRNAs and mRNAs were extracted from TarBase (<http://www.grnpedia.org/tarbase/>)², miRTarBase (<http://mirtarbase.mbc.nctu.edu.tw/>)³, and miRecords (<http://mirecords.umn.edu>), while the miRNA-lncRNA interactions were obtained from starBase (<https://rnasysu.com/encori/index.php>)⁴ and DIANA-lncBase (<https://diana.e-ce.uth.gr/lncbasev3>).⁵ The ceRNA network was visualized using Cytoscape (<https://cytoscape.org>).⁶ For the elaboration of the possible relationships between a drug and a gene, the DGI dB (<https://www.dgldb.org/>)⁷ was used, and then these interactions were illustrated by network diagrams constructed using Cytoscape software. For Gene Ontology (GO) and KEGG pathway enrichment analysis of both DEGs and hub genes, the database for annotation, visualization, and integrated discovery database was used (<https://david.ncicrf.gov/>)⁸ with a FDR cutoff of 0.05. For Kyoto Encyclopedia of Genes and Genomes (KEGG) pathway analysis, R packages DOSE⁹, Hs.egENSEMBL, and clusterProfiler¹⁰ were used. Ethical approval was granted by the Institutional Review Board (NEU/2024/128-1900).

RESULTS

Four datasets were analyzed to detect DEGs, miRNAs, and lncRNAs related to PCOS. In GSE84958, composed of 22 normal, and 15 PCOS samples, 2054 genes had differential expression, with 1036 overexpressed ($\log_2 \text{ fold change} \geq 1$) and 1018 underexpressed ($\log_2 \text{ fold change} \geq 1$). GSE156067, with nine control samples and nine PCOS samples, revealed 796 DEGs, including 341 overexpressed and 455 underexpressed genes. A comparative analysis revealed 37 commonly upregulated, and 34 commonly downregulated genes between two datasets. Furthermore, our analysis of miRNAs expression from GSE138572 (five control and five PCOS samples) identified 11 DE-miRNAs. GSE159466, which includes three control and three PCOS samples, identified 203 DE-lncRNAs. GO and KEGG pathway analyses revealed the involvement of biological processes such as signal transduction, cell-cell adhesion. Mapped genes were predominantly located in the plasma membrane, mitochondria, and sarcoplasmic reticulum. Enrichment analysis showed that the genes were involved in hydrolase activity, focal adhesion, metabolic regulation, and cell-matrix adhesion. KEGG pathway analysis identified associations with viral myocarditis, Cushing's syndrome, and NK cell-mediated cytotoxicity (Figure 1A). A ceRNA network was constructed to examine interactions among lncRNAs, miRNAs, and mRNAs. Network analysis identified hsa-miR-561-5p, hsa-miR-1299, and hsa-miR-19b-1-5p as key miRNAs with the highest degree of interactions. GSE159466, composed of three control and three PCOS samples, identified 203 DE-lncRNAs. GO and KEGG pathway analyses determined the involvement of biological processes such as signal transduction, cell-cell adhesion. The mapped genes were found to be primarily located in the plasma membrane, mitochondria, and sarcoplasmic reticulum. Enrichment analysis showed molecular functions related to hydrolase activity and focal adhesion, as well as pathways involved in metabolic regulation and cell-matrix adhesion. KEGG pathway analysis identified associations with viral myocarditis, Cushing's syndrome, and NK cell-mediated cytotoxicity. To examine interactions among lncRNAs, miRNAs, and mRNAs, a ceRNA network was constructed. Network analysis pinpointed hsa-miR-561-5p, hsa-miR-1299, and hsa-miR-19b-1-5p as key miRNAs with the highest degree of interactions. NEAT1, H19, and KCNQ10T1 presented high connectivity with genes linked to PCOS (see Figure 1B). The drug-gene interaction (DGI) database analysis revealed 71 DEGs of potential therapeutic relevance, and nine hub genes were identified: PDE5A, ETFB, COL11A1, SLC25A20, DAPK1, ICAM1, FABP5, GBE1, and SLC2A3 (Figure 1C). Furthermore, the functional annotation of these hub genes via GO and KEGG analyses indicated their localization to secretory granule membranes, extracellular vesicles, and postsynaptic density (Figure 1D). Further analysis integrated hub genes from the DGI network into the ceRNA regulatory framework. Several hub genes, including PDE5A, COL11A1, and ICAM1, were found to be regulated by multiple miRNAs. For instance, hsa-miR-767-5p targeted lncRNAs H19, LINC00840, and NEAT1, which in turn regulated DAPK1, COL11A1, and ICAM1. Similarly, hsa-miR-940 was associated with SLC25A20 through interactions with H19 and NEAT1. Additionally, hsa-miR-19b-1-5p was linked to lncRNAs H19, DANCR, and KCNQ10T1, affecting the expression of PDE5A (Figure 1E).

DISCUSSION

The current study uncovers key molecular pathways and networks associated with PCOS pathogenesis. This result is in line with prior work that implicated these pathways involved in ovarian dysfunction and metabolic abnormalities in PCOS.¹¹⁻¹³ KEGG pathway analysis has

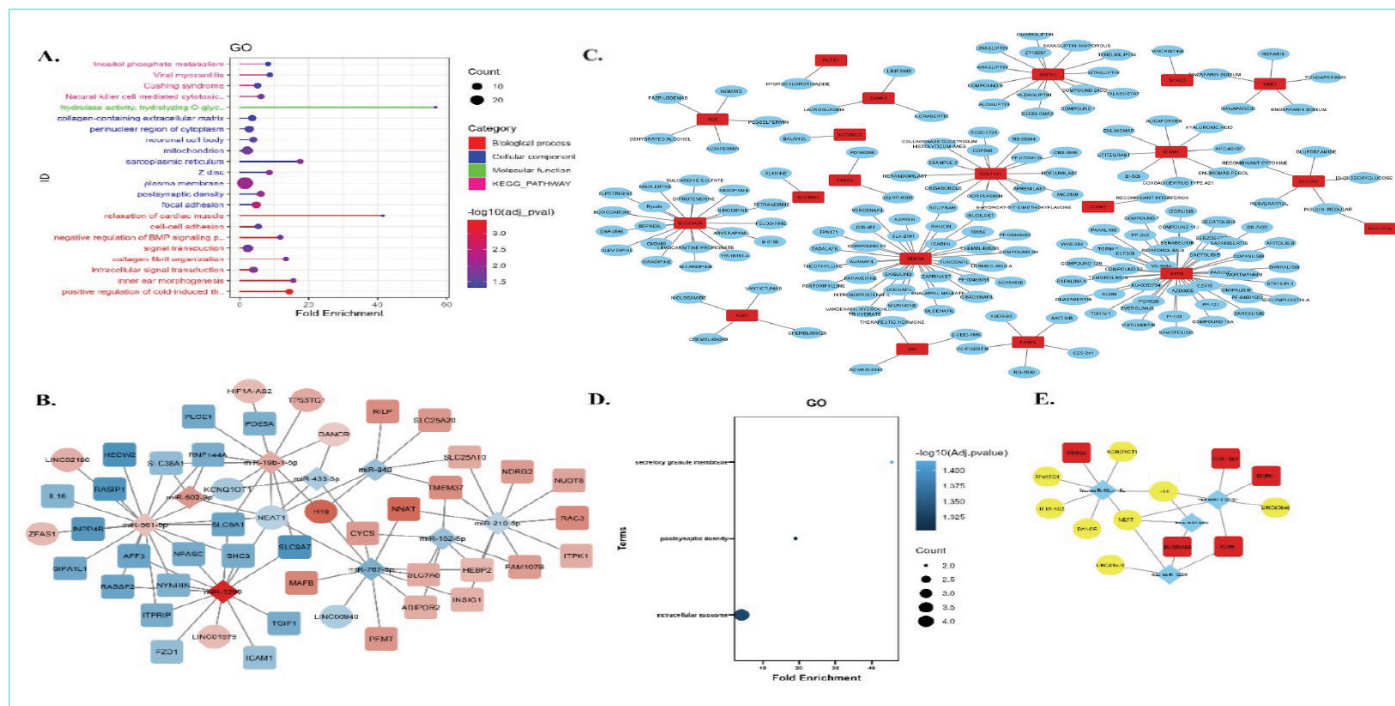


Figure 1. A) KEGG pathway and GO enrichment analysis for DEGs. B) ceRNA network: prism nodes indicate miRNAs. Quadrilateral nodes indicate the mRNA. Circles nodes that lncRNAs. C) Drug gene interaction network: The orange octagonal nodes indicate medications for PCOS, while the blue oval nodes represent FDA-approved drugs. The red rectangles are hub genes, and the prism nodes indicate miRNAs. The quadrilateral nodes indicate mRNA, while the circles indicate lncRNAs. The blue prism nodes indicate miRNAs, the red square nodes indicate genes, and the yellow circle nodes indicate lncRNAs. D) KEGG pathway and GO enrichment analysis for hub genes. E) The lncRNA-miRNA-mRNA network: blue prism nodes indicate miRNAs. Red square nodes indicate genes. Yellow circle nodes indicate lncRNAs

lncRNAs: Long non-coding RNAs, miRNA: MicroRNAs, PCOS: Polycystic ovary syndrome, FDA: Food and Drug Administration, DEGs: Differentially expressed genes, GO: Gene Ontology, KEGG: Kyoto Encyclopedia of Genes and Genomes, DEGs: Differentially expressed genes, GO: Gene Ontology, KEGG: Kyoto Encyclopedia of Genes and Genomes, DEGs: Differentially expressed genes

been shown to have an association with viral myocarditis, Cushing's syndrome, and NK cell-mediated cytotoxicity. Previous studies have established a link between these conditions and chronic inflammation and hormonal imbalance in PCOS.^{14,15}

These findings reinforce the multifactorial pathogenesis of PCOS with both immune and metabolic dysregulation. To further characterize the post-transcriptional regulatory network, we performed a ceRNA network analysis and found several key lncRNAs (NEAT1, H19, and KCNQ10T1) and miRNAs (hsa-miR-767-5p and hsa-miR-19b-1-5p) as central regulatory players. These non-coding RNAs have already been demonstrated to be involved in ovarian follicle development and insulin signaling¹⁶⁻¹⁸, which supports their functional relevance in the pathophysiology of PCOS. Additionally, hub genes identified through DGI analysis, including PDE5A, DAPK1, and COL11A1, were found to be involved in vascular function, apoptosis, and extracellular matrix remodeling. PDE5A, in particular, is associated with metabolic pathways linked to nitric oxide signaling, a pathway frequently impaired in PCOS-related endothelial dysfunction.¹⁹⁻²¹ We also predict that DAPK1 interacts with the antidiabetic drug sitagliptin. This may be a therapeutic target; however, experimental evidence supporting this will need validated. Integrating ceRNA networks with DGIs provides a novel perspective on post-transcriptional regulation in PCOS. Additionally, hsa-miR-767-5p was found to regulate DAPK1 and ICAM1 via H19 and NEAT1, which offers a potential mechanism by which non-coding RNAs modulate immune and metabolic pathways. Similarly, it was predicted that hsa-

miR-19b-1-5p influences PDE5A expression through its interactions with H19 and KCNQ10T1, suggesting a regulatory pathway involved in vascular homeostasis and glucose metabolism. While these findings are primarily derived from computational analyses, they align with previous experimental reports demonstrating miRNA-mediated regulation of insulin sensitivity and steroidogenesis in PCOS models. The findings are significant because they revealed the hub genes, including SLC2A3 and COL11A1, that play key roles in glucose transport and extracellular matrix remodeling.^{22,23}

Study Limitations

While many datasets have been analyzed, some groups may have insufficient sample sizes to provide conclusive evidence regarding the patterns of expression and regulatory mechanisms in PCOS. Secondly, empirical validation of bioinformatic predictions with respect to biological relevance is warranted. Laboratory studies, such as qRT-PCR, western blot, or in vivo studies, are needed.

CONCLUSION

In conclusion, this study explores the cellular pathophysiology of PCOS by analyzing DEGs, miRNAs, and lncRNAs across multiple datasets. Additionally, investigations of the KEGG and GO pathways highlighted important biological functions such as cell adhesion and signal transmission. Significantly, hub genes were found to be located in important signaling-related cellular areas, highlighting their possible

involvement in the pathophysiology of PCOS, with core miRNAs emerging as major regulatory nodes and their interactions with lncRNAs and mRNAs, the development of a ceRNA network revealed important interactions among miRNAs, lncRNAs, and mRNAs. Furthermore, the discovery of 71 DEGs as therapeutic targets provided information on FDA-approved medications that might be useful for the treatment of PCOS.

MAIN POINTS

- MicroRNAs and long non-coding RNAs were shown to affect the polycystic ovary syndrome (PCOS) related RNA expression.
- Food and Drug Administration-approved drugs could potentially target these identified differentially expressed genes.
- Enrichment analyses showed that the hub genes in PCOS were predominantly linked to functions related to secretory granule membranes, extracellular exosomes, and postsynaptic density.

ETHICS

Ethics Committee Approval: Ethical approval was granted by the Near East University Institutional Review Board (approval number: 128-1900, date: 2024).

Informed Consent: Not available.

Footnotes

Authorship Contributions

Concept: P.T., Design: P.T., Analysis and/or Interpretation: B.O.H., Z.L.S., P.O.H., Literature Search: P.O.H., P.T., Writing: B.O.H., Z.L.S., P.T.

DISCLOSURES

Conflict of Interest: No conflict of interest was declared by the authors.

Financial Disclosure: The authors declared that this study had received no financial support.

REFERENCES

1. (NCBI) NCFBI. Gene Expression Omnibus (GEO).
2. Skoufos G, Kakoulidis P, Tastsoglou S, Zacharopoulou E, Kotsira V, Miliotis M, et al. TarBase-v9.0 extends experimentally supported miRNA–gene interactions to cell-types and virally encoded miRNAs. *Nucleic Acids Res.* 2023; 52(1): 304-10.
3. Huang H-Y, Lin Y-C-D, Cui S, Huang Y, Tang Y, Xu J, et al. miRTarBase update 2022: an informative resource for experimentally validated miRNA–target interactions. *Nucleic Acids Res.* 2021; 50(1): 222-30.
4. starBase v2.0: decoding miRNA-ceRNA, miRNA-ncRNA and protein-RNA interaction networks from large-scale CLIP-Seq data. *Nucleic Acids Res.* 2014; 42: 92-7.
5. Thessaly Uo. DIANA-LncBase v3: indexing experimentally supported miRNA targets on non-coding transcripts. 2020.
6. Consortium C. Cytoscape: An Open-Source Platform for Complex Network Analysis.
7. Cannon M, Stevenson J, Stahl K, Basu R, Coffman A, Kiwala S, et al. DGIdb 5.0: rebuilding the drug–gene interaction database for precision medicine and drug discovery platforms. *Nucleic Acids Res.* 2024; 52(1): 1227-35.
8. Huang DW, Sherman BT, Lempicki RA. Systematic and integrative analysis of large gene lists using DAVID bioinformatics resources. *Nature protocols.* 2009; 4(1): 44-57.
9. Yu G, Wang L-G, Yan G-R, He Q-Y. DOSE: an R/Bioconductor package for disease ontology semantic and enrichment analysis. *Bioinformatics.* 2014; 31(4): 608-9.
10. Yu G, Wang L-G, Han Y, He Q-Y. clusterProfiler: an R Package for Comparing Biological Themes Among Gene Clusters. *OMICS.* 2012; 16(5): 284-7.
11. Li X, Gao B, Gao B, Li X, Xia X. Transcriptome profiling reveals dysregulation of inflammatory and protein synthesis genes in PCOS. *Sci Rep.* 2024; 14(1): 16596.
12. Zou J, Li Y, Liao N, Liu J, Zhang Q, Luo M, et al. Identification of key genes associated with polycystic ovary syndrome (PCOS) and ovarian cancer using an integrated bioinformatics analysis. *J Ovarian Res.* 2022; 15(1): 30.
13. Devarbhavi P, Telang L, Vastrad B, Tengli A, Vastrad C, Kotturshetti I. Identification of key pathways and genes in polycystic ovary syndrome via integrated bioinformatics analysis and prediction of small therapeutic molecules. *Reprod Biol Endocrinol.* 2021; 19(1): 31.
14. Liu L, He D, Wang Y, Sheng M. Integrated analysis of DNA methylation and transcriptome profiling of polycystic ovary syndrome. *Mol Med Rep.* 2020; 21(5): 2138-50.
15. Li D, Xu D, Xu Y, Chen L, Li C, Dai X, et al. MicroRNA-141-3p targets DAPK1 and inhibits apoptosis in rat ovarian granulosa cells. *Cell Biochem Funct.* 2017; 35(4): 197-201.
16. Zhen J, Li J, Li X, Wang X, Xiao Y, Sun Z, et al. Downregulating lncRNA NEAT1 induces proliferation and represses apoptosis of ovarian granulosa cells in polycystic ovary syndrome via microRNA-381/IGF1 axis. *J Biomed Sci.* 2021; 28(1): 53.
17. Li L, Wei J, Hei J, Ren Y, Li H. Long non-coding RNA H19 regulates proliferation of ovarian granulosa cells via STAT3 in polycystic ovarian syndrome. *Arch Med Sci.* 2019; 17(3): 785-91.
18. Dieter C, Lemos NE, Corrêa NRdF, Assmann TS, Crispim D. The impact of lncRNAs in diabetes mellitus: a systematic review and in silico analyses. *Front Endocrinol.* 2021; 12: 602597.
19. Wang H, Ren R, Yang Z, Cai J, Du S, Shen X. The COL11A1/Akt/CREB signaling axis enables mitochondrial-mediated apoptotic evasion to promote chemoresistance in pancreatic cancer cells through modulating BAX/BCL-2 function. *J Cancer.* 2021; 12(5): 1406-20.
20. Champion HC, Bivalacqua TJ, Takimoto E, Kass DA, Burnett AL. Phosphodiesterase-5A dysregulation in penile erectile tissue is a mechanism of priapism. *Proc Natl Acad Sci U S A.* 2005; 102(5): 1661-6.
21. Meng C. Nitric oxide (NO) levels in patients with polycystic ovary syndrome (PCOS): A meta-analysis. *J Int Med Res.* 2019; 47(9): 4083-94.
22. Lynch CS, Kennedy VC, Tanner AR, Ali A, Winger QA, Rozance PJ, et al. Impact of placental SLC2A3 deficiency during the first-half of gestation. *Int J Mol Sci.* 2022; 23(20): 12530.
23. Cheon D-J, Tong Y, Sim M-S, Dering J, Berel D, Cui X, et al. A collagen-remodeling gene signature regulated by TGF- β signaling is associated with metastasis and poor survival in serous ovarian cancer. *Clin Cancer Res.* 2014; 20(3): 711-23.

Stimulation by Exosomes Under Hypoxia Enhances Tumorigenic Properties of Primary and Metastatic Colon and Breast Cancer Cells

İbrahim Halil Gürçınar¹, Hilal Kabadayı Ensarioğlu², Remziye Kendirci-Katirci³, Hafize Seda Vatansever^{2,4*}

¹Department of Surgery, Technical University of Munich Faculty of Medicine, Munich, Germany

²Department of Histology and Embryology, Manisa Celal Bayar University Faculty of Medicine, Manisa, Türkiye

³Department of Histology and Embryology, Akdeniz University Faculty of Medicine, Antalya, Türkiye

⁴DESAM Research Institute, Near East University, Nicosia, North Cyprus

Abstract

BACKGROUND/AIMS: Exosomes are small vesicles that transport bioactive molecules between cells and play a key role in tumor progression. Hypoxic conditions in tumors promote processes such as angiogenesis, metastasis, and drug resistance, primarily through hypoxia-inducible factors (HIF)-1 α and HIF-2 α . This study investigates exosome production and stemness properties of cancer cells under hypoxic conditions, in primary and metastatic breast and colon carcinoma cell lines.

MATERIALS AND METHODS: Primary breast (MCF7) and colon (Colo320), as well as metastatic breast (M4A4) and colon (Colo741) cancer cell lines, were cultured under hypoxic (3% O₂) and normoxic conditions. Exosomes were isolated using the miRCURY™ Exosome Isolation Kit. The distribution of CD9, CD63, CD133, and HIF-1 α was analyzed by immunohistochemical staining, and total miRNA was quantified by NanoDrop.

RESULTS: Under hypoxia, CD63 expression increased in primary cell lines (MCF7 and Colo320) compared to metastatic lines (M4A4 and Colo741). CD133 immunoreactivity was strong in all cells under hypoxia, while HIF-1 α levels remained similar across all conditions. Total miRNA levels in Colo320 and Colo741 were unchanged under hypoxia but increased in MCF7 and decreased in M4A4 under hypoxia.

CONCLUSION: Hypoxia significantly enhances exosome secretion and may increase the stemness properties of primary breast and colon cancer cells. Exosomes in the tumor microenvironment could contribute to the malignancy and metastatic potential of aggressive tumors.

Keywords: Exosome, hypoxia, cancer cells, cell differentiation

INTRODUCTION

During tumor development and progression, stromal and cancer cells often have limited access to nutrients and oxygen, a phenomenon known as tumor hypoxia. Hypoxia is a critical factor in promoting cancer progression by causing resistance to radiotherapy and chemotherapy, as well as enhancing the metastatic potential of cancer cells.¹ Hypoxia drives tumor cells to adapt to low oxygen conditions

primarily through the activation of hypoxia-inducible factors (HIFs), particularly HIF-1 α and HIF-2 α , which are responsible for initiating survival pathways under stress.^{2,3} These transcription factors not only promote angiogenesis and metabolic reprogramming but also contribute to cancer cell survival in harsh microenvironments.⁴ The tumor microenvironment (TME) comprises not only cancer cells but also various stromal components such as fibroblasts, immune cells, extracellular matrix proteins, and secreted factors.⁵ This dynamic

To cite this article: Gürçınar İH, Kabadayı Ensarioğlu H, Kendirci-Katirci R, Vatansever HS. Stimulation by exosomes under hypoxia enhances tumorigenic properties of primary and metastatic colon and breast cancer cells. Cyprus J Med Sci. 2025;10(Suppl 1):78-82

ORCID IDs of the authors: İ.H.G. 0000-0001-8960-5265; H.K.E. 0000-0001-7429-1478; R.K.K. 0000-0002-6839-8823; H.S.V. 0000-0002-7415-9618.



Corresponding author: Hafize Seda Vatansever
E-mail: seda.vatansever@cbu.edu.tr/seda.vatansever@neu.edu.tr
ORCID ID: orcid.org/0000-0002-7415-9618

Received: 02.01.2025
Accepted: 03.03.2025
Publication Date: 04.06.2025



Copyright© 2025 The Author. Published by Galenos Publishing House on behalf of Cyprus Turkish Medical Association.
This is an open access article under the Creative Commons AttributionNonCommercial 4.0 International (CC BY-NC 4.0) License.

environment plays a crucial role in tumor progression, invasion, and immune evasion.⁶ Cancer stem cells (CSCs), a subpopulation of cancer cells within the TME, have been shown to contribute significantly to tumor initiation, metastasis, and resistance to therapies. CSCs maintain their stemness properties within the TME due to the supportive interactions with both cellular and physical factors.⁷ Colorectal cancer, the second leading cause of cancer-related deaths in Western countries, represents a prime example of the complex interactions between tumor cells and their microenvironment. These interactions stimulate tumor growth, progression, and metastasis, as well as the development of treatment resistance.⁸ Breast cancer, the most commonly diagnosed cancer among women, is influenced by a variety of risk factors, including genetic mutations, reproductive history, and lifestyle factors.^{9,10} Early detection and personalized treatment strategies are critical for both colon and breast cancer. Exosomes, small extracellular vesicles (30-100 nm), have garnered attention as potential biomarkers due to their unique molecular cargo, which includes proteins, miRNAs, and lncRNAs.¹¹ Exosomes differ from other extracellular vesicles in their biogenesis and lipid composition, and they are secreted by various cell types into bodily fluids like blood, saliva, and lymph.¹² The analysis of exosome content from cancer cells provides insights into tumor biology, enabling the identification of novel diagnostic and therapeutic targets.¹³

In cancer, exosome-mediated signaling contributes to tumor progression by facilitating communication between tumor cells and the surrounding stroma. This promotes processes such as angiogenesis, invasion, metastasis, and immune evasion.^{14,15} Hypoxia has been shown to increase exosome secretion, and the content of these exosomes often reflects the hypoxic state of the tumor, further influencing tumor behavior.¹⁶ In this study, we aim to analyze the presence and content of exosomes in cell culture media under hypoxic and normoxic conditions in primary and metastatic breast and colon carcinoma cell lines, and to evaluate their potential role in promoting stemness properties in cancer cells.

MATERIALS AND METHODS

Cell culture: Primary colon adenocarcinoma (Colo320, HTL95027, Interlab Cell Line Collection, Genova, Italy) and metastatic colon adenocarcinoma (Colo741, HTL95008, Interlab Cell Line Collection, Genova, Italy) cell lines were cultured in RPMI-1640 (F-1213, Biochrom, Berlin, Germany) supplemented with 10% fetal bovine serum [(FBS), S 0113, Biochrom, Berlin, Germany], 2 mM L-glutamine (K 0283, Biochrom, Berlin, Germany), and 1% penicillin-streptomycin. Similarly, breast cancer cell lines, primary (MCF7, HTB-22, ATCC) and metastatic (M4A4, CRL-2914, ATCC), were cultured in Dulbecco's Modified Eagle Medium containing 10% FBS, 1% penicillin-streptomycin, and 2 mM L-glutamine. All cell lines were incubated at 37 °C with 5% CO₂ in both normoxic and hypoxic (3% O₂) conditions. Each experimental condition was performed in triplicate to ensure reproducibility and reliability of the results.

Statistical Analysis

Immunocytochemical analysis: Cells in all groups were fixed with 4% paraformaldehyde and then incubated with 3% H₂O₂ (Merck, K31355100 303) for 15 min. After washing, permeabilization was performed with 0.1% Triton-X100 (Applichem, Mt 646). The blocking solution (Invitrogen, 859043) was applied, followed by the addition

of primary antibodies against CD63 (Santa Cruz Biotechnology, sc-5275), CD9 (Santa Cruz Biotechnology, sc-13118), HIF1 α (GeneTex, GTX127309), and CD133 (BiorBy, orb99113) and were incubated overnight at 4 °C. After washing, secondary antibody (Invitrogen, 859043) and diaminobenzidine chromogen (ScyTek, ACC125) were applied. They were stained for 3 minutes with Mayer's hematoxylin (05-06002/L) and then examined under a light microscope (Olympus BX31).

Exosome derivation: After collecting culture medium from all groups, the miRCURY™ Exosome Isolation Kit (Exiqon 300102) was used for the exosome derivation according to the manufacturer's protocol.

RNA derivation: Lysis buffer (600 μ L) was added to the cell pellets and incubated at room temperature for 5 min. Then 70% ethanol (1:1 ratio with lysis buffer) was added, the mixture was vortexed, and transferred to the column. After centrifugation, 50 μ L of elution buffer was added. At the end of the other centrifugation, the amount of RNA was measured with a NanoDrop spectrophotometer.

RESULTS

Semi-adherent adhesion feature of Colo320 (Figure 1A, B), epithelial-shaped feature of Colo741 (Figure 1C, D), fusiform structure of M4A4 (Figure 1E, F) and adherent epithelial feature of MCF-7 (Figure 1G, H) were the same after culturing under both hypoxic (Figure 1A, C, E, G) and normoxic (Figure 1B, D, F, H) conditions. HIF1 α immunoreactivity was detected as very weak in both hypoxic and normoxic conditions in all types of cells (Figures 2, 3). Very weak CD9 immunoreactivity was observed in Colo320, Colo741, and M4A4, and weak CD9 immunoreactivity was observed in MCF-7, in both hypoxic (Figure 2) and normoxic (Figure 3) conditions. CD63 immunoreactivity was positive in the Colo320, MCF7, and M4A4 cell lines, while it appeared negative in Colo741 cells under both hypoxic (Figure 2) and normoxic (Figure 3) conditions. The immunoreactivity of CD133 was similar for the Colo741 cell line in both normoxic and hypoxic conditions; however, in hypoxic conditions, increased immunoreactivity was detected in the other cell types (Figures 2, 3). After exosome analysis, the total miRNA in hypoxic, and normoxic conditions was similar in the Colo320 and Colo741 cells. The total amount of miRNA in hypoxic conditions in MCF7 cells was found to be higher than that in the normoxic conditions. In M4A4 cells, the amount of total miRNA in hypoxic conditions was less than in normoxic conditions.

DISCUSSION

In this study, exosome production was investigated in both primary and metastatic breast and colon cancer cells under hypoxic and normoxic conditions. Our findings showed a significant increase in exosome production in breast cancer cells under hypoxia, suggesting that hypoxia enhances exosome-mediated communication in the TME, potentially promoting tumor progression. The upregulation of CD63 expression in primary cells further supports the idea that exosome production is heightened in response to hypoxic stress. In contrast, hypoxia had a less pronounced effect on exosome production in colon cancer cells, indicating that these cells may utilize alternative adaptive mechanisms or rely less on exosome-mediated signaling. The differential responses between breast and colon cancer cells to hypoxia highlight the complexity of tumor biology and the distinct ways various cancer types interact with their microenvironment.

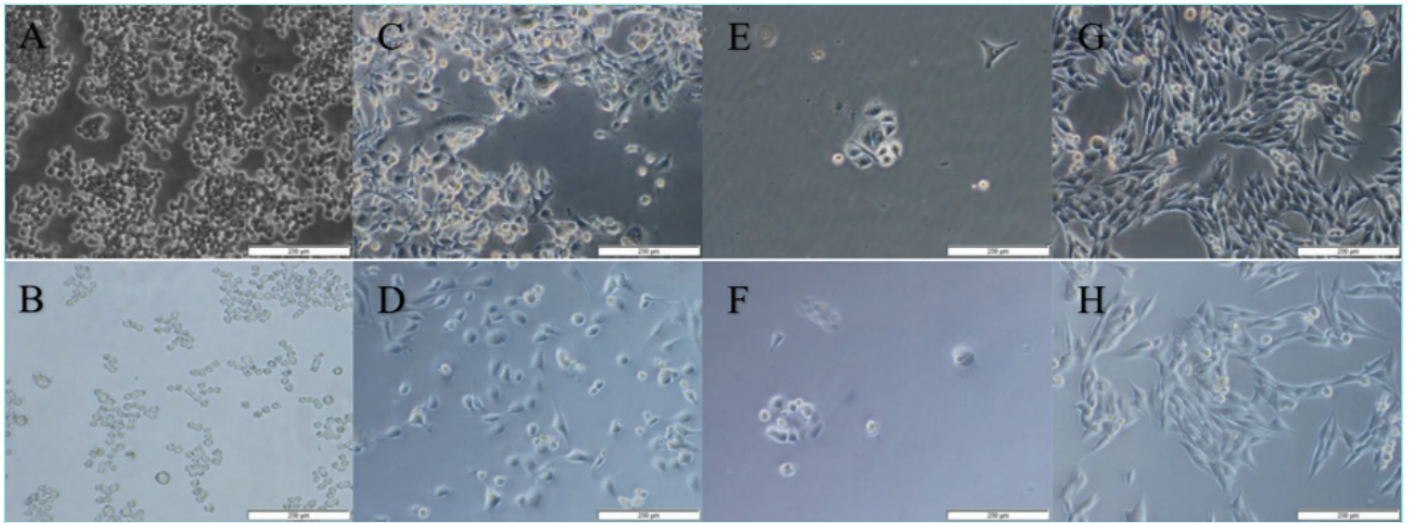


Figure 1. Colo320 (A, B), Colo741 (C, D), MCF7 (E, F) and M4A4 (G, H) cells were cultured in hypoxic (A, C, E, G) and normoxic (B, D, F, H) conditions. Scale bars: 200 µm.

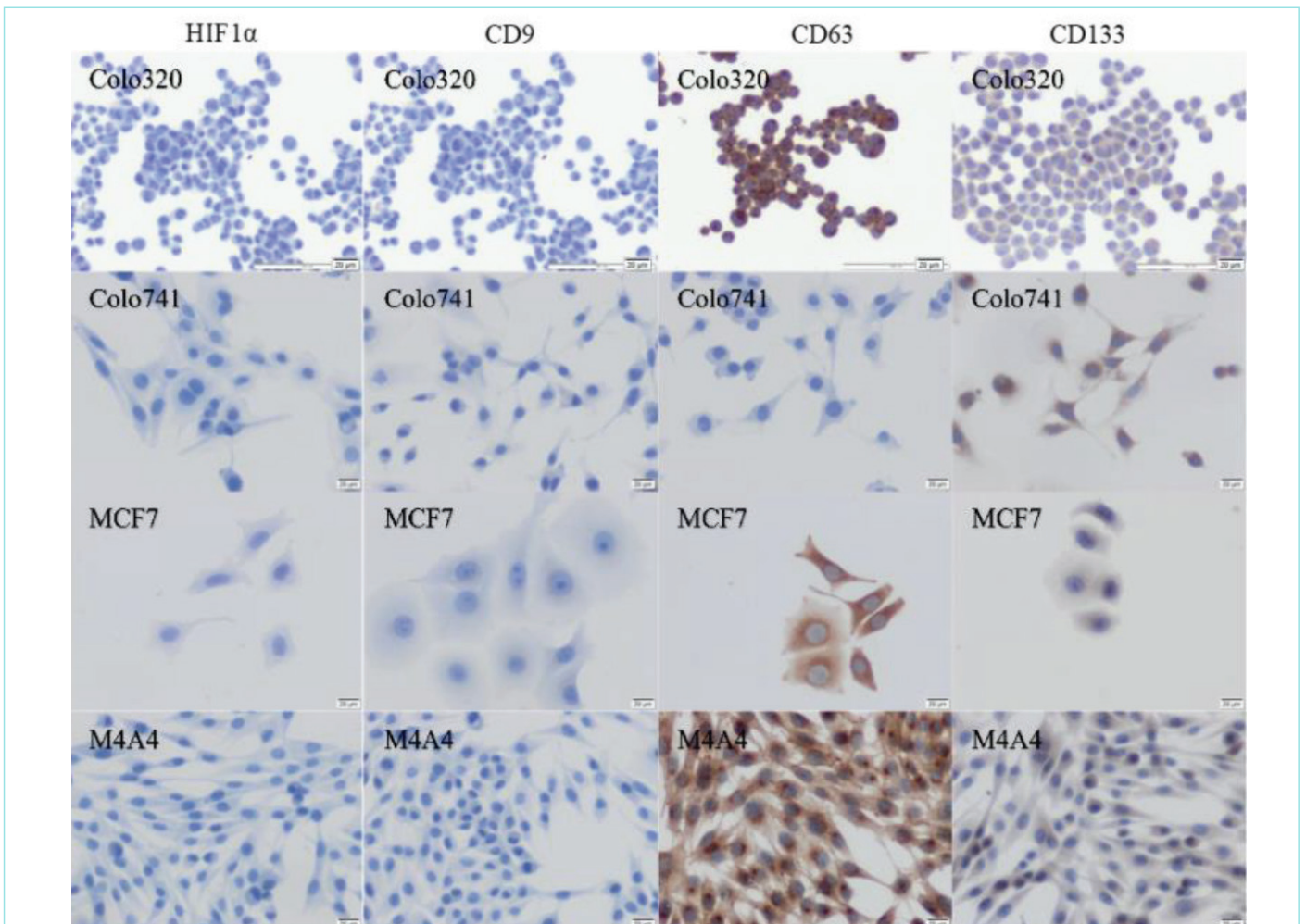


Figure 2. HIF1α, CD9, CD63 and CD133 immunoreactivities of Colo320, Colo741, MCF7 and M4A4 cell lines in hypoxic condition. Scale bars: 20 µm.

HIF: Hypoxia-inducible factors.

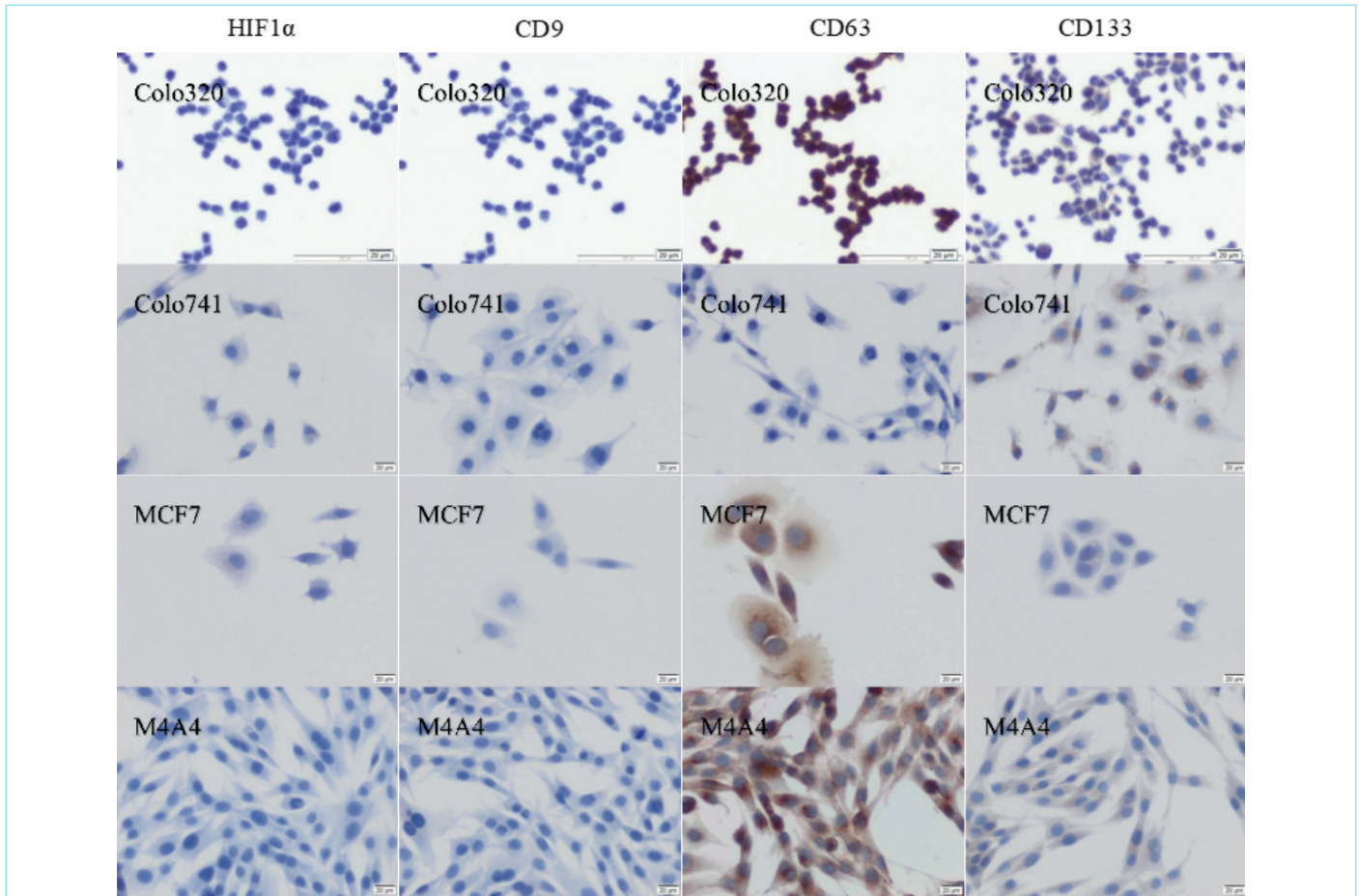


Figure 3. HIF1 α , CD9, CD63 and CD133 immunoreactivities of Colo320, Colo741, MCF7 and M4A4 cell lines in normoxic condition. Scale bars: 20 μ m.

HIF: Hypoxia-inducible factors.

Moreover, the increase in CD133 immunoreactivity under hypoxic conditions suggests that hypoxia may support CSC properties, which are crucial for tumor initiation and progression.¹⁷ Changes in miRNA profiles in response to hypoxia also imply that exosomes play a role in modulating tumor growth and metastasis through altered miRNA signaling.

CONCLUSION

Overall, this study demonstrates that hypoxia-induced exosome production may influence cancer stemness and tumor cell interactions with the microenvironment. The observed differences in exosome production across cancer types offer valuable insights into cancer biology and may guide the development of personalized therapeutic strategies in the future.

MAIN POINTS

- Hypoxia significantly enhances exosome secretion and may increase the stemness properties of primary breast and colon cancer cells.
- Exosomes from hypoxic conditions show distinct miRNA profiles compared to normoxic conditions, which could impact tumor progression.

- CD63 expression was notably increased in primary cancer cells under hypoxia, while metastatic lines showed less response.
- Exosome-mediated signaling in the tumor microenvironment contributes to malignancy and metastasis, particularly in aggressive tumors.

ETHICS

Ethics Committee Approval: Not applicable.

Informed Consent: Not applicable.

Footnotes

Authorship Contributions

Concept: İ.H.G., H.K.E., H.S.V., Design: İ.H.G., H.K.E., H.S.V., Data Collection and/or Processing: İ.H.G., H.K.E., R.K.K., H.S.V., Analysis and/or Interpretation: İ.H.G., H.K.E., R.K.K., H.S.V., Literature Search: İ.H.G., H.K.E., R.K.K., H.S.V., Writing: İ.H.G., H.K.E., H.S.V.

DISCLOSURES

Conflict of Interest: No conflict of interest was declared by the authors.

Financial Disclosure: This study supported by TUBITAK 2209-A scholarship program (1919B011502966).

REFERENCES

1. Petrova V, Annicchiarico-Petruzzelli M, Melino G, Amelio I. The hypoxic tumour microenvironment. *Oncogenesis*. 2018; 7(1): 10.
2. Huang X, Ding L, Bennewith KL, Tong RT, Welford SM, Ang KK, et al. Hypoxia-inducible mir-210 regulates normoxic gene expression involved in tumor initiation. *Mol Cell*. 2009; 35(6): 856-67.
3. Balkwill FR, Capasso M, Hagemann T. The tumor microenvironment at a glance. *J Cell Sci*. 2012; 125(Pt 23): 5591-6.
4. Lu J, Getz G, Miska EA, Alvarez-Saavedra E, Lamb J, Peck D, et al. MicroRNA expression profiles classify human cancers. *Nature*. 2005; 435(7043): 834-8.
5. Bhome R, Mellone M, Emo K, Thomas GJ, Sayan AE, Mirnezami AH. The colorectal cancer microenvironment: strategies for studying the role of cancer-associated fibroblasts. *Methods Mol Biol*. 2018; 1765: 87-98.
6. Laitman Y, Feldman DM, Sklair-Levy M, Yosepovich A, Barshack-Nakar I, Brodsky M, et al. Abnormal findings detected by multi-modality breast imaging and biopsy results in a high-risk clinic. *Clin Breast Cancer*. 2018; 18(4): 695-8.
7. Voinnet O. Origin, biogenesis, and activity of plant microRNAs. *Cell*. 2009; 136(4): 669-87.
8. Shao C, Yang F, Miao S, Liu W, Wang C, Shu Y, et al. Role of hypoxia-induced exosomes in tumor biology. *Mol Cancer*. 2018; 17(1): 120.
9. Gilkes DM, Semenza GL, Wirtz D. Hypoxia and the extracellular matrix: drivers of tumour metastasis. *Nat Rev Cancer*. 2014; 14(6): 430-9.
10. Semenza GL. Targeting HIF-1 for cancer therapy. *Nat Rev Cancer*. 2003; 3(10): 721-32.
11. Zhou J, Schmid T, Schnitzer S, Brüne B. Tumor hypoxia and cancer progression. *Cancer Lett*. 2006; 237(1): 10-21.
12. Rankin EB, Giaccia AJ. The role of hypoxia-inducible factors in tumorigenesis. *Cell Death Differ*. 2008; 15(4): 678-85.
13. Joyce JA, Pollard JW. Microenvironmental regulation of metastasis. *Nat Rev Cancer*. 2009; 9(4): 239-52.
14. Reina-Campos M, Moscat J, Diaz-Meco M. Metabolism shapes the tumor microenvironment. *Curr Opin Cell Biol*. 2017; 48: 47-53.
15. Harris AL. Hypoxia-a key regulatory factor in tumour growth. *Nat Rev Cancer*. 2002; 2(1): 38-47.
16. Gilkes DM, Semenza GL, Wirtz D. Hypoxia and the extracellular matrix: drivers of tumour metastasis. *Nat Rev Cancer*. 2014; 14(6): 430-9.
17. Lin SP, Lee YT, Wang JY, Miller SA, Chiou SH, Hung MC, et al. Survival of cancer stem cells under hypoxia and serum depletion via decrease in PP2A activity and activation of p38-MAPKAPK2-Hsp27. *PLoS One*. 2012; 7(11): 49605.

Molecular Characterization of Newcastle Disease Virus Circulating in Pakistan

✉ Uswa Siddique¹, ✉ Ijaz Ali²

¹Department of Medical Microbiology and Clinical Microbiology, Near East University Faculty of Healthy Sciences, Nicosia, North Cyprus

²Department of Biosciences, COMSATS University Islamabad Faculty of Health Sciences, Islamabad, Pakistan

Abstract

BACKGROUND/AIMS: Newcastle disease (ND) is a highly contagious disease in poultry caused by the ND virus (NDV). In Pakistan, NDV epidemics occur frequently, leading to massive economic losses; however, the genetic diversity of NDV in Pakistan is not well known. This study aims to investigate the genetic variation between the vaccine and circulating strains of NDV among poultry in Pakistan.

MATERIALS AND METHODS: Three vaccine strains [ND-Lasota, ND-infectious bronchitis (IB), ND-clone] were analyzed alongside 67 field samples collected from ND outbreaks. NDV samples were inoculated into 9-10-day-old eggs. Allantoic fluid was harvested, followed by a hemagglutination test. RNA was extracted from positive HA samples. Complementary DNA was prepared using reverse transcriptase-polymerase chain reaction (PCR). The *fusion (F)* gene was amplified through PCR using specific primers, and PCR products, measured in base pairs (bp), were analyzed using gel electrophoresis.

RESULTS: Among 67 field samples, the HA tests were positive in 50 samples, accounting for 75%. On gel, the *F1* gene of field NDV showed variable band size (250 bp, 350 bp, 400 bp), while *F2* and *F3* had band sizes of 650 bp and 500 bp, respectively. The band sizes *F1*, *F2*, and *F3* of ND-Lasota and ND-IB were each 100 bp. The band sizes of the *F1*, *F2*, and *F3* genes of ND-clone were 100 bp, 150 bp, and 150 bp, respectively.

CONCLUSION: Variability among *F1* gene sizes indicates the emergence of mutations or new subgenotypes. Sequencing-based studies are needed to monitor circulating NDV strains, to modify vaccines.

Keywords: Newcastle disease virus, hemagglutination test, RT-PCR, Gel electrophoresis

INTRODUCTION

Newcastle disease virus (NDV), also known as Avian paramyxovirus-1, causes ND when birds are infected with a virulent strain.¹ It is the most lethal among avulaviruses, infecting approximately 236 bird species globally and causing significant economic losses in poultry.² Between 2006 and 2009, countries reported 56 to 68 ND outbreaks. NDV consists of single-stranded, negative-sense RNA and six structural proteins. These proteins are the nucleocapsid, matrix, phosphoprotein, fusion (F), hemagglutinin-neuraminidase, and polymerase (L).³

In Pakistan, ND caused the death of 45 million broiler chickens during 2011-12, resulting in a loss of 6 billion PKR. In 2012, NDV outbreaks affected peacocks in Lahore and Sindh.⁴ Despite strict biosecurity efforts, NDV remains prevalent, transmitted largely via wild birds. Symptoms include shivering, spasms, and paralysis, leading to death from inability to eat or drink. There are four NDV pathotypes: asymptomatic enteric, lentogenic, mesogenic, and velogenic strains. The virus is highly contagious, with an incubation period of 2-15 days, and there is no treatment available.¹ Genetic recombination drives NDV evolution, with chimeric sequences identified in its genome. An intrinsic error rate of RNA L and the lack of proofreading ability during viral replication

To cite this article: Siddique U, Ali I. Molecular characterization of newcastle disease virus circulating in Pakistan. Cyprus J Med Sci. 2025;10(Suppl 1):83-86

ORCID IDs of the authors: U.S 0009-0002-2790-1901; I.A. 0000-0003-2163-8874.



Corresponding author: Uswa Siddique
E-mail: uswasiddique16@gmail.com
ORCID ID: orcid.org/0009-0002-2790-1901

Received: 03.12.2024
Accepted: 08.03.2025
Publication Date: 04.06.2025



Copyright © 2025 The Author. Published by Galenos Publishing House on behalf of Cyprus Turkish Medical Association.
This is an open access article under the Creative Commons Attribution-NonCommercial 4.0 International (CC BY-NC 4.0) License.

are the primary reasons behind the diversity and evolution of NDV.¹ This study investigates genetic variation between NDV vaccine strains (VS) and circulating field strains (FS) in Pakistan, focusing on the *F* gene, which is critical for virulence. The circulating strains belong to genotypes XIIIb and VIIi, while vaccines are from genotype II, showing a 17% evolutionary distance.⁴ There is a pressing need for vaccines that are both safe to use and compatible with the genotype of the circulating FS to effectively combat ND.²

MATERIALS AND METHODS

This study was conducted in the Molecular Virology Lab at COMSATS University, Islamabad. Three VSs [ND-infectious bronchitis (IB), ND Lasota, and ND clone] commonly utilized in Pakistan poultry vaccination programs were selected for this study. A total of 67 samples were analyzed. Among 67 field samples, 42 were collected from poultry farms located in Lahore, Sargodha, Islamabad, and Rawalpindi, while 25 samples were obtained from the outbreak-affected farms in Lahore and Sargodha. Field samples included the liver, trachea, and lungs. Embryonated eggs, aged nine to ten days, were collected, and candling was performed. Vaccine and field samples were prepared and inoculated in the eggs. After 24 and 48 hours, allantoic fluid was harvested, and the Hemagglutination test was conducted to detect the presence of NDV. Two methodologies were employed for RNA extraction: guanidinium thiocyanate (manual method) and the nucleic acid extraction kit (Tianlong, Xi'an, China). RNA quantification was performed by a Nanophotometer. Complementary DNA (cDNA) was synthesized through reverse transcriptase-polymerase chain reaction (RT-PCR), and the quantity was measured by a Nanophotometer. The *F* gene was amplified through PCR, and the resulting products were analyzed on the agarose gel. Ethical approval for this study was granted by the Ethics Review Board of COMSATS University Islamabad, Pakistan.

Statistical Analysis

No statistical analysis is needed for this study.

RESULTS

Viral Inoculation and Harvesting

All vaccine and field samples were inoculated in 9-10 embryonated eggs. After harvesting allantoic fluid (Figure 1a), the effects on the chicks

of the VS and FS were meticulously observed. Notably, chicks exposed to FS exhibited hemorrhaging, resulting in mortality, while those exposed to VS remained healthy with no observable lesions, as depicted in Figure 1b.

Hemagglutination Test

The hemagglutination (HA) test was employed to detect viral presence in the samples. All 3 VS tested positive for HA. Out of 67 field samples, 50 were confirmed positive for the NDV strain, while the remaining 17 samples gave negative results. Viral titer in positive samples was calculated following standard protocols, based on the last hazy well observed before bead formation.

RNA Extraction and Quantification

RNA extraction was conducted on the HA-positive samples utilizing 2 methods: the guanidinium thiocyanate method and a nucleic acid extraction kit. The ND Lasota VS and ND-IB VS along with 20 field samples of NDV were processed using the nucleic acid extraction kit. Conversely, RNA extraction of ND clone and the remaining 30 NDV field samples was performed via the guanidinium thiocyanate method. RNA concentration was quantified using a nanophotometer.

Complementary DNA Preparation and Quantification

cDNA was synthesized using RT-PCR, followed by quantification using a Nanophotometer.

Fusion Gene Amplification

Amplification of the *F* gene was conducted using three sets of primers, as outlined in Table 1.⁵ Each set of primers was applied sequentially for both vaccine and FS samples. The resultant PCR products were subjected to gel electrophoresis for band size analysis.

Newcastle Disease Virus Vaccine Samples

Using the F1, F2, and F3 sets of primers, 100 base pairs (bp) bands were successfully observed at different temperatures ranging from 61 °C to 70 °C in both the Lasota and ND-IB samples, as depicted in Figure 2a. In ND Clone, the *F1* and *F2* gene primers yielded 100 bp PCR products, while the *F3* gene primer generated a 150 bp product, as depicted in Figure 2b. These results were consistent across repeated experimental trials.



Figure 1. Harvesting of allantoic fluid and samples effects on the embryo.

Table 1. Primers of fusion (F) gene used⁵

Primer names	Sequence of primers
NDV-F330	5'-AGGAAGGAGACAAAAACGTTTATAGG-3'
NDV-R700	5'-TCAGCTGAGTTAATGCAGGGGAGG-3'
NDV-F640	5'-CTAACTGAATTAACACTACAGTATTCGGG-3'
NDV-R1290	5'-GTCTAATGATAAGACATTGCACGAATG-3'
NDV-F1200	5'-ATGTACAGACCCTCTGGTATCATATC-3'
NDV-R1740	5'-CTTAAGTCTTATACTTGACAGGTTATC-3'

Newcastle disease forward primer = NDV-F, Newcastle disease reverse primer = NDV-R.

Newcastle Disease Virus Field Samples

In most field samples, band visibility was limited due to low concentration; however, in some instances, bands of varying bp were detected.

Utilizing *F1* gene primers, 350 bp bands were identified in three distinct samples (Figure 3a). PCR product of different sizes of field NDV strains is observed in Figure 3b. Left to right, Lane 1 has a 100 bp ladder. Lane 2 shows *F1* fragment of 250 bp at 67.5 °C, lane 3 depicts *F1* fragment of 400 bp at 67.5 °C, lane 4 shows *F2* fragment of 650 bp at 68.3 °C and lane 5 shows *F2* fragment of 650 bp at 68.3 °C (Figure 3b).

Notably, four of these samples were collected from a poultry farm in Islamabad, while three originated from a poultry farm in Sargodha. A single sample exhibited a 400 bp band, as illustrated in Figure 3b.

For the *F2* gene, a 650 bp band was also observed in 2 NDV samples (Figure 3b).

For the *F3* gene, a 500 bp band was detected in 1 NDV sample (Figure 4).

DISCUSSION

In Pakistan, NDV outbreaks occur two-to-three times a year, making it the top fatal disease in poultry. This study examined three ND vaccines (ND Lasota, ND IB, and ND clone) in order to isolate, characterize, and compare the *F* gene of vaccine and FS from various regions. The *F* gene is vital for assessing the virulence of NDV, and significant variability was found, consistent with previous research, indicating a notable genetic distance among NDV strains.⁵ ND prevalence peaks in January, February, June, July, and September in both Pakistan and Egypt.⁵ Analysis revealed discrepancies in the band sizes in the *F1* gene products when compared to the results of other studies, likely due to the high mutation rates of RNA viruses.^{6,7} These results indicated that there is a large genetic distance between the two NDV strains. In Pakistan, new subgenotypes of NDV keep emerging, especially VII subgenotypes, due to the uncontrolled vaccination programs.⁸⁻¹⁰

Current vaccines are insufficient against contemporary strains, highlighting a mismatch between available vaccines and circulating variants.^{9,10} Despite the historical success of ND vaccines developed during the 1930s-1970s, they have proven inadequate against novel NDV variants emerging in recent years.¹¹ Given the historical success of ND vaccines, there is an urgent need for updated formulations that

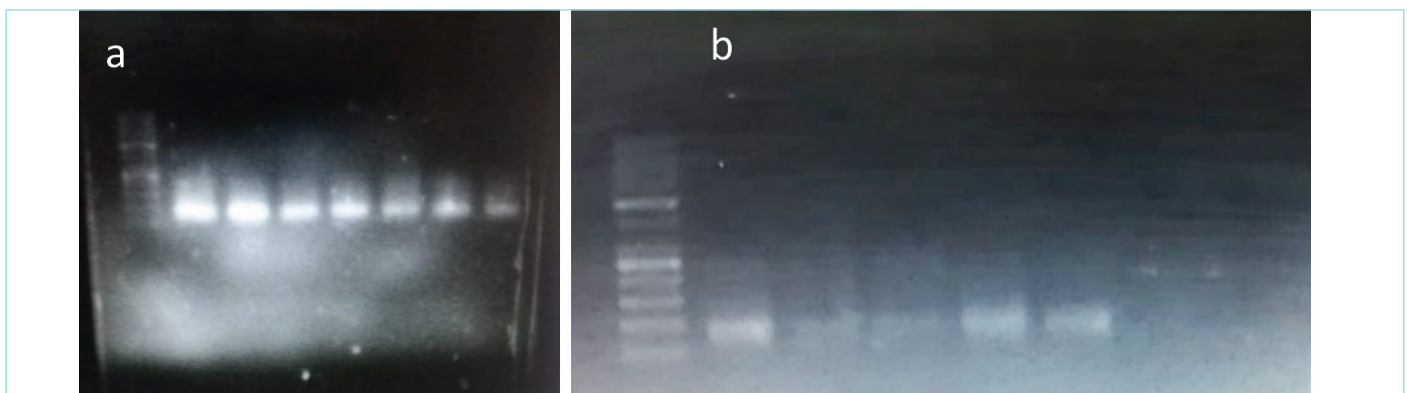


Figure 2. Gradient PCR results showing optimization of the *fusion* gene.

PCR: Polymerase chain reaction.

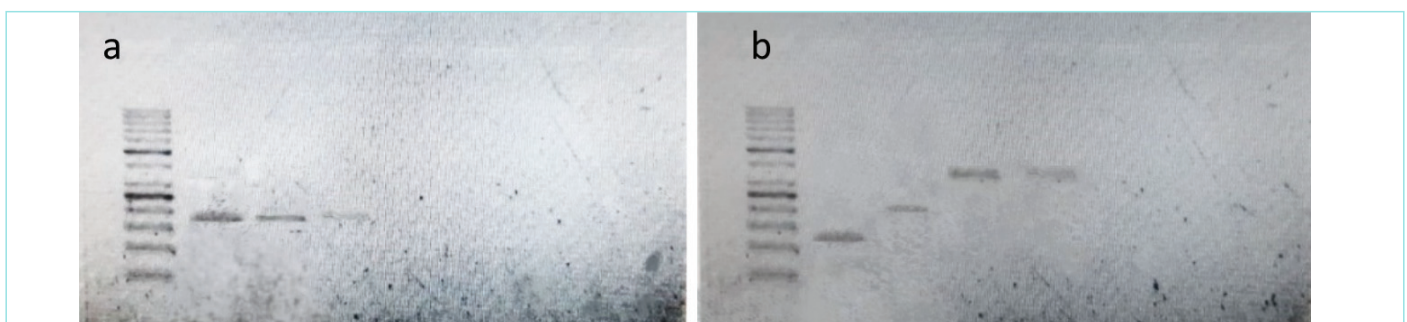


Figure 3. PCR products of different sizes.

PCR: Polymerase chain reaction.



Figure 4. A gradient PCR result for the optimization of the F3 gene.
PCR: Polymerase chain reaction.

align with current strains. Regular surveillance and strain identification are essential for developing more effective vaccines. Improved strategies are crucial to mitigate the economic impact of ND and address the ongoing evolution of the virus, emphasizing the importance of sequencing and phylogenetic analysis in future studies. Reducing genetic diversity between vaccine and FS may aid in the control and eventual elimination of ND.

Study Limitations

Sequencing and phylogenetic analysis could not be performed because of time limitations. Future studies, must be performed to identify NDV FS. According to recent findings, a new vaccine should be formulated immediately to combat the NDV situation.

CONCLUSION

In conclusion, our study revealed large genetic differences between the VS and the FS. Furthermore, variability was observed among F1 gene sizes indicating mutations or evolutions of new subgenotypes. Future studies must be performed regarding the identification of NDV FS. According to which new vaccines should be formulated immediately to combat the NDV situation.

MAIN POINTS

- Large genetic distance observed between the field strain (FS) and vaccine strains (VS).
- VS are lentogenic while FS are velogenic.
- Variability among *F1* gene sizes indicates mutations or the emergence of new subgenotypes.

ETHICS

Ethics Committee Approval: Ethical approval for this study was granted by the Ethics Review Board of COMSATS University Islamabad, Pakistan. (approval number: CUI/Bio/ERB/10-2024/1, date: 01.01.2024).

Informed Consent: Not available.

Footnotes

Authorship Contributions

Surgical and Medical Practices: U.S., Concept: I.A., Design: U.S., Data Collection and/or Processing: U.S., Analysis and/or Interpretation: U.S., Literature Search: U.S., Writing: U.S.

DISCLOSURES

Conflict of Interest: No conflict of interest was declared by the authors.

Financial Disclosure: The authors declared that this study had received no financial support.

REFERENCES

1. Suarez DL, Miller PJ, Koch G, Mundt E, Rautenschlein S. Newcastle disease, other avian paramyxoviruses, and avian metapneumovirus infections. *Diseases of poultry*. 2020 Jan 13:109-66.
2. Hu Z, He X, Deng J, Hu J, Liu X. Current situation and future direction of Newcastle disease vaccines. *Vet Res*. 2022; 53(1): 99.
3. Qiu X, Jia Y, Zhang Z, Fo X, Wang W. Characterization of chicken-derived genotype VII Newcastle Disease Virus isolates from Northwest China. *J Poult Sci*. 2023; 60(2): 2023010.
4. Tanveer S, Malik HA, Shahid N, Salisu IB, Ahmed N, Latif A, et al. Production of proinflammatory cytokines by expressing Newcastle disease vaccine candidates in corn. *J King Saud Univ Sci*. 2023; 35(3): 102537.
5. Selim KM, Selim A, Arafa A, Hussein HA, Elsanousi AA. Molecular characterization of full fusion protein (F) of Newcastle disease virus genotype VII isolated from Egypt during 2012-2016. *Vet World*. 2018; 11(7): 930-8.
6. Sarcheshmei M, Dadras H, Mosleh N, Mehrabanpour MJ. Comparative evaluation of the protective efficacy of different vaccination programs against a virulent field strain of the Newcastle disease virus in broilers. *Braz J Poult Sci*. 2016; 18: 363-70.
7. Roohani K, Tan SW, Yeap SK, Ideris A, Bejo MH, Omar AR. Characterization of genotype VII Newcastle disease virus (NDV) isolated from NDV vaccinated chickens, and the efficacy of LaSota and recombinant genotype VII vaccines against challenge with velogenic NDV. *J Vet Sci*. 2015; 16(4): 447-57.
8. Shabbir MZ, Abbas M, Yaqub T, Mukhtar N, Subhani A, Habib H, et al. Genetic analysis of Newcastle disease virus from Punjab, Pakistan. *Virus Genes*. 2013; 46(2): 309-15.
9. Siddique N, Naeem K, Abbas MA, Malik AA, Rashid F, Rafique S, et al. Sequence and phylogenetic analysis of virulent Newcastle disease virus isolates from Pakistan during 2009-2013 reveals circulation of new subgenotype. *Virology*. 2013; 444(1-2): 37-40.
10. Munir MT, Chowdhury MR, Ahmed Z. Emergence of new sub-genotypes of Newcastle disease virus in Pakistan. *J Avian Res*. 2016; 2(1): 1-7.
11. Mehmood A, Rasool MH, Anjum AA, Zahoor MA, Shafique M. pathotyping and genetic characterization of a highly virulent newcastle disease virus strain isolated from recent outbreak in district Okara, Pakistan. *Pak Vet J*. 2019; 39(3) 353-8.

Does RAB31 Continue to Play a Role in Exosome Biogenesis of Adipose-Derived Mesenchymal Stem Cells in 2D and 3D Culture Conditions in a Hypoxic Environment?

✉ Hafize Seda Vatansever^{1,2}, ✉ Hilal Kabadayı Ensarioğlu¹, ✉ Aslınur Aktaş¹, ✉ Burak Kutlu Aydın¹, ✉ Nadire Kiyak³,
✉ Mehmet Vatansever⁴

¹Department of Histology and Embryology, Manisa Celal Bayar University Faculty of Medicine, Manisa, Türkiye

²DESAM Research Institute, Near East University, Nicosia, North Cyprus

³Department of Histology and Embryology, Near East University Faculty of Medicine, Nicosia, North Cyprus

⁴Department of Occupation Therapy, Near East University Faculty of Health Sciences, Nicosia, North Cyprus

Abstract

BACKGROUND/AIMS: Mesenchymal stem cells (MSCs) are considered potential candidates in regenerative medicine due to their angiogenic, anti-apoptotic, and immunomodulatory properties. Among the secretory products of MSCs are biomolecules such as cytokines, chemokines, growth factors, and particularly exosomes. Exosomes are nanovesicles, ranging from 20 to 100 nm, that can be isolated from various body fluids. RAB31 plays a role in an endosomal sorting complex required for transport-independent pathway. Our study aims to determine the changes in exosome biogenesis and secretion of RAB31 from adipogenic mesenchymal stem cells (AMSCs), cultured in 2D and 3D culture conditions under normoxic and hypoxic environments.

MATERIALS AND METHODS: AMSCs were cultured in 2D and 3D conditions, and the study groups were formed as follows: normoxic 2D AMSC culture (group 1), normoxic 3D AMSC culture (group 2), hypoxic 2D AMSC culture (group 3), and hypoxic 3D AMSC culture (group 4). After culturing all groups of cells under normoxic and hypoxic conditions for 48 hours, exosomes were collected from culture medium, and the presence of RAB31, Rab7, CD9, and CD63 proteins was evaluated using indirect immunocytochemistry.

RESULTS: The exosome secretion was different after normoxic and hypoxic conditions. In addition, the distributions of RAB31 and RAB7 were different, but the intensity of CD9 and CD63 immunoreactivity was similar in 2D conditions. CD9 immunoreactivity was not affected under hypoxic or normoxic conditions. However, increased immunoreactivity of CD63 was observed. Moderate and negative RAB7 immunoreactivity was observed in 3D hypoxic and normoxic conditions, respectively. RAB31 immunoreactivity was higher in hypoxic conditions than in normoxic conditions.

CONCLUSION: Exosome secretion from AMSCs was affected after culture conditions. Especially hypoxic conditions triggers the secretion of RAB31, and co-localization of CD63 and RAB31 under these conditions points out that exosome biogenesis controls RAB31 in AMSCs under hypoxic conditions.

Keywords: Exosome, biogenesis, RAB31, adipogenic mesenchymal stem cells

To cite this article: Vatansever HS, Kabadayı Ensarioğlu H, Aktaş A, Aydın BK, Kiyak N, Vatansever M. Does RAB31 continue to play a role in exosome biogenesis of adipose-derived mesenchymal stem cells in 2D and 3D culture conditions in a hypoxic environment? Cyprus J Med Sci. 2025;10(Suppl 1):87-91

ORCID IDs of the authors: H.S.V. 0000-0002-7415-9618; H.K.E. 0000-0001-7429-1478; A.A. 0009-0000-4168-5753; B.K.A. 0000-0002-5837-0026; N.K. 0000-0002-7126-2775; M.V. 0009-0005-6155-3076.



Corresponding author: Hafize Seda Vatansever
E-mail: seda.vatansever@cbu.edu.tr/seda.vatansever@neu.edu.tr
ORCID ID: orcid.org/0000-0002-7415-9618

Received: 01.01.2025
Accepted: 03.03.2025
Publication Date: 04.06.2025



Copyright© 2025 The Author. Published by Galenos Publishing House on behalf of Cyprus Turkish Medical Association.
This is an open access article under the Creative Commons AttributionNonCommercial 4.0 International (CC BY-NC 4.0) License.

INTRODUCTION

Exosomes are nanovesicles with a size of 20-100 nm, are secreted from many cells in the body, and have been isolated from body fluids such as blood, urine, breast milk, amniotic fluids, and bronchial alveolar lavage.¹ Exosomes belong to the group of extracellular vesicles (EVs) along with ectosomes, microvesicles, membrane vesicles, and apoptotic bodies. Although the content of exosomes varies depending on the cells of origin, they can generally be considered vesicles containing proteins, lipids, and nucleic acids.² Its structure includes cytoskeleton proteins (actin, tubulin, cofilin, moesin); adhesion molecules tetraspanins (CD9, CD37, CD53, CD63, CD81, CD82); integrins; endosomal sorting complex required for transport (ESCRT) proteins; transport/binding proteins (annexins, galectin, rab family, GTPases); as well as ALIX and TSG101 proteins and heat shock proteins (HSP70, HSP90) that act as markers and participate in exosome biogenesis.³ Due to the similarity of the exosome membrane with the cell membrane structure, due to its fusion with other cells, and due to its ability to easily pass through many barriers due to its small diameter, research on exosome biogenesis continues.⁴⁻⁶

Although the content of exosomes varies depending on the cells of origin, they can generally be considered as vesicles containing proteins, lipids, and nucleic acids.^{2,7} Various proteins are involved in exosome biogenesis. Two main pathways have been explained: ESCRT-dependent and independent pathways.⁸ There are three Rab-GTPases described in EVs biogenesis and secretion: RAB11, RAB35, and RAB27A.^{9,10} Due to the secretion of intraluminal vesicles (ILVs) from ESCRT-depleted cells, when the level of the Rab-related protein in brain (RAB) 31, which is a member of the RAB5 subfamily of Rab GTPases, is higher than RAB7, RAB31 inactivates RAB7, rescuing lysosomal degradation, and therefore ILVs are secreted as exosomes.¹¹

Stem cells can be obtained from fetal and adult tissues. They have the potential to proliferate on their own and differentiate in appropriate culture environments. Mesenchymal stem cells (MSCs), which are favored in the field of medicine due to their angiogenic, anti-apoptotic, and immunomodulatory properties, are often used because they can be taken from the person himself/herself. In addition, MSCs do not cause ethical problems in their use even when sourced from different people. MSC-derived EVs retain the biological activity of parental MSCs and demonstrate a similar therapeutic potential.¹¹⁻¹⁴ Several studies have explored the potential of stem cell-derived exosomes collected under normoxic and hypoxic conditions for advancing regenerative medicine.¹⁴ Hypoxia modulates the secretion, composition, and function of exosomes, especially various cancers.⁸ While hypoxia increased exosome release via upregulation of RAB27a and reducing RAB7^{9,10} the secretion of RAB31 via hypoxia remains unclear.

We aim to determine the changes in exosome biogenesis and the secretion of RAB31 in the context of the culture of adipogenic mesenchymal stem cells (AMSCs) in 2D and 3D culture conditions under normoxic and hypoxic environments.

MATERIALS AND METHODS

2D and 3D Culture of AMSCs in Hypoxic and Normoxic Conditions

AMSCs were thawed rapidly in a water bath at 37 °C, then transferred to Dulbecco's Modified Eagle Medium culture medium containing 10%

exosome-free fetal bovine serum (Capricorn Scientific, FBS-ED-12B), 1% penicillin/streptomycin, and 1% L-glutamine, and centrifuged at 1000 rpm for 5 minutes. After the supernatant is discarded, 5 mL of culture medium is added to the pellet, and it is cultured in a 25 cm² flask, with the culture medium changed every 2 days until it reached 80% confluency. AMSCs were then subdivided into four groups: normoxic 2D culture, normoxic 3D culture, hypoxic 2D culture, and hypoxic 3D culture. For 2D conditions, they were cultured in 24-well plates according to standard cell culture protocols. For 3D conditions, matrigel was prepared at a concentration of 5 mg/mL, and 100 µL was added to each well of a 24-well culture plate. After incubating for 30 minutes at 37 °C and 5% CO₂, 30 µL of AMSCs suspension (at a concentration of 5x10⁶ cells/mL) was mixed into 270 µL of Matrigel solution, resulting in a final cell density of 5x10⁵ cells/mL. This mixture was incubated for 30-45 minutes at 37 °C and 5% CO₂. Afterward, 2 mL of culture medium was added to each well, and the cells were cultured. AMSCs were incubated for 48 hours in normoxic (5% CO₂, 95% O₂) and hypoxic (5% CO₂, 5% O₂, 90% N₂) conditions. All cell culture studies were performed in three replicates.

Statistical Analysis

Immunocytochemical Analysis

All groups of cells were fixed with 4% paraformaldehyde (Merck, Cat. No: TP70404 415) and distributions of RAB31 (Affinity Biosciences, DF4401), RAB7 (Affinity Biosciences, DF6288), CD9 (Santa Cruz, sc-13118), and CD63 (Santa Cruz, sc-5275) were analyzed using indirect immunoperoxidase staining. For the permeabilization process, the samples were kept in 0.1% Triton-X 100 solution on ice for 10 min. Cells were washed with phosphate buffered saline and then treated with 3% H₂O₂ for 5 min to inhibit tissue endogenous peroxidase. The blocking solution was incubated for 60 min. After removal of the blocking solution, primary antibodies were added overnight. After washing steps, biotin-streptavidin horseradish peroxidase secondary (Thermo Scientific, Cat. No: TP-125-HL) antibodies were applied. Diaminobenzidine (Thermo Scientific, Cat. No: TA-125-HD) was used for chromogen and Mayer's hematoxylin (Atom Scientific Ltd, Cat. No: TTSP60) for background staining. Immunocytochemical staining was performed in three replicates.

RESULTS

Fusiform structures of AMSCs were observed after 2D, and culture under normoxic and hypoxic conditions (Figure 1). The shape of AMSCs after 3D culture was spheroid in both normoxic and hypoxic conditions (Figure 1). Intensities of CD9 and CD63 were similar in both 2D hypoxic and normoxic conditions, while CD9 immunoreactivity was negative, but moderate staining of CD63 was detected (Figure 2). CD9 immunoreactivity was similar in both conditions in 3D culture, and it was very weak (Figure 2). The intensity of CD63 was strong and similar in both 3D hypoxic and normoxic conditions (Figure 2). RAB7 and RAB31 immunoreactivities were higher in the 2D hypoxic conditions than in the 2D normoxic conditions (Figure 2). Moderate and absent RAB7 immunoreactivity was observed in 3D hypoxic and normoxic conditions, respectively, (Figure 2). However, RAB31 immunoreactivity was higher in 3D hypoxic conditions than in normoxic conditions (Figure 2).

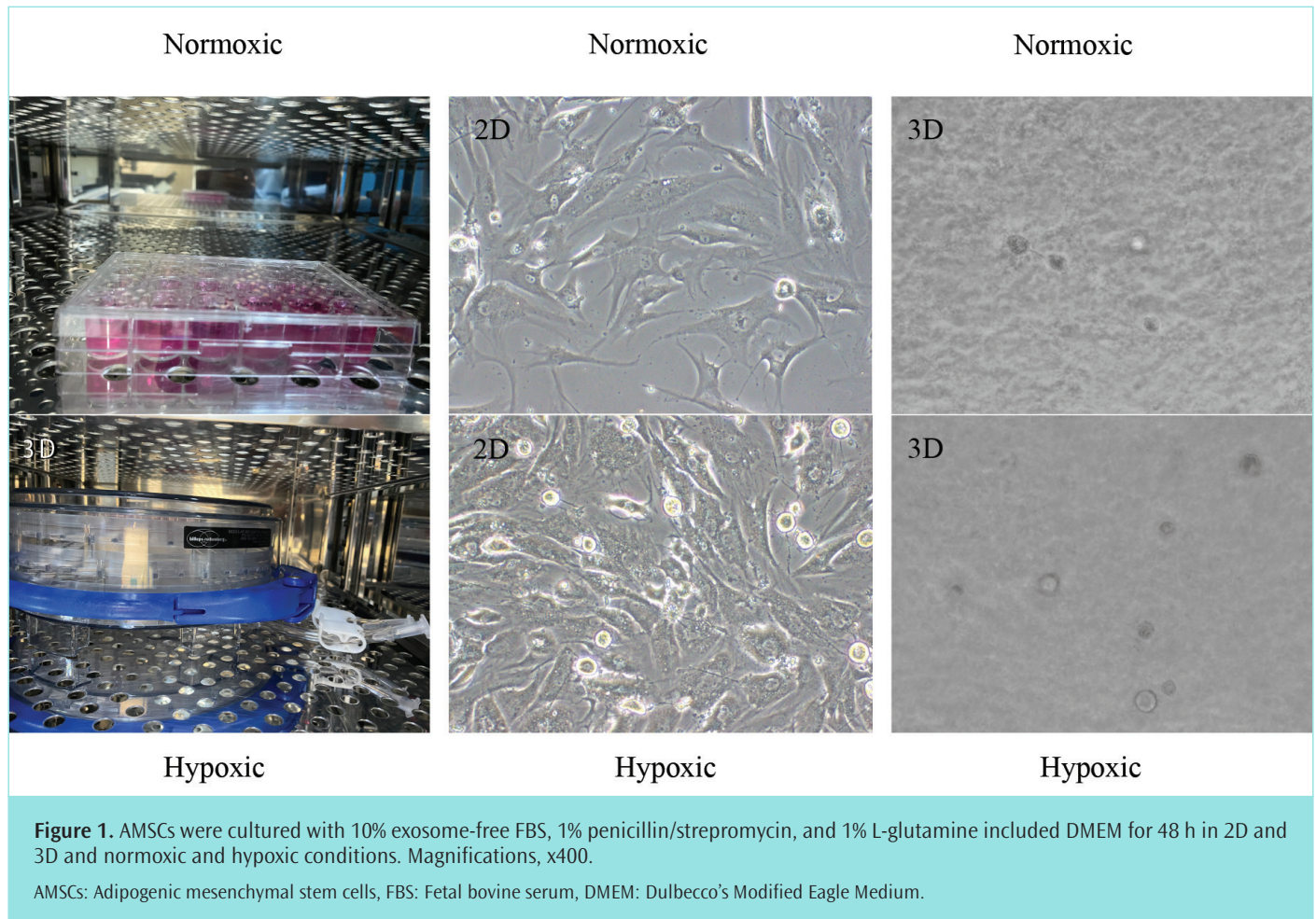


Figure 1. AMSCs were cultured with 10% exosome-free FBS, 1% penicillin/streptomycin, and 1% L-glutamine included DMEM for 48 h in 2D and 3D and normoxic and hypoxic conditions. Magnifications, x400.

AMSCs: Adipogenic mesenchymal stem cells, FBS: Fetal bovine serum, DMEM: Dulbecco's Modified Eagle Medium.

DISCUSSION

The exosome lipid bilayer is highly asymmetrical, which could be particularly advantageous for its interaction with the plasma membrane and especially with their target cells.^{3,4} During the biogenesis of exosomes, endocytosis and plasma membrane invagination allow proteins, lipids, metabolites, small molecules, ions, and cell surface proteins to enter cells.⁷ Improved understanding of the physical properties of exosomes and the mechanism of their biogenesis is leading to new approaches to increase yield and uniformity of their production. Both stem cells and exosomes have their place in a treatment protocol. Therefore, the EVs of MSCs are potential therapeutic tools, which have advantages over cell therapy in terms of safety, ease of storage/transportation, and clinical use.¹¹⁻¹⁴ Instead of examining the biogenesis of exosomes, it should be examined how exosome content is affected by environmental changes. In our results, we demonstrated that exosome secretion from AMSCs was affected by culture conditions. In both 2D and 3D conditions, RAB31 secretion was affected in hypoxic conditions. Higher intensity

and intracellular co-localization of CD63 and RAB31 were observed. This indicating that hypoxia triggers exosome biogenesis via RAB31.

Study Limitations

During the studies, some proteins were not evaluated by immunocytochemical analysis, therefore, in future investigations, the protein levels will be evaluated by immunoblotting.

CONCLUSION

Understanding the mechanisms of exosome biogenesis and the influence of microenvironmental conditions on their content and secretion is critical to harnessing their full potential. This study highlights the impact of hypoxic conditions on exosome biogenesis in AMSCs, with RAB31 playing a significant role in this process. Modification of stem cell-derived exosomes and/or artificial synthesis of exosomes will be the new therapeutic approaches for treating diseases. It is very important to understand and control exosome secretion or biogenesis under different microenvironments.

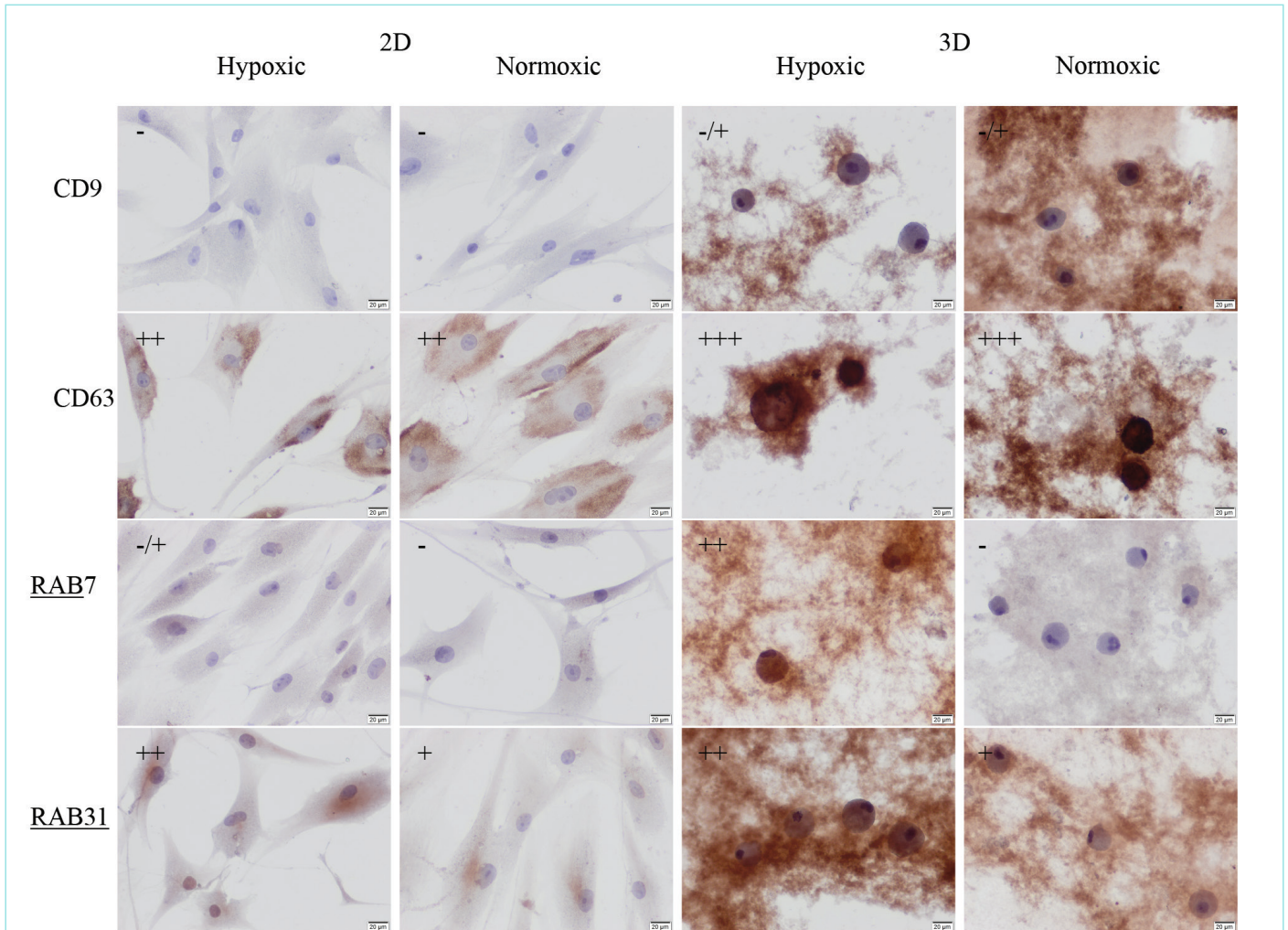


Figure 2. Immunoreactivity of CD9, CD63, RAB7, and RAB31 of AMSCs in 2D and 3D hypoxic and normoxic conditions. Scale bars: 20 μm. AMSCs: Adipogenic mesenchymal stem cells.

MAIN POINTS

- Exosome secretion from adipogenic mesenchymal stem cells (AMSCs) was affected after culture conditions.
- Hypoxic condition, trigger the secretion of RAB31 from AMSC.
- The biogenesis of exosomes should be evaluated under different culture conditions.

ETHICS

Ethics Committee Approval: Not applicable.

Informed Consent: Not applicable.

Footnotes

Authorship Contributions

Concept: H.S.V., H.K.E., Design: H.S.V., H.K.E., Data Collection and/or Processing: H.S.V., H.K.E., A.A., B.K.A., N.K., M.V., Analysis and/or Interpretation: H.S.V., H.K.E., A.A., B.K.A., N.K., M.V., Literature Search: H.S.V., H.K.E., A.A., B.K.A., N.K., M.V., Writing: H.S.V., H.K.E.

DISCLOSURES

Conflict of Interest: No conflict of interest was declared by the authors.

Financial Disclosure: This work was supported by Research Fund of Near East University (project number: SAG-2023-1-026).

REFERENCES

1. Choi DS, Kim DK, KimYK, Gho YS. Proteomics, transcriptomics and lipidomics of exosomes and ectosomes. *Proteomics*. 2013; 13(10-11): 1554-71.
2. Mathieu M, Martin-Jaular L, Lavieuv G, Théry C. Specificities of secretion and uptake of exosomes and other extracellular vesicles for cell-to-cell communication. *Nat Cell Biol*. 2019; 21(1): 9-17.
3. Kimiz-Gebologlu I, Oncel SS. Exosomes: large-scale production, isolation, drug loading efficiency, and biodistribution and uptake. *J Control Release*. 2022; 347; 533-43.
4. Du S, Guan Y, Xie A, Yan Z, Gao S, Li W, et al. Extracellular vesicles: a rising star for therapeutics and drug delivery. *J Nanobiotechnology*. 2023; 21(1): 231.
5. Wang X, Huang J, Chen W, Li G, Li Z, Lei J. The updated role of exosomal proteins in the diagnosis, prognosis, and treatment of cancer. *Exp Mol Med*. 2022; 54: 1390-400.

6. Gurunathan S, Kang MH, Jeyaraj M, Qasim M, Kim JH. Review of the isolation, characterization, biological function, and multifarious therapeutic approaches of exosomes. *Cells*. 2019; 8(4): 307.
7. Skotland T, Hessvik NP, Sandvig K, Llorente A. Exosomal lipid composition and the role of ether lipids and phosphoinositides in exosome biology. *J Lipid Res*. 2019; 60(1): 9-18.
8. Han QF, Li WJ, Hu KS, Gao J, Zhai WL, Yang JH, et al. Exosome biogenesis: machinery, regulation, and therapeutic implications in cancer. *Mol Cancer*. 2022; 21(1): 207.
9. Wei D, Zhan W, Gao Y, Huang L, Gong R, Wang W, et al. RAB31 marks and controls an ESCRT-independent exosome pathway. *Cell Res*. 2021; 31(2): 157-77.
10. Dorayappan KDP, Wanner R, Wallbillich JJ, Saini U, Zingarelli R, Suarez AA, et al. Hypoxia-induced exosomes contribute to a more aggressive and chemoresistant ovarian cancer phenotype: a novel mechanism linking STAT3/Rab proteins. *Oncogene*. 2018; 37(28): 3806-21.
11. Qiu G, Zheng G, Ge M, Wang J, Huang R, Shu Q, et al. Functional proteins of mesenchymal stem cell-derived extracellular vesicles. *Stem Cell Res Ther*. 2019; 10(1): 359.
12. Hade MD, Suire CN, Suo Z. Mesenchymal stem cell-derived exosomes: applications in regenerative medicine. *Cells*. 2021; 10(8): 1959.
13. Gomzikova MO, James V, Rizvanov AA. Therapeutic application of mesenchymal stem cells derived extracellular vesicles for immunomodulation. *Front Immunol*. 2019; 10: 2663.
14. Braga CL, da Silva LR, Santos RT, de Carvalho LRP, Mandacaru SC, de Oliveira Trugilho MR, et al. Proteomics profile of mesenchymal stromal cells and extracellular vesicles in normoxic and hypoxic conditions. *Cytotherapy*. 2022; 24(12): 1211-24.

Protocol for Obtaining Stem Cells from Menstrual Blood

Aslinur Aktaş¹, Hilal Kabadayı Ensarioğlu², Yıldız Uyar³, Hafize Seda Vatansever^{2,4}

¹Department of Histology and Embryology, Manisa Celal Bayar University Institute of Health Sciences, Manisa, Türkiye

²Department of Histology and Embryology, Manisa Celal Bayar University Faculty of Medicine, Manisa, Türkiye

³Department of Obstetrics and Gynaecology, Manisa Celal Bayar University Faculty of Medicine, Manisa, Türkiye

⁴DESAM Research Institute, Near East University, Nicosia, North Cyprus

Abstract

BACKGROUND/AIMS: Stem cells that have the ability to differentiate into other somatic cells are special cells in tissue and play a role in the repair and regeneration of tissues. Menstrual blood stem cells (MenSCs), a subtype of mesenchymal stem cells derived from the endometrium during menstruation, present an accessible and non-invasive source for stem cell research. This study aimed to create a protocol to obtain MenSCs from menstrual blood.

MATERIALS AND METHODS: Samples were collected from fertile women aged 18-45 on the second day of their menstrual cycles. Two methods: Ficoll and collagenase, were applied for cell isolation. In the Ficoll method, solution was slowly added in equal proportions and then centrifuged at 2000 rpm for twenty minutes (min). MenSCs were collected, centrifuged at 1000 rpm for 10 min, and then cultured in MenSCs culture medium at 37 °C with 5% CO₂ in air. In the collagenase technique, 0.5 mg/mL collagenase 1 was added to the samples in a 1:1 ratio and left to incubate for 1 hour at 37 °C with 5% CO₂ in air. After centrifugation, MenSCs were cultured and were then passaged three times. Distributions of CD31 and CD44 were used to characterize the cells via the indirect immunoperoxidase technique.

RESULTS: Cells isolated using both methods exhibited epithelioid morphology, cytoplasmic lipid droplets and colony formation. However, cells obtained with the collagenase method demonstrated faster proliferation and formed bigger colonies. Morphology and immunoreactivity remained consistent across passages.

CONCLUSION: MenSCs isolated with collagenase method showed better proliferation than those obtained with ficoll. The immunocytochemistry results, showing CD31 negativity and CD44 positivity, confirmed the mesenchymal stem cell characteristics of the isolated cells.

Keywords: Mesenchymal stem cells, menstrual blood stem cells, collagenase 1, ficoll

INTRODUCTION

Mesenchymal stem cells (MSCs) are multipotent and, under suitable conditions, have the ability to differentiate into various cell types. MSCs can be obtained from bone marrow, dental pulp, adipose tissue, etc.^{1,2} The proliferation of MSCs by adhering to plastic culture surfaces and their differentiation into at least three lines in vitro is considered to be the gold standard.³ MSCs have become an important focus in the

treatment of disease due to their biological properties, as well as their potential to repair and regenerate damaged tissues.⁴ Menstrual blood stem cells (MenSCs) were adult stem cells derived from the endometrial epithelium and were first obtained in 2007. MenSCs have attracted attention due to their accessibility, potential in regenerative medicine given their non-invasive collection methods, ease of acquisition, and lack of ethical issues.⁴ MenSCs have the ability to self-renew, differentiate into other types of cells, and culture long-term.^{5,6} In addition, MenSCs

To cite this article: Aktaş A, Kabadayı Ensarioğlu H, Yıldız Uyar Y, Vatansever HS. Protocol for obtaining stem cells from menstrual blood. Cyprus J Med Sci. 2025;10(Suppl 1):92-95

ORCID IDs of the authors: A.A. 0009-0000-4168-5753; H.K.E. 0000-0001-7429-1478; Y.U. 0000-0003-1104-2786; H.S.V. 0000-0002-7415-9618.



Corresponding author: Hafize Seda Vatansever
E-mail: seda.vatansever@cbu.edu.tr, seda.vatansever@neu.edu.tr
ORCID ID: orcid.org/0000-0002-7415-9618

Received: 22.11.2024
Accepted: 13.03.2025
Publication Date: 04.06.2025



Copyright © 2025 The Author. Published by Galenos Publishing House on behalf of Cyprus Turkish Medical Association.
This is an open access article under the Creative Commons Attribution-NonCommercial 4.0 International (CC BY-NC 4.0) License.

have increased proliferation and differentiation potential compared to stromal bone marrow-derived MSCs.⁷ For this reason, MSCs derived from menstrual blood may have the potential to be a new and easily available cell-based treatment. MenSCs are positive for markers such as CD44, CD73, CD90, SSEA-4, OCT-4, etc., but negative for CD34, STRO-1, etc.⁸ Due to these advantages of MenSCs, it is very important to obtain the appropriate number of MenSCs with the desired characteristics. The aim is to analyze the culture and differentiation potential of MenSCs using different protocols.

MATERIALS AND METHODS

MenSCs Derivation and Culture

The project was supported by Manisa Celal Bayar University Health Sciences Ethics Committee (approval number: E-20478486-050.04-706680, date: 18.01.2024). All participants were given detailed information about the study and voluntary consent was obtained from the before the study started. To obtain MenSCs, samples were collected from 5 patients, and 10 mL samples were collected from each patient. The selection criteria were the collection of menstrual blood from fertile patients, on the 2nd day of their menstrual cycle. Blood samples were then divided into two tubes for two different protocols. They were first centrifuged at 1000 rpm for five minutes (min). For the first protocol, Ficoll protocol, blood samples were diluted 1:1 ratio with Ficoll (Biochrom, cat no: L 6115) and centrifuged at 2000 rpm for twenty min. MenSCs in buffy coat layer were collected and washed with DMEM F12 (Sigma Life Science, cat no: RNBG7035), 5% fetal bovine serum (Gibco, 2440087), 1% pen-strep (Capricorn, PS-B), and centrifuged at 1000 rpm for five min. Culture medium was added to the pellet after discharge of the supernatant. The cells were then incubated at 37 °C in 5% CO₂. The second protocol was the collagenase protocol. 0.5 mg/mL type 1 collagenase (Sigma Aldrich, 9001-12-1) was added to the menstrual blood and incubated for sixty min in an incubator. MenSCs were collected after being centrifuged at 1000 rpm for five min and cultured with culture medium following the same Ficoll protocol. The medium was changed every two days, and cells were passaged at least three times with Trypsin-EDTA (Capricorn, TRY-4265) solution.

Characterization of MenSCs

MenSCs from two protocols were fixed in 4% paraformaldehyde (Merck, Cat. No: TP70404 415), and the distribution of MSC markers CD34 (Santa Cruz, Cat. No: sc-74499) and CD44 (Proteintech, Cat. No: 15675-1-AP) was analyzed using a biotin-streptavidin (Thermo Scientific, Cat. No: TP-125-HL) based on indirect immunoperoxidase staining protocol. Diaminobenzidine (Thermo, TA-125-HD) was used for chromogen and Mayer's hematoxylin (Atom Scientific Ltd, Cat. No: TTSP60) for background staining.

The osteogenic, chondrogenic, and adipogenic differentiation potential of MenSCs was also evaluated. For induction of differentiation for three lineages, 1×10⁴ cells/well were cultured for one week according to their manufacturer's protocols (Bio BASIC, cat no: C14H07SNa; Chem Cruz, cat no: sc-203749A; Carlo Erba cat no:428561, respectively). After induction, phosphate buffer solution was added for washing and fixation was performed with paraformaldehyde. Differentiation potential was analyzed using Alizarin Red S (ARS) (osteogenic), Alcian Blue (chondrogenic), and Oil Red O (ORO) (adipogenic) staining.

Statistical Analyses

There was no data for statistical analyses in this article.

RESULTS

MenSCs Derivation and Culture

Both Ficoll (Figure 1A, B) and collagenase 1 (Figure 1C, D) isolated MenSCs exhibited an epithelioid morphology after 3 days of culture time. After 1 week of culture, MenSCs derived from two protocols were also able to form colonies (Figure 1B, D). Notably, MenSCs isolated with collagenase 1 reached confluence more quickly and displayed more defined colony structures (Figure 1C, D). Additionally, no significant changes in cell proliferation were observed up to the fourth passage.

Immunocytochemical Assay

Immunocytochemical results demonstrated that MenSCs obtained from both the collagenase 1 (Figure 2) and ficoll (Figure 3) protocols were positive for CD44 (Figure 2A, Figure 3A), which is a positive marker of MSCs, and negative for CD34 (Figure 2B, Figure 3B), a negative marker for MSCs.

Differentiation Assay

After 1 week of differentiation assay, ORO staining was performed on both collagenase 1 and Ficoll-derived MenSCs. Cytoplasmic adipogenic droplets were observed (orange-red staining) in MenSCs derivatives after the collagenase 1 protocol. However, MenSCs, which were collected via Ficoll protocol, were not stained with ORO. MenSCs were not stained with ARS (osteogenic) or Alcian Blue (chondrogenic) after 1 week of culture (data not shown) (Figure 4).

DISCUSSION

In recent years, there has been a growing interest in the clinical potential of MCS due to their high proliferative potential, their remarkable versatility and the fact that they can be obtained non-invasively, unlike other sources of MCS derived from adult tissues.⁷ Menstrual blood is an

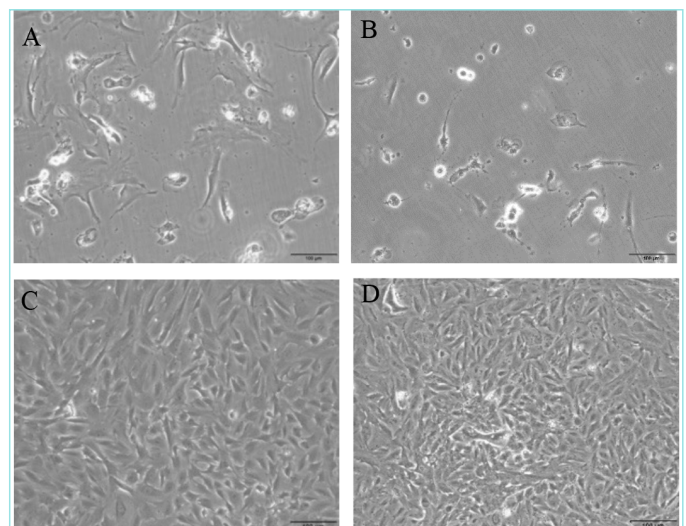


Figure 1. Menstrual blood stem cells obtained from menstrual blood by ficoll (A, B) and collagenase 1 (C, D) from day 3 (A, C) and 1 week (B, D). Scale bars:100 µm.

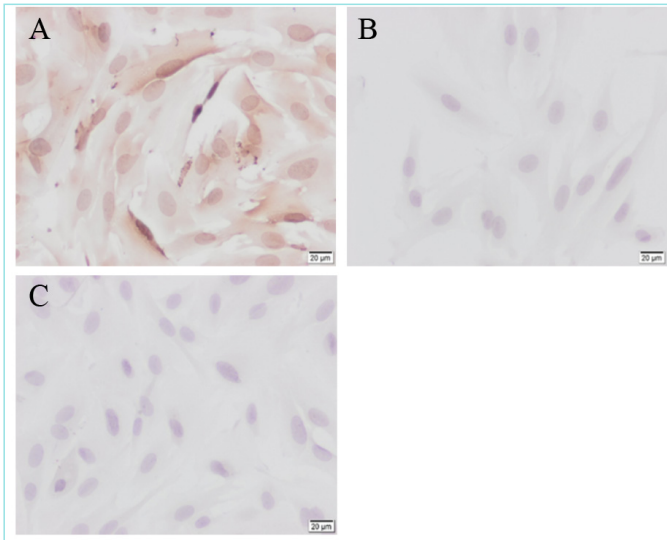


Figure 2. CD44 (A), CD34 (B), control (C) immunohistochemical staining for mesenchymal stem cell characterization obtained from menstrual blood with collagenase 1 protocol. Scale bars: 100 µm.

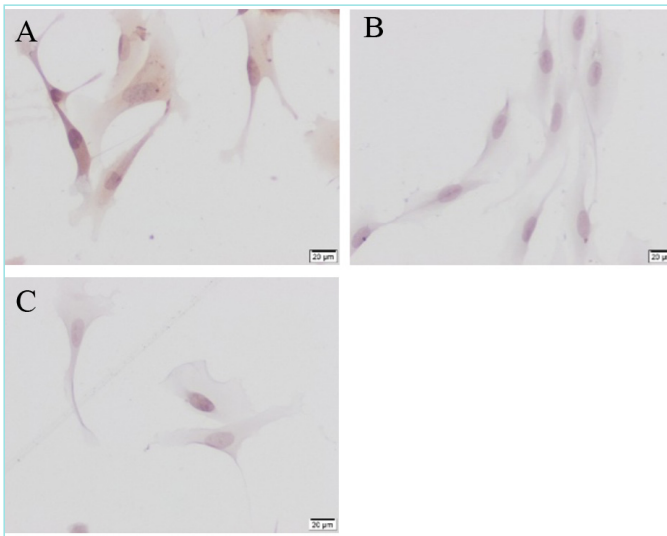


Figure 3. CD44 (A), CD34 (B), control (C) immunohistochemical staining for mesenchymal stem cell characterization obtained from menstrual blood with Ficoll protocol. Scale bars: 100 µm.

emerging and intriguing source of MenSCs for researchers, as these cells offer advantages over stem cells derived from other sources.⁹ In this study, MenSCs were derived from menstrual blood using two different protocols and exhibited adherent cells with a fibroblast-like morphology, formed circular colonies and showed multiple proliferation patterns, consistent with the findings of Meng et al.⁵ Dalirfardouei et al.¹⁰ also obtained and cultured MenSCs according to two different protocols: the culture of whole blood cells and Ficoll. In this study, the first protocol was found to be more effective in obtaining MenSCs.

Our findings regarding the characterization of MenSCs revealed that CD44, one of the MSC markers, was highly expressed and exhibits a

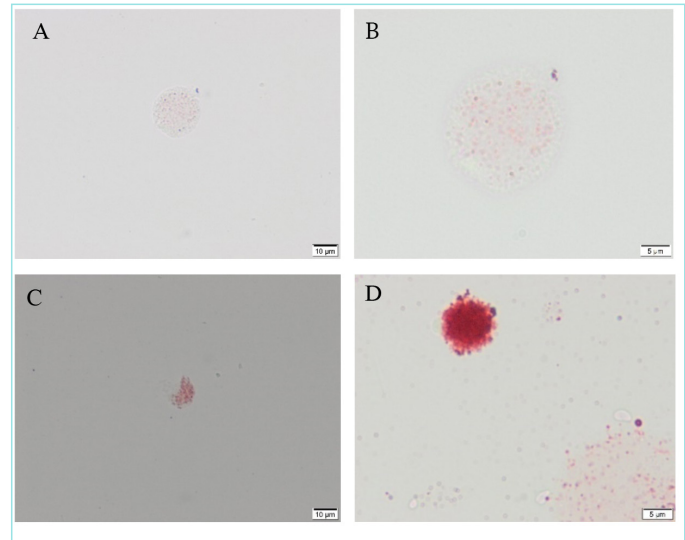


Figure 4. Oil Red staining of MenSCs obtained in the Ficoll protocol (A,B). Oil Red staining of MenSCs obtained with collagenase 1 (C,D). Scale bars: 100 µm (A,B), Scale bar: 5 µm (C).

MenSCs: Menstrual blood stem cells.

similar CD marker pattern to Sheikholeslami et al.¹¹ results. Also, ORO staining of both Ficoll and collagenase 1 derived cells showed that collagenase 1 derived cells have more differentiation ability compared to Ficoll-derived cells. In our study, MenSCs were derived from blood cells characterized by positive CD44 immunoreactivity, and ORO staining, leading us to identify these cells as mesenchymal-like stem cells.

Study Limitations

The limitation of this study is the insufficient number of stem cells obtained from patients. Additionally, the study was limited by a restricted number of available patients, which may have affected the generalizability of the findings. Furthermore, the study focused on a limited set of markers to characterize MenSCs, which may not fully encompass the complete spectrum of their characteristics. Future research with larger sample sizes and a broader array of markers would provide a more comprehensive understanding of MenSCs.

CONCLUSION

Menstrual blood provides a non-invasive and easily accessible source for deriving MSCs (MenSCs), offering significant potential for clinical applications due to their high proliferation rate and versatility. Therefore, obtaining a suitable protocol for having menstrual stem cells is important.

MAIN POINTS

- Collagenase 1 demonstrated a greater ability to obtain more stem cells than the Ficoll protocol.
- Menstrual blood stem cells (MenSCs) successfully expressed the stem cell marker, CD44.
- Differentiation potential of MenSCs derived from collagenase 1 was higher than Ficoll protocol.

ETHICS

Ethics Committee Approval: The project was supported by Manisa Celal Bayar University Health Sciences Ethics Committee (approval number: E-20478486-050.04-706680, date: 18.01.2024).

Informed Consent: All participants were given detailed information about the study and voluntary consent was obtained from the before the study started.

Footnotes

Authorship Contributions

Concept: H.S.V., H.K.E., A.A., Design: H.S.V., A.A., Data Collection and/or Processing: H.S.V., H.K.E., A.A., Y.U., Analysis and/or Interpretation: H.S.V., H.K.E., A.A., Literature Search: H.S.V., H.K.E., A.A., Writing: H.S.V., H.K.E. A.A.

Conflict of Interest: No conflict of interest was declared by the authors.

Financial Disclosure: The study was funded by Manisa Celal Bayar University Scientific Research Projects Office (project no: 2024-068).

REFERENCES

1. Uzielienė I, Urbonaitė G, Tachtamisevaite Z, Mobasher A, Bernotienė E. The potential of menstrual blood-derived mesenchymal stem cells for cartilage repair and regeneration: novel aspects. *Stem Cells Int.* 2018; 5748126.
2. Augello A, De Bari C. The regulation of differentiation in mesenchymal stem cells. *Hum Gene Ther.* 2010; 21(10): 1226-38.
3. Can A. Kök hücre biyolojisi, türleri ve tedavide kullanımları. Ankara: Akademişen Tıp Kitapevi; 2014.
4. Faramarzi H, Mehrabani D, Fard M, Akhavan M, Zare S, Bakhshalizadeh S, et al. The potential of menstrual blood-derived stem cells in differentiation to epidermal lineage: a preliminary report. *World J Plast Surg.* 2016; 5(1): 26-31.
5. Meng X, Ichim TE, Zhong J, Rogers A, Yin Z, Jackson J, et al. Endometrial regenerative cells: a novel stem cell population. *J Transl Med.* 2007; 5: 57.
6. Pushkala K, Gupta PD. Menstrual blood mesenchymal stem cells: boon in therapeutics. *J Biotechnology and Bioprocessing.* 2021; 2(4): 1-6.
7. Chen L, Qu J, Cheng T, Chen X, Xiang C. Menstrual blood-derived stem cells: toward therapeutic mechanisms, novel strategies, and future perspectives in the treatment of diseases. *Stem Cell Res Ther.* 2019; 10(1): 406.
8. Chen L, Qu J, Xiang C. The multi-functional roles of menstrual blood-derived stem cells in regenerative medicine. *Stem Cell Res Ther.* 2019; 10(1): 1.
9. Skliutė G, Baušytė R, Borutinskaitė V, Valiulienė G, Kaupinis A, Valius M, et al. Menstrual blood-derived endometrial stem cells' impact for the treatment perspective of female infertility. *Int J Mol Sci.* 2021; 22(13): 6774.
10. Dalirfardouei R, Jamialahmadi K, Mahdipour E. A feasible method for the isolation of mesenchymal stem cells from menstrual blood and their exosomes. *Tissue Cell.* 2018; 55: 53-62.
11. Sheikholeslami A, Kalhor N, Sheykhasan M, Jannatifar R, Sahraei SS. Evaluating differentiation potential of the human menstrual blood-derived stem cells from infertile women into oocyte-like cells. *Reprod Biol.* 2021; 21(1): 100477.

Synthesis of Chitosan Functionalized Zinc Oxide Nanocomposite using *Moringa Stenopetala* Extract and Assessment of its Antibacterial and Cytotoxic Potentials

© Huzaifa Umar¹, © Maryam Rabi Aliyu², © Natacha Usanase^{1,3}, © Basil Bartholomew Duwa¹, © Dilber Uzun Ozsahin^{1,4,5}

¹Operational Research Centre in Healthcare, Near East University, Nicosia, North Cyprus

²Department of Energy System Engineering, Cyprus International University Faculty of Engineering, Nicosia, North Cyprus

³Department of Biomedical Engineering, Near East University Faculty of Engineering, Nicosia, North Cyprus

⁴Department of Medical Diagnostic Imaging, University of Sharjah College of Health Sciences, Sharjah, United Arab Emirates

⁵Research Institute for Medical and Health Sciences, University of Sharjah, Sharjah, United Arab Emirates

Abstract

BACKGROUND/AIMS: Nanomaterials, especially nanocomposites, have garnered much attention due to their potential uses in antibacterial and cancer therapies. This research used *Moringa stenopetala* extract as a chelating agent to create a chitosan-functionalized zinc oxide nanocomposite (CZNM), and its cytotoxic and antibacterial properties were carefully assessed.

MATERIALS AND METHODS: The effective production of the nanocomposites was confirmed by their characterisation using fourier-transform infrared spectroscopy, energy-dispersive X-ray spectroscopy, X-ray diffraction, scanning electron microscopy, and UV-vis spectroscopy.

RESULTS: With an average size of 19 nm, the CZNMs had a spherical shape, and their stability was verified by zeta potential and UV-Vis studies. The produced CZNMs showed strong antibacterial action against *Escherichia coli* and *Salmonella typhi*. MDA-MB 231, and MCF-7, breast cancer cell lines were used in cytotoxicity tests, and the results showed concentration-dependent actions with IC50 values that were 63.4 µg/mL and 78.5 µg/mL, respectively.

CONCLUSION: Overall, CZNMs made from *Moringa stenopetala* extract have encouraging cytotoxic and antimicrobial properties, making them promising candidates for antimicrobial and cancer treatment.

Keywords: UV-vis spectroscopy, scanning electron microscopy, spherical morphology, *Salmonella typhi*, *Escherichia coli*

INTRODUCTION

Nanotechnology has emerged as a broad and advanced field focusing on developing eco-friendly methods to synthesize biosynthetic nanoparticles, such as zinc oxide (ZnO), silver, gold, and sodium nanoparticles. The distinct physicochemical features of these nanoparticles make them non-toxic, chemically stable, biocompatible,

and useful as therapeutics for cancer,¹ as diabetes drugs,² as antibacterial agents,³ in cell imaging devices,⁴ as biological sensors,⁵ as carriers for drugs,⁶ and in aesthetics.⁷ Before the development of green synthesis techniques, metal oxide nanoparticles were usually made by chemical processes involving dangerous chemicals, which made the synthesis time-consuming, expensive, and toxic.⁸ At the same time, to change and improve the materials' electrical work, optics, and mechanical

To cite this article: Umar H, Aliyu MR, Usanase N, Duwa BB, Uzun Ozsahin D. Synthesis of chitosan functionalized zinc oxide nanocomposite using *Moringa stenopetala* extract and assessment of its antibacterial and cytotoxic potentials. Cyprus J Med Sci. 2025;10(Suppl 1):96-100

ORCID IDs of the authors: H.U. 0000-0003-2508-9710; M.R.A. 009-005-7359-6620; N.U. 0000-0002-0901-4439; B.B.D. 0000-0002-1690-6830; D.U.O. 0000-0002-3873-1410.



Corresponding author: Huzaifa Umar
E-mail: huzaifee27@gmail.com
ORCID ID: orcid.org/0000-0003-2508-9710

Received: 02.11.2024
Accepted: 17.02.2025
Publication Date: 04.06.2025



Copyright © 2025 The Author. Published by Galenos Publishing House on behalf of Cyprus Turkish Medical Association.
This is an open access article under the Creative Commons AttributionNonCommercial 4.0 International (CC BY-NC 4.0) License.

characteristics, as well as their external chemical makeup, some nanoparticles, like metal oxide, are modified by completely replacing some metal ions with designated atoms.⁹

Therefore, this research study aims to provide an eco-friendly pathway that fits in the production of modified nanocomposites ZnO [chitosan-functionalized zinc oxide nanocomposites (CZNMs)], which involves the application of chitosans and of *Moringa stenopetala* extract, primarily as reducing and stabilising agents and zinc nitrate solution as a precursor, respectively. This approach has several advantages: simplicity, environmental coherence, affordability, high-purity precursors, and few by-products.¹⁰ Furthermore, the synthesis of CZNMs does not include any toxic substances and occurs at an acceptable temperature.¹¹ This study fills a gap in the literature by synthesising a new, environmentally friendly, and sustainable CZNM for the multipurpose use in antibacterial therapies and cancer treatment using extract from *Moringa stenopetala*, an organic and naturally occurring resource. The individual uses of ZnO nanoparticles (ZnO NPs) and *Moringa* extract have been the subject of many investigations, but little work has integrated them to create an nanocomposite system that offers a thorough evaluation of both antimicrobial and cytotoxic properties.

MATERIALS AND METHODS

Synthesis of Chitosan-functionalized Zinc Oxide Nanocomposites

CZNMs using chitosan and *Moringa stenopetala* were attained using the method developed by Kavaz et al.¹² CZNMs were synthesized using 0.1 M zinc nitrate hexahydrate [$\text{Zn}(\text{NO}_3)_2 \cdot 6\text{H}_2\text{O}$] procured from Gibco by Life Technologies, United States of America. The synthesis was performed in a conical flask at a controlled temperature of 45 °C for 72 hours, with water serving as the solvent for the extraction process. Chitosan and *Moringa stenopetala* aqueous extract was introduced by drops to the zinc nitrate solution (1:1:9) while stirring continuously at 60 °C for 5 hours to enhance complex formation. Furthermore, the blend was vigorously calcined in a muffle furnace, as shown in Figure 1. The resulting residue comprised the synthesized CZNMs.

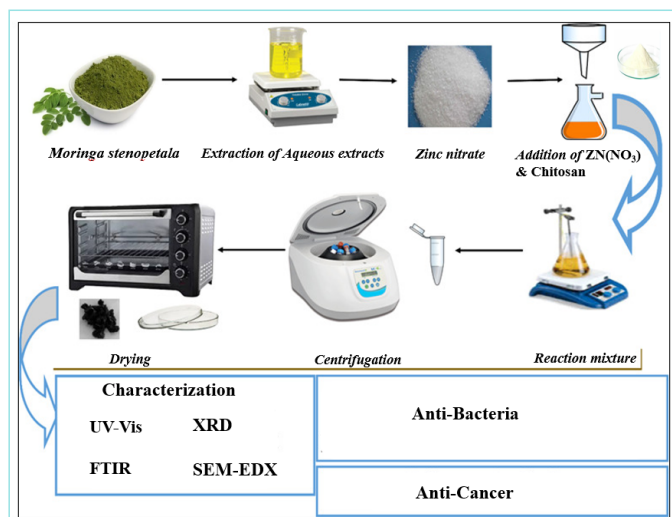


Figure 1. The representation of combined zinc oxide nanocomposites.

XRD: X-ray diffraction, FTIR: Fourier transform infrared, SEM: Scanning electron microscopy.

Characterization

Several analytical methods were used to characterize CZNMs. A Shimadzu UV-2450 UV-Vis spectrophotometer was used to capture the spectrum of UV-Vis absorption after the CZNMs were filtered via a 0.45 µm membrane, sonicated to achieve a constant dispersion, and then dissolved in deionized water. A 10 mm optical pathlength container was used to obtain ambient temperature spectra in the 300-800 nm wavelength range. Fourier transform infrared (FTIR) spectroscopy, used to find the functional categories in the CZNMs, was used, which has a frequency range of 500 to 4,000 cm^{-1} and a resolution of 4 cm^{-1} . The shape and structure of the nanocomposites were examined using scanning electron microscopy (SEM), and their crystallization was assessed with X-ray diffraction (XRD) employing a Rigaku ZSX Primus II.

Antimicrobial Activity

The antibacterial activity of synthesized CZNMs on *Salmonella typhi* (B-4420) and *Escherichia coli* (ATCC 8739) was assessed on Müller hinton's culture trays.¹³ The sterilized empty disc was filled with an established amount of CZNMs, with ciprofloxacin (10 µg/disc) as a reference. Antibacterial efficacy was assessed with 30% DMSO.

Trypan Blue Assay

The CZNMs' toxicity has been determined on MDA-MB 231 and MCF-7 cell lines using a slightly modified method of Umar.¹⁴ The cells were cultured in Dulbecco's modified Eagle's medium supplemented with 5% fetal bovine serum and L-glutamate (2%), and then grown to confluence in an incubator at 37 °C, 5% CO_2 . The cells were subjected to nanoparticle concentrations (500, 250, 50, 10, 5, and 0 µg/mL) and then cultivated for 24 and 48 hours at 37 °C. After incubation, the treatment was removed, and the number of living and dead cells was counted independently. In the results section, the mean ± standard deviation was displayed.

Proliferation Assay

The 3-(4,5-dimethylthiazol-2-yl)-2,5-diphenyltetrazolium bromide (MTT) assay was used to measure cell growth, following the methodology developed by Umar and Aliyu.¹⁵ MDA-MB 231 cells ($3 \times 10,000$) were incubated for 24 hours after exposure to CZNM doses of 0, 5, and 10 µg/mL. After incubation, the wells were filled with 600 µL of new growth media containing 150 µL of MTT solution (5 mg/mL) (Sigma-Aldrich Inc.). Using an ELX 800TM Absorption Microplate Reader, the absorption was measured at 570 nm. The experiment was carried out in triplicate to guarantee dependability, with each treatment repeated thrice.

Ethical Concern

The study involves using cell lines, not human subjects, and does not require ethical approval or informed consent.

Statistical Analysis

Data are shown as means ± SEM. The statistical analysis was performed using IBM SPSS Statistics version 21. The data were analysed using one-way ANOVA and the Student's t-test. All studies were done in triplicate ($n \geq 3$), and statistical significance was regarded as a p-value <0.05.

RESULTS

The biosynthesis of CZNMs using *Moringa stenopetala* and chitosan as reducing and stabilizing agents was confirmed by a visible color change and various characterization techniques. The UV-visible

spectrophotometer analysis showed a strong absorption peak at 380 nm (Figure 2a), indicating the formation of ZnO nanoparticles. The zeta sizer analysis determined the average particle size to be approximately 19 nm and confirmed the colloidal stability through zeta potential measurements.

FTIR spectroscopy revealed characteristic bands at 1446 cm⁻¹ and 1033 cm⁻¹ corresponding to C=C methyl groups and ZnO bonds, respectively (Figure 2b). The presence of alcohol groups suggests their role in stabilizing the nanoparticles. XRD analysis showed distinct diffraction peaks at 31.70°, 34.34°, 47.54°, 56.48°, 62.78°, 67.66°, 72.53°, and 76.58° (Figure 2c), consistent with the hexagonal wurtzite crystalline structure of ZnO nanoparticles. SEM imaging confirmed the spherical shape of the nanoparticles, with an average size of 19 nm (Figure 2d).

The antibacterial potential of the synthesized NPs was tested on *S. typhi* and *E. coli*, adopting the disc diffusion technique (Table 1). CZNMs had higher antibacterial activities than chitosan on both bacteria, with a significant difference compared to standard (p<0.05; n≥3; Table 1).

The cytotoxic effect of CZNMs was evaluated on MDA-MB 231 and MCF-7 breast cancer cell lines using MTT and trypan blue assays. A concentration-dependent decrease in cell viability was observed, with the highest cytotoxic effect at 500 µg/mL after 24 hours of incubation (Figure 3a, b). No significant cytotoxicity was observed at lower concentrations (5 and 10 µg/mL), which were further tested for anti-

proliferative potential (Figure 3c).

DISCUSSION

The biosynthesis of CZNMs using green methods was supported by the colour change and characteristic UV-Vis absorption peak at 380 nm, aligning with earlier findings by Kavaz et al.¹⁶ The FTIR analysis confirmed the presence of functional groups from plant extract and chitosan that contribute to capping and stabilizing the nanoparticles, helping to prevent agglomeration.¹⁷ Furthermore, the crystalline nature confirmed via XRD patterns is typical of ZnO nanoparticles and consistent with previous literature.¹⁸ The SEM results further verified the uniform spherical morphology. Prior studies have emphasized that nanoparticle size and shape influence their interaction with cells and biological targets.¹⁹ The nanoparticle size (19 nm) and high zeta potential support the synthesis of stable and monodispersed nanostructures. Smaller particle sizes often exhibit superior surface activity, improving biological interactions and stability.²⁰

The significant antibacterial activity of CZNMs against *E. coli* and *S. typhi* demonstrates their potential as antimicrobial agents. Their enhanced efficacy over chitosan or zinc nitrate alone suggests synergistic effects when both components are combined. This is especially relevant for combating resistant bacterial strains.

In the cytotoxicity assays, the concentration-dependent effects are

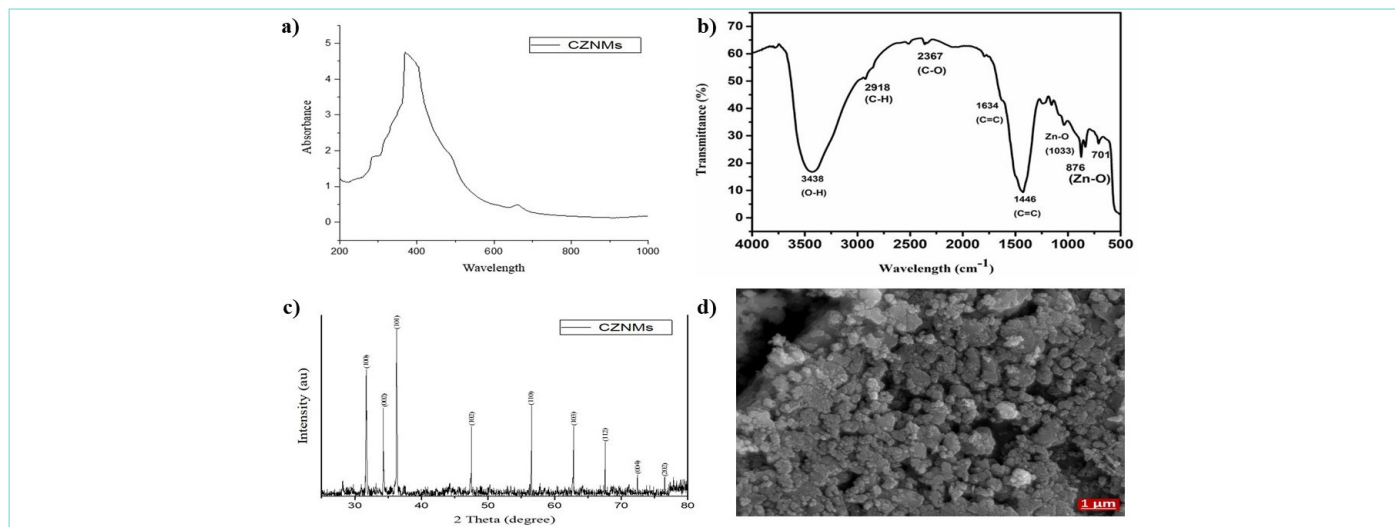


Figure 2. a) Absorption spectra of the CZNMs by UV-visible Spectrophotometer. b) FTIR of the CZNMs. c) XRD pattern of CZNMs. d) SEM image of CZNMs (scale bar 1µm).

CZNMs: Chitosan-functionalized zinc oxide nanocomposites, XRD: X-ray diffraction, FTIR: Fourier transform infrared, SEM: Scanning electron microscopy.

Table 1. Anti-microbial activity of chitosan-functionalized zinc oxide nanocomposites (CZNMs)

Zone of Inhibition (mm)		
Bacterial strains	<i>Escherichia coli</i> (mean ± SEM)	<i>Salmonella typhi</i> (mean ± SEM)
Standard ciprofloxacin (10 µg/disc)	14.0±0.20	12.53±0.50
CZNMs	11.6±0.47**	10.80±0.20**
Chitosan	5.8±0.15**	6.20±0.10**
Zinc nitrate solution (0.1M)	1.20±0.10**	1.22±0.20**
DMSO (30%)	-	-

CZNMs: Chitosan-functionalized zinc oxide nanocomposites, DMSO: Dimethyl sulfoxide, SEM: Scanning electron microscopy, ** p<0.01 vs. control (standard group).

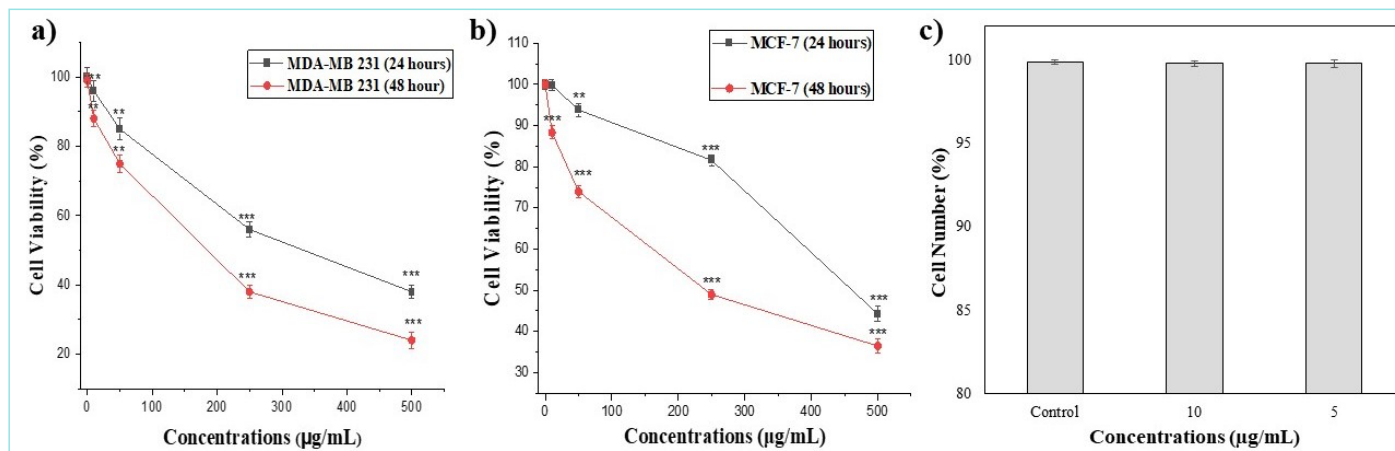


Figure 3. Effect of CZNMs on the viability of a) MDA-MB 231, and b) MCF-7 cells. c) Effect of CZNMs on the viability of a) MDA-MB 231 cells. CZNMs: Chitosan-functionalized zinc oxide nanocomposites.

consistent with existing literature on green-synthesized ZnO NPs.²¹ The more pronounced cytotoxicity observed in MDA-MB 231 cells compared to MCF-7 suggests possible differential sensitivity between triple-negative and hormone receptor-positive breast cancer cells. Furthermore, lower concentrations did not significantly affect viability, indicating that the CZNMs might be safe at low doses—an essential consideration for therapeutic applications. Our findings are in agreement with prior studies, such as those by Taher et al.²² who showed that chitosan-based nanoparticles have dose-dependent anti-proliferative effects. Similarly, thymoquinone-loaded nanoparticles also demonstrated comparable apoptotic activity, reinforcing the potential of natural product-based nanocarriers in cancer therapy.²³

Study Limitations

The absence of other analyses, such as lateral mobility, migration, and invasion assays, is a study limitation. These tests are required to verify that concentrations determined to be non-toxic to cells have no discernible effects on cellular behaviours, including proliferation.

CONCLUSION

In conclusion, there is considerable antibacterial and cytotoxic potential in the manufacture of CZNMs utilizing extract from *Moringa stenopetala*. In addition to their dose- and time-dependent cytotoxic effects on MDA-MB 231 and MCF-7 breast cancer cells, the nanocomposites demonstrated potent antibacterial activity against *S. typhi* and *E. coli*. These results imply that the CZNMs have potential as therapeutic candidates, especially in cancer treatment, due to their efficacy and biocompatibility. More research into their mode of action and *in vivo* efficacy is necessary to explore their clinical potential.

MAIN POINTS

- The chitosan-functionalized zinc oxide nanocomposites (CZNMs) were successfully synthesized using *Moringa stenopetala* extract, and characterized using various spectroscopic and microscopic techniques in which spherical morphology and an average size of 19 nm was observed.

- The synthesized CZNMs revealed potent antibacterial effects against *Escherichia coli* and *Salmonella typhi*. Compared to chitosan and zinc nitrate solution alone, suggesting their effectiveness as an antibacterial agent.
- Dose-dependent cytotoxicity on MCF-7 and MDA-MB 231 breast cancer cell lines was observed when treated with CZNMs.

ETHICS

Ethics Committee Approval: Not available.

Informed Consent: Not available.

Footnotes

Authorship Contributions

Concept: H.U., N.U., B.B.D., D.U.O., M.R.A., Design: H.U., N.U., D.U.O., M.R.A., Data Collection and/or Processing: H.U., B.B.D., D.U.O., M.R.A., Analysis and/or Interpretation: H.U., N.U., D.U.O., Literature Search: H.U., B.B.D., D.U.O., M.R.A., Writing: H.U., N.U., B.B.D., D.U.O., M.R.A.,

DISCLOSURES

Conflict of Interest: No conflict of interest was declared by the authors.

Financial Disclosure: The authors declared that this study had received no financial support.

REFERENCES

- Nirmala M, Anukaliani A. Synthesis and characterization of undoped and TM (Co, Mn) doped ZnO nanoparticles. Mater Lett. 2011; 65(17): 2645-8.
- Hassan HF, Mansour AM, Abo-Youssef AM, Elsadek BE, Messiha BA. Zinc oxide nanoparticles as a novel anticancer approach; in vitro and in vivo evidence. Clin Exp Pharmacol Physiol. 2017; 44(2): 235-43.
- Xu D, Liu M, Zou H, Tian J, Huang H, Wan Q, et al. A new strategy for fabrication of water dispersible and biodegradable fluorescent organic nanoparticles with AIE and ESIPT characteristics and their utilization for bioimaging. Talanta. 2017; 17: 803-8.

4. Rosi NL, Mirkin CA. Nanostructures in biodiagnostics. *Chem Rev.* 2005; 105(4): 1547-62.
5. El-Gharbawy RM, Emara AM, Abu-Risha SE. Zinc oxide nanoparticles and a standard antidiabetic drug restore the function and structure of beta cells in Type-2 diabetes. *Biomed Pharmacother.* 2016; 84: 810-20.
6. Albrecht MA, Evans CW, Raston CL. Green chemistry and the health implications of nanoparticles. *Green Chem.* 2006; 8(5): 417-32.
7. Emakpor OL, Edo GI, Yousif E, Samuel PO, Jikah AN, Zainulabdeen K, et al. The interplay of nutrition, exercise, and dietary intervention for enhanced performance of athletes and general well-being of non-athletes: a review. *OBM Integr Complement Med.* 2024; 9(2): 1-41.
8. Li H, Carter JD, Labean TH. Nanofabrication by DNA self-assembly. *Mater Today.* 2009; 12(5): 24-32.
9. Altıntaş YO, Unalan HE, Durucan C. Highly efficient room temperature synthesis of silver-doped zinc oxide (ZnO:Ag) nanoparticles: structural, optical, and photocatalytic properties. *J Am Ceram Soc.* 2013; 9(3): 766-73.
10. Govindaraju K, Khaleel Basha S, Ganesh Kumar V, Singaravelu GJ. Silver, gold and bimetallic nanoparticles production using single-cell protein (*Spirulina platensis*) Geitler. *Mater Sci.* 2008; 43: 5115-22.
11. Umar H, Aliyu MR, Ozsahin DU. Iron oxide nanoparticles synthesized using *Mentha spicata* extract and evaluation of its antibacterial, cytotoxicity and antimigratory potential on highly metastatic human breast cells. *Biomed Phys Eng Express.* 2024; 10(3): 035019.
12. Kavaz D, Umar H, Zimuto T. Biosynthesis of gold nanoparticles using *Scytosiphon luminaria* (Brown algae) and *Spyridia filamentosa* (Red algae) from Kyrenia region and evaluation of their antimicrobial and antioxidant activity. *Hacetatepe J Biol Chem.* 2019; 47(4): 367-82.
13. Mustapha A, Abushoufa FS, Alsharksi AN, Adakole NC, Umar H, Ghali UM. Invitro evaluation of antibacterial activity and in-silico insights of canarium schwenfurthii against multi-drug resistant klebsiella pneumoniae. *Afr J Bio Sci.* 2024; 6(5): 9534-48.
14. Umar H. Morphological changes caused by synthesized zinc oxide nanoparticles in MDA-MB 231 cells and prediction with multi-linear regression. *Trop J Nat Prod Res.* 2023; 7(12).
15. Umar H, Aliyu MR. Moringa oleifera-mediated iron oxide nanoparticles, characterization and their anti-proliferative potential on MDA-MB 231 human breast cancer cells. *Pak J Pharm Sci.* 2023; 36: 1875-83.
16. Kavaz D, Umar H, Aliyu MR. Green synthesized metallic oxide nanomaterials for diverse applications. *J Nanoworld.* 2022; 8(1): 14-22.
17. Umar H, Kavaz D, Abubakar AL, Aliyu MR, Rizaner N. Synthesis of zinc oxide nanoparticles using *Ficus thonningii* aqueous extract and evaluation of its antioxidant and antimicrobial activities. *Bulgar Chem Commun.* 2022; 277: 1.
18. Edo GI, Ndudi W, Makia RS, Ainyanbhor IE, Yousif E, Gaaz TS, et al. Beta-glucan: An overview in biological activities, derivatives, properties, modifications, and current advancements in food, health, and industrial applications. *Process Biochem.* 2024; 147: 347-70.
19. Nagarajan S, Kuppusamy KA. Extracellular synthesis of zinc oxide nanoparticles using seaweeds of Gulf of Mannar, India. *J Nanobiotechnol.* 2013; 11: 39.
20. Umar H, Kavaz D, Rizaner N. Biosynthesis of zinc oxide nanoparticles using *Albizia lebbek* stem bark, and evaluation of its antimicrobial, antioxidant, and cytotoxic activities on human breast cancer cell lines. *International journal of nanomedicine,* 2019: 87-100.
21. Khan I, Saeed K, Khan I. Nanoparticles: Properties, applications, and toxicities. *Arab J Chem.* 2019; 12(7): 908-31.
22. Taher FA, Ibrahim SA, El-Aziz AA, Abou El-Nour MF, El-Sheikh MA, El-Husseiny N, et al. Anti-proliferative effect of chitosan nanoparticles (extracted from crayfish *Procambarus clarkii*, Crustacea: Cambaridae) against MDA-MB-231 and SK-BR-3 human breast cancer cell lines. *Int J Biol Macromol.* 2019; 126: 478-87.
23. Yıldırım M, Acet Ö, Acet BÖ, Karakoç V, Odabaşı M. Innovative approach against cancer: Thymoquinone-loaded PHEMA-based magnetic nanoparticles and their effects on MCF-7 breast cancer. *Biochem Biophys Res Commun.* 2024; 734: 150464.

Investigation of Single Nucleotide Polymorphisms within the *FSHR* Gene and Biological Network Analysis of Non-Coding RNAs in Polycystic Ovary Syndrome Patients

© Sana Madhher¹, © Bita Ostad-Hasanzadeh¹, © Burcu Özbakır^{2,3}, © Ali Cenk Özay^{2,3}, © Pinar Tulay^{3,4}

¹Department of Medical Genetics, Near East University Faculty of Medicine, Nicosia, North Cyprus

²Department of Obstetrics and Gynecology, Near East University Faculty of Medicine, Nicosia, North Cyprus

³Near East University, DESAM Research Institute, Nicosia, North Cyprus

⁴Near East University, Center of Excellence, Genetics and Cancer Diagnosis, Nicosia, North Cyprus

Abstract

BACKGROUND/AIMS: Polycystic ovary syndrome (PCOS) is associated with numerous health issues. The study aims to examine the allelic frequencies of the *follicle stimulation hormone receptor (FSHR)* gene, specifically for the oogenesis-regulating variants p.Ser680Asn (c.2039C>T; rs6166) and p.Ala307Thr (c.919G>A; rs6165). Further in biological network analysis, the aim is to investigate the relationship of the *FSHR* gene with non-coding RNAs, symptoms of PCOS, and drugs used for PCOS treatment.

MATERIALS AND METHODS: One hundred and twenty whole blood samples were collected from non-PCOS and PCOS females. Real-time polymerase chain reaction was applied in the assessment of single nucleotide polymorphisms (SNPs) in the *FSHR* gene. The relationship of this gene with miRNAs and lncRNAs and the association of *FSHR* with drugs, symptoms of PCOS, and other associated diseases were investigated.

RESULTS: The outcome of this project did not show significance in the investigated *FSHR* polymorphisms between PCOS patients and the control group. Biological network analysis showed that this gene was associated with a number of miRNAs and lncRNAs. Furthermore, this gene was associated with a number of PCOS symptoms besides other women's health anomalies.

CONCLUSION: The SNPs of the *FSHR*, p.Ser680Asn (c.2039C>T; rs6166) and p.Ala307Thr (c.919G>A; rs6165), did not seem to have an association with the pathophysiology of PCOS. Therefore, it remains a possibility that *FSHR* polymorphisms involved in symptoms or progression of PCOS. However, these SNPs have been associated with many symptoms. Thus, further analysis must be performed to investigate these in larger populations.

Keywords: Polycystic ovary syndrome, polymorphism, SNP

INTRODUCTION

Polycystic ovary syndrome (PCOS) is a multifactorial and complex disorder where patients may have metabolic abnormalities and obesity.^{1,2} PCOS is a multifaceted condition influenced by a

combination of genetic³ and environmental factors.^{4,5} Single nucleotide polymorphisms (SNPs) may affect hormonal regulation, influencing normal oocyte development, in which hormonal imbalances can lead to the development of PCOS.⁶ Around 80% of females with PCOS produce high levels of androgens.⁷ PCOS has been linked to ovarian

To cite this article: Madhher S, Ostad-Hasanzadeh B, Özbakır B, Özay AC, Tulay P. Investigation of single nucleotide polymorphisms within the *FSHR* gene and biological network analysis of non-coding RNAs in polycystic ovary syndrome patients. *Cyprus J Med Sci*. 2025;10(Suppl 1):101-105

ORCID IDs of the authors: S.M. 0000-0001-8548-4208; B.O.-H. 0009-0000-9496-6276; B.Ö. 0000-0002-0895-0487; A.C.Ö. 0000-0002-6082-7101; P.T. 0000-0002-6793-7805.



Corresponding author: Pinar Tulay
E-mail: pinar.tulay@neu.edu.tr
ORCID ID: orcid.org/0000-0002-6793-7805

Received: 01.11.2024
Accepted: 16.03.2025
Publication Date: 04.06.2025



Copyright © 2025 The Author. Published by Galenos Publishing House on behalf of Cyprus Turkish Medical Association.
This is an open access article under the Creative Commons Attribution-NonCommercial 4.0 International (CC BY-NC 4.0) License.

hormone abnormalities resulting in anovulation, hyperinsulinemia, and hyperandrogenemia. Additionally, studies prove that females with PCOS are at an increased risk of endometrial cancer.⁸

Since studies have shown a possible genetic and epigenetic regulation in PCOS development, investigation of molecular mechanisms regulating PCOS has become a hot topic. follicle stimulation hormone (FSH) mediates its function through the follicle stimulation hormone receptor (FSHR),⁹ and it is responsible for development of follicles, regulation of steroid synthesis and maturation of oocytes.¹⁰ Previously published studies genotyped the FSHR Ala307Thr and FSHR Ser680Asn and analysed the association with PCOS, showing a statistically significant correlation between FSHR Ala307Thr and FSHR Ser680Asn polymorphisms and PCOS patients.¹¹ Another study in China revealed a clear correlation between Ser680Asn and PCOS;¹² Ala307Thr is statistically correlated with PCOS in Italian patients.¹³ On the contrary, no such association was reported for Ala307Thr and Ser680Asn between PCOS patients and controls in the Turkish population.¹⁴ Similarly, no association between Ser680Asn polymorphism and PCOS patients was reported in the Han ethnic population in China,¹⁵ and in the Netherlands.¹⁶

Since the evaluation of SNPs has proven important in identifying regulatory functions in disease development, such as PCOS, especially in genes like FSHR where discrepancies have been reported, this practice is crucial. This study aimed to examine the allelic frequencies of the *FSHR* gene, specifically for the oogenesis-regulating variants p.Ser680Asn (c.2039C>T; rs6166) and p.Ala307Thr (c.919G>A; rs6165). Further biological network analysis was aimed at investigating the relationship of the *FSHR* gene with non-coding RNAs, the symptoms of PCOS, and drugs used for PCOS treatment.

MATERIALS AND METHODS

Sample Collection and Genotype Analysis

In this project, samples from patients undergoing gynaecological assessment were taken at the Near East University Hospital Scientific Research Ethics Committee (approval number: YDU/2019/67-784, date: 28.03.2019) granted the ethical approval, and each patient signed the informed consent. The inclusion criteria for both groups included subjects ages 18-35 years with a normal body mass index (BMI). The control group included patients undergoing routine check-up in the gynaecology clinic who have a normal menstrual cycles with normal ovarian morphology. Patients with PCOS were diagnosed according to the Rotterdam criteria by an expert gynecologist. The exclusion criteria included patients with secondary causes of PCOS, such as those diagnosed due to hormonal therapy. Additionally, subjects with syndromes such as Down syndrome were excluded from the study. One hundred and twenty subjects were divided into two groups consisting of 65 PCOS patients and 55 subjects with no PCOS diagnosis. All the subjects are of Turkish origin.

DNA extraction was performed using a commercial kit (Pure Link Genomic DNA Mini Kit, Thermo Fisher Scientific) following the manufacturer's instructions. The NanoDrop ND-200 (Thermo Scientific, Pittsburgh, United States of America) was utilized to determine the quantity and quality of the DNA obtained. The real-time polymerase chain reaction (PCR) followed by high resolution melting (HRM) analyses were applied to examine the *FSHR*, p.Ser680Asn (c.2039C>T; rs6166) and p.Ala307Thr (c.919G>A; rs6165), following manufacturer's protocol (LightCycler SYBR Green 480) with a final primer concentration of 2.5

µM. The primer sequences were obtained from a previously published study.¹⁷ The results were analyzed using dedicated software.

Statistical Analysis

Version 25 of the SPSS statistical program was used to analyze the data. Fisher's exact test was used to analyze the heterozygosity of the SNPs within the *FSHR* gene in both PCOS and control groups. Statistical significance was determined as a *p* value < 0.05, and the HWE test was conducted for the PCOS group of FSHR p.Ala307Thr (c.919G>A; rs6165).

Biological Network Analysis

The relationship of *FSHR* gene variations with the PCOS symptoms and related women's health issues was studied.¹⁸ The relationship between the *FSHR* gene, along with the other genes within the GnRH signalling pathway, was examined to analyse the drug association using the DGIdb site.¹⁹ Finally, the relationship between the *FSHR* gene and microRNAs and lncRNAs was investigated.^{20,21}

RESULTS

The primary goal of the project was to examine the two SNPs of *FSHR* implicated in PCOS. The whole blood samples used for this project consisted of 65 PCOS patients and 55 females without PCOS. In both groups, the mean age was 20 years, and the BMI was 17.

The SNP analysis of the *FSHR* gene, p.Ser680Asn (c.2039C>T; rs6166) and p.Ala307Thr (c.919G>A; rs6165), was performed using real-time PCR and HRM, in which the generated amplicon was progressively melted. In the PCOS group, the heterozygosity of *FSHR* Ala307Thr was 96.6%, while in the control group, it was 100% (Figure 1). Consequently, no statistically significant difference was found between the two groups (*p*=0.498). Due to the absence of PCR amplification, six samples from the PCOS category and four samples from the control category were ruled out from the project. For *FSHR* Ser680Asn, both the PCOS and control groups exhibited 100% heterozygosity. Due to the absence of PCR amplification, six samples from the PCOS group and one sample from the control group were ruled out from the project. The chi-square test for HWE in the PCOS group of FSHR p.Ala307Thr (c.919G>A; rs6165) was 51,271, and none (0.0%) have expected frequencies less than 5. The minimum expected frequency is 14.8.

In the second part of this study, a number of biological network analyses were performed. The association of *FSHR* gene, along with the FSHB, CGA, and GNAS, which also function in the GnRH signalling pathway, was shown to interact with a number of drugs, such as cisplatin, mifepristone, and urofollitropin (Figure 2). The SNPs investigated were associated with a number of PCOS symptoms as well as related women's health issues (Figure 3). Additionally, *FSHR* was shown to interact with a number of miRNAs and lncRNAs (Figure 4).

DISCUSSION

PCOS is a common and complex endocrine disorder where the pathophysiology is believed to be significantly influenced by both genetic and environmental factors.²² In this investigation, real-time PCR and HRM analysis were used to investigate the association of *FSHR* Ala307Thr and *FSHR* Ser680Asn with PCOS. The study's findings did not show any significance in heterozygosity status for two FSHR polymorphisms investigated in the PCOS and control groups. Thus, this study suggests that the p.Ala307Thr and p.Ser680Asn *FSHR* gene

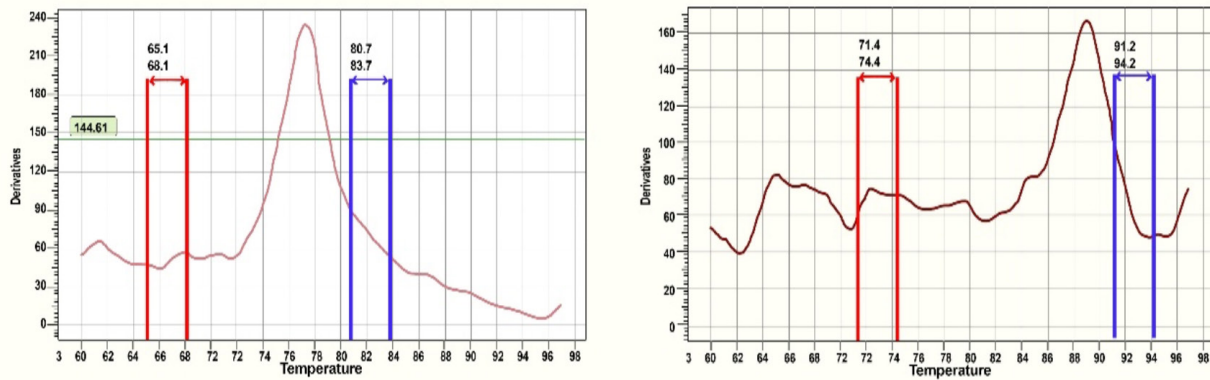


Figure 1. (a) HRM image showing the amplification of mutant type allele p.Ala 307Thr(c.919 G<A; rs6165). (b) HRM image showing the amplification of wild type allele p.Ala307Thr.

HRM: High resolution melting.

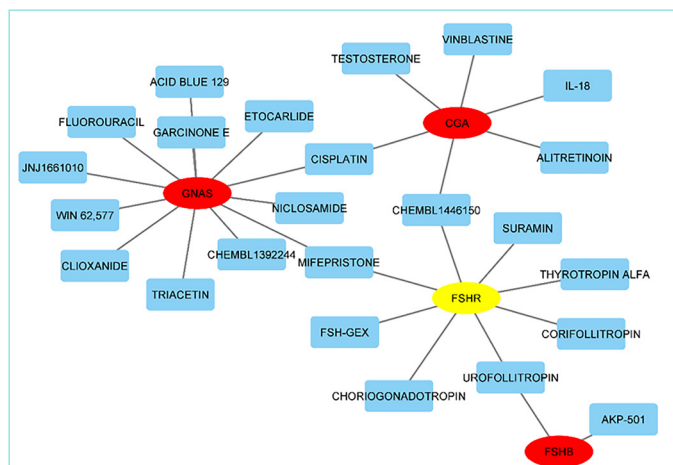


Figure 2. The association of drugs on selected genes.

FSHR: Follicle stimulation hormone receptor.

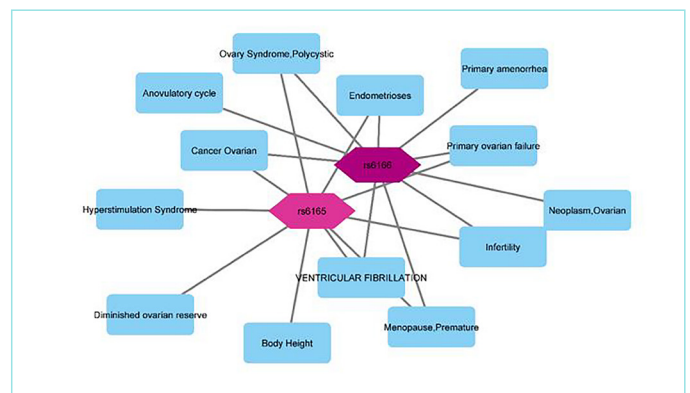


Figure 3. The association of FSHR SNPs with PCOS symptoms and related women's health abnormalities.

FSHR: Follicle stimulation hormone receptor, SNPs: Single nucleotide polymorphisms, PCOS: Polycystic ovary syndrome.

polymorphisms may not have a significant impact on PCOS in the studied group. In accordance with our findings, several studies also showed that there was no significant association between PCOS and FSHR Ala307Thr and FSHR Ser680Asn.¹⁴⁻¹⁶ In conflict with our results, a number of studies indicated a statistically significant link between FSHR Ala307Thr¹³ and FSHR Ser680Asn²¹ polymorphisms in females diagnosed with PCOS,^{14,15} in different populations. These contrasts among different studies may be due to variations in ethnicity or the sample size.

Biological network analysis was shown to be a valuable tool in health sciences to understand the possible interactions of gene variations, diseases, and their symptoms. An association between drug response or resistance and several genes has been reported, including FSHR. In the Caucasian populations, a number of genes including FSHR were reported as potential candidates to predict drug response and resistance for PCOS treatment. It was reported that PCOS patients with G/G *FSHR* polymorphism (rs6166) has lower chance in restoring ovulation under clomiphene citrate treatment.²³ The results of this study showed that *FSHR* SNPs are particularly associated with a

number of PCOS symptoms. A previously published study reported that there is no association between *FSHR* (rs6166, rs6165, rs2349415) and PCOS symptoms, though an association was reported with SNVs *ESR2* rs4986938 and *LHCGR* rs2293275.²⁴ It is possible that, with an increased sample size or in a different ethnic group, outcomes would differ. Thus, to better understand the involvement of FSHR polymorphisms, a large cohort study should be organized. Numerous studies have utilized bioinformatics tools to investigate gene expression levels and their correlation with miRNA and lncRNAs. Since non-coding RNAs have a critical role in the modulation of gene expression, the biological network analyses have played an important role in identifying the underlying mechanisms of the molecular regulation as well as the possible biomarkers. A recently published study investigated the lncRNA-miRNA-mRNA interaction networks *via* coding-non-coding gene co-expression networks and ceRNA network analysis showing that *FSHR* was down-regulated in PCOS patients and that there was both positive and negative correlation of lncRNAs with the six genes, including *FSHR25*.

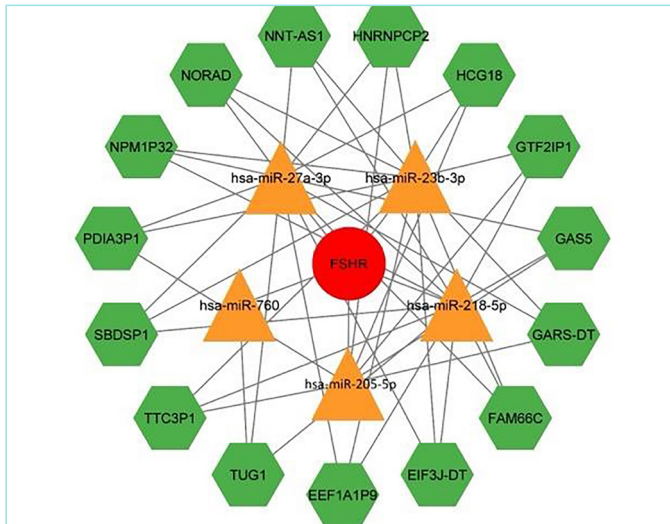


Figure 4. The relationship between *FSHR* gene and miRNAs and lncRNAs.

FSHR: Follicle stimulation hormone receptor.

CONCLUSION

In conclusion, this study found no significant difference in the heterozygosity of the *FSHR* gene polymorphisms, p.Ser680Asn (c.2039C>T; rs6166) and p.Ala307Thr (c.919G>A; rs6165), between the PCOS and control groups in the Turkish population. Biological network analysis was employed to investigate the possible association between PCOS symptoms and gene variations. Additionally, the association of *FSHR* with non-coding RNAs was investigated. This study postulates a foundation for future research, focusing on the regulation of the *FSHR* gene by non-coding RNAs and the potential identification of PCOS biomarkers.

MAIN POINTS

- No association of *FSHR* p. Ala307Thr (c.919G>A; rs6165) and p. Ser680Asn (c.2039C>T; rs6166) was observed in PCOS patients of Turkish origin.
- Biological network analysis of the *FSHR* gene in association with PCOS showed associations with miRNA and lncRNA.
- Biological network analysis for *FSHR* gene showed an association between PCOS-related symptoms and women's health abnormalities.

ETHICS

Ethics Committee Approval: Ethics committee approval was received for this study from Near East University Hospital Scientific Research Ethics Committee (approval number: YDU/2019/67-784, date: 28.03.2019).

Informed Consent: The patients signed the informed consent.

Footnotes

Authorship Contributions

Surgical and Medical Practices: B.Ö., A.C.Ö., Concept: P.T., Design: P.T., Data Collection and/or Processing: B.Ö., A.C.Ö., Analysis and/or Interpretation: S.M., B.O.-H., Literature Search: S.M., P.T., Writing: S.M., B.O.-H., P.T.

DISCLOSURES

Conflict of Interest: The authors declare no conflicts of interest.

Financial Disclosure: The authors declared no financial support for this study.

REFERENCES

1. Maffazioli GDN, Lopes CP, Heinrich-Oliveira V, Lobo RA, Hayashida SAY, Soares JM Jr, et al. Prevalence of metabolic disturbances among women with polycystic ovary syndrome in different regions of Brazil. *Int Gynaecol Obstet.* 2020; 151(3): 383-91.
2. Neves LPP, Marcondes RR, Maffazioli GN, Simões RS, Maciel GAR, Soares JM Jr, et al. Nutritional and dietary aspects in polycystic ovary syndrome: insights into the biology of nutritional interventions. *Gynecol Endocrinol.* 2020; 36(12): 1047-50.
3. Fauser BC JM, Diedrich K, Bouchard P, Domínguez F, Matzuk M, Franks S, et al. Contemporary genetic technologies and female reproduction. *Hum Reprod Update.* 2011; 17(6): 829-47.
4. Qu F, Wang FF, Yin R, Ding GL, El-Prince M, Gao Q, et al. A molecular mechanism underlying ovarian dysfunction of polycystic ovary syndrome: hyperandrogenism induces epigenetic alterations in the granulosa cells. *J Mol Med (Berl).* 2012; 90(8): 911-23.
5. Wang P, Zhao H, Li T, Zhang W, Wu K, Li M, et al. Hypomethylation of the LH/choriogonadotropin receptor promoter region is a potential mechanism underlying susceptibility to polycystic ovary syndrome. *Endocrinology.* 2014; 155(4): 1445-52.
6. Goodarzi MO, Dumesic DA, Chazenbalk G, Azziz R. Polycystic ovary syndrome: etiology, pathogenesis and diagnosis. *Nat Rev Endocrinol.* 2011; 7(4): 219-31.
7. Fauser BC JM, Tarlatzis BC, Rebar RW, Legro RS, Balen AH, Lobo R, et al. Consensus on women's health aspects of polycystic ovary syndrome (PCOS): the Amsterdam ESHRE/ASRM-Sponsored 3rd PCOS Consensus Workshop Group. *Fertil Steril.* 2012; 97(1): 28-38.
8. Barry JA, Azizia MM, Hardiman PJ. Risk of endometrial, ovarian and breast cancer in women with polycystic ovary syndrome: a systematic review and meta-analysis. *Hum Reprod Update.* 2014; 20(5): 748-58.
9. Fauser BC, Van Heusden AM. Manipulation of human ovarian function: physiological concepts and clinical consequences. *Endocr Rev.* 1997; 18(1): 71-106.
10. Gu BH, Park JM, Baek KH. Genetic variations of follicle stimulating hormone receptor are associated with polycystic ovary syndrome. *Int J Mol Med.* 2010; 26(1): 107-12.
11. Kim JJ, Choi YM, Hong MA, Chae SJ, Hwang K, Yoon SH, et al. FSH receptor gene p. Thr307Ala and p. Thr307Ala and p. Asn680Ser polymorphisms are associated with the risk of polycystic ovary syndrome. *J Assist Reprod Genet.* 2017; 34(8): 1087-93.
12. Du J, Zhang W, Guo L, Zhang Z, Shi H, Wang J, et al. Two *FSHR* variants, haplotypes and meta-analysis in Chinese women with premature ovarian failure and polycystic ovary syndrome. *Mol Genet Metab.* 2010; 100(3): 292-5.
13. Dolfen E, Guani B, Lussiana C, Mari C, Restagno G, Revelli A. FSH-receptor Ala307Thr polymorphism is associated to polycystic ovary syndrome and to a higher responsiveness to exogenous FSH in Italian women. *J Assist Reprod Genet.* 2011; 28(10): 925-30.
14. Unsal T, Konac E, Yesilkaya E, Yilmaz A, Bideci A, Onen HI, et al. Genetic polymorphisms of *FSHR*, *CYP17*, *CYP11A1*, *CAPN10*, *INSR*, *SERPINE1* genes in adolescent girls with polycystic ovary syndrome. *J Assist Reprod Genet.* 2009; 26(4): 205-16.
15. Fu L, Zhang Z, Zhang A, Xu J, Huang X, Zheng Q, et al. Association study between *FSHR* Ala307Thr and Ser680Asn variants and polycystic ovary

- syndrome (PCOS) in Northern Chinese Han women. *J Assist Reprod Genet.* 2013; 30(5): 717-21.
16. Valkenburg O, Uitterlinden AG, Piersma D, Hofman A, Themmen AP, de Jong FH, et al. Genetic polymorphisms of GnRH and gonadotrophic hormone receptors affect the phenotype of polycystic ovary syndrome. *J Hum Reprod.* 2009; 24(8): 2014-22.
 17. Branavan U, Muneeswaran K, Wijesundera S, Jayakody S, Chandrasekharan V, Wijeyaratne C. Identification of selected genetic polymorphisms in polycystic ovary syndrome in Sri Lankan women using low cost genotyping techniques. *PLoS One.* 2018; 13(12): e0209830.
 18. DISGENET, Data for Tomorrow's Health [Internet] MedBioinformatics Solutions SL, 2024 [Cited 2024 October 1] Available from: <https://disgenet.com>
 19. Interaction Database (DGIdb 4.0) with open crowdsourcing efforts. Freshour SL, Kiwala S, Cotto KC, Coffman AC, McMichael JF, Song JJ, et al. *Nucleic Acids Res.* 2021; 49(1): 1144-51.
 20. Diana Tools LncBase [Internet] Univ. of Thessaly, Pasteur Institute Powered by Angular / PostgreSQL & Java 2019. [Cited 2024 October 1] Available from: <https://diana.e-ce.uth.gr/lncbasev3>
 21. López I, Valdivia IL, Vojtesek B, Fähræus R, Coates PJ. Re-appraising the evidence for the source, regulation and function of p53-family isoforms. *Nucleic Acids Res.* 2024 Nov 11;52(20):12112-12129. doi: 10.1093/nar/gkæ855. PMID: 39404067; PMCID: PMC11551734. Available from: <https://rnasysu.com/encori/index.php>
 22. Shen Y, Wang L, Zhao Y, You L, Geng L, Gu HF, et al. Evaluation of the association between GHR exon 3 polymorphism and polycystic ovary syndrome among Han Chinese women. *Growth Horm IGF Res.* 2011; 21(5): 248-51.
 23. Valkenburg O, van Santbrink EJP, König TE, Themmen APN, Uitterlinden AG, Fauser BCJM, et al. Follicle-stimulating hormone receptor polymorphism affects the outcome of ovulation induction in normogonadotropic (World Health Organization class 2) anovulatory subfertility. *Fertil Steril* 2015; 103(4): 1081-8.
 24. Lidaka L, Bekere L, Rota A, Isakova J, Lazdane G, Kivite-Urtane A, et al. Role of single nucleotide variants in FSHR, GNRHR, ESR2 and LHCGR genes in adolescents with polycystic ovary syndrome. *Diagnostics (Basel).* 2021; 11(22): 2327.
 25. Zhou W, Zhang T, Lian Y, Zhang W, Yang M, Li Y, et al. Exosomal lncRNA and mRNA profiles in polycystic ovary syndrome: bioinformatic analysis reveals disease-related networks. *Reprod Biomed Online.* 2021; 44(5): 777-90

Phenolic Profile and Antioxidant Properties of Sariulak Olive Fermented with Red Beetroot

Şebnem Güler¹, Hüseyin Erten², Mehmet Karagözlü^{1,3}

¹Department of Food Engineering, Near East University Faculty of Agriculture, Nicosia, North Cyprus

²Department of Food Engineering, Çukurova University Faculty of Agriculture, Adana, Türkiye

³Research Center for Science, Technology and Engineering (BILTEM), Near East University, Nicosia, North Cyprus

Abstract

BACKGROUND/AIMS: Phenolic compounds are essential for enhancing the quality of table olives, contributing to their taste, aroma, color, and shelf life. Their antioxidant properties also provide health benefits, including protection against low-density lipoprotein oxidation and prevention of oxidative damage. The purpose of this study is to analyze the phenolic composition and antioxidant characteristics of the Sariulak olive variety, which is fermented alongside red beetroot (*Beta vulgaris* L.).

MATERIALS AND METHODS: In this study, geographically certified Tarsus Sariulak olives sourced from Mersin, Türkiye, and red beets obtained from Bursa, Türkiye, were utilized. Preliminary trials demonstrated that the optimal outcome was achieved with a 20% red beetroot ratio. The fermentation process, which lasted 128 days, was conducted using 10 kg of green olives in 9 liters of 7% brine solution. Fermentation was carried out in 12 L PVC-reinforced polyethylene airtight containers. Phenolic compounds were identified through high-performance liquid chromatography, while total phenolic content and antioxidant activity were evaluated using a spectrophotometer.

RESULTS: Olives contain around 30 phenolic compounds, with total phenolic content ranging from 100 to 800 mg/kg. Fresh olives, rich in oleuropein and hydroxytyrosol, have higher phenolic content than processed ones. In this study: oleuropein content in fresh olives ranged between 667.16 and 721.18 mg/kg, but dropped to 17.35-20.91 mg/kg during fermentation. Red beetroot addition further reduced oleuropein levels to 14.25-22.41 mg/kg, indicating enhanced hydrolysis. Hydroxytyrosol levels increased by 38% in red beet-added olives, while they decreased by 54% in the control group. Antioxidant activity improved significantly, reaching 32.43% with red beet addition, compared to 12.67% in the control.

CONCLUSION: The results demonstrate that incorporating red beetroot during olive fermentation enhances the hydrolysis of oleuropein, increases hydroxytyrosol levels, and boosts antioxidant activity. These effects contribute to producing a healthier olive product with higher functional value. Future studies are recommended to further explore the underlying mechanisms and long-term stability of these benefits.

Keywords: Sariulak olive, red beetroot, fermentation, phenolic compounds, antioxidants

INTRODUCTION

Olive cultivation is primarily practiced in Mediterranean countries like Spain, Türkiye, Greece, Italy, and others, and Italy, due to the specific climate requirements of olive trees. Currently, 93% of the world's olive trees are in these regions. In the 2022/2023 season, Türkiye ranked second

in global olive oil production with 380,000 tons after Spain's 665,800 tons, while Greece produced 345,000 tons, and Italy, 288,900 tons. These countries are key players in global olive oil production.¹ The Sariulak olive variety, cultivated in Mersin and Adana, accounts for approximately 6% of the olive trees in the Mediterranean region. This variety yields medium-sized, cylindrical fruits with an oil content ranging from 18% to

To cite this article: Güler Ş, Erten H, Karagözlü M. Phenolic profile and antioxidant properties of sariulak olive fermented with red beetroot. Cyprus J Med Sci. 2025;10(Suppl 1):106-110

ORCID IDs of the authors: Ş.G. 0009-0002-8050-8850; H.E. 000-0003-1537-2416; M.K. 0000-0002-6737-6702.



Corresponding author: Şebnem Güler
E-mail: sebnem.guler@neu.edu.tr
ORCID ID: orcid.org/0009-0002-8050-8850

Received: 10.11.2024
Accepted: 25.02.2025
Publication Date: 04.06.2025



Copyright© 2025 The Author. Published by Galenos Publishing House on behalf of Cyprus Turkish Medical Association.
This is an open access article under the Creative Commons AttributionNonCommercial 4.0 International (CC BY-NC 4.0) License.

22% and can be utilized for both green and black table olives.² Sensitive to low temperatures, the Tarsus Sariulak variety originates from Tarsus in Mersin.^{3,4} The primary objective of table olive processing is to remove⁵ phenolic acids, flavonoids, sugars (approximately 95% sucrose), vitamins (A, B1, B2, B3, C, folate), and essential minerals (calcium, potassium, magnesium, iron). Betalains in red beet prevent oxidation, scavenge free radicals, and offer health benefits, including probiotic effects and enhanced antioxidant activity. They also improve nutritional and sensory quality by increasing microbial diversity during fermentation.⁶⁻¹⁴ Red beetroot is rich in betalains, pigments that give it red and yellow hues. These include red betacyanins and yellow betaxanthins, with betanin being the dominant betacyanin, making up 75-95% of betalains. Betanin is widely used as a food colorant (E162). Interest in betalains is growing due to their stability in mildly acidic conditions and better water solubility compared to anthocyanins, making them a preferred natural colorant in the food industry.¹⁵⁻¹⁷ Phenolic compounds are key elements that improve the quality of table olives by enhancing their taste, aroma, color, and shelf life, alongside providing their antioxidant benefits. Additionally, these compounds are recognized for their positive effects on human health, including anti-inflammatory and antimicrobial properties, which contribute to overall well-being.^{18,19} Phenolic compounds in olives are essential for health benefits, owing to their antioxidant properties, protective effects against low-density lipoprotein oxidation, and potential to prevent oxidative damage.⁵ These compounds, including flavonoids and phenolic acids, significantly contribute to the sensory qualities and health effects of olive products. Oleuropein, a major secoiridoid in olives, provides strong antioxidant properties and acts as a natural defense against pests.¹⁸ Oleuropein consists of three key components: an apolar elenolic acid, a secoiridoid water-soluble glucose molecule, and hydroxytyrosol (HTz), a polyphenol with antioxidant properties. While elenolic acid has no direct function, it helps form oleuropein, a strong antioxidant, when glucose and hydroxytyrosol are added.^{5,20,21} This study aims to identify the phenolic profile and antioxidant properties of the Sariulak olive variety fermented with red beetroot (*Beta vulgaris* L.) while also evaluating the feasibility of producing beetroot-enriched olives.

MATERIALS AND METHODS

Olive Samples and Experimental Design

In this study, geographically registered Tarsus Sariulak olives from Mersin, Türkiye, and red beets from Bursa, Türkiye, were used. The fermentation lasted 128 days, involving 10 kg of green olives in 9 liters of 7% brine. The olives were fermented in two salt solutions: 7% NaCl (Sample Y) and 7% NaCl + 20% red beetroot (sample K). They were placed in 25 kg polyethylene crates, stacked up to three high in a closed truck, and transported to the Food Engineering Department of Çukurova University on the same day. The peels of the red beets were removed, and chopped into small pieces before being added to the olive fermentation process (day 0). Preliminary studies showed that the optimal red beetroot supplement was 20% (2 kg beetroot). The fermentation was conducted in airtight vessels kept in a cool, dark environment under controlled conditions, with salt concentrations maintained at 7%. After fermentation, the olives were stored at -20 °C for further analysis.

Chemicals

Methanol (CAS No 67-56-1), acetic acid (CAS No 64-19-7), and hexane (CAS NO 110-54-3) of high-performance liquid chromatography (HPLC) grade were obtained from Merck (Darmstadt, Germany). Standards for phenolic compounds, including hydroxytyrosol (3,4-Dihydroxyphenyl Ethanol, CAS NO

10597-60-1), Tyrosol (CAS NO 501-94-0), verbascoside (CAS NO 61276-17-3), p-coumaric acid (CAS NO 501-98-4), vanillic acid (CAS NO 121-34-6), oleuropein (CAS NO 32619-42-4), rutin (CAS NO 153-18-4), and apigenin-7-glucoside (CAS NO 578-74-5), were supplied by Sigma-Aldrich [St. Louis, MO, United States of America (USA)] and Fluka Chemie GmbH (Buchs, Switzerland). The chemicals Trolox (6-hydroxy-2,5,7,8-tetramethylchroman-2-carboxylic acid CAS NO 53188-07-1) and the Folin-Ciocalteu (CAS NO 12111-13-6) phenol reagent were sourced from Merck, while 2,2-diphenyl-1-picrylhydrazyl (DPPH) (CAS NO 1898-66-4) was purchased from Sigma-Aldrich.

Preparation of Sample Extracts

One point five grams of olive with the pit removed, ground into a paste using a grinder, was weighed and 20 mL of 80% methanol was added. After being broken down using an ultraturrax, the sample was washed twice with n-hexane (CAS NO 110-54-3) to remove the oil, and homogenized by vortexing. The extract was obtained by centrifuging at 6000 rpm for 10 minutes (min). After passing through a Durapore 0.45 µm, 47 mm PTFE (Polytetrafluoroethylene) membrane filter, the sample was directly injected into the HPLC system. For the phenolic compound analysis, 20 mL of methanol (80:20) was added to the 1.5 g olive sample, and the extract was obtained by centrifugation. The sample was blended and washed twice with 10 mL of n-hexane to remove the oil.

Determination of Total Phenolic Content

The method proposed by^{22,23} was carried out with slight modifications. In the proposed method, phenolic compounds reduce phosphomolybdic-phosphotungstic agents in the Folin-Ciocalteu solution to form a blue-colored complex; this color change is measured spectrophotometrically at 765 nm.

Determination of Antioxidant Activity

In the analysis of olive extracts, the spectrophotometric method proposed by²⁴ was adapted to be suitable for this purpose. For the analysis, 100 µL of extract was combined with 3000 µL of 1,1-diphenyl-2-picrylhydrazyl (DPPH*; 0.025 g/L in 80% methanol). For the control sample, 100 µL of pure water was used instead. The samples were subsequently blended and kept in the dark for one hour to allow the reaction to stabilize. After this incubation period, the absorbance of the samples was recorded at 515 nm using a spectrophotometer (Perkin Elmer Lambda 25 UV/VIS, Massachusetts, USA, 2005), with an 80% methanol solution serving as the reference.

High-Performance Liquid Chromatography Analysis of Phenolic Compounds

The phenolic compounds in the extracts were analyzed using HPLC on a Shimadzu LC-20AT system (Kyoto, Japan, 2006) with a diode array detector and a 4.6 mm × 250 mm i.d., 5 µm particle size reversed-phase C18 column (Waters, USA). The mobile phase consisted of water with 5% formic acid (solvent A) and acetonitrile (solvent B), with a gradient elution starting at 5% formic acid, progressing to 10% B at 15 min, 15% B at 20 min, 25% B at 30 min, 35% B at 50 min, 55% B at 75 min, 40% B at 53 min, 75% B at 90 min, and finally 100% B at 93 min. The column was maintained at 30 °C with a flow rate of 1 mL/minute and an injection volume of 40 µL. Detection occurred at wavelengths of 280 nm and 320 nm. The phenolic compounds were identified and quantified by comparing their retention times with those of standard compounds, and the results were expressed as mg/kg on a wet weight basis.

Statistical Analysis

The results of the analysis of raw olives and those obtained during fermentation were subjected to analysis of variance. Duncan's multiple range test was used to assess significant differences, with IBM SPSS Statistics 22 statistical software employed for the analysis.

RESULTS

Total Phenolic Content and Antioxidant Activity of Table Olives

The total phenolic content and antioxidant activity of the studied olives are presented in Figures 1, 2. Table olives and olive oils are noted to be valuable sources of "functional foods" due to the phenolic antioxidant compounds they contain.²⁵ It has been reported that the total phenolic content in olives varies depending on the variety.²⁶ The total phenolic content of olives at the start of fermentation ranged from 4601.17 to 4879.49 mg gallic acid/kg, decreasing to 1451.76 to 1827.74 mg/kg by the end. The highest phenolic content was observed at day 0, with a slight decrease by day 60 and more noticeable reduction in the control sample compared to the red beet-enriched olives. In a study on green olive fermentation with 10% and 20% red beet,²⁷ reported an initial total phenolic content of 3584.70 mg gallic acid/kg. As fermentation progressed, total phenolic content decreased, with a slight increase at the end. Antioxidant activity was higher at the start (52.49%-54.50%) than at day 60 and day 128, showing a significant difference between day 60 and day 128 ($p < 0.05$). Previous studies have shown that unfermented green olives have the highest antioxidant capacity (89%), with a decline observed during fermentation.^{28,29} In this study, the lowest antioxidant activity at the end of fermentation (12.67%) was recorded in the control sample, while the highest value (32.43%) was observed in the olives with red beet addition. The increase in antioxidant activity was attributed to the red beet supplementation. Antioxidant activity values decreased during the middle of the fermentation process. It has been suggested that the reduction in antioxidant capacity during processing is linked to the decrease in total phenolic compounds, with a linear relationship

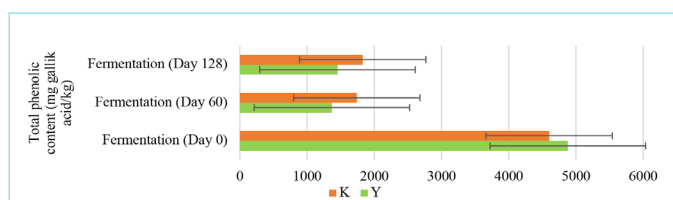


Figure 1. Total phenolic content of table olives (on a wet basis). Bars with different letters indicate significant differences ($p < 0.05$). Y represents 7% NaCl and K represents 7% NaCl + 20% red beetroot.

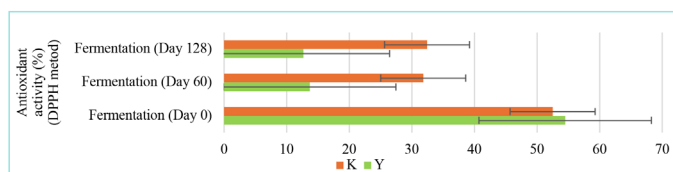


Figure 2. Antioxidant activity of table olives (on a wet basis). Bars with different letters indicate significant differences ($p < 0.05$). Y represents 7% NaCl and K represent 7% NaCl + 20% red beetroot. DPPH: 2,2-diphenyl-1-picrylhydrazyl.

between total phenolics and antioxidant capacity.^{26,30} Several studies have reported that betalains exhibit strong antioxidant activity, indicating that the addition of red beet enhances the antioxidant activity of olives. This is due to the positive correlation between betalain content and antioxidant properties. Plants rich in betalains are recognized for their high antioxidant capabilities.³¹ A study showed that olives with red beet had higher antioxidant capacity at the start, which decreased during fermentation, peaking in the middle. Increased red beet content also raised antioxidant activity.²⁷

Phenolic Compounds Profile of Table Olives

The amounts of phenolic compounds in the table olives are presented in Table 1. Monounsaturated fats and phenolic compounds are key contributors to the nutritional value of olive products, with phenolic compounds comprising 1-2% of fresh olives.¹⁹ Olive fruit contains various phenolic compounds, including glycosides like oleuropein, ligstroside, verbascoside, rutin, anthocyanins, as well as simple phenols and phenolic acids.³² Olives contain about 30 simple phenolic compounds, with total phenolic content ranging from 100 to 800 mg/kg.³³ In their study on Tunisian olives,¹⁹ identified 13 simple phenolic compounds in the olive fruit flesh, noting that the main components were hydroxytyrosol, tyrosol, and vanillic acid. Studies by^{34,35} have shown that the concentration of phenolic compounds in olives and olive oil typically ranges from 50 to 800 mg/kg. Significant variations in phenolic content were observed among different table olive samples. The phenolic compounds identified across all samples included hydroxytyrosol, tyrosol, verbascoside, p-coumaric acid, vanillic acid, oleuropein, rutin, and apigenin-7-glucoside. At the start of fermentation, oleuropein levels ranged from 624.36 mg/kg to 997.33 mg/kg, decreasing substantially by the end to 21.65 mg/kg (sample K) and 45.79 mg/kg (sample Y). These phenolic compounds in olives are typically in complex forms, which break down into simpler compounds like hydroxytyrosol and tyrosol. Oleuropein and hydroxytyrosol are the predominant phenolic compounds in fresh olives, with hydroxytyrosol being formed because of oleuropein hydrolysis. Hydroxytyrosol is a critical marker for monitoring the reduction in bitterness in olives.³⁶ At the start of fermentation, hydroxytyrosol levels were similar across samples (221.20 mg/kg to 221.81 mg/kg). However, hydroxytyrosol increased in the red beet-enriched samples, reaching 357.72 mg/kg by the end, a 38% increase, while the control sample saw a 54% decrease. Tyrosol levels decreased during fermentation, with final values of 11.89 mg/kg (sample Y) and 13.64 mg/kg (sample K), showing significant differences ($p < 0.05$). Rutin levels also decreased, from 58.48 mg/kg (sample Y) and 65.46 mg/kg (sample K) to 1.76 mg/kg (sample K) and 3.27 mg/kg (sample Y) by the end. Statistically significant differences in rutin levels were observed among the samples, consistent with previous research that reported higher rutin contents in raw Sariulak variety olives.³⁷ The initial vanillic acid levels in the table olives ranged from 19.16 mg/kg in sample Y to 33.66 mg/kg in sample K, decreasing over fermentation. By day 128, the content dropped to 3.24 mg/kg in sample Y and 4.04 mg/kg in sample K. However, red beet-enriched olives showed an increase in vanillic acid, with a significant difference between samples ($p < 0.05$). Verbascoside levels started at 719.72 mg/kg in sample Y and 835.32 mg/kg in sample K, declining during fermentation to 19.56 mg/kg and 650.22 mg/kg, respectively, with a significant difference ($p < 0.05$). The variation in verbascoside was attributed to the addition of red beet. Apigenin levels increased from 6.92 mg/kg (sample Y) and 9.60 mg/kg (sample K) to 27.54 mg/kg and 28.80 mg/kg, respectively, with no significant difference ($p > 0.05$). p-Coumaric acid levels decreased, with a slight increase in sample K (red beet-enriched) at the end, but no significant difference was observed between samples ($p > 0.05$).

Table 1. Phenolic compounds of table olives in mg/kg on wet basis

Phenolic compound		Fermentation (day 0)	Fermentation (day 60)	Fermentation (day 128)
Verbascosid	Y	769.95±6.52 ^d	20.07±0.69 ^e	19.56±0.80 ^f
	K	835.32±11.90 ^c	441.15±12.27 ^b	650.22±18.13 ^b
Vanillic acid	Y	19.16±2.26 ^b	3.71±0.63 ^{ab}	3.24±0.01
	K	33.66±1.33 ^a	0.98±0.26 ^c	4.04±0.38
Oleuropein	Y	714.17±9.91 ^c	46.31±0.13 ^a	45.79±2.51 ^a
	K	956.48±8.90 ^b	24.30±0.36 ^c	21.65±1.06 ^a
Rutin	Y	58.48±0.66 ^c	1.85±0.13 ^b	3.27±3.75
	K	65.46±0.53 ^a	2.33±0.97 ^b	1.76±0.24
Apigenin-7-glukozid	Y	9.60±3.73	29.52±1.19	28.80±5.22 ^{ab}
	K	6.92±0.59	26.27±0.78	27.54±0.13 ^b
P-coumaric acid	Y	3.05±0.05 ^{ab}	0.40±0.06 ^b	0.49±0.10
	K	4.34±0.98 ^a	0.32±0.00 ^b	0.56±0.01
Hydroxytyrosol	Y	221.81±6.92 ^b	200.70±6.94 ^d	101.10±9.90 ^d
	K	221.20±9.21 ^b	265.32±17.42 ^b	357.72±11.71 ^a
Tyrosol	Y	167.54±12.39 ^{ab}	15.65±2.72 ^c	11.89±1.10 ^c
	K	166.68±0.61 ^{ab}	10.03±11.07 ^c	13.64±2.25 ^c

Means with different superscript letters in the same row are significantly different ($p < 0.05$). Y: 7% NaCl and K: 7% NaCl + 20% red beetroot.

DISCUSSION

Table olives and olive oils are recognized as functional foods due to their rich phenolic composition, which contributes to health-promoting antioxidant properties.^{5,29} The results indicate a general decline in total phenolic content and antioxidant activity over fermentation, consistent with previous findings.^{26,30} However, the addition of red beet significantly reduced the extent of these losses, indicating that betalains from red beet enhanced antioxidant properties.^{20,21,31} The increased hydroxytyrosol content in the red beet-supplemented samples supports the hypothesis that oleuropein hydrolysis is more pronounced in these conditions.³⁶ This compound is also linked to bitterness reduction during olive fermentation. While rutin, vanillic acid, and verbascoside typically degrade over time, the enriched samples retained higher levels, suggesting a protective or synergistic role from red beet components.^{19,27,31-33} These findings align with Ardiç,²⁷ who reported increased phenolic retention and antioxidant activity in beet-supplemented green olives.²⁷ Overall, this study confirms the positive effect of red beet addition on preserving the bioactive properties of table olives. The findings contribute to the growing body of knowledge supporting the use of natural plant-based fortification strategies in fermented vegetable products.^{18,21,31}

CONCLUSION

The incorporation of red beet into table olive production improved the fermentation process. Although overall phenolic compound content decreased during fermentation, the addition of red beet reduced this decline, leading to higher antioxidant activity in the red beet-infused samples. The highest antioxidant activity recorded was 32.43%. Oleuropein levels declined rapidly during fermentation, but red beet promoted a faster breakdown compared to the control. Red beet-enriched olives also showed higher hydroxytyrosol levels, with a 38% increase in the enriched sample (K) compared to a 54% decrease in the control (Y). The study highlights the potential benefits of red beet in improving the quality and functional properties of table olives, emphasizing their importance in economy and health benefits. Further research is needed to explore future applications of this approach.

MAIN POINTS

- Red beet boosted the antioxidant activity in olives to 32.43% of their content, making it about 2.5 times higher than the control group.
- It slowed the decline of phenolic compounds during fermentation and increased hydroxytyrosol levels by 38%.
- It also accelerated the natural hydrolysis of oleuropein, improving phenolic transformation and health benefits.

ETHICS

Ethics Committee Approval: Not applicable.

Informed Consent: Not applicable.

Footnotes

Authorship Contributions

Concept: H.E., Ş.G., Design: H.E., Ş.G., M.K., Data Collection and/or Processing: H.E., Ş.G., Analysis and/or Interpretation: H.E., Ş.G., Literature Search: Ş.G., Writing: H.E., Ş.G., M.K.

DISCLOSURES

Conflict of Interest: No conflict of interest was declared by the authors.

Financial Disclosure: This study was supported by Scientific Research Projects, Çukurova University (Grant Number FBA-2021-13430).

REFERENCES

1. IOC. Olive production. International Olive Council. (serial online). 2023 (cited 2024 July 14): 1(1): Available from: URL: <https://www.internationaloliveoil.org/>.
2. Kaya H. Zeytinde çeşit tanımlama ve çeşitlerimiz, İzmir Zeytincilik Araştırma Enstitüsü. (serial online). 2017:20(C3): Available from: URL: <https://www.tarimorman.gov.tr/BUGEM/kumelenme/Belgeler/Budama/Zeytinde>.

3. Efe R, Soykan A, Curebal I, Sönmez S. Chapter one transhumance in northwestern turkey: karadere highlands (Burhaniye) case study. *Environment and Ecology in the Mediterranean Region II*; 2014.p.1-12.
4. Özkaya MT. Bölüm IV: standart zeytin çeşitlerimiz ve bazı özellikleri, zeytin yetiştiriciliği, İstanbul: Hasad Yayıncılık; 2008.p. 25-38.
5. Albuquerque TG, Costa HS, Oliveira MBP. An overview of portuguese olive oils and table olives with protected designation of origin. *European Journal of Lipid Science and Technology*. 2019; 121(5): 1800129.
6. Baião DDS, da Silva DV, Del Aguila EM, Paschoalin VMF. Nutritional, bioactive and physicochemical characteristics of different beetroot formulations. *Food Additives*. 2017; 6(6): 21-43.
7. Casciano F, Mayr H, Nissen L, Putti A, Zoli F, Gianotti A, et al. Red beetroot fermentation with different microbial consortia to develop foods with improved aromatic features. *Foods*. 2022; 11(19): 3055.
8. Chhikara N, Kushwaha K, Sharma P, Gat Y, Panghal A. Bioactive compounds of beetroot and utilization in food processing industry: A critical review. *Food Chem*. 2019; 272: 192-200.
9. Garrido-Fernández A, Fernández-Díez M, Adams M. Table olives: production and processing. London: Chapman and Hall; 1997.p.15-22.
10. Klewicka E, Cyzowska A. Biological stability of lactofermented beetroot juice during refrigerated storage. *Polish Journal of Food and Nutrition Sciences*. 2011; 61(4): 251-6.
11. López-García E, Romero-Gil V, Arroyo-López FN, Benítez-Cabello A. Impact of lactic acid bacteria inoculation on fungal diversity during Spanish-style green table olive fermentations. *Int Journal of Food Microbiology*. 2024; 417: 110689.
12. Panghal A, Virkar K, Kumar V, Dhull SB, Gat Y, Chhikara N. Development of probiotic beetroot drink. *Current Research in Nutrition and Food Science*. 2017; 5(3): 257-62.
13. Wróblewska B, Kuliga A, Wnorowska K. Bioactive Dairy-fermented products and phenolic compounds. Together or Apart. *Molecules*. 2023; 28(24): 8081.
14. Yoon KY, Woodams EE, Hang YD. Fermentation of beet juice by beneficial lactic acid bacteria. *LWT*. 2005; 38(1): 73-5.
15. Ferrara L. Food benefits and nutraceutical properties of the red beet. *Austin Journal of Nutrition Metabolism*. 2020; 7(3): 1084.
16. Özcan K, Bilek SE. Production and Stability of Food Colorant from Red Beetroot. *Academic Food Journal*. 2018; 16(4): 439-49.
17. Tomar O, Yıldırım G. Antimicrobial effect of red beet (*beta vulgaris* var. *cruenta* alef.) on some foodborne pathogens. *Turkish Journal of Agriculture-Food Science and Technology*. 2019; 7(1): 54-60.
18. Artık N, Anlı ER, Konar N, Vural N, editors. *Gıdalarda bulunan fenolik bileşikler*. İzmir:Türkiye; Sidas Medya; 2016.
19. Ben Othman N, Roblain D, Thonart P, Hamdi M. Tunisian table olive phenolic compounds and their antioxidant capacity. *J Food Sci*. 2008; 73(4): 235-40.
20. Blatchly R, Nircan DZ, O'Hara P, editors. *Zeytinlikten sofraya zeytinyağının hikayesi*. İstanbul: Türkiye: İş Bankası Kültür Yayınları. 2020.
21. Ötleş S, Özyurt VH. Oleuropein ve önemi. *Zeytin Bilimi*. 2012; 3(1): 59-71.
22. Abdulkasım P, Songchitsomboon S, Techagumpuch M, Balee N, Swatsitang P, Sungpuag N. Antioxidant capacity, total phenolics and sugar content of selected thai health beverages. *International Journal of Food Sciences and Nutrition*. 2007; 58(1): 77-85.
23. Akan S, Horzum Ö, Güneş NT. Fonksiyonel gıda kaynağı kırmızı pancar. *Proceedings Book of 5th International Eurasian Congress on Natural Nutrition, Healthy Life and Sport*; 2019 October 2-06; Ankara: Türkiye; 2019. pp.1537-50.
24. Klimczak I, Malecka M, Szlachta M, Gliszczyńska-Świgło A. Effect of storage on the content of polyphenols, vitamin c and the antioxidant activity of orange juices. *Journal of Food Composition and Analysis*. 2007; 20: 313-22.
25. Irmak Ş, Güngör FÖ, Susamcı E. The Determination of Total Phenol Quantities of Some Turkish Table Olive Varieties and the Effects of Processing Methods on These Compounds. *Zeytin Bilimi*. 2010; 1(2): 57-64.
26. Kiai H, Hafidi A. Chemical composition changes in four green olive cultivars during spontaneous fermentation. *LWT-Food Science and Technology*. 2014; 57(2): 663-70.
27. Ardiç Z. Sofralık Yeşil zeytin fermantasyonunda kırmızı pancar ve siyah havuç. *Sivas Cumhuriyet Üniversitesi, Fen Bilimleri Enstitüsü, Yüksek Lisans Tezi, Sivas*. 2022.
28. Jiang LQ, Takamura H. Radical-scavenging compounds in olive fruits and their changes during table olive preparation. *Applied Mechanics and Materials*. 2013; 295(298): 118-22.
29. Chranoti C, Kotzekidou P, Gerasopoulos D. Effect of Starter cultures on fermentation of naturally and alkali-treated cv. *conservolea* green olives. *LWT*. 2018; 89: 403-8.
30. Aprile A, Negro C, Sabella E, Luvisi A, Nicolì F, Nutricati E, et al. Antioxidant activity and anthocyanin contents in olives (cv *cellina di nardò*) during ripening and after fermentation. *Antioxidants*. 2019; 8(5): 138.
31. Bucur L, Țarălungă G, Schroder V. The betalains content and antioxidant capacity of red beet (*beta vulgaris* L. subsp. *vulgaris*) root. *Farmacia*. 2016; 64(2): 198-201.
32. Keçeli T, Gordon MH. The antioxidant activity and stability of the phenolic fraction of green olives and extra virgin olive oil. *Journal of the Science of Food and Agriculture*. 2001; 81(14): 1391-6.
33. Öztürk Aİ, Yılmaz Ö, Özer T, editors. *Her derde deva mucizevi bitki zeytin ve zeytinyağı analizleri*. İstanbul: Türkiye; Hiperayın. 2020.
34. Visioli F, Caruso D, Plasmati E, Patelli R, Mulinacci N, Romani A, et al. Hydroxytyrosol, as a component of olive mill waste water, is dose-dependently absorbed and increases the antioxidant capacity of rat plasma. *Free Radic Res*. 2001; 34(3): 301-5.
35. Perona JS, Cabello-Moruno R, Ruiz-Gutierrez V. The role of virgin olive oil components in the modulation of endothelial function. *The Journal of Nutritional Biochemistry*. 2006;17(7): 429-445.
36. Anagnostopoulos DA, Goulas V, Xenofontos E, Vouras C, Nikoloudakis N, Tsaltas D. Benefits of the use of lactic acid bacteria starter in green cracked cypriot table olives fermentation. *Foods*. 2020;9(1): 17.
37. Arslan D, Özcan MM. Phenolic profile and antioxidant activity of olive fruits of the turkish variety sarulak from different locations. *Grasas y Aceites*. 2011; 62(4): 453-461.

Ensemble Learning for Diabetes Classification Using Voting Classifier on CDC Health Indicators Dataset

✉ Bardia Arman¹, ✉ Kian Jazayeri², ✉ Erbug Celebi³, ✉ Kezban Alpan⁴, ✉ Kamil Dimililer⁵

¹Artificial Intelligence Application and Research Center, Cyprus International University Faculty of Engineering, Nicosia, North Cyprus

²Department of Information Technology, Cyprus International University School of Applied, Nicosia, North Cyprus

³Artificial Intelligence Application and Research Center, Cyprus International University, Nicosia, North Cyprus

⁴HND Digital Technologies Programme, David Game Higher Education, London, United Kingdom

⁵Department of Electrical and Electronic Engineering Applied Artificial Intelligence Research Centre Near East University, Nicosia, North Cyprus

Abstract

BACKGROUND/AIMS: Diabetes is one of the paramount public health challenges, affecting millions worldwide. Classification models can boost early detection and aid in treatment, particularly for diabetes type 2. This study, therefore, uses an ensemble learning approach for classifying diabetes type 2, utilizing a soft voting classifier, using multiple machine learning techniques on the Centers for Disease Control and Prevention Health Indicators Dataset.

MATERIALS AND METHODS: An ensemble model was developed in which the predictions of five machine learning algorithms were combined: XGBoost, Random Forest, Gradient Boosting, Support Vector Machine, and convolutional neural network-long short-term memory. Each model is trained using bootstrapped re-sampling, and predictions are aggregated through soft voting to improve classification performance on the test set.

RESULTS: On the test set, it achieved a classification accuracy of 87.8%, precision of 99.5%, recall of 99.51%, and an F1 score of 99.2%, hence proving high efficacy in identifying diabetes type 2 cases.

CONCLUSION: It follows that the proposed ensemble model efficiently classifies diabetes type 2 with high precision and recall; hence, it underpins the importance of ensemble learning in boosting the accuracy of classification. This may provide a reliable tool for early detection of diabetes, contributing to better patient outcomes through timely intervention.

Keywords: Convolutional neural network-long short-term memory, disease control and prevention, Support Vector Machine, XGBoost

INTRODUCTION

Diabetes mellitus is a chronic disease that impairs the body's ability to convert food into energy, resulting in elevated blood sugar levels due to insufficient or ineffective insulin production.¹ Type 2 diabetes accounts for 90-95% of cases, in which insulin is produced but is inadequate in its action. High blood sugar can damage blood vessels and organs,

leading to severe complications such as cardiovascular disease, kidney failure, and neuropathy. Moreover, undiagnosed diabetes can reduce life expectancy by up to 8 years, highlighting the urgent need for early detection and intervention.²

Common symptoms include frequent thirst, nighttime urination, fatigue, unplanned weight loss, slow wound healing, increased hunger,

To cite this article: Arman B, Jazayeri K, Celebi E, Alpan K, Dimiller L. Ensemble learning for diabetes classification using voting classifier on CDC health indicators dataset. Cyprus J Med Sci. 2025;10(Suppl 1):111-115

ORCID IDs of the authors: B.A. 0009-0001-9449-2688; K.J. 0000-0003-2843-7354; E.Ç. 0000-0003-3289-3328; K.A. 0000-0002-0492-1275; K.D. 0000-0002-2751-0479.



Corresponding author: Bardia Arman
E-mail: bardia.arman@gmail.com
ORCID ID: orcid.org/0009-0001-9449-2688

Received: 18.11.2024
Accepted: 15.04.2025
Publication Date: 04.06.2025



Copyright© 2025 The Author. Published by Galenos Publishing House on behalf of Cyprus Turkish Medical Association.
This is an open access article under the Creative Commons AttributionNonCommercial 4.0 International (CC BY-NC 4.0) License.

and blurred vision.³ Diagnosis primarily relies on blood glucose measurement,⁴ influenced by various health indicators. Research indicates that obesity, high blood pressure (HighBP), high cholesterol (HighCol), stroke history, and cardiovascular diseases are significant risk factors for diabetes.⁵⁻⁷ These health-related factors complicate diabetes management, necessitating effective predictive models.

In public health, classifying patients as diabetic or non-diabetic using advanced machine learning techniques can significantly enhance early detection and treatment strategies. This study aims to leverage ensemble learning models to improve classification accuracy for type 2 diabetes, integrating multiple machine learning algorithms through a voting classifier. This approach seeks to provide a reliable tool for healthcare professionals to identify at-risk individuals, ultimately contributing to better patient outcomes.

Previous studies have explored various machine learning approaches for diabetes prediction. For instance, Singh and Singh⁸ achieved 83.6% accuracy with a stacking-based ensemble framework. Kibria et al.⁹ reached 90% accuracy using a soft voting classifier. Dogru et al.¹⁰ developed a hybrid model achieving 99.6% accuracy. Sunny et al.¹¹ also proposed a soft voting ensemble method for accurate diabetes risk diagnosis.

MATERIALS AND METHODS

Statistical Analysis

To conduct this study and the proposed method, the Centers for Disease Control and Prevention (CDC) Diabetes Health Indicators Dataset was selected. The dataset contains 253,680 samples with 35 features, consisting of medical and behavioural data of individuals. The proposed method is implemented in the feature group shown in Table 1. Since this study primarily focuses on the classification of diabetes based on medical data, five medical features were selected from the dataset: including individuals' HighBP, HighCol, body mass index (BMI), which determines whether they are at a healthy weight, whether they have had a stroke in their medical history, and whether they have any history of heart disease or heart attack. The age and gender of individuals were used as demographic data.

Machine Learning Algorithms

Random forest: Random Forest allows the generation of various models and classifications by training each decision tree on a different observation sample. The algorithm creates a decision tree for each example and determines the estimated value of each decision tree.¹²

Table 1. Selected features for the study 1= diabetes		
Feature	Description	Definition
HighBP	High blood pressure	0= No, 1= Yes
HighCol	High cholesterol	0= No, 1= Yes
BMI	Body mass index	Numerical
Stroke	Stroke history	0= No, 1= Yes
Heart disease or attack	Heart disease history	0= No, 1= Yes
Age	Age of individual	Numerical
Sex	Biological classification	0= Female, 1= Male
Education	Education level	Scale 1 to 6
Diabetes binary	Target value	0= No diabetes, 1= Diabetes

Gradient boosting: In the first stage, an initial tree is created. It then calculates an error based on the difference between the actual value of the target variable and the value predicted by the tree a second tree is created to reduce this error. The second tree is used to estimate the negative gradient of the error predicted by the first tree.¹⁴

eXtreme gradient boosting: XGBoost is one of the ensemble methods that operates on decision trees, unlike traditional GB, which aims to minimize the errors of the model.

$$L(y, \hat{y}) + \Omega(f) \quad (1)$$

Support vector machines: As represented in Figure 1, support vector machine (SVM) is a supervised learning technique used for classification and regression. The SVM algorithm draws lines to separate sets of two or more points that are placed on a plane. Considering two data sets, this line aims to maximize the distance between the points of both sets. The decision boundary that needs to be determined for separation finds the best margin between classes and defines the hyperplane.¹⁵

Convolutional-longitudinal-short-term neural network: A deep learning architecture formed by the combination of CNN and LSTM networks is known as CNN-LSTM, and represented in Figure 2. CNNs capture spatial relationships within the dataset through convolution. LSTM, a type of recurrent neural network, is successful in capturing long-term dependencies. The combination of CNN-LSTM enables learning both spatial and temporal features of the data.¹⁶

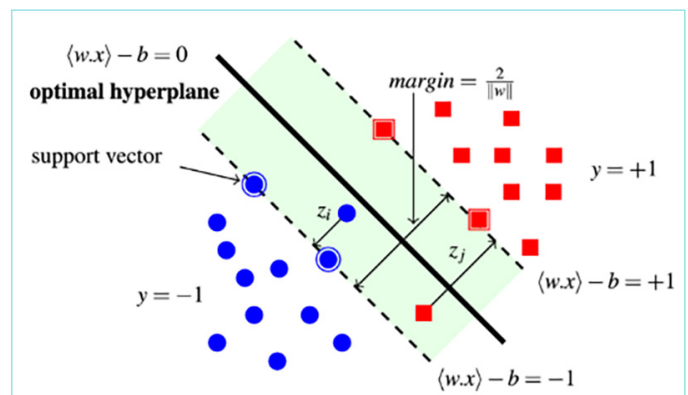


Figure 1. Classification of the datapoints into two classes with SVM.¹⁷

SVM: Support vector machine.

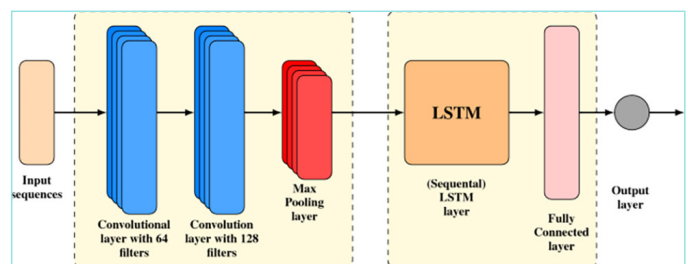


Figure 2. Example CNN-LSTM model.¹⁸

CNN-LSTM: Convolutional neural network-long short-term memory.

Correlation: Figure 3 illustrates the correlation between Diabetes Binary and eight characteristic variables. Health-related factors such as HighBP, BMI, HighCol, and heart disease show a positive correlation with diabetes. Among demographic variables, education level shows a negative correlation and stands out as significant, even when compared among medical factors. Examining both positive and negative correlations provides a comprehensive view of the dataset.

Proposed model: The dataset underwent an loading, preprocessing, and an 80-20 train-test split, followed by feature standardization. Bootstrap resampling was applied to the training set to enhance model robustness. Multiple models (XGBoost, Random Forest, Gradient Boosting, SVM, and CNN-LSTM) were trained on resampled datasets (Figure 4). The predictions were combined using soft voting, with the probabilities averaged for the predictions. The model’s performance was evaluated using accuracy, precision, recall, and F1 score. This ensemble approach improves robustness and mitigates overfitting.

RESULTS

Performance Analysis

The effectiveness of different machine learning algorithms in binary classification varies. The accuracy of measurements evaluates models such as Decision Tree, Random Forest, K-nearest neighbor (KNN), CatBoost, Gaussian Naive Bayes, Logistic Regression, Linear Discriminant, Gradient Boosting, and the proposed model. As shown in Table 2 and Figure 5, the proposed model achieved the highest accuracy (87.8%) in classifying the CDC Diabetes Indicator Dataset.

Beyond accuracy, precision, recall, and F1 score provide deeper insight into model performance. Random Forest and KNN excel in these metrics, demonstrating strong predictive power and minimizing false positives and false negatives. While the proposed model has the highest accuracy, its recall and F1 score confirm its ability to correctly classify positive cases. In contrast, Gaussian naive Bayes and logistic regression show moderate accuracy with lower precision, recall, and F1 scores,

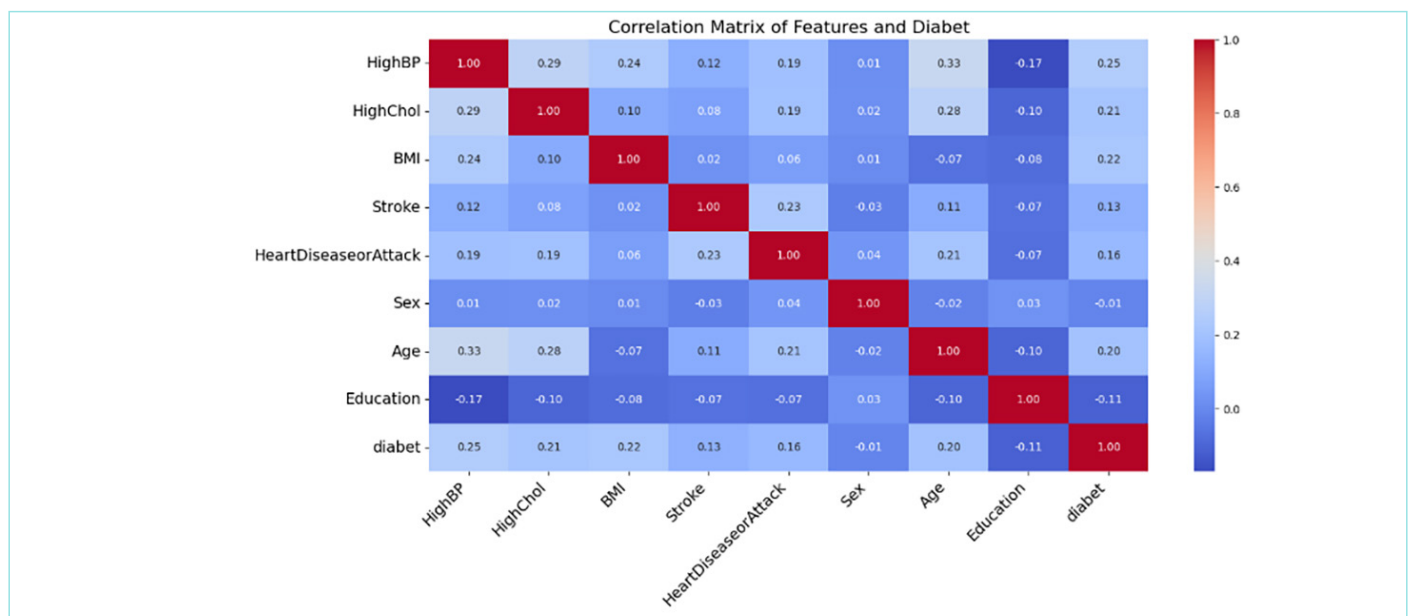


Figure 3. Correlation diagram.

HighBP: High blood pressure, HighCol: High cholesterol, BMI: Body mass index.

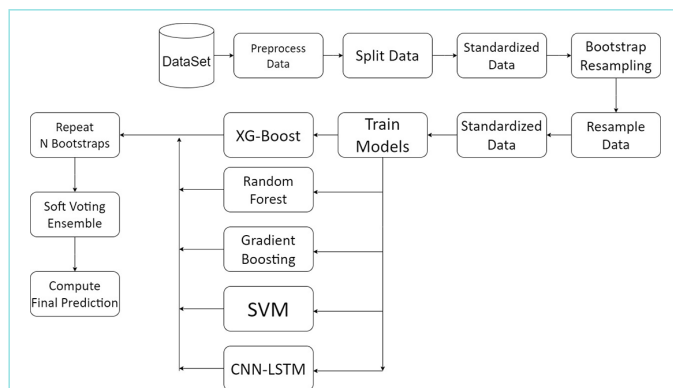


Figure 4. Model flowchart.

SVM: Support vector machine, CNN-LSTM: convolutional neural network-long short-term memory.

Model	Accuracy	Precision	Recall	F1 score
Decision tree	80.2%	97%	97.2%	97.8%
Random forest	84.9%	99%	99%	99%
KNN	85.4%	98%	98.5%	98.48%
Cat boost	86.6%	94.3%	94%	95.1%
Gaussian Naïve Bayes	74.1%	95.4%	96.5%	93.4%
Logistic regression	72.9%	89.7%	92.1%	91%
Linear discriminant	72.1%	96.3%	96.3%	97%
Gradient boosting	83.8%	97.4%	96.8%	97.2%
Proposed model	87.8%	99.5%	99.51%	99.2%

KNN: K-nearest neighbor

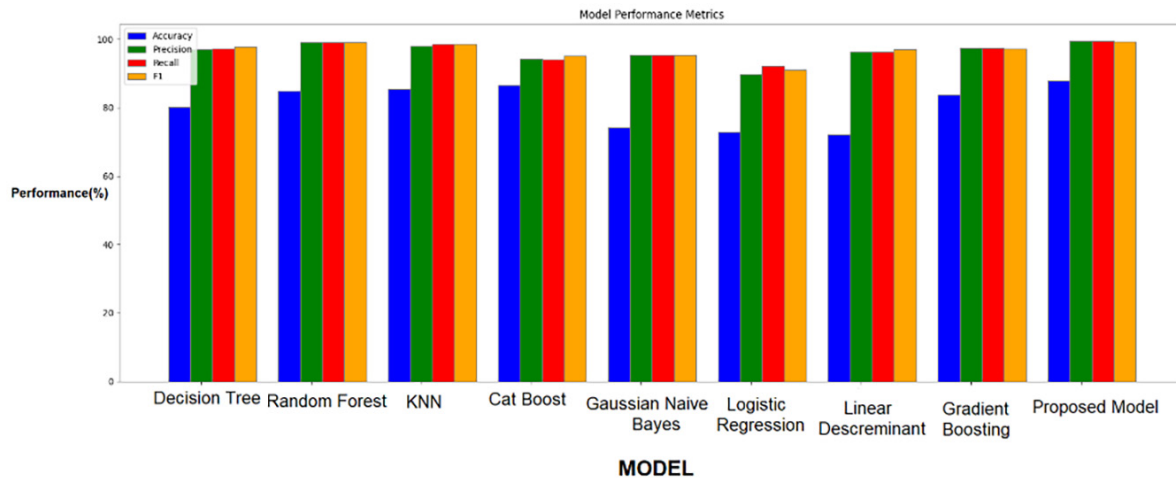


Figure 5. Model performance comparison.

KNN: K-nearest neighbor

indicating a higher rate of misclassification. Decision Trees and Linear Models, though less accurate, outperform Gaussian Naive Bayes and Logistic Regression in precision, recall, and F1 score.

Finally, Gradient Boosting shows competitive performance with high precision, recall, and F1 score, although the sentence is incomplete.

It is slightly weaker than Random Forest and KNN. Overall, this analysis emphasizes the importance of examining different metrics beyond accuracy to fully evaluate model performance, especially in scenarios where the costs of false positives and false negatives are different.

DISCUSSION

This study presents a robust ensemble learning model for classifying type 2 diabetes, utilizing five machine learning algorithms: XGBoost, Random Forest, Gradient Boosting, SVM, and CNN-LSTM. The ensemble approach, employing soft voting, achieved a classification accuracy of 87.8%; with precision, recall, and F1 scores of 99.5%, 99.51%, and 99.2%, respectively. These results demonstrate the model's effectiveness in accurately identifying diabetic patients while minimizing false positives and negatives, which is crucial in clinical settings.

The high performance of the ensemble model is attributed to its ability to leverage the strengths of diverse algorithms. Each algorithm contributes unique insights, allowing the ensemble to capture complex patterns in the data. For instance, Random Forest handles overfitting through its ensemble of decision trees, while XGBoost optimizes predictive accuracy via gradient boosting. The integration of CNN-LSTM captures both spatial and temporal features, which is beneficial for analyzing health-related time-series data.

However, the study has limitations. Reliance on a single dataset may restrict the generalizability of findings across different populations. Future research should validate the model on diverse datasets to ensure broader applicability. Additionally, the complexity of the ensemble

model may pose challenges in real-time clinical implementation and interpretability. Simplifying the model or employing explainable AI techniques could enhance usability for healthcare professionals. In conclusion, this study highlights the potential of ensemble learning in diabetes prediction, offering a powerful tool for early detection and intervention.

Study Limitations

This study's reliance on a single dataset may limit the generalizability of findings across diverse populations. Additionally, the model's complexity could present challenges in real-time implementation and interpretability in clinical settings.

CONCLUSION

Diabetes prediction remains essential in public health for early intervention and management. This study's ensemble model, leveraging the strengths of various machine learning techniques, achieved superior predictive accuracy and reliability in classifying diabetes based on health indicators. With high scores in precision, recall, and F1 metrics, the model proves valuable for accurately identifying diabetic patients and minimizing classification errors. Although further work is needed to enhance interpretability and generalizability, the findings suggest that ensemble learning offers a powerful approach for diabetes prediction, potentially aiding clinicians in early detection and reducing the impact of diabetes on patient health outcomes.

MAIN POINTS

- An ensemble learning model combining XGBoost, Random Forest, Gradient Boosting, SVM, and CNN-LSTM was developed for diabetes type 2 classification.
- The model achieved high performance with 87.8% accuracy, 99.5% precision, 99.51% recall, and 99.2% F1 score.

- The results highlight the potential of ensemble models in improving early detection and management of diabetes.

ETHICS

Ethics Committee Approval: Not available.

Informed Consent: Not available.

Footnotes

Authorship Contributions

Concept: B.A., K.J., E.Ç., K.A., K.D., Design: B.A., K.J., E.Ç., K.A., Data Collection and/or Processing: B.A., E.Ç., K.A., K.D., Analysis and/or Interpretation: B.A., K.J., K.D., Literature Search: B.A., K.J., E.Ç., K.A., K.D., Writing: B.A., K.J., E.Ç., K.A., K.D.

DISCLOSURES

Conflict of Interest: No conflict of interest was declared by the authors.

Financial Disclosure: The authors declared that this study had received no financial support.

REFERENCES

1. Alberti KG, Zimmet PZ. Definition, diagnosis and classification of diabetes mellitus and its complications. Part 1: Diagnosis and classification of diabetes mellitus. Provisional report of a WHO consultation. *Diabet Med*. 1998; 15(7): 539-53.
2. Halim R, Dahi Z, Halim NM. Tip 2 diyabette devamlı egzersiz ve safran kullanımının insülin direnci ve glikozun hücre içine alınımına etkisi. In 5th International Students Science Congress. (2021).
3. Tachkov K, Mitov K, Koleva Y, Mitkova Z, Kamusheva M, Dimitrova M, et al. Life expectancy and survival analysis of patients with diabetes compared to the non-diabetic population in Bulgaria. *PloS one*. 2020; 15(5): 0232815.
4. American Diabetes Association. Diagnosis and classification of diabetes mellitus. *Diabetes Care*. 2010; 33(Suppl 1): 62-9.
5. Inzucchi SE. Diagnosis of diabetes. *N Engl J Med*. 2012; 367(6): 542-50.
6. Lu W, Resnick HE, Jablonski KA, Jones KL, Jain AK, Howard WJ, et al. Non-HDL cholesterol as a predictor of cardiovascular disease in type 2 diabetes: the strong heart study. *Diabetes care*. 2003; 26(1): 16-23.
7. Lehto S, Rönnemaa T, Pyörälä K, Laakso M. Cardiovascular risk factors clustering with endogenous hyperinsulinaemia predict death from coronary heart disease in patients with type 2 diabetes. *Diabetologia*. 2000; 43(2): 148-55.
8. Singh N, Singh P. A stacked generalization approach for diagnosis and prediction of type 2 diabetes mellitus. *Computational Intelligence in Data Mining: Proceedings of the International Conference on ICCIDM*. 2020; 559-70.
9. Kibria HB, Nahiduzzaman M, Goni MOF, Ahsan M, Haider J. An ensemble approach for the prediction of diabetes mellitus using a soft voting classifier with an explainable AI. *Sensors*. 2022; 22(19): 7268.
10. Dogru A, Buyrukoglu S, Arı M. A hybrid super ensemble learning model for the early-stage prediction of diabetes risk. *Med Biol Eng Comput*. 2023; 61(3): 785-97.
11. Sunny S, Pinky S, Jalal S, Kayser M, Wadud M, Mansoor N. Soft voting ensemble-based approach for diagnosing diabetes mellitus. 2024 International Conference on Advances in Computing, Communication, Electrical, and Smart Systems. 2024; 1-6.
12. Biau G, Scornet E. A random forest guided tour. 2015; 25(2): 197-227.
13. Sahour H, Gholami V, Torkaman J, Vazifedan M, Saeedi S. Random forest and extreme gradient boosting algorithms for streamflow modeling using vessel features and tree-rings. *Environmental Sciences*. 2021; 80: 1-14.
14. Natekin A, Knoll A. Gradient boosting machines, a tutorial. *Front Neurobot*. 2013; 7: 21.
15. Aldino A, Saputra A, Nurkholis A, Setiawansyah S. Application of Support Vector Machine (SVM) Algorithm in classification of low-cape communities in lampung timur. *Building of Informatics, Technology and Science (BITS)*. 2021; 3(3): 325-30.
16. Mutegeki R, Han DS. A CNN-LSTM approach to human activity recognition. In 2020 international conference on artificial intelligence in information and communication (ICAIC). 2020; 362-6.
17. Do TN. Automatic learning algorithms for local Support Vector Machines. *SN Computer Science*.
18. World Health Organization. Diabetes [Internet]. Geneva: World Health Organization; 2024 Aug 8 [cited 2025 Jun 3]. Available from: <https://www.who.int/healthtopics/diabetes#tab=tab1>

Synthesis and Cytotoxic Effects of Various Thiosemicarbazide Compounds on Primary and Metastatic Breast Cancer Cell Lines

© Hilal Kabadayı Ensarioğlu¹, © Eda Becer², © Faika Başoğlu³, © Nuray Ulusoy Güzeldemirci⁴, © Hafize Seda Vatansever^{1,5}

¹Department of Histology and Embryology, Manisa Celal Bayar University Faculty of Medicine, Manisa, Türkiye

²Department of Biochemistry, Eastern Mediterranean University Faculty of Pharmacy, Famagusta, North Cyprus

³Department of Pharmaceutical Chemistry, European University of Lefke Faculty of Pharmacy, Lefke, North Cyprus

⁴Department of Pharmaceutical Chemistry, Istanbul University Faculty of Pharmacy, İstanbul, Türkiye

⁵DESAM Research Institute, Near East University, Nicosia, North Cyprus

Abstract

BACKGROUND/AIMS: Thiosemicarbazides and their metal complexes are known for their antiviral, antibacterial, and antitumor properties. This research describes the synthesis of four novel thiosemicarbazide derivatives (5, 8, 13, and 14) and investigates their cytotoxic effects on primary (MCF-7) and metastatic (M4A4) breast cancer cells. The study explored the Wnt/ β -catenin signaling pathway as well as key factors associated with proliferation, and stemness, that play a vital role in breast cancer development.

MATERIALS AND METHODS: Hydrazone derivatives containing imidazo[2,1-b]thiazole ring were synthesized through a conventional method. The MCF-7 and M4A4 cells were cultivated and exposed to different concentrations (200 μ M, 400 μ M, 800 μ M) of the all compounds for 24 and 48 hours. Cytotoxicity was investigated using the 3-(4,5-Dimethylthiazol-2-yl)-2,5-Diphenyltetrazolium Bromide (MTT) assay. The distribution of β -catenin, GSK 3 β , LGR5, Wnt 5a, Ki-67, Cxcl1, and CD44 were analyzed using indirect immunoperoxidase staining.

RESULTS: A 200 μ M dose for all compounds for 24 hours was selected based on MTT assay for further analyses. Immunohistochemical analysis exhibited that compounds 5, 8, and 14 stimulated the Wnt/ β -catenin pathway in both cell lines, with an elevation in the immunoreactivity of β -catenin, GSK 3 β , and LGR5 also observed. Compound 13 reduced the proliferation of M4A4 cells, but an increase in stemness was also observed.

CONCLUSION: Various thiosemicarbazide compounds affected primary and metastatic breast cancer cell lines differently. Among these, compound 13 showed an ability to reduce the growth of metastatic breast cancer cells. However, additional research about the stemness properties of breast cancer should be evaluated in further investigations.

Keywords: Thiosemicarbazide, Wnt/ β -catenin, stemness, breast cancer

To cite this article: Kabadayı Ensarioğlu H, Becer E, Başoğlu F, Ulusoy Güzeldemirci N, Vatansever HS. Synthesis and cytotoxic effects of various thiosemicarbazide compounds on primary and metastatic breast cancer cell lines. Cyprus J Med Sci. 2025;10(Suppl 1):116-120

ORCID IDs of the authors: H.K.E. 0000-0001-7429-1478; E.B. 0000-0002-2378-128X; F.B. 0000-0002-4890-3124; N.U.G. 0000-0002-4495-4282; H.S.V. 0000-0002-7415-9618.



Corresponding author: Hafize Seda Vatansever
E-mail: seda.vatansever@cbu.edu.tr, seda.vatansever@neu.edu.tr
ORCID ID: orcid.org/0000-0002-7415-9618

Received: 22.11.2024
Accepted: 13.03.2025
Publication Date: 04.06.2025



Copyright © 2025 The Author. Published by Galenos Publishing House on behalf of Cyprus Turkish Medical Association.
This is an open access article under the Creative Commons AttributionNonCommercial 4.0 International (CC BY-NC 4.0) License.

INTRODUCTION

Breast cancer is the most prevalent type of cancer in females.¹ Thiosemicarbazides and their metal complexes are known for their antiviral, antibacterial, and antitumor properties. Levamisole featuring an imidazo[2,1-b]thiazole structure was initially authorized as an anticancer agent by Başoğlu et al.^{2,3} which led to a significant increase in global research on this chemical framework. This trend continued with thiosemicarbazide, which followed the development of Triapine, thioacetazone, and methisazone. The Wnt/ β -catenin signaling pathway plays an important role in regulating key biological functions of cells such as proliferation and differentiation.^{4,6} Dysregulation of Wnt signaling is a feature of oncogenic transformation. Knockdown of Wnt5a has been demonstrated to reduce cellular senescence by reducing p16INK4A levels, reducing β -gal-positive cells counts, and suppressing the senescence associated secretory phenotype (SASP), which encompasses key SASP genes such as IL6, IL16, Cxcl1, Cxcl5, Cxcl12.^{7,8,9} The objective of this study is to develop four novel thiosemicarbazide compounds (5, 8, 13, and 14) and evaluate their cytotoxic effects on MCF-7 and M444 cell lines. The study also explored the involvement of this signaling pathway and essential factors associated with senescence, proliferation, and stemness in breast cancer progression.

MATERIALS AND METHODS

General synthesis pathway of 2-[(6-(4-methoxyphenyl)imidazo[2,1-b]thiazole-3-yl)acetyl]-N-alkyl/arylhydrazinecarbothioamides: the compounds were synthesized by heating 0.01 mol of each of compound 5, compound 8, compound 13, and compound 14 under reflux in 30 mL of ethanol on a water bath until a clear solution was obtained. Subsequently, 0.01 mol of alkyl isothiocyanate is added, and the mixture is heated for 3 hours. After the reaction is complete and the mixture has cooled to room temperature, the resulting precipitate is filtered and purified by washing with hot ethanol. The characterization of all synthesized compounds was performed using various spectroscopic techniques, including fourier transform infrared spectroscopy (FT-IR), ¹H-NMR, and MS. In this study, only precisely characterized compounds were used for further analysis.

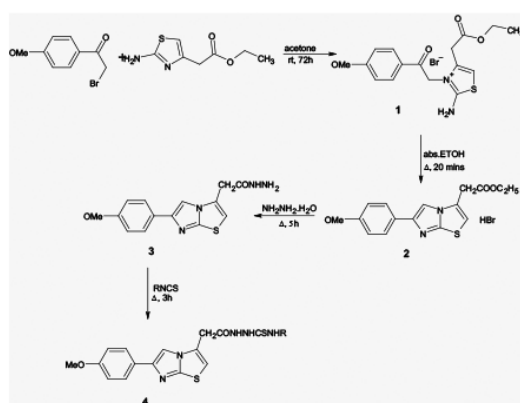
Cytotoxicity assay: Primary (MCF-7, HTB-22, ATCC) and metastatic (M444, CRL-2914, ATCC) breast cancer cell lines were cultured in medium [RPMI-1640 (F-1213, Biochrom), 10% fetal bovine serum (10270-106, Gibco), 1% pen-strep (PS-B, Capricorn Scientific) and 2 mM L-glutamine (K0283, Biochrom, Berlin, Germany)] in a humidified atmosphere at 37 °C and 5% CO₂. Cells (2x10³ cells/mL) in 96 well plates were then treated with various concentrations (10 μ M, 25 μ M, 50 μ M, 100 μ M, 200 μ M) of compounds 5, 8, 13 and 14 for 24 and 48 h. MTT (5 mg/mL, GC4568, Glentham Life Sciences) solution was added to each well, and incubated for 4 h and 50 μ L of dimethyl sulfoxide (DMSO) was added and reaction was evaluated using microplate reader (ELX800UV, BioTek Instruments Inc) at a reference wavelength of 540 nm.

Experimental groups and immunocytochemistry assay: The cells were grouped into five separate experimental groups: control (cell culture medium only), compound 5, compound 8, compound 13, and compound 14. After a 30 minutes (min) fixation with 4% paraformaldehyde (1.04004.0800, Merck), they were permeabilized with 0.1% Triton-X-100 (A4975,0100, AppliChem) on ice for 15 min; then 3% hydrogen peroxide (H₂O₂, 1.08597.2500, Merck) was added. They were incubated with blocking solution (TA-125-UB, ThermoFisher) for

1 h at RT before being exposed to primary antibodies against β -catenin (9562, Cell Signaling Technology), GSK 3 β (27C10, Cell Signaling Technology), LGR5 (HPA012530, Sigma Aldrich), Wnt 5a (2392S, Cell Signaling Technology), Ki-67 (PRM325AA, Biocare Medical), Cxcl1 (MBS422132, MyBiosource) and CD44 (15675-I-AP, Proteintech) for 18 h at 4°C. After the washing step, secondary antibodies (biotinylated rabbit anti-mouse, and streptavidin-conjugated hydrogen peroxidase-TP-125-UB, ThermoFisher) were applied. Diaminobenzidine (DAB, 38611, ScyTek Laboratories) was used as chromogen; Mayer's hematoxylin (Bio-Optica, 05-06002/L Milano, Italy) was used for counterstaining. Immunoreactivities were semi-quantitatively graded using the H-score. The Kruskal-Wallis test was utilized to perform the analysis, and statistical significance was evaluated at a p-value less than 0.05.

RESULTS

Chemistry



Compounds	R
5	Phenyl
8	Phenethyl
13	4-Chlorophenyl
14	4-Flourophenyl

Schema 1. The general synthesis pathway of the thiosemicarbazides

Compound-5: White solid, yield: 70% (1.84 g), mp: 201-202 °C. Anal. Calcd. C₁₇H₁₅N₃S₂: C 57.65, H 4.38, N 16.01%; Found: C 57.16, H 4.27, N 15.60%. FT-IR (cm⁻¹): 3176 (N-H), 1687 (C=O), 1172 (C=S). ¹H-NMR (DMSO-d₆, 500 MHz): δ 10.40 (s, NH-Ph), 10.23 (s, CS-NH), 7.48-7.15 (m, 5H, ar. CH), 3.78 (s, 3H, OCH₃). ESI (+) MS m/z (%): 437.9 M+, 438.9 (M+H)+

Compound-8: White solid, yield: 74% (2.06 g), mp: 200 °C. Anal. Calcd. C₁₉H₁₇N₃S₂: C 59.33, H 4.98, N 15.04%; Found: C 58.86, H 4.73, N 14.76%. FT-IR (cm⁻¹): 3159 (N-H), 1699 (C=O), 1172 (C=S). ¹H-NMR (DMSO-d₆, 500 MHz): δ 10.18 (s, NH-Ph), 9.54 (s, CS-NH), 7.31-7.19 (m, 5H, ar. CH), 3.76 (s, 3H, OCH₃).

Compound-13: White solid, yield: 79% (2.06 g), mp: 204 °C. Anal. Calcd. C₁₈H₁₄N₃S₂: C 53.44, H 3.84, N 14.84%; Found: C 52.81, H 3.71, N 14.53%. FT-IR (cm⁻¹): 3211, 3130 (N-H), 1682 (C=O), 1166 (C=S). ¹H-NMR (DMSO-d₆, 500 MHz): δ 10.51 (s, NH-Ph), 10.40, 10.29 (s, CS-NH), 7.57-7.38 (m, 4H, ar. CH), 3.78 (s, 3H, OCH₃).

Compound-14: White solid, yield: 93% (2.53 g), mp: 200 °C. Anal. Calcd. C₁₈H₁₄N₃S₂·C₆H₅OH: C 55.08, H 4.82, N 13.96%; Found: C 54.37, H 4.50, N 14.21%. FT-IR (cm⁻¹): 3122 (N-H), 1681 (C=O), 1167

(C=S). ¹H-NMR (DMSO-d₆, 500 MHz): δ 10.39 (s, NH-Ph), 10.21 (s, CS-NH), 7.44-7.16 (m, 4H, ar. CH), 3.78 (s, 3H, OCH₃).

Cell viability and cytotoxicity: MCF-7 exhibited adherence characteristics and an epithelial morphology, as depicted in Figure 1A. The metastatic breast cancer cell line M4A4 also displayed an epithelial morphology, with observations of a fusiform structure, highlighted in Figure 1B. After treated of cells with different concentrations of compound 5, 8, 13 and 14 for 24 (A, C) and 48 (B, D) hours, 200 μM dose and 24 h application were determined in both MCF-7(Figure 2 A, B) and M4A4 (Figure 2 C, D) cells.

Experimental groups and immunocytochemistry assay: β-catenin immunoreactivity was moderate in the control group, strongly positive in compound 5 and compound 14 applied groups, and it was weak in the compound 13 group in MCF -7 cell line (Figure 3A). Statistical analyses revealed that only the group treated with compound 13 exhibited a significant difference from the control group (p=0.029) (Figure 4A). In M4A4 cells, β-catenin immunoreactivity was moderate in control, groups treated with compound 13 and compound 14, while it was strongly positive and weak in groups treated with compound 8

and compound 5, respectively (Figure 3A). Immunoreactivity for GSK 3β was strongly positive in all groups where compounds were applied except the compound 13 group, which was moderate in both cell lines (Figure 3A), and it was statistically significant in MCF-7 cells for GSK 3β (p=0.015) when compared to the control group. Wnt5a and Cxcl1 immunoreactivities were weak or negative in all groups for MCF-7 and M4A4 cells (Figure 3B). Ki67 immunoreactivity was strongly positive in control and compound 14 applied groups, and it was moderate in compound 5 and 8 groups, while it was weak in compound 13 group for both type of cells (Figure 3C). Furthermore, in MCF-7 cells, the compound 13-applied group was statistically significantly different (p value is 0.008) compared to the control group. CD44 immunoreactivity was strongly positive in all groups where compounds were applied,

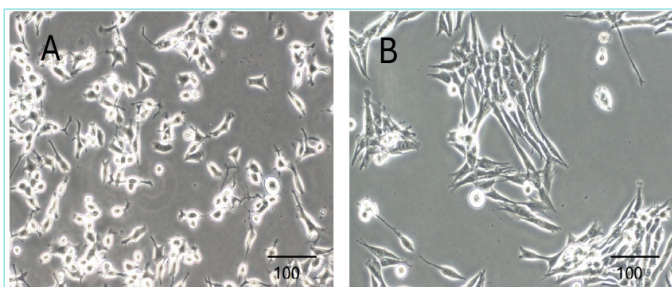


Figure 1. Cell culture photographs of MCF-7 (A) and M4A4 (B). Scale bars: 100μm.

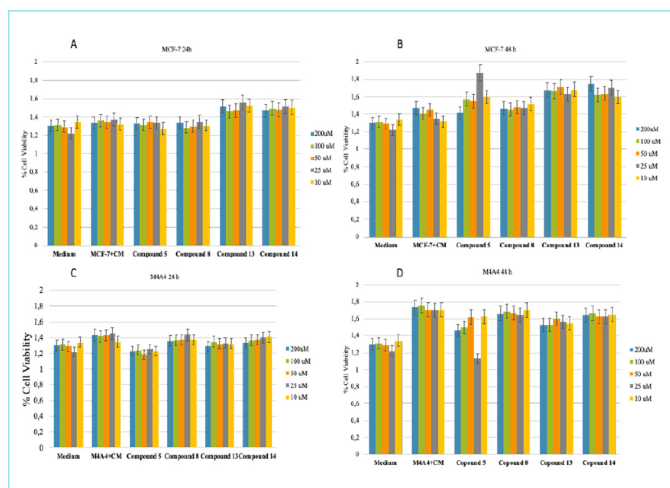


Figure 2. Cell viability assay of compound 5, compound 8, compound 13 and compound 14 for 24 (A,C) and 48 (B,D) h for MCF-7 and M4A4 cells. CM: Culture medium.

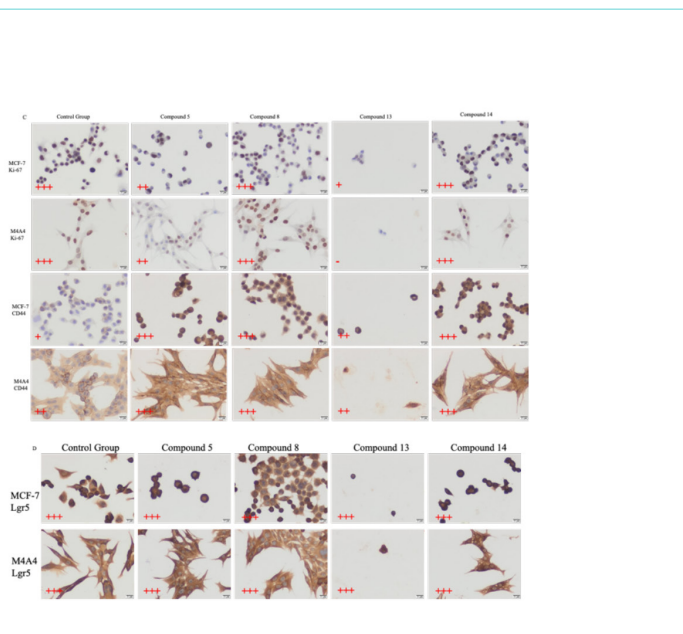
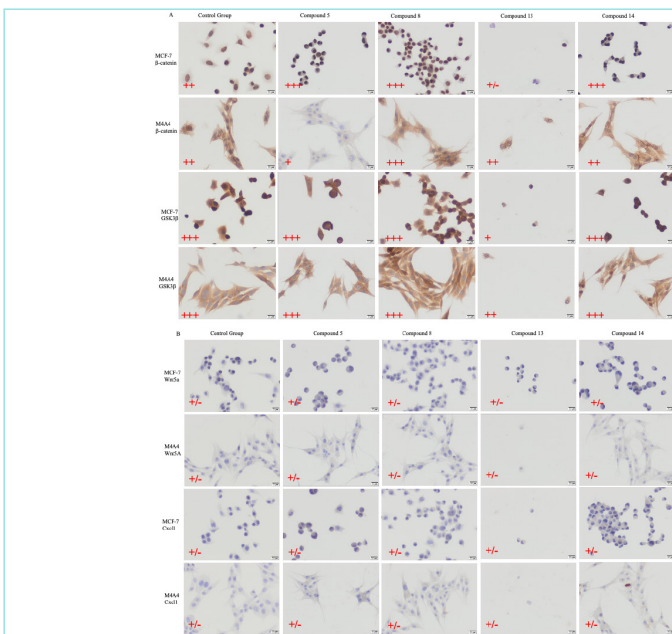
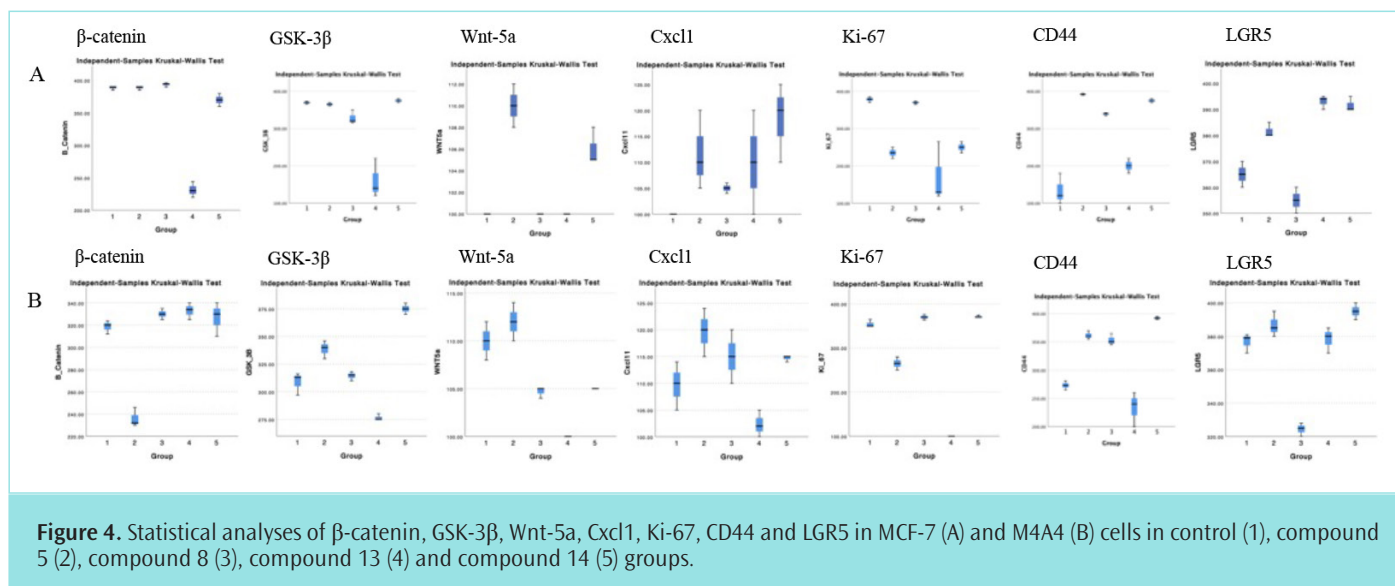


Figure 3. Distribution of β-catenin (A), GSK3β (A), Wnt5a (B), Cxcl1 (B), Ki-67 (C), CD44 (C) and LGR5 (D) after immunocytochemistry of control, compound 5, compound 8, compound 13 and compound 14. Scale bars: 20 μm.



except in the control group, and was weak or moderate in MCF-7 and M4A4 cells, respectively (Figure 3C). Finally, immunoreactivity for LGR-5 was strongly positive in all groups where compounds were applied except the compound 13 group, which was moderate in both cell lines (Figure 3D), and it was statistically significant in MCF-7 cells for LGR-5 ($p=0.027$) when compared to the control group. All statistical analyses were shown in Figure 4.

DISCUSSION

After synthesizing the hydrazone compound containing the 4-methoxy-substituted imidazo[2,1-b]thiazole core structure, we prepared thiosemicarbazide derivatives with yields ranging from 70% to 90% by reacting the hydrazone with four different aryl isothiocyanates using our previously reported method from our earlier study. The synthesized compounds were characterized by various spectroscopic techniques.³ The most significant evidence confirming the formation of the desired compounds was observed in the FT-IR spectra, where the characteristic double band associated with the NH^2 group disappeared, and a new band in the range of 1200-1050 cm^{-1} , corresponding to the $\text{C}=\text{S}$ stretching vibration, appeared. In the $^1\text{H-NMR}$ spectra, the absence of signals attributed to NH^2 protons further supported the conversion of NH^2 to $\text{N}=\text{C}$. Additionally, an increase in integral values from 7 to 8 ppm, corresponding to aromatic protons, was observed, with distinct peaks assigned to the hydrogens of phenyl, phenethyl, 4-chlorophenyl, and 4-fluorophenyl groups. Mass spectroscopy of the phenyl derivative selected as the prototype was conducted, and the M^+ peak of the compound with a molecular weight of 437 was observed as the base peak with an abundance of 100%. The spectra of the synthesized compounds are provided in the supplementary material file.

Our study investigated the effects of thiosemicarbazide compounds 5, 8, 13, and 14 on MCF-7 and M4A4 breast cancer cell lines. Notably, applying compounds 5, 8, and 14 resulted in an accumulation of β -catenin and GSK3 β in the cytoplasm and nucleus. This observation supports the activation of the canonical Wnt/ β -catenin pathway, which may drive cell proliferation and differentiation. However, in certain conditions, thiosemicarbazides might stimulate proliferation if they induce stress responses or activate pathways that promote cell survival

or regeneration. In our study, if compounds like thiosemicarbazide derivatives (such as 5, 8, 13, and 14) are triggering increased proliferation in breast cancer cell lines (as indicated by Ki-67 levels), it may suggest that these compounds are activating signaling pathways that support cell growth, potentially through the Wnt/ β -catenin pathway or other cell survival mechanisms. However, it is noteworthy that the application of compound 13 resulted in reduced immunoreactivity for investigated proteins, indicating a different mode of action or a potential inhibitory effect on this pathway. The proliferation marker Ki-67 showed increased immunoreactivity with compounds 8 and 14 in both MCF-7 and M4A4 cell lines, suggesting enhanced cell proliferation in response to these compounds. In contrast, compound 5, decreased Ki-67 levels compared to the control group. In addition, compound 13 reduced the number of cells. This reduction in Ki-67 supports the notion that these compounds may inhibit cell proliferation, with compound 13 showing particular effectiveness. Interestingly, all compounds appeared to enhance stemness properties in both MCF-7 and M4A4 cells. This weak intensity of Wnt5a and Cxcl1 may indicate a limited role for these factors in the context of the treatments applied. Furthermore, LGR5, a downstream target of the canonical Wnt pathway, showed decreased expression associated with increased senescence. However, our results suggest that none of the tested compounds significantly impacted senescence in MCF-7 and M4A4 cells, indicating that their effects may primarily be on proliferation and stemness rather than on senescent cell populations.

Study Limitations

An *in vitro* cell culture model was used in this study, but this does not capture the complexity of tumor microenvironments, including immune responses, stromal interactions, or pharmacokinetics. The effects of compounds may differ in a more complex *in vivo* setting. Future studies could focus on evaluating the efficacy of these thiosemicarbazide compounds in 3D spheroid models to better mimic the tumor microenvironment.

CONCLUSION

Overall, our findings highlight the diverse impacts of thiosemicarbazide compounds on both primary and metastatic breast cancer cell lines. In particular, compound 13 shows promise for reducing the proliferation

of metastatic breast cancer cells, although further investigation is warranted to evaluate its impact on stemness properties. The balance between proliferation and stemness should be controlled. Understanding the balance between proliferation, differentiation, and stemness in response to these compounds could inform future treatment strategies for breast cancer.

MAIN POINTS

- Synthesized thiosemicarbazide derivatives affected breast cancer cell lines.
- The cytotoxic effects of derivatives differed, and compounds 8 and 14 activated the canonical Wnt/ β -catenin pathway, promoting cell proliferation, while compound 13 inhibited proliferation.
- All compounds were found to enhance stemness properties in both MCF-7 and M4A4 cells.

ETHICS

Ethics Committee Approval: Not available.

Informed Consent: Not available.

Footnotes

Authorship Contributions

Concept: H.S.V., E.B., H.K.E., F.B., N.U.G., Design: H.S.V., E.B., H.K.E., F.B., Data Collection and/or Processing: H.S.V., E.B., H.K.E., F.B., N.U.G., Analysis and/or Interpretation: H.S.V., E.B., H.K.E., F.B., N.U.G., Literature Search: H.S.V., E.B., H.K.E., F.B., N.U.G., Writing: H.S.V., E.B., H.K.E., F.B., N.U.G.

DISCLOSURES

Conflict of Interest: No conflict of interest was declared by the authors.

Financial Disclosure: The authors declared that this study had received no financial support.

REFERENCES

1. Sung H, Ferlay J, Siegel RL, Laversanne M, Soerjomataram I, Jemal A, et al. Global Cancer Statistics 2020: GLOBOCAN Estimates of Incidence and Mortality Worldwide for 36 cancers in 185 countries. *CA Cancer J Clin.* 2021; 71(3): 209-49.
2. Bařođlu F, Ulusoy-Güzeldemirci N, Akalın-Çiftçi G, Çetinkaya S, Ece A. Novel imidazo[2,1-b]thiazole-based anticancer agents as potential focal adhesion kinase inhibitors: synthesis, in silico and in vitro evaluation. *Chem Biol Drug Des.* 2021; 98(2): 270-82.
3. Bařođlu-Ünal F, Becer E, Ensariođlu HK, -Güzeldemirci NU, Kuran ED, Vatansever HS. A newly synthesized thiosemicarbazide derivative trigger apoptosis rather than necroptosis on HEPG2 cell line. *Chem Biol Drug Des.* 2024; 103(1): 14355.
4. Corda G, Sala A. Non-canonical WNT/PCP signalling in cancer: Fzd6 takes centre stage. *Oncogenesis.* 2017; 6(7): 364.
5. Raut D, Vora A, Bhatt LK. The Wnt/ β -catenin pathway in breast cancer therapy: a pre-clinical perspective of its targeting for clinical translation. *Expert Rev Anticancer Ther.* 2022; 22(1): 97-114.
6. Rapp J, Jaromi L, Kvell K, Miskei G, Pongracz JE. WNT signaling - lung cancer is no exception. *Respir Res.* 2017; 18(1): 167.
7. Chen M, Li Y, Xiao L, Dai G, Lu P, Rui Y. Noncanonical Wnt5a signaling regulates tendon stem/progenitor cells senescence. *Stem Cell Res Ther.* 2021; 12(1): 544.
8. Sarabia-Sánchez MA, Robles-Flores M. WNT signaling in stem cells: a look into the non-canonical pathway. *Stem Cell Rev Rep.* 2024; 20(1): 52-66.
9. Fodde R, Brabletz T. Wnt/beta-catenin signaling in cancer stemness and malignant behavior. *Curr Opin Cell Biol.* 2007; 19(2): 150-8.
10. Khan AA, Ahmad R, Alanazi AM, Alsaif N, Abdullah M, Wani TA, et al. Determination of anticancer potential of a novel pharmacologically active thiosemicarbazone derivative against colorectal cancer cell lines. *Saudi Pharm J.* 2022; 30(6): 815-24.

Adipose Mesenchymal Stem Cell-Derived Exosomes Prevent Testicular Torsion Injury by Controlling Apoptosis and Necroptosis

© Hilal Kabadayı Ensarioğlu¹, © Fatma Bilgecan Şimşek², © Hafize Seda Vatanserver^{1,3}, © Hasan Çayırılı⁴, © Aydın Şencan⁴

¹Department of Histology and Embryology, Manisa Celal Bayar University Faculty of Medicine, Manisa, Türkiye

²Clinic of Pediatric Surgery, University of Health Sciences Türkiye, Gülhane Training and Research Hospital, Ankara, Türkiye

³DESAM Research Institute, Near East University, Nicosia, North Cyprus

⁴Department of Pediatric Surgery, Manisa Celal Bayar University Faculty of Medicine, Manisa, Türkiye

Abstract

BACKGROUND/AIMS: Testicular torsion, which occurs as a result of twisting of the spermatic cord, disrupts blood flow and causes ischemic damage, and reperfusion damage occurs when circulation is restored. Our earlier study revealed that exosomes originating from adipogenic mesenchymal stem cells (ADSCs) effectively reduce ischemia-reperfusion injury in experimental models of testicular torsion. This study investigates how these exosomes influence cell death pathways, specifically apoptosis and necroptosis.

MATERIALS AND METHODS: Twenty-one Wistar albino rats at a prepubertal stage were divided into sham, control, and treatment groups. The left testis was rotated to induce testicular torsion, then it was detorsed to allow reperfusion. The control group received ADSCs culture medium post-detorsion, while the treatment group was administered ADSC-derived exosomes (ADSC-Exos). The immunoreactivity of apoptotic (caspase 3, 8, 9, Bcl-2, Bax), necroptotic [receptor-interacting serine/threonine protein kinases 1, receptor-interacting protein 3 (RIPK1, RIP3), mixed lineage kinase domain-like (MLKL)] and spermatogonial stem cell [G-protein coupled receptor 125 (Gpr125)] markers was analyzed by indirect immunoperoxidase staining. The intensity of marker expression was evaluated by HSCORE. The results were statistically evaluated, and a p-value of <0.05 was considered significant.

RESULTS: The treatment group exhibited lower levels of caspase 3, 8, and 9 compared to the control group. Bcl-2 intensity was similar in all groups, but the Bax/Bcl-2 ratio was significantly reduced in the treatment group. The immunolabel of MLKL in the treatment group differed compared to the sham group (p=0.053). RIPK1 immunoreactivity was strong in the control torsion group compared to the other groups (p=0.000 and p=0.254, respectively), while RIP3 immunoreactivity was similar between the treatment group and sham group and lower compared to the control torsion group. Additionally, the highest intensity of Gpr125 was detected in the treatment group.

CONCLUSION: In the experimental testicular torsion-detorsion model, necroptosis was found more effective than apoptosis in affecting cell viability negatively. ADSC-Exos significantly reduced necroptosis in testicular cells. Additionally, exosomes had a positive effect on spermatogonial stem cells and helped prevent cell death after testicular torsion.

Keywords: Testicular torsion injury, exosomes, apoptosis, necroptosis

To cite this article: Kabadayı Ensarioğlu H, Şimşek FB, Vatanserver HS, Çayırılı H, Şencan A. Adipose mesenchymal stem cell-derived exosomes prevent testicular torsion injury by controlling apoptosis and necroptosis. Cyprus J Med Sci. 2025;10(Suppl 1):121-125

ORCID IDs of the authors: H.K.E. 0000-0001-7429-1478; F.B.Ş. 0000-0003-0826-3721; H.S.V. 0000-0003-3619-5666; H.Ç. 0000-0001-8422-2417; A.Ş. 0000-0002-8892-4907.



Corresponding author: Aydın Şencan
E-mail: aydin.sencan@yahoo.com.tr
ORCID ID: orcid.org/0000-0002-8892-4907

Received: 13.11.2024
Accepted: 17.02.2025
Publication Date: 04.06.2025



Copyright© 2025 The Author. Published by Galenos Publishing House on behalf of Cyprus Turkish Medical Association.
This is an open access article under the Creative Commons AttributionNonCommercial 4.0 International (CC BY-NC 4.0) License.

INTRODUCTION

Testicular torsion is a critical urological condition caused by the rotation of the testis and funiculus spermaticus that obstructs blood supply and leads to ischemia. The pathophysiological process involves ischemia caused by the twisting, followed by reperfusion once the cord is untwisted. The severity of injury is contingent on both the duration of torsion and the degree of twisting. Ischemia-reperfusion (I/R) injury initiates a cascade of pathological events, including neutrophil recruitment, the production of substance, release of proinflammatory cytokines, lipid peroxidation, cell death, anoxia, and disruptions in microvascular blood flow.¹

Adipogenic mesenchymal stem cells (ADSCs) have shown promise in mitigating I/R injuries through their biological properties which are controlled with ADSCs.^{2,3} Local application of ADSCs has been shown to preserve fertility in animal models of testicular torsion.^{4,5} However, transplanted mesenchymal stromal cells often face poor survival in ischemic environments post-infarction⁶, suggesting that their therapeutic effects are likely mediated by paracrine mechanisms, particularly through the release of exosomes.⁷

Exosomes are tiny vesicles (30-150 nm) surrounded by a membrane, and mediate intercellular communication by transferring molecular signals between cells. These vesicles, found in fluids like blood, urine, and semen, engage with recipient cells through various mechanisms, including ligand-receptor binding and membrane fusion.⁸ Exosomes and their linked microRNAs (miRNAs) play a key role in testis development, regulating vital processes such as proliferation of spermatogonial stem cells and the meiosis of spermatocytes, while also preserving the stability of the testicular immune microenvironment.⁸

Exosomes derived from ADSC (ADSC-Exos) have shown effectiveness in reducing I/R injury in multiple organs, including the brain⁹, heart¹⁰, and kidneys.¹¹ These exosomes have also been shown to improve erectile function in diabetic and post-prostatectomy models.^{12,13} Our previous work emphasized the protective role of ADSC-Exos against testicular torsion-induced I/R injury.¹⁴ This investigation aims to further explore the role of ADSC-Exos, particularly how they impact cell death mechanisms, such as apoptosis and necroptosis, in a testicular torsion model.

MATERIALS AND METHODS

Cell Culture and Study Groups

The research was approved by the Experimental Animal Ethics Committee of Manisa Celal Bayar University (approval number: E-77637435-050.04.04-582692, date: 21.07.2023). Adipose-derived mesenchymal stem cells were cultured and characterized following the methods outlined in our previous study¹⁴ Briefly, ADSCs were cultured in minimum essential medium alpha (Capricorn Scientific MEMA-XRA) containing 15% fetal bovine serum, 1% Penicillin-Streptomycin, and 1% L-Glutamine, maintained until they reached 85% confluency. The culture medium was harvested and exosomes were isolated using the miRCURY Exosome Isolation Kit (Exiqon 300102). There were three study groups, namely, sham, control, and treatment, and for each group, 7 Wistar albino male prepubertal rats were randomly assigned. In the sham group, rats underwent a left scrotal incision without any additional intervention. The sentence appears to logically misrepresent the experimental setup by suggesting treatment procedures for a control

group, but since details of the study's context are necessary for further revision and such details have not been provided, the sentence remains as is. Ensure the correct experimental context before publication. After 4 hours of torsion, the testis was detorsioned, and ADSCs culture medium, without fetal bovine serum, was administered into the testicular parenchyma, followed by a 4-hour reperfusion period. In the treatment group, the same procedure was performed, but the rats were administered ADSC-Exos instead of culture medium. Following the completion of the experimental procedures, the experimental animals were euthanized and the testicular tissues were collected. These tissues were fixed in Bouin's solution, processed through a standard paraffin embedding protocol, and sectioned into 5 µm slices for further analyses.

Apoptotic and Necroptotic Evolution via Immunohistochemistry

Immunoreactivity of apoptotic markers (caspases 3, 8, 9, Bcl-2, Bax), necroptotic markers [receptor-interacting serine/threonine protein kinases 1, receptor-interacting protein 3 (RIPK1, RIP3), mixed lineage kinase domain-like (MLKL)] and spermatogonial stem cell [G-protein coupled receptor 125 (Gpr125)] markers were assessed using the indirect immunoperoxidase technique. After deparaffinization, tissue sections were treated with two changes of xylene. To rehydrate the sections, they were dipped into the graded alcohol series and rinsed with distilled water. Following this, they were dipped into phosphate buffer solution (PBS) for five minutes (min). Next, they were incubated with a trypsin solution at 37 °C for 30 min. The sections were treated with 3% hydrogen peroxide (Merck, 1.08597.2500), followed by additional washes. Blocking solution (ThermoFisher, TA-125-UB) was then incubated for 1 hour at room temperature, before being added overnight at 4 °C with primary antibodies anti-caspase 3 (Bioassay Technology Laboratory, BT-AP01199), anti-caspase 8 (Bioss antibodies, BS-0052R) anti-caspase 9 (Bioss antibodies, BS-0049R), anti-Bcl-2 (Delta Biolabs, DB001), anti-Bax (Santa Cruz Biotechnology, sc-526), anti-RIPK1 (Bioss antibodies, 5805R), anti-RIP3 (Santa Cruz Biotechnology, sc-374639), anti-MLKL (Santa Cruz Biotechnology, sc-293201) and anti-Gpr125 (abcam, ab51705). Following PBS washing, the tissue samples were incubated with biotinylated rabbit anti-mouse secondary antibody for 30 min, followed by streptavidin-hydrogen peroxidase for an additional 30 min (ThermoFisher, TP-125-UB). After washing steps, the chromogen (DAB, 38611, ScyTek Laboratories) was applied to the slides for 5 min. Mayer's hematoxylin was added to stain the nuclei and the sections were mounted (DMM-125, Spring Bioscience). The degree of immunolabeling was evaluated by two researchers using light microscopy. The intensity of staining was graded semi-quantitatively using the H-score method. The H-score was determined using the following formula: $\sum (i + 1)$, where "i" represents the staining intensity (scored as 1, 2, or 3 for weak, moderate or strong, respectively) and "T" denotes the percentage of cells stained at each intensity level, ranging from 0 to 100%.

Statistical Analysis

Statistical comparisons between groups were performed using the Kruskal-Wallis test. A p-value of less than 0.05 was considered statistically significant.

RESULTS

Immunohistochemical analyses revealed that the immunoreactivity of caspase 3 (a), caspase 8 (b) and caspase 9 (c) was reduced in the treatment (Figure 1C-a, b, c) group in contrast to the control torsion (Figure 1B-a, b, c) group, though this difference was not statistically significant

(Figure 2). Bcl-2 immunoreactivity was lower in the treatment group (Figure 1C-d), and the difference with the sham group (Figure 1A-d) was significant ($p=0.044$) (Figures 1, 2). MLKL intensity was similar in the treatment group (Figure 1C-h) to the control group (Figures 1B-h, 2). Higher immunoreactivity of RIPK1 was detected in the control torsion group (Figure 1B-f), compared to the sham (Figure 1A-f) and treatment groups (Figure 1C-f), (p values were 0.000 and 0.254, respectively) (Figure 2); RIP3 (g) immunoreactivity was similar in the sham (Figure 1A-g) and treatment (Figure 1C-g) groups and lower than in the control torsion group (Figure 1B-g), although this was not statistically significant (Figure 2). Bax (e) immunoreactivity was higher in the control torsion group (Figure 1B-e) compared to the sham, (Figure 1A-e) and treatment (Figure 1C-e) groups. Treatment group Gpr125 (Figure 1C-i) immunoreactivity was higher than the control (Figure 1B-i) groups and the sham (Figure 1A-i) group (p -values 0.001 and 0.017, respectively).

DISCUSSION

In recent years, stem cell therapies and exosome-based treatments, a cell-free alternative, have gained prominence as promising options for various pathological conditions due to their advantages, including superior stability, storability, absence of toxicity and aneuploidy risks, low likelihood of immune rejection, and efficient targeting of damaged areas. Stem cell therapies have also been recognized for their potential in these conditions.^{15,14} The outlined effects of exosomes present a promising option for testicular torsion, offering potential benefits in preventing or mitigating I/R damage and preserving spermatogenic functions. Exosomes derived from mesenchymal stem cells modulate cellular activity and paracrine signaling by transferring proteins, lipids, mRNA, and miRNAs to recipient cells.¹⁶

In this study, we specifically aimed to explore the impact of ADSC-Exos particularly on apoptosis and necroptosis, in a model of testicular

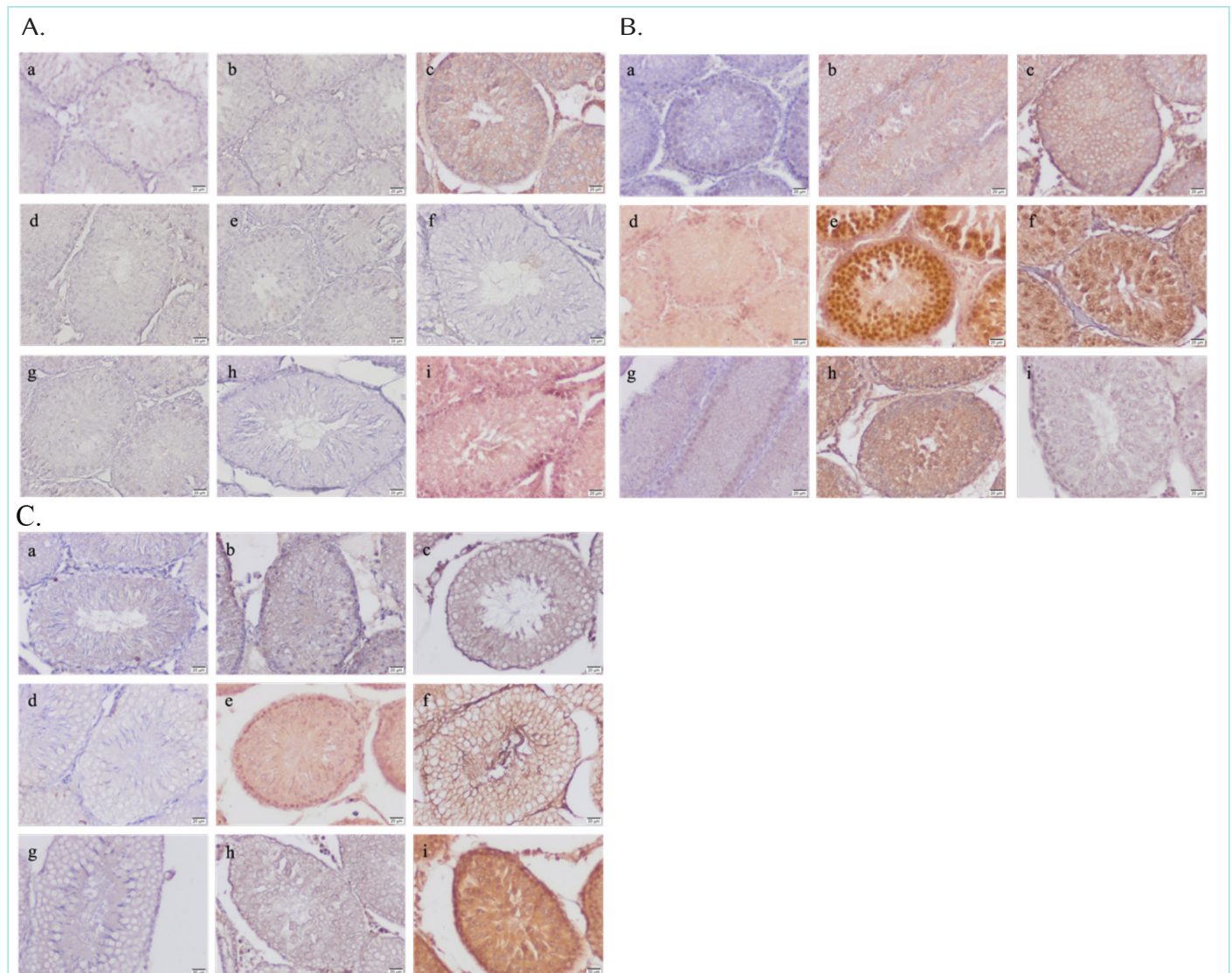


Figure 1. Distribution of caspases 3 (a), 8 (b), 9 (c), Bcl-2 (d), Bax (e), RIPK1 (f), RIP3 (g), MLKL (h), Gpr125 (i) after immunocytochemistry in the sham group (A), control torsion group (B), treatment group (C) testicles. Scale bars: 20 μ m.

RIPK1: Receptor-interacting serine/threonine protein kinases 1, RIP3: Receptor-interacting protein 3, MLKL: Mixed lineage kinase domain-like, Gpr125: G-protein coupled receptor 125.

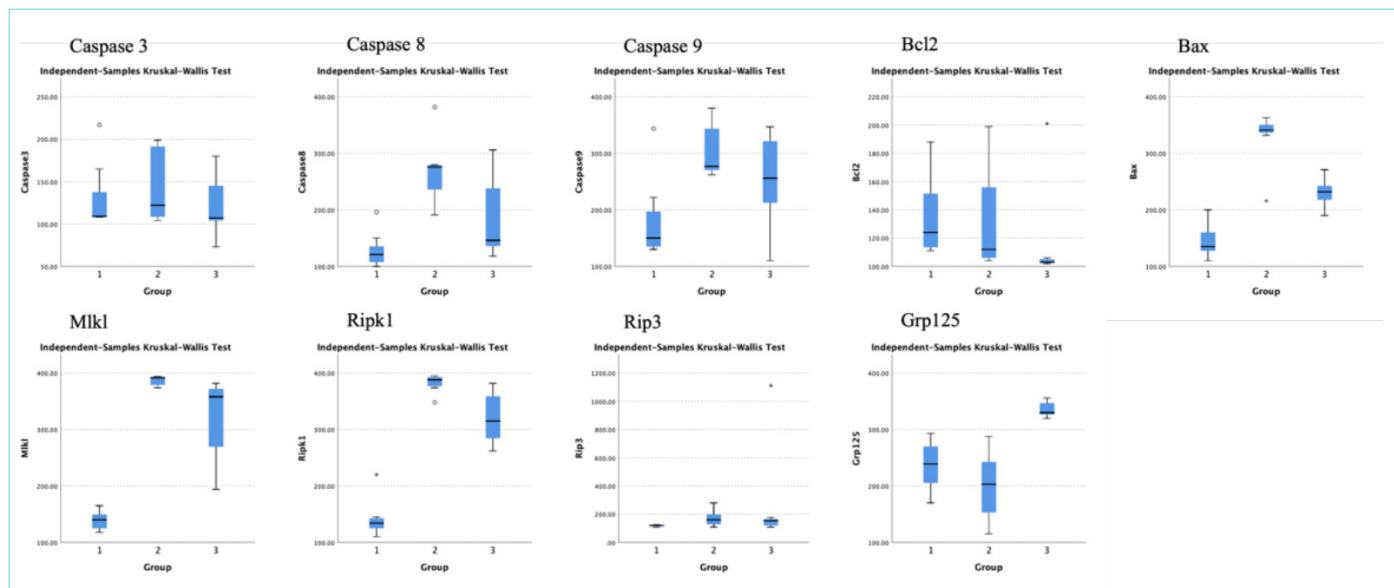


Figure 2. Statistical analyses of apoptotic (caspases 3, 8, 9, Bcl2, Bax) and necroptotic (RIPK1, RIP3 and MLKL) markers in sham (1), control (2), treatment (3) groups.

RIPK1: Receptor-interacting serine/threonine protein kinases 1, RIP3: Receptor-interacting protein 3, MLKL: Mixed lineage kinase domain-like, Gpr125: G-protein coupled receptor 125.

torsion-detorsion in rats. Previous studies have demonstrated the therapeutic potential of ADSC-Exos in various I/R injury models. For instance, Liu et al.⁶ observed that ADSCs exosomes exhibited notable therapeutic potential in mitigating oxidative stress-induced ischemia/reperfusion injury, particularly through modulation of the signaling pathways, especially PI3K/AKT and MAPK/ERK1/2. Similarly, our previous study showed that ADSC-Exos effectively helped prevent ischemia reperfusion injury in a testicular torsion model, as evidenced by improvements in tissue morphology and TUNEL staining analysis.¹⁴

In the present study, immunocytochemistry findings showed that exosome treatment reduced the immunoreactivity of caspases 3, 8 and 9, although these changes were not statistically significant. In contrast, the difference between anti-apoptotic Bcl-2, and apoptotic Bax values was significant, suggesting a shift toward cell survival. Furthermore, the reduced intensities of necroptotic markers RIPK1, and MLKL in the treatment group suggested that exosomes can reduce the harmful effects of I/R injury by modulating key apoptotic and necroptotic pathways. These findings support the potential role of exosomes in improving tissue survival, preserving spermatogonial stem cells, and ultimately enhancing the regenerative capacity of the testicular tissue.

This study adds to the growing body of evidence that ADSC-Exos are a viable therapeutic strategy for testicular torsion-detorsion injury. Their ability to target multiple pathways involved in cell death and survival underscores their potential for broader applications in ischemic and other pathological conditions requiring precision therapy.

Study Limitations

The study relies on an animal model, which may not perfectly replicate human pathophysiology. Therefore, translating these findings directly to human clinical applications might require additional validation in

larger models. Moreover, the study focuses on short-term outcomes after exosome treatment. However, the long-term effects of exosome therapy on tissue are not addressed. Additionally, investigation is needed to analyse the content of the exosomes.

CONCLUSION

Our experimental model of testicular torsion-detorsion indicated that necroptosis has a greater negative impact on cell viability than apoptosis. Furthermore, exosomes obtained from ADSCs were found to significantly mitigate necroptosis in testicular cells, while also promoting the survival of spermatogonial stem cells. Our findings indicate that exosomes have beneficial effects on cell death following testicular torsion and spermatogonial stem cell survival.

MAIN POINTS

- Exosomes derived from adipose-derived stem cells (ADSCs-Exos) offer a promising, cell-free therapeutic approach for testicular torsion by mitigating ischemia-reperfusion injury, reducing oxidative stress, and preserving spermatogenic functions.
- Exosome treatment reduced immunoreactivity of caspases 3, 8, and 9, while significantly increasing anti-apoptotic Bcl-2, and decreasing apoptotic Bax levels, indicating a shift toward cell survival. Additionally, lower expression of necroptotic markers RIPK1 and MLKL suggests a protective effect against cell death mechanisms.
- The ability of ADSCs-Exos to regulate multiple cell death and survival pathways highlights their potential for treating testicular torsion-detorsion injury.

ETHICS

Ethics Committee Approval: The research was approved by the Experimental Animal Ethics Committee of Manisa Celal Bayar University (approval number: E-77637435-050.04.04-582692, date: 21.07.2023).

Informed Consent: Not applicable.

Footnotes

Authorship Contributions

Surgical and Medical Practices: H.K.E., F.B.Ş., H.Ç., A.Ş., Concept: A.Ş., H.S.V., F.B.Ş., H.K.E., H.C., Design: A.Ş., H.S.V., H.K.E., F.B.Ş., Data Collection and/or Processing: H.K.E., F.B.Ş., H.S.V., H.Ç., A.Ş., Analysis and/or Interpretation: H.K.E., F.B.Ş., H.S.V., H.Ç., A.Ş., Literature Search: H.K.E., F.B.Ş., H.S.V., H.Ç., A.Ş., Writing: H.K.E., F.B.Ş., H.S.V., H.Ç., A.Ş.

DISCLOSURES

Conflict of Interest: No conflict of interest was declared by the authors.

Financial Disclosure: The study was funded by Manisa Celal Bayar University Scientific Research Projects Office (Project no: 2021-072).

REFERENCES

- Karaguzel E, Kadihasanoglu M, Kutlu O. Mechanisms of testicular torsion and potential protective agents. *Nat Rev Urol*. 2014; 11(7): 391-9.
- Yip HK, Chang YC, Wallace CG, Chang LT, Tsai TH, Chen YL, et al. Melatonin treatment improves adipose-derived mesenchymal stem cell therapy for acute lung ischemia-reperfusion injury. *J Pineal Res*. 2013; 54(2): 207-21.
- Yip HK, Lee MS, Sun CK, Chen KH, Chai HT, Sung PH, et al. Therapeutic effects of adipose-derived mesenchymal stem cells against brain death-induced remote organ damage and post-heart transplant acute rejection. *Oncotarget*. 2017; 8(65): 108692-711.
- Hsiao CH, Ji AT, Chang CC, Cheng CJ, Lee LM, Ho JH. Local injection of mesenchymal stem cells protects testicular torsion-induced germ cell injury. *Stem Cell Res Ther*. 2015; 6(1): 113.
- Hsiao CH, Ji AT, Chang CC, Chien MH, Lee LM, Ho JH. Mesenchymal stem cells restore the sperm motility from testicular torsion-detorsion injury by regulation of glucose metabolism in sperm. *Stem Cell Res Ther*. 2019; 10(1): 270.
- Liu H, Shi M, Li X, Lu W, Zhang M, Zhang T, et al. Adipose mesenchymal stromal cell-derived exosomes prevent testicular torsion injury via activating PI3K/AKT and MAPK/ERK1/2 pathways. *Oxid Med Cell Longev*. 2022; 16: 8065771.
- Song Y, Li Z, He T, Qu M, Jiang L, Li W, et al. M2 microglia-derived exosomes protect the mouse brain from ischemia-reperfusion injury via exosomal miR-124. *Theranostics*. 2019; 9(10): 2910-23.
- Li CY, Liu SP, Dai XF, Lan DF, Song T, Wang XY, et al. The emerging role of exosomes in the development of testicular. *Asian J Androl*. 2023; 25(5): 547-55.
- Huang X, Ding J, Li Y, Liu W, Ji J, Wang H, et al. Exosomes derived from PEDF modified adipose-derived mesenchymal stem cells ameliorate cerebral ischemia-reperfusion injury by regulation of autophagy and apoptosis. *Exp Cell Res*. 2018; 371(1): 269-77.
- Chai HT, Sheu JJ, Chiang JY, Shao PL, Wu SC, Chen YL, et al. Early administration of cold water and adipose derived mesenchymal stem cell derived exosome effectively protects the heart from ischemia-reperfusion injury. *Am J Transl Res*. 2019; 11(9): 5375-89.
- Lin KC, Yip HK, Shao PL, Wu SC, Chen KH, Chen YT, et al. Combination of adipose-derived mesenchymal stem cells (ADMSC) and ADMSC- derived exosomes for protecting kidney from acute ischemia-reperfusion injury. *Int J Cardiol*. 2016; 216: 173-85.
- Chen F, Zhang H, Wang Z, Ding W, Zeng Q, Liu W, et al. Adipose-derived stem cell-derived exosomes ameliorate erectile dysfunction in a rat model of type 2 diabetes. *J Sex Med*. 2017; 14(9): 1084-94.
- Li M, Lei H, Xu Y, et al. Exosomes derived from mesenchymal stem cells exert therapeutic effect in a rat model of cavernous nerves injury. *Andrology*. 2018; 6(6): 927-35.
- Şimşek FB, Şencan A, Vatansever HS. Exosomes obtained from adipose mesenchymal stem cells prevent ischemia-reperfusion injury after torsion-detorsion in rat testes. *Pediatr Surg Int*. 2023; 39(1): 204.
- Basu J, Ludlow JW. Exosomes for repair, regeneration and rejuvenation. *Expert Opin Biol Ther*. 2016; 16(4): 489-506.
- Jiang N, Xiang L, He L, Yang G, Zheng J, Wang C, et al. Exosomes mediate epithelium-mesenchyme crosstalk in organ development. *ACS nano*. 2017; 11(8): 7736-46.